

ASI/PINSON  
1 KILOWATT HIGH RELIABILITY  
WIND SYSTEM DEVELOPMENT

Phase I - Design and Analysis

Technical Report

March 1982

R.B. No11  
N.D. Ham  
H.M. Drees  
L.B. Nichol

Prepared by

Aerospace Systems Inc.  
Burlington, MA 01803

Pinson Energy Corporation  
Marstons Mills, MA 02648

Natural Power Inc.  
New Boston, NH 03070

For

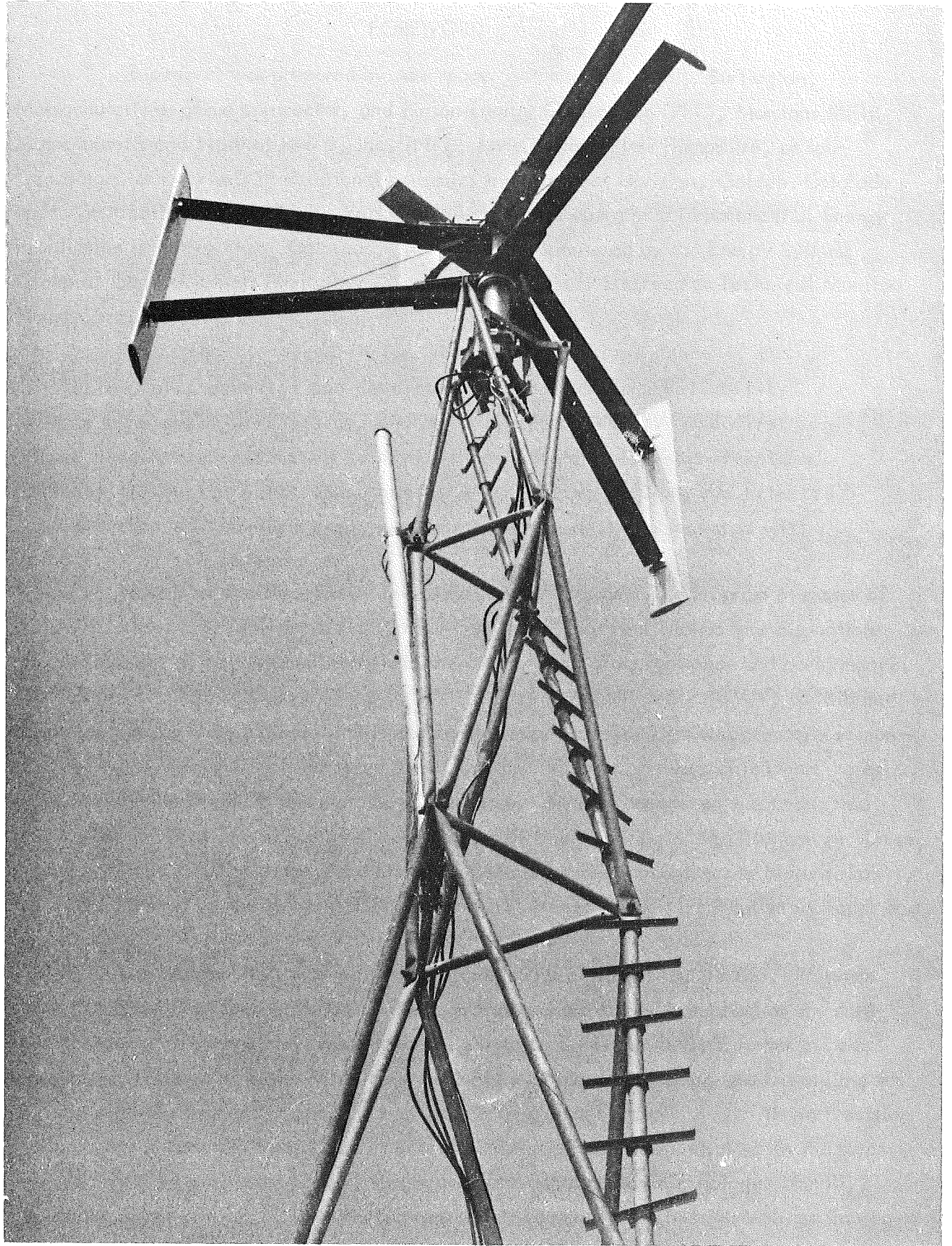
Rockwell International Corporation  
Energy Systems Group  
Rocky Flats Plant  
Wind Systems Program  
Golden, CO 80402-0464

Subcontract No. PF-71777-F

As part of the  
UNITED STATES DEPARTMENT OF ENERGY  
WIND ENERGY TECHNOLOGY DIVISION  
FEDERAL WIND ENERGY PROGRAM

Contract No. DE-AC04-76DP03533

0001200 1000 05 JUL



ASI/Pinson 1 Kilowatt High Reliability Cycloturbine  
(Prototype - 1979 Photo)

## FOREWORD

This report was prepared by Aerospace Systems, Inc. (ASI), Burlington, Massachusetts as prime contractor, and Pinson Energy Corporation (PEC), Marstons Mills, Massachusetts and Natural Power, Inc. (NPI), New Boston, New Hampshire, as sub-contractors for Rockwell International, Atomic International Division, Golden, Colorado under Contract No. PF71777-F. Rockwell International operates a Department of Energy installation at Rocky Flats, Colorado. The study was sponsored by the Energy Systems Group at the Rocky Flats Plant. Mr. Warren S. Bollmeier, II served as Technical Monitor of the contract.

This report, issued in two volumes, summarizes Phase I, Design Evaluation, of the design and development of a 1-kW High Reliability Cycloturbine small wind energy conversion system (SWECS). The first volume presents an executive summary of the effort. The second volume presents the design philosophy, analysis and tests; reviews the selected configuration and construction; and examines the costs associated with production of the selected design.

The effort was directed by Mr. John Zvara, President and Program Manager of ASI. Mr. Richard B. Noll served as Project Engineer. Mr. Paul Soohoo was responsible for development of computer software and the computation of design loads and performance. Dr. Norman D. Ham, Director of the V/STOL Technology Laboratory at MIT, contributed to the program as technical consultant and co-investigator. Dr. Ham was primarily responsible for the development of the aerodynamic and performance analyses which were based on his unpublished work in those areas. Development of the rotor system was conducted under subcontract to Pinson Energy Corporation under the direction of Mr. Herman M. Drees, President of PEC. The electrical system was developed under subcontract to Natural Power, Inc. Mr. Richard L. Katzenberg, President of NPI, served as the NPI Program Manager and Mr. Leander B. Nichols served as their Project Engineer.

The design effort was facilitated by a number of consultants to ASI. Professor Ernst G. Frankel of the Department of Ocean Engineering at MIT consulted on the reliability aspects of the program. Dr. James L. Kirtley, Jr. of the Electric Power Systems Engineering Laboratory in the MIT Department of Electrical Engineering was responsible for investigation of alternator modelling and test. Mr. Walter S. Harrington of Helio Precision Products, Inc., Bedford, Massachusetts and Mr. Paul A. Thibodeau consulted on the rotor and electrical system, respectively, in the area of manufacturing technology. Finally, Dr. F. A. Fisher and Mr. Edward C. Schrom of the General Electric High Voltage Laboratory, Pittsfield, Massachusetts reviewed the lightning protection aspects of the design.

## ABSTRACT

Aerospace Systems, Inc. (ASI) joined with Pinson Energy Corporation (PEC) and Natural Power, Inc. (NPI) to develop a high-reliability version of a unique vertical-axis machine called the Cycloturbine<sup>®</sup>. The final design is a 15-ft diameter turbine with three straight 8-ft blades controlled by a tilt-cam mechanism. The tilt-cam mechanism controls blade cyclic pitch amplitudes in a manner similar to a helicopter swash plate. The turbine has a power coefficient of 0.4 at an optimum tip speed ratio of  $\sim 3.0$  which results in a rotational speed of 112 RPM in a 9 m/sec wind.

The electrical system provides 1-kW of 24 V DC power in a 9 m/sec wind by means of a flux-switching alternator. The electronic circuitry, designed with high-reliability components, consists of a voltage regulator and a power rectifier. A dump-load circuit is provided as an option. Two transient protection networks are included, one on the tower for the alternator and the other to protect circuitry in the control building.

The unique configuration of the Cycloturbine necessitated the development of aerodynamic, performance, and structural analyses to evaluate the design. The resultant analyses were implemented on a computer. The alternator proved to be a non-linear device and, therefore, a semi-empirical approach was used in its analysis.

The theoretical analyses were complemented with various tests. A commercial Cycloturbine was instrumented and tested to verify the aerodynamic, performance and structural analyses. The alternator was tested to provide data to characterize its performance. A number of towers were tested to determine their dynamic characteristics before a 42.5-ft Octahedron tower was recommended for use with the 1-kW SWECS.

Manufacturing costs were evaluated and the design scrutinized to improve cost. The estimated total cost for the 1,000<sup>th</sup> production unit (in 1977 dollars) was \$1,994.

Completion of the design of the 1-kW High-Reliability Cycloturbine SWECS constitutes Phase I of the joint effort. Fabrication of three prototype units for testing will be done during Phase II.

---

<sup>®</sup>Cycloturbine is a registered trademark of the Pinson Energy Corporation.

## TABLE OF CONTENTS

<u>Section</u>	<u>Page</u>
	iii
	iv
1	1 - 1
2	2 - 1
2.1	2 - 1
2.2	2 - 1
2.2.1	2 - 1
2.2.2	2 - 4
2.2.3	2 - 6
2.2.4	2 - 11
2.3	2 - 13
3	3 - 1
3.1	3 - 1
3.1.1	3 - 1
3.1.2	3 - 8
3.2	3 - 31
3.2.1	3 - 31
3.2.2	3 - 41
4	4 - 1
4.1	4 - 2
4.2	4 - 18
4.3	4 - 21

TABLE OF CONTENTS (Continued)

<u>Section</u>		<u>Page</u>
	4.3.1 Dynamic Stall . . . . .	4 - 22
	4.3.2 Additional Drag Effect . . . . .	4 - 26
	4.3.3 Effect of Wind Shift . . . . .	4 - 29
4.4	Gusts . . . . .	4 - 32
4.5	Structural Loads . . . . .	4 - 32
	4.5.1 Stress Analysis . . . . .	4 - 34
	4.5.2 Maximum Operational Stresses . . . . .	4 - 60
	4.5.3 Maximum Stresses Due to Gusts . . . . .	4 - 63
	4.5.4 Failure Analysis . . . . .	4 - 77
	4.5.5 Ice Buildup Stresses . . . . .	4 - 77
4.6	Dynamics Analysis . . . . .	4 - 89
	4.6.1 Aeroelastic Analysis . . . . .	4 - 89
	4.6.2 Dynamic Response of Cycloturbine/ Tower System . . . . .	4 - 94
4.7	Total System Performance . . . . .	4 - 99
5	DEVELOPMENTAL TESTING . . . . .	5 - 1
5.1	Cycloturbine . . . . .	5 - 1
	5.1.1 Measurement of Performance and Stress Levels . . . . .	5 - 1
	5.1.2 Strut Outboard Tang Structural Test . . . . .	5 - 24
	5.1.3 Tilt-Cam Control System Operational Tests . . . . .	5 - 25
5.2	Electrical System . . . . .	5 - 27
	5.2.1 Electrical Circuit Temperature Tests . . . . .	5 - 27
	5.2.2 Transient Suppression Network Tests . . . . .	5 - 30

## TABLE OF CONTENTS (Continued)

<u>Section</u>		<u>Page</u>
	5.2.3 Alternator Characteristics Tests .....	5 - 32
6	RELIABILITY .....	6 - 1
	6.1 Failure Mode Effects Analysis (FMEA) .....	6 - 2
	6.2 Critical Components .....	6 - 10
	6.3 Component Failure Rates and Reliability .....	6 - 20
	6.3.1 Cycloturbine Failure Rate Estimates .....	6 - 20
	6.3.2 Electrical System Failure Rates .....	6 - 28
	6.4 System Reliability .....	6 - 32
	6.4.1 Cycloturbine Reliability .....	6 - 33
	6.4.2 Electrical Reliability .....	6 - 38
	6.4.3 Total System Reliability .....	6 - 38
	6.5 Maintenance .....	6 - 41
	6.6 Critical Component Tests .....	6 - 42
	6.6.1 Bearings .....	6 - 42
	6.6.2 Castings .....	6 - 42
	6.6.3 Tilt-Cam Vane/Wing Assembly Tests .....	6 - 43
	6.6.4 Transient-Suppression Circuit Tests .....	6 - 44
	6.7 Summary of Conclusions .....	6 - 44
7	MANUFACTURING COSTS .....	7 - 1
	7.1 Cycloturbine .....	7 - 1
	7.1.1 Cost Improvement Curve Considerations .....	7 - 1
	7.1.2 Growth Estimates .....	7 - 9
	7.1.3 Labor Cost .....	7 - 11

TABLE OF CONTENTS (Continued)

<u>Section</u>		<u>Page</u>
	7.1.4 Materials and Parts Costs .....	7 - 13
	7.1.5 Total Cost .....	7 - 13
7.2	Electrical System .....	7 - 23
	7.2.1 Manufacturing Cost Considerations .....	7 - 23
	7.2.2 Growth Estimates .....	7 - 24
	7.2.3 Labor Cost .....	7 - 26
	7.2.4 Materials and Parts Cost .....	7 - 26
	7.2.5 Total Cost .....	7 - 28
8	TOWER .....	8 - 1
	8.1 Foundation Specification .....	8 - 1
	8.2 Tower Specification .....	8 - 3
	8.2.1 Cycloturbine/Tower System Analysis .....	8 - 3
	8.2.2 Preliminary Tower Characteristics .....	8 - 5
	8.2.3 Tower Test Program .....	8 - 9
9	PRODUCT LIABILITY AND SAFETY .....	9 - 1
	9.1 Product Liability .....	9 - 2
	9.2 Safety Requirements .....	9 - 3
10	PHASE II TEST PLAN .....	10 - 1
	10.1 Weld Tests .....	10 - 1
	10.2 Test Stand Tests .....	10 - 2
	10.2.1 Cycloturbine .....	10 - 2
	10.2.2 Electrical System .....	10 - 7

TABLE OF CONTENTS (Concluded)

<u>Section</u>		<u>Page</u>
10	10.3 Prototype Tests .....	10 - 8
	10.3.1 Cycloturbine .....	10 - 8
	10.3.2 Electrical System .....	10 - 9
	REFERENCES .....	R - 1
<u>Appendices</u>		
A	NOMENCLATURE .....	A - 1
B	TOWER VIBRATION TEST DATA FOR: 34-FT OCTAHEDRON (500 LB CYCLOTURBINE), AND 40-FT ROHN (570 LB DEADWEIGHT) .....	B - 1

## LIST OF ILLUSTRATIONS

<u>Figure</u>		<u>Page</u>
1-1	Pinson Energy Corporation Cycloturbine, Model C2E . . . . .	1 - 3
1-2	1-kW High-Reliability WECS Program Organization . . . . .	1 - 5
2-1	Mean and Maximum Gust Factors for 5-Minute Mean Speeds . . .	2 - 5
2-2	Soderberg Diagram . . . . .	2 - 8
2-3	Wind Speed Distribution Comparison . . . . .	2 - 14
2-4	Wind Speed Distribution: 10 MPH Average . . . . .	2 - 15
3-1	High Reliability Cycloturbine Layout . . . . .	3 - 2
3-2	Cycloturbine Components . . . . .	3 - 3
3-3	General Dimensions . . . . .	3 - 6
3-4	Blade Construction Options . . . . .	3 - 12
3-5	Blade Construction . . . . .	3 - 13
3-6	Blade Planform Detail . . . . .	3 - 14
3-7	Strut Construction Methods Considered . . . . .	3 - 15
3-8	Hub - Strut Connection Options . . . . .	3 - 17
3-9	Strut Root Casting . . . . .	3 - 18
3-10	Hub - Strut Connection . . . . .	3 - 19
3-11	Strut Root Casting . . . . .	3 - 20
3-12	Selected Hub - Strut Connection . . . . .	3 - 21
3-13	Blade/Strut Attachment Assembly . . . . .	3 - 23
3-14	Bearing Cartridge/Weldment . . . . .	3 - 24
3-15	Considered Transmission Options . . . . .	3 - 26
3-16	Morse Double-Reduction Gearbox . . . . .	3 - 27
3-17	Heli-Cal Stainless Steel Flexible Coupling . . . . .	3 - 28

LIST OF ILLUSTRATIONS (Continued)

<u>Figure</u>		<u>Page</u>
3-18	Operation of Tilt-Cam Cyclic Pitch Control . . . . .	3 - 30
3-19	Tilt-Cam Detail . . . . .	3 - 32
3-20	Vane and Wing Construction Details . . . . .	3 - 33
3-21	Electrical System Block Diagram . . . . .	3 - 35
3-22	Preliminary Electrical System Circuit Diagram . . . . .	3 - 36
3-23	Typical System Configuration . . . . .	3 - 38
3-24	Revised Electrical System Circuit Diagram . . . . .	3 - 40
3-25	Selected Electrical System Circuit Diagram . . . . .	3 - 42
3-26	NPI 1-kW High-Reliability Alternator . . . . .	3 - 43
3-27	Alternator Comparison . . . . .	3 - 45
3-28	NPI Alternator Characteristics . . . . .	3 - 49
3-29	Comparison of 1-kW Alternator Test Data and Curve Fit . . . . .	3 - 50
3-30	Computer Model Characteristics of 1-kW Alternator . . . . .	3 - 51
3-31	Main Control Box Layout . . . . .	3 - 54
4-1	Turbine and Blade Geometry . . . . .	4 - 3
4-2	Section Lift Coefficient for NACA-0015 Airfoil . . . . .	4 - 5
4-3	Section Drag Coefficient for NACA-0015 Airfoil . . . . .	4 - 7
4-4	Sinusoidal Blade Pitch Schedule . . . . .	4 - 10
4-5	Blade Aerodynamic Load: 15-Ft Cycloturbine . . . . .	4 - 11
4-6	Representation of the Operation of Cycloturbine C2E . . . . .	4 - 13
4-7	Effect of Dynamic Stall Velocity Parameter $\frac{\alpha_c}{U}$ . . . . .	4 - 24
4-8	Effect of Dynamic Stall on Blade Normal Aerodynamic Load . . . . .	4 - 25
4-9	Effect of Dynamic Stall on Turbine Power Coefficient . . . . .	4 - 27

## LIST OF ILLUSTRATIONS (Continued)

<u>Figure</u>		<u>Page</u>
4-10	Effect of Additional Drag on the Power Coefficient for 15-ft Cycloturbine . . . . .	4 - 30
4-11	Critical Load Points . . . . .	4 - 33
4-12	Blade Load Distribution and Bending Moments . . . . .	4 - 35
4-13	Stress at Blade Spar Center: Nominal Operating Condition . .	4 - 39
4-14	Stress at Blade/Strut Connection: Nominal Operating Condition . . . . .	4 - 41
4-15	Strut Radial Loading . . . . .	4 - 43
4-16	Strut Tangential Loading . . . . .	4 - 45
4-17	Strut Root Stress: Nominal Operating Condition . . . . .	4 - 47
4-18	Main Bearing and Shaft Loading . . . . .	4 - 49
4-19	Main Shaft Stress: Nominal Operating Condition . . . . .	4 - 51
4-20	Blade/Pitch Actuation System . . . . .	4 - 53
4-21	Moment About Blade Pivot: Nominal Operating Condition . . . . .	4 - 56
4-22	Force on the Pull Rod Root: Nominal Operating Condition . . . . .	4 - 59
4-23	Maximum Operational Stresses: Blade Center Spar, S <sub>1</sub> ; Blade/Strut Connection, S <sub>2</sub> ; Strut Root, S <sub>3</sub> ; and Main Shaft, S <sub>4</sub> . . . . .	4 - 61
4-24	Maximum Operational Stress: Pull Rod Root, S <sub>5</sub> . . . . .	4 - 62
4-25	Soderberg Diagram: Nominal Operating Condition . . . . .	4 - 64
4-26	Maximum Stresses on Stopped Rotor . . . . .	4 - 66
4-27	Effect of Sharp-Edged Gust . . . . .	4 - 70
4-28	Maximum Operational Stresses Due to Gusts . . . . .	4 - 72
4-29	Maximum Stresses on Stopped Rotor Due to Gusts . . . . .	4 - 74

## LIST OF ILLUSTRATIONS (Continued)

<u>Figure</u>		<u>Page</u>
4-30	Failure Analysis . . . . .	4 - 78
4-31	Failure Analysis with Gust . . . . .	4 - 81
4-32	Uniform Ice Buildup on Rotor System . . . . .	4 - 85
4-33	Effect of Clear Ice Accumulation . . . . .	4 - 86
4-34	Elastic Blade Geometry . . . . .	4 - 90
4-35	Cycloturbine/Tower Dynamic Response at Cycloturbine . . . . .	4 - 98
4-36	High-Reliability Cycloturbine Annual Energy Production . . . . .	4 - 101
4-37	High-Reliability Cycloturbine Power Output . . . . .	4 - 102
5-1	C2E Transmission and Weldment . . . . .	5 - 3
5-2	Instrumentation Block Diagram . . . . .	5 - 5
5-3	Experimental Calibration Curves . . . . .	5 - 8
5-4	Sample Performance Data Run . . . . .	5 - 11
5-5	Sample Data Reduction Sheet . . . . .	5 - 12
5-6	Sample Performance Data . . . . .	5 - 13
5-7	Effect of Wind Speed Reading Error . . . . .	5 - 14
5-8	Comparison of Experimental and Analytical Performance . . . . .	5 - 16
5-9	Blade and Strut Loading Waveform . . . . .	5 - 18
5-10	Comparison of Experimental and Analytical Blade Loads . . . . .	5 - 21
5-11	Strut Outboard Tang Failure Modes . . . . .	5 - 26
5-12	Voltage Control Relay Temperature Test Data . . . . .	5 - 28
5-13	Voltage Limiter Control Temperature Test Data . . . . .	5 - 29
5-14	Main Rectifier Heat Sink Temperature Test . . . . .	5 - 31
5-15	NPI Alternator Friction and Windage Loss . . . . .	5 - 33

## LIST OF ILLUSTRATIONS (Concluded)

<u>Figure</u>		<u>Page</u>
5-16	NPI Alternator Saturation Curve . . . . .	5 - 34
5-17	Temperature Rise in NPI Alternator . . . . .	5 - 37
6-1	1-kW High-Reliability SWECS Components . . . . .	6 - 3
6-2	1-kW High-Reliability SWECS Functional Flow Chart . . . . .	6 - 4
6-3	Cycloturbine Tilt-Cam Control System and Bearing Location . . . . .	6 - 7
6-4	System Diagrammatic Block Diagram of Cycloturbine . . . . .	6 - 34
7-1	Cycloturbine Cumulative Average Productivity Factor versus Unit Number Produced . . . . .	7 - 2
7-2	Assumed Cycloturbine Production Rate . . . . .	7 - 10
7-3	Assumed Cycloturbine Cumulative Production . . . . .	7 - 12
8-1	Nonconcrete-Guyed Footings . . . . .	8 - 2
8-2	Effect of Weight and Damping Ratio On Cycloturbine/Tower Dynamic Response . . . . .	8 - 4
8-3	Towers Under Consideration . . . . .	8 - 6
8-4	Octahedron Tower First Mode Natural Frequency versus Tower Height . . . . .	8 - 7
8-5	Preliminary Measurement of Natural Frequency versus Weight Aloft for 40-ft Rohn SSV Tower . . . . .	8 - 8
8-6	Excitation Frequency versus SWECS RPM . . . . .	8 - 10
8-7	Tower Test Data . . . . .	8 - 13

## LIST OF TABLES

<u>Table</u>		<u>Page</u>
1-1	1-kW High-Reliability Cycloturbine Design Features and Development History . . . . .	1 - 7
2-1	Key Design Specifications . . . . .	2 - 2
2-2	Extreme Environmental Conditions . . . . .	2 - 3
2-3	1-kW High-Reliability Cycloturbine Operating Ranges . . . . .	2 - 4
3-1	High-Reliability Cycloturbine Selected Design . . . . .	3 - 7
3-2	NPI Alternator Specifications . . . . .	3 - 44
4-1	Calculation of Strut Drag . . . . .	4 - 28
4-2	Effect of Wind Direction Shift on Turbine Power Coefficient . . . . .	4 - 31
4-3	Cycloturbine Yield Stresses . . . . .	4 - 60
4-4	Cycloturbine Margins of Safety . . . . .	4 - 77
4-5	Ice Accumulation on Blades . . . . .	4 - 84
4-6	Effect of Ice on Stresses at High Wind Speeds . . . . .	4 - 88
4-7	Bending Frequencies of Nonrotating Blade . . . . .	4 - 92
4-8	Blade Torsional Frequencies . . . . .	4 - 93
6-1	1-kW High-Reliability SWECS Failure Modes and Effects Analysis . . . . .	6 - 11
6-2	Critical Bearings List . . . . .	6 - 22
6-3	Bearing MTBF and Reliability . . . . .	6 - 27
6-4	Electrical System Reliability . . . . .	6 - 32
6-5	Bearing Pair Reliability . . . . .	6 - 36
7-1	Summary of Cycloturbine First Unit Manufacturing Labor Hours . . . . .	7 - 3
7-2	Cycloturbine First Unit Manufacturing Labor Hours . . . . .	7 - 4
7-3	Summary of Cycloturbine Materials and Parts Costs . . . . .	7 - 14

## LIST OF TABLES (Concluded)

<u>Table</u>		<u>Page</u>
7-4	Cycloturbine Materials and Parts Costs . . . . .	7 - 15
7-5	Summary of Cycloturbine Cost Elements . . . . .	7 - 21
7-6	1-kW High Reliability Cycloturbine Weight Estimation . . .	7 - 22
7-7	Electrical System Manufacturing Testing . . . . .	7 - 23
7-8	Electrical System Manufacturing Capital Improvements . . . .	7 - 25
7-9	Summary of Electrical System Materials and Manufacturing Labor Costs . . . . .	7 - 27
7-10	Summary of Electrical System Cost Elements . . . . .	7 - 28
7-11	Summary of Total System Cost Elements . . . . .	7 - 29

## SECTION 1

### INTRODUCTION

Rockwell International, under contract with the Department of Energy (DOE) to manage the Small Wind Systems Program, has initiated programs to develop prototype wind machines in the one-, eight-, and forty-kilowatt (kW) ranges. Rockwell manages the program for DOE at the Rocky Flats Plant near Golden, Colorado. In particular, the program for the 1-2 kW size wind machine has the following objectives:

- To develop a technology base for design, fabrication, and production of a high-reliability wind machine in the 1-2 kW size range for use in rural and remote applications.
- To provide fabrication cost data in sufficient detail to determine economic viability of wind machines in the 1-2 kW size range.
- To fabricate and deliver three high-reliability 1-2 kW prototype wind machine units for testing at the Rocky Flats Wind Systems Test Center.

The design and fabrication of a highly reliable, durable yet cost effective small wind energy conversion system (SWECS) is a challenging undertaking. The development of a machine that is expected to run and withstand extremely adverse conditions while unattended or, even in some applications, unseen for a year at a time is a difficult task by any engineering standards. The wind system must be designed to operate automatically and to be able to adjust its operation to the varying conditions. To be durable, the rotor must be designed to withstand highly irregular wind-induced loads as well as operationally-induced cyclic loads under extreme environmental conditions. The rotor design must incorporate a comprehensive fatigue analysis, and the aeroelastic behavior of the rotor must be well understood. Cost effectiveness calls for a design which is simple to manufacture, inexpensive and easy to transport and install.

Aerospace Systems, Inc. (ASI) investigated the possibility of implementing a vertical-axis configuration to achieve the stress and reliability requirements of a 1-2 kW high-reliability SWECS. A vertical-axis wind turbine configuration offers several advantages over the classical horizontal-axis configuration. The rotor accepts variations in wind direction instantly without completely reorienting the rotor thereby eliminating gyroscopically-induced stresses. The vertical shaft allows an alternator or generator to be placed below the rotor, out of the rotor influence area and driven by the working shaft, thereby eliminating flow interference with the rotor. In addition, flow interference with the tower which can cause undesirable cyclic loads is also eliminated. This configuration also eliminates the need for slip rings, which are susceptible to wear and failure, as would be required on horizontal-axis wind machines. A vertical-axis wind machine affords accessibility for maintenance of the drive train and electrical subsystems.

As a result of the investigation of SWECS designs, ASI joined with Pinson Energy Corporation (PEC) and Natural Power, Inc. (NPI) in offering a unique vertical-axis wind machine for development as a high-reliability SWECS. The wind turbine developed by PEC, is called the Cycloturbine (References 1 and 2) and is pictured in Figure 1-1. The turbine has three untwisted, straight blades which are held to a central shaft by streamlined support struts. The blades follow a preset schedule of angle changes during each revolution of the rotor. This cyclic blade pitch motion is activated by a cam mechanism which is oriented relative to the wind by a wind-direction tracking vane (similar to a weather vane) mounted above the machine. By introducing sufficient blade angle into the cyclic pitch schedule, the Cycloturbine, unlike the vertical-axis Darrieus turbine, becomes self-starting. In high winds, it is possible to pivot the blades to a position of least wind resistance.

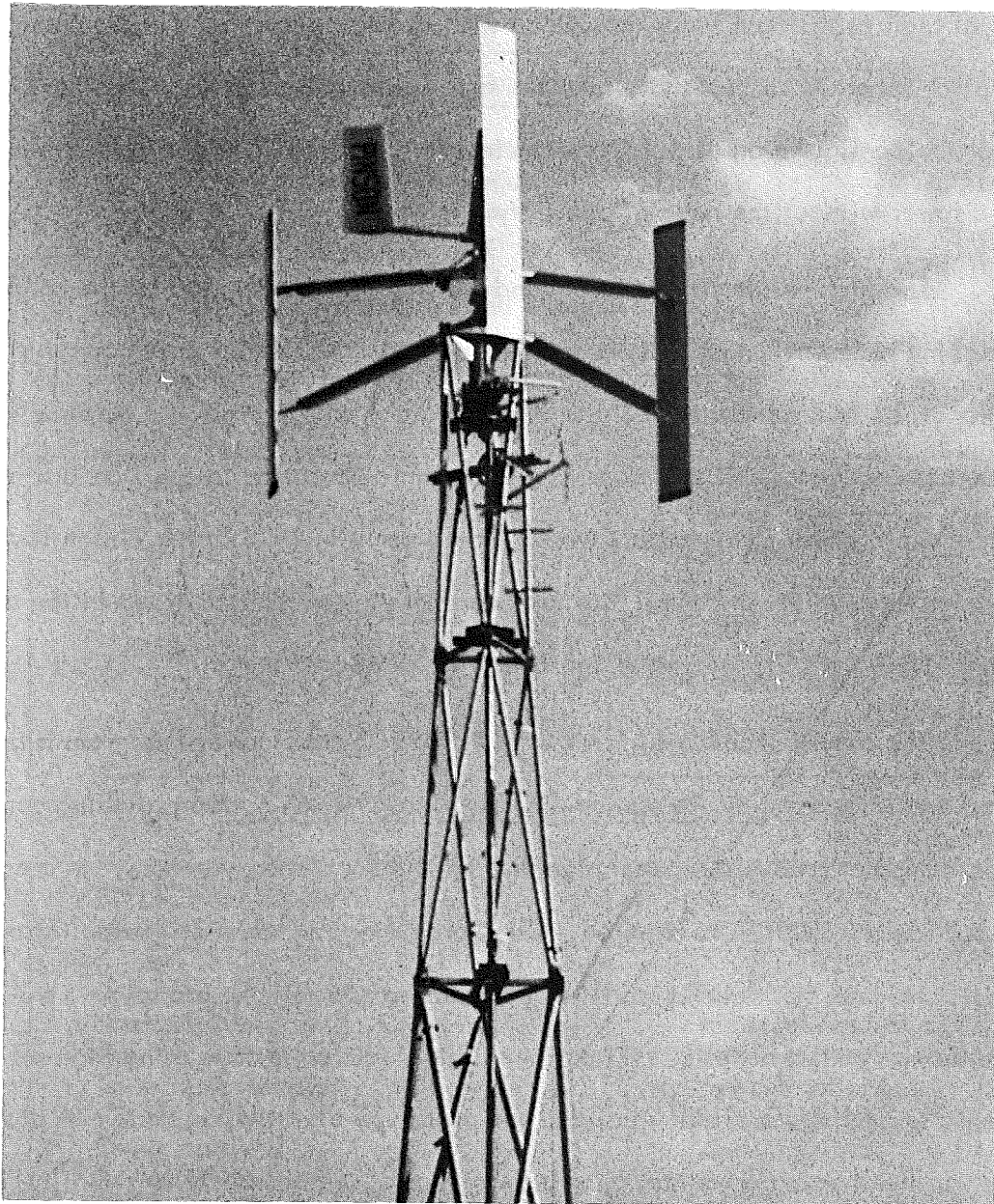


Figure 1-1. Pinson Energy Corporation Cycloturbine, Model C2E.  
(Machine developed prior to high reliability prototype design)

making the rotor aerodynamically self-limiting. This is achieved through a mechanism which, at high centrifugal loads associated with increased rotational rate, changes the cyclic pitch schedule so that the blades are aerodynamically stalled. Another convenience of the configuration of the Cycloturbines is that it can be cantilever-mounted on top of a tower without the need of auxiliary guy wires.

The high reliability 1-2 kW wind machine design is based on the original Cycloturbine rotor/transmission system developed by PEC. Originally conceived and built at the Massachusetts Institute of Technology with a National Science Foundation grant (Reference 1), it is similar in aerodynamic operation to the Darrieus turbine. Testing of a prototype Cycloturbine was initiated early in 1976 at the Pinson test facility at New Seabury, Massachusetts. The test program yielded data utilized in the design of an improved second prototype which is now available commercially.

The overall 1-2 kW high-reliability SWECS development program is being managed and integrated by Aerospace Systems, Inc., which is also providing aerodynamic computer analysis and test planning for the wind energy system. In areas where particular expertise is required, ASI is providing for technical consultation. PEC will fabricate the high-reliability Cycloturbine and test the prototype SWECS prior to delivery to Rockwell. NPI designed the electrical system using high reliability electronic technology and will fabricate the prototype electrical systems. A block diagram of the program organization showing areas of responsibility is given in Figure 1-2.

The Cycloturbine wind energy system is one of three designs presently being developed for Rockwell International to meet the objectives of their low-cost, high reliability program. The joint effort by ASI, PEC and NPI is being conducted in two

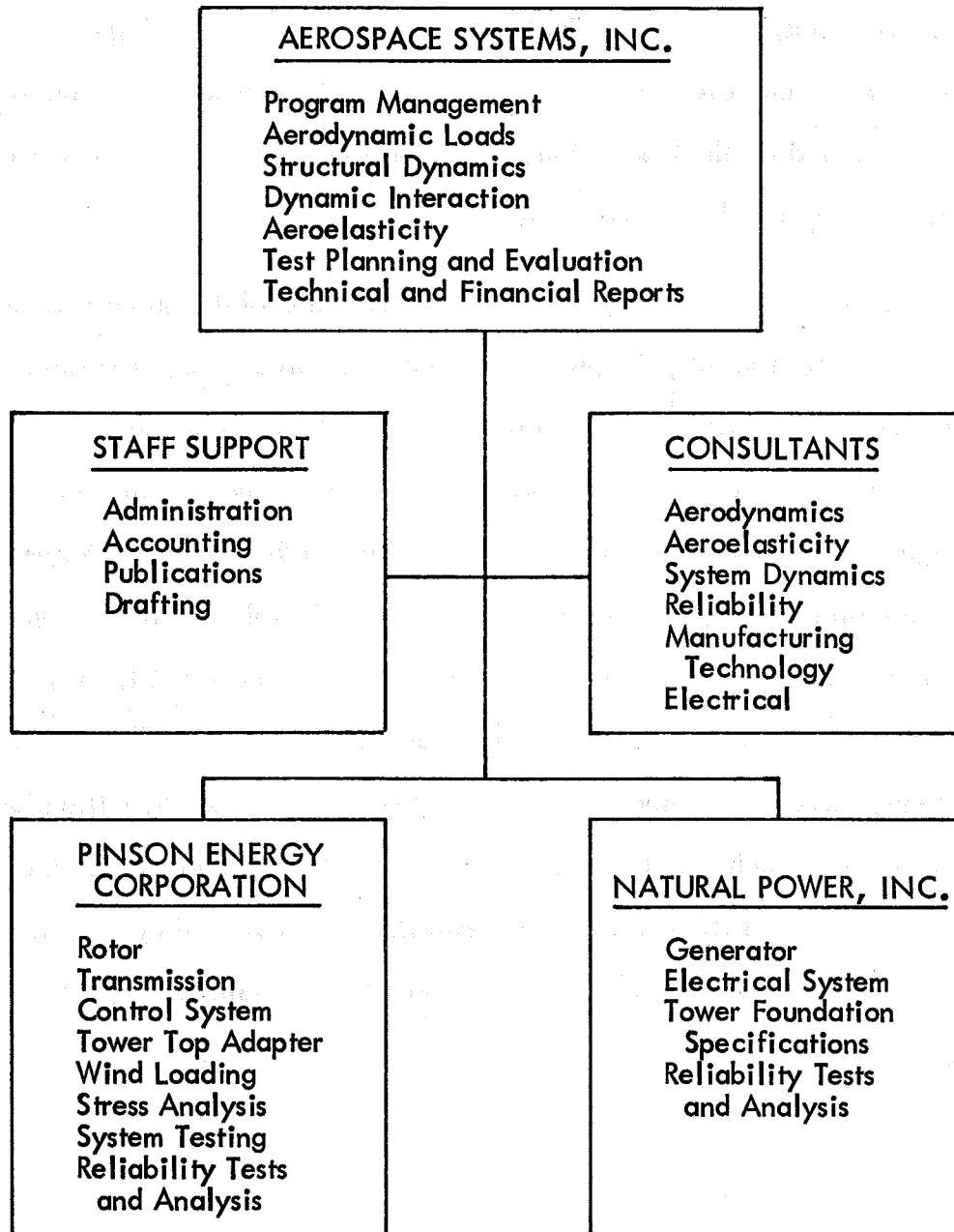


Figure 1-2. 1-kW High-Reliability SWECS Program Organization.

phases: Phase I providing for the design and development of a 1-2 kW system; and Phase II providing for the construction of three prototype units for testing by Rockwell at its wind systems test center. The final Phase I design of the 1-kW high-reliability Cycloturbine and its electrical system has been approved by Rockwell International and authorization granted for the fabrication of three prototype machines. The design features and development history are outlined in Table 1-1.

This volume begins in Section 2 with a discussion of design considerations including design requirements, design criteria and trade-off studies. The selected configuration and construction details of both the Cycloturbine and the electrical system are presented in Section 3. Section 4 reviews the analyses developed and used in the design. Analyses include those for aerodynamic loads, structural stresses, dynamics, and total system performance. Tests performed on the machine components and on similar configurations are discussed in Section 5. The reliability of the Cycloturbine and the electrical system is discussed and analyzed in Section 6 and the manufacturing costs are presented for each subsystem in Section 7. Specifications for a tower on which the high-reliability Cycloturbine will be mounted are presented in Section 8. Product liability and safety considerations are reviewed in Section 9. The proposed Phase II test plan is given in Section 10. This volume concludes with supporting references and appendices.

Table 1-1. 1-kW High-Reliability Cycloturbine Design Features and Development History.

Description	Proposed	PDR	CDR	FDR
<b>GENERAL CONFIGURATION</b>				
Output Power (kW) @ Rated Wind $\bar{V}$	1-2 @ 20	1 @ 20	1 @ 20	1 @ 20
Axis Orientation	Vertical	Vertical	Vertical	Vertical
Rotor Location (Upwind/Downwind)	NA*	NA	NA	NA
Rotor/Cone Diameter (ft); (Width and Height - Vertical Axis)	12 x 8	12 x 8	15 x 8	15 x 8
Number of Blades	3-4	3	3	3
Centerline Hub Height (ft)	40	40	40	40
Method of Power Regulation	Variable Pitch	Variable Pitch	Variable Pitch	Variable Pitch
Type of Output Voltage and $\phi$	24 VAC/3 $\phi$	24 VAC/3 $\phi$	24 VAC/3 $\phi$	24 VAC/3 $\phi$
Total System Weight (lbs)	464	464	508	508
System Cost - 1st/1000th Units	15000/2250	5454/1769	5500-8500/ 2000-4000	5300/1994
<b>PERFORMANCE PARAMETERS</b>				
$C_p$ @ Rated Wind Velocity	0.41	0.45	0.4	0.4
Cut-in Wind Velocity (mph)	5	5	5	5
Cut-out Wind Velocity (mph)	NS	40	40	40
Survival Wind Velocity (mph)	165	165	190	190
<b>ANNUAL OUTPUT (kWh)</b>				
(For average wind velocity measured @ 30 ft., based upon NASA Wind Distribution)				
@ 12 mph	NS**	NS	2682	2682
@ 15 mph	NS	NS	4562	4562
@ 18 mph	NS	NS	6089	6089
<b>ROTOR (Including Blades/Hub)</b>				
Rotor Swept Area (ft <sup>2</sup> )	96	96	120	120
Coning Angle (Deg.)	NA	NA	NA	NA
Rotor/Hub Weight (lbs.)	174	174	290 (approx.)	290 (approx.)
<b>Blades:</b>				
Airfoil	NACA 0015	NACA 0015	NACA 0015	NACA 0015
Material	Aluminum	Aluminum	Aluminum	Aluminum
Length (ft)	8	8	8	8
Weight (lbs.)	13	13	21	18
<b>Type of Hub:</b>				
Material	Steel	Steel	Steel	Steel
Weight (lbs.)	75***	75***	24/each	24/each
<b>CONTROL SYSTEM</b>				
Pitch Control Method	Variable Pitch with Vane Cam	Tilt-Cam	Tilt-Cam	Tilt-Cam
Shutdown Provisions	NS	Tilt-Cam	Tilt-Cam	Tilt-Cam
<b>TRANSMISSION/SPEED CHANGER</b>				
Type	Timing Belt	Gearbox	Gearbox	Gearbox
Ratio	$\approx$ 9:1	$\approx$ 9:1	15:1	15:1
Weight (lbs.)	NS	NS	60	60
<b>BEARINGS (Main)</b>				
Type and Number	NS	Sealmaster-SFC (2)	Sealmaster-SFC (2)	Sealmaster-SFC (2)
Material	NS	NS	Steel	Steel
Weight (lbs.)	NS	NS	8/each	8/each

\*Not applicable.  
 \*\*Not supplied.  
 \*\*\*2 hubs plus shaft.

Table 1-1. 1-kW High-Reliability Cycloturbine Design Features and Development History (Concluded).

Description	Proposed	PDR	CDR	FDR
<b>GENERATOR</b>				
Type	NPI Flux-Switch Alternator	NPI Flux-Switch Alternator	NPI Flux-Switch Alternator	NPI Flux-Switch Alternator
Output Power (kW) @ Rated RPM	1-2 @ NS	1 @ 1650	1 @ 1650	@ 1650
Maximum Output Power (kW)	1-2	1	1.3	1.3
Weight (lbs.)	35	35	35	35
<b>TOWER</b>				
Type of Construction/Features	Octahedron	Octahedron	Octahedron	Octahedron
Materials	Steel	Steel	Steel	Steel
Height (ft)	34	34	34	42.5
Weight (lbs.)	NS	NS	NS	NS
Access	NS	NS	NS	NS
<b>AUXILIARY ELECTRICAL EQUIPMENT REQUIRED</b>				
Power Output to User	NS	NS	NS	NS
Form of Voltage	NS	NS	NS	NS
<b>COSTS (1st/1000th Units)</b>				
Rotor: (Blades, Struts, Shaft)	NS/NS	NS/746	862*/562.26*	1210/400
Blades	NS/NS	NS/210	181.57*/103.21*	300/218
Hub (Shaft)	NS/NS	NS/95	154.34*/133.43*	290/103
Control System	NS/NS	NS/93	169.64*/91.38*	295/36
Transmission/Speed Changer	NS/NS	NS/450	372.72*/340.87*	370/234
Bearings	NS/NS	NS/260	151.42*/132.8*	245/110
Generator	NS/NS	NS/406	5410/1292	3000/640
Tower	NS/NS	NS/NS	NS/NS	NS/NS
Auxiliary Electrical Equipment	NA/NA	NA/NA	NA/NA	NA/NA
<b>VALUE INDICATORS (1st/1000th Units)</b>				
\$/kW	15000/2250	5454/1769	5500-8500/2000-4000	5300/1994
\$/Rotor Area, ft <sup>2</sup>	159.28/23.44	56.81/18.32	45.83-70.83/16.67-33.33	44.17/16.62
\$/System Weight (lbs.)	32.33/4.85	11.75/3.81	10.83-16.73/3.94-7.87	10.43/3.93
\$/System Weight (lbs.)/kW:				
Total	NS	-	-	-
Tower	NS	-	-	-
Above Tower	464	464	508	508
Rotor	174	174	290	290
Blades Only	39	39	63	63
System Weight (lbs.)/ft <sup>2</sup> : (ft <sup>2</sup> /lbs.):				
Total	NS : NS	NS : NS	NS : NS	NS/NS
No Tower	4.83 : 0.207	4.83 : 0.207	4.23 : 0.236	4.23 : 0.236
\$/kWh:				
12 mph site	NS/NS	NS/NS	NS/NS	NS/NS
15 mph site	NS/NS	NS/NS	NS/NS	NS/NS
18 mph site	NS/NS	NS/NS	NS/NS	NS/NS
kWh/System Weight (lbs.):				
12 mph site	NS	NS	NS	NS
15 mph site	NS	NS	NS	NS
18 mph site	NS	NS	NS	NS
kWh/SWECS Weight (lbs.), (No Tower):				
12 mph site	NS	NS	3.34	3.34
15 mph site	NS	NS	5.54	5.54
18 mph site	NS	NS	7.44	7.44
kWh/Rotor Swept Area (ft <sup>2</sup> ):				
12 mph site	NS	NS	14.15	14.15
15 mph site	NS	NS	23.44	23.44
18 mph site	NS	NS	31.48	31.48

\*Manufacturing costs only (material and labor).

## SECTION 2

### DESIGN CONSIDERATIONS

The design of the 1-kW high reliability WECS is an iterative process involving numerous trade-offs in order to meet the design specifications and environmental conditions. This section outlines the design requirements, sets forth criteria used in various stages of the design, and reviews key trade-offs.

#### 2.1 DESIGN REQUIREMENTS

The design requirements established for the 1-kW high reliability WECS consisted of design specifications and extreme environmental conditions which had to be withstood. The key design specifications are outlined in Table 2-1 and the extreme environmental conditions are established in Table 2-2. Design specifications which were particularly important were reliability, durability and capital cost goal whereas temperature range and lightning protection were the most important environmental conditions driving the design.

#### 2.2 DESIGN CRITERIA

In order to meet the design requirements, a number of criteria were established. These criteria pertained to operating ranges, gust velocities, critical load points, and fatigue analysis.

##### 2.2.1 OPERATING RANGES

The 1-kW Cycloturbine designed for the high reliability WECS has a 15-ft diameter. Throughout the specified wind range of up to 165 mph (a combination of 120 mph steady wind speed with a 45 mph gust), the machine has several operational conditions ranging from static (i.e., stopped) to stalled. These operating ranges are specified in Table 2-3.

Table 2-1. Key Design Specifications.

<u>Reliability:</u>	MTBF 10 Years Minimum.
<u>Maintainability:</u>	One Maintenance Day/Year
<u>Durability:</u>	Continuous Operation in Extreme Weather.
<u>Power Output:</u>	1-2 kW at 9 m/s (20 mph) Wind Speed.
<u>Power Form:</u>	26 ± 2 Volts DC with Voltage Regulation to Control Charging of 24 Volt Battery System.
<u>Survival Wind Speed:</u>	Steady Winds 54 m/s (120 mph), Gusts 75 m/s (165 mph).
<u>Rotor Speed and Yaw Control:</u>	Optional Design.
<u>System Life Goal:</u>	25 Years.
<u>Capital Cost Goal:</u>	\$1,500/kW at 9 m/s (20 mph) Wind

Table 2-2. Extreme Environmental Conditions.

<u>Temperature:</u>	-70°C to +60°C (-94°F to 140°F).
<u>Rain:</u>	Torrential Downpour with Winds.
<u>Snow, Sleet, Icing:</u>	Ice Buildup to 60 mm (2-1/2 in) Thick on Rotor System.
<u>Hail:</u>	Impact by Hail up to 40 mm (1-1/2 in) Diameter.
<u>Wind:</u>	Steady Wind 54 m/s (120 mph), Gusts 75 m/s (165 mph).
<u>Salt Water Spray:</u>	Heavy Ocean Spray.
<u>Dust:</u>	Fine Sand and Dust with Wind Gusts to 45 m/s (100 mph).
<u>Corrosive Atmosphere:</u>	Heavy Industrial Atmosphere Coupled with Salt Fog or Spray.
<u>Lightning:</u>	Repeated Strikes During Severe Thunderstorms.

NOTE: Values Represent Probable  
Extremes from Worldwide  
Applications.

Table 2-3. 1-kW High-Reliability Cycloturbine Operating Ranges.

Operating Range	V (MPH)	$\Omega$ (RPM)	Collective Pitch (Degrees)	Cyclic Pitch (Degrees)
Nominal	20	112	0	-10
No Load	0 - 5	0 - 28	0	-10
Normal	5 - 28	28 - 160	0	-10
RPM Limited	28 - 40	160	0	-10
Stalled	40	160	-45 (collective) 0 (tilt-cam)	10 10
Static (Stopped)	40 - 120	0	-45 (collective) 0 (tilt-cam)	10 10
	165 (120 mph and 45 mph gust)	0	-45 (collective) 0 (tilt-cam)	10 10

### 2.2.2 GUST VELOCITY

The value of the gust velocity to be considered was not specified except for maximum wind condition of 165 mph which was achieved by the combination of a 120 mph wind with a 45 mph gust. Gust velocity criteria were established based on available statistical measurements of gust velocities and average wind speed. Data used for developing the criteria are shown in Figure 2-1. Comparison of the Boulder data with averages from other sites indicates that Boulder has more severe conditions than the other locations in terms of gust factor. The gust velocity is determined by

$$V_G = \bar{V} (F_G - 1) \quad (2-1)$$

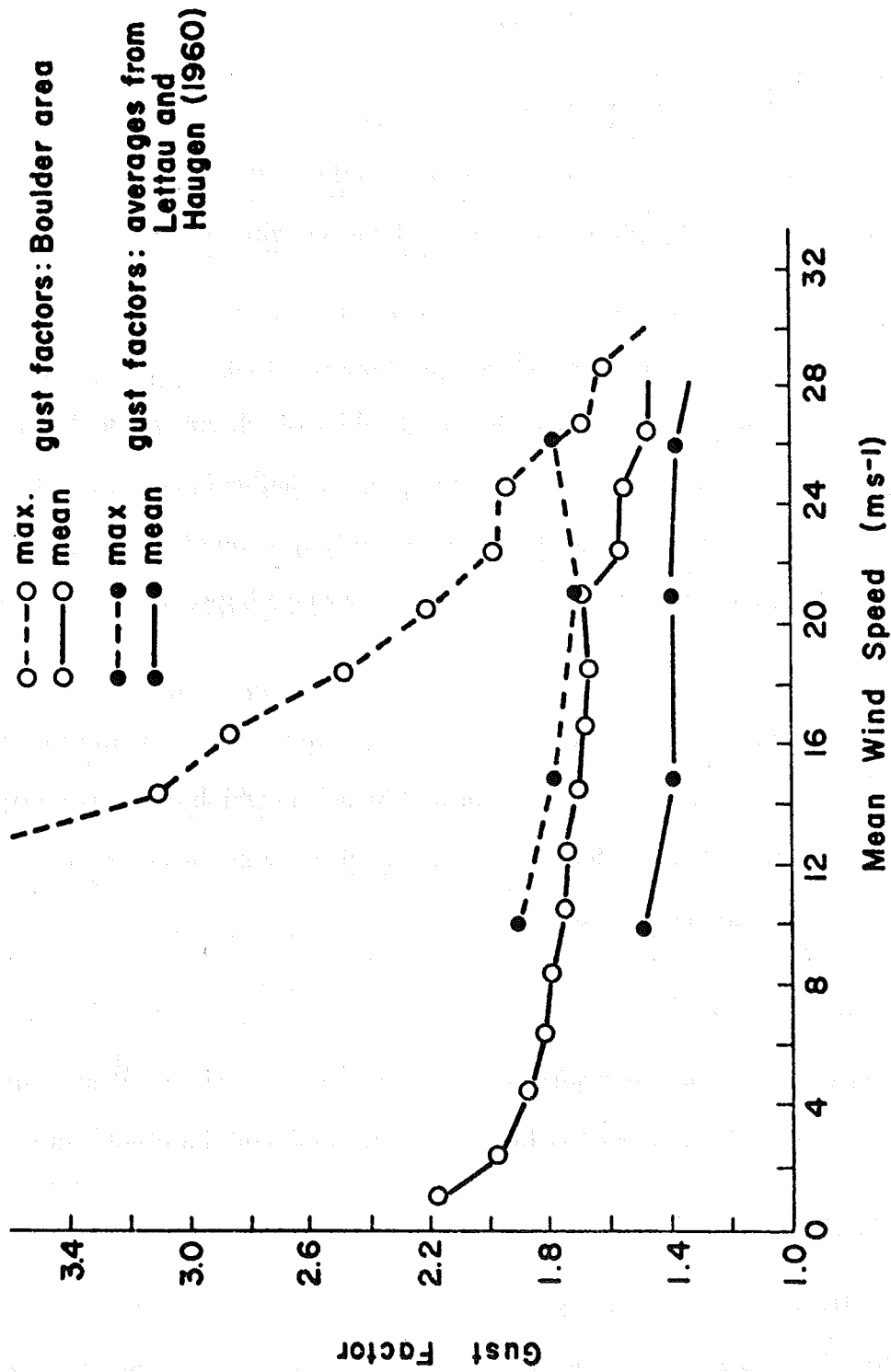


Figure 2-1. Mean and Maximum Gust Factors for 5-Minute Mean Speeds (Reference 3).

where

$V_G$  = gust velocity

$\bar{V}$  = mean wind speed

$F_G$  = gust factor

Examining the Boulder data reveals that for maximum gust factors, gust velocities between about 34 mph to 70 mph are possible in the mean wind speed range of 31 mph to 67 mph.

Unfortunately, data below 34 mph were not available. However, it is seen in Figure 2-1 that the mean gust factors for Boulder which are available in the desired speed range of 2 to 18 m/sec (~5 to 40 mph) are similar in magnitude to maximum values at other locations within the normal operating range of the Cycloturbine. Gust velocities based on mean gust factors for Boulder range between about 5 mph to 31 mph.

Based on these data, a gust velocity of 40 mph was used for all gust effect calculations except for analysis at speeds above 120 mph in which a gust velocity of 45 mph was used. The 40 mph value exceeds the maximum value measured at numerous locations and exceeds the mean Boulder values.

### 2.2.3 CRITICAL LOADS

Certain of the design requirements (Subsection 2.1) can result in critical loads. These are described separately for the Cycloturbine and the electrical system.

#### 2.2.3.1 CYCLOTURBINE

Critical loads are normally determined based on the selected operating conditions. These loads are then used to size the structure and to select appropriate

components. This process was not used in the design of the 1-kW High-Reliability Cycloturbine. The turbine design was basically an extrapolation of commercially available versions produced by PEC. A design analysis was developed for the vertical-axis configuration (see Section 4) and implemented on the ASI computer. The selected design was checked over the various operating ranges specified in Table 2-3.

The system life goal of 25 years required that the Cycloturbine be designed with adequate margins of safety. These margins were already inherent in commercially-available Cycloturbines. Nonetheless, it was necessary to check critical areas for the stresses imposed by aerodynamic, centrifugal and inertial loads. Critical structural loads were determined at points where bending moments and/or combined axial loads reach a maximum. These points (see Figure 4-11) include the center of the blade spar, the blade/spar connection, the strut root, the main shaft at the main bearings, and the pull rods in the control actuation system.

The life of the Cycloturbine is also affected by the oscillatory stresses imposed upon it, which can result in fatigue of the structure. In order to evaluate the severity of the fatigue condition, the Soderberg diagram is used (see Reference 4). In this diagram, experimental fatigue data are used to establish an operational boundary. The Soderberg diagram is recommended for use in design because it is on the safe side of the test results and is, therefore, considered to be conservative.

The Soderberg diagram is shown in Figure 2-2 where the oscillatory stresses are plotted as a function of the mean stress. In the diagram, points A, B, C and D are defined as follows:

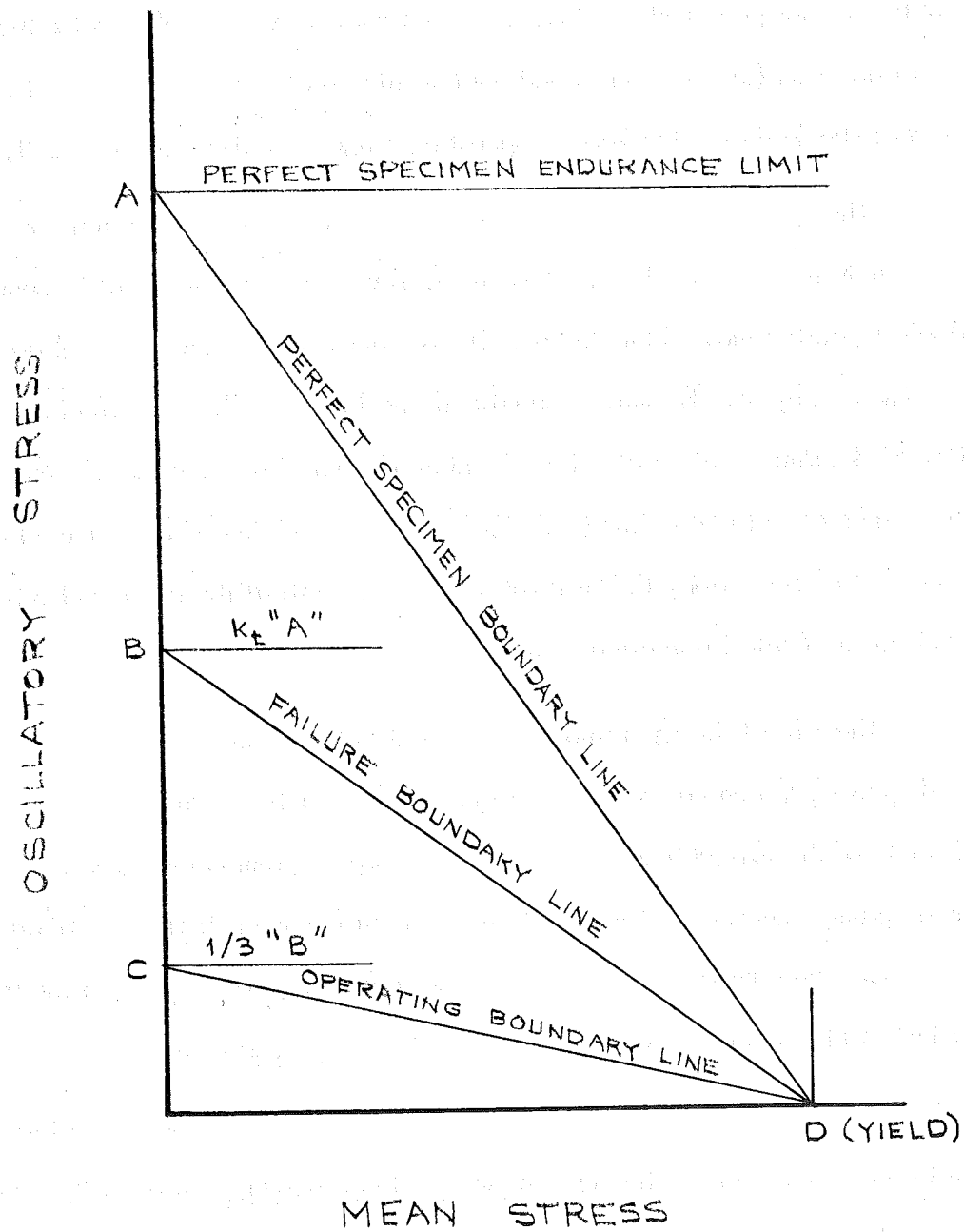


Figure 2-2. Soderberg Diagram.

- A - Unnotched (or perfect) specimen fatigue strength derived from endurance tests.
- B - Notched specimen fatigue strength derived from endurance tests; if data are not available, often taken as 1/2 the magnitude of point A.
- C - Margin of safety of 2 from point B, that is, 1/3 the magnitude of point B; defines the operating boundary line.
- D - Yield stress of material.

If the calculated stresses lie below the operating boundary line, this is considered adequate substantiation for unlimited fatigue life.

The requirement to operate in the specified extreme environmental conditions, while resulting in numerous design modifications and trade-offs, did not impose critical loads on the machine. Similarly, the reliability requirements resulted in the selection of bearings with higher load-bearing capacity but did not cause more critical loads in itself.

#### 2.2.3.2 ELECTRICAL SYSTEM

The thermal loading of electrical system components as influenced by load voltage, load current and lightning strikes is most critical for the electrical system. The thermal impedance to heat produced in the system is the major limiting factor with respect to component capacity and reliability. Therefore, the electrical system was designed to ensure that the thermal limits of components are not exceeded during any conceivable mode of operation.

The area of primary concern was the power rectifier. It was necessary to reject heat from the power rectifiers to the atmosphere so as to keep the hot spot temperature of the silicon pellet below 200°C. Above that temperature, structural damage is done to the rectifier junction. Given the upper ambient temperature specification of 60°C and using reasonably-sized heat sinks, the temperature at the case of

the diode cannot exceed 85°C or the junction will overheat. This required that the maximum stress level for a silicon device be limited to 60 percent. Silicon was chosen over germanium for its superior high temperature characteristics.

It was also desirable to limit the voltage stress ratio of the rectifier to 70 percent or less in order to obtain maximum reliability. The low voltage of the electrical system presented no problem in this area, but it should be noted that the price of diodes is not particularly sensitive to their voltage rating and that voltage ratings of 600 volts are easily obtainable. Even using the 200-volt devices employed for the 24-volt system, there would be no degradation to system performance if the load voltage were increased to 120 volts. A higher load voltage would have the advantage of reducing the current stress level and reducing  $I^2R$  losses in the generator and transmission line for the same power level.

The stresses imposed on the system from lightning strikes are many orders of magnitude above normal operating stresses; however, these lightning-induced stresses are infrequent, and short lived. The electrical system circuitry was designed to prevent lightning-induced energy from entering the alternator and main control panel. Only a few components designed to tolerate infrequent, extreme overloads are allowed to interact with lightning-induced energy. Lightning currents have the potential to damage bearing surfaces and insulation, melt solder joints, cause semiconductor punch-through, vaporize tower joints and footings, to name a few effects, so special paths have been designed to conduct the bulk of its energy. Fortunately, metals are excellent conductors of electricity and even a piece of 22 AWG copper wire normally used for telephone circuits can withstand a momentary peak current of 80,000 amperes for the duration of an average lightning strike without vaporizing. Thus, most of the mechanical components can withstand momentary high electrical current (a load they are not usually designed to withstand) with little or no degradation.

#### 2.2.4 WIND SPEED PROFILE

The magnitude and duration of the mean wind speed is an important factor (Reference 5) in the design of a SWECS. The actual power that can be achieved from a wind turbine of rated power is dependent upon the distribution of the various wind speeds and on the cut-in and cut-out wind speeds. A number of wind speed distributions are currently in use. Initially, the Wentink distribution (Reference 6) based on work by Dinkelacker was used. The probability density function is given by

$$f(x) = kx^3 e^{-ax} - 1 \quad (2-2)$$

where

$$x = V/\bar{V}$$

$$V = \text{wind speed}$$

$$\bar{V} = \text{average wind speed}$$

$$a = 3.5$$

$$k = 23.2$$

Although the Wentink distribution has been used within the wind energy industry, it is not widely used elsewhere. Therefore, after the preliminary design phase was completed, the widely used Weibull distribution was used. Comparison of wind data in terms of a Weibull statistical distribution with experimental results shows good agreement (see Reference 7). The Weibull probability density function is given by

$$f(x) = \frac{K}{c} x^{K-1} e^{-x^K} \quad (2-3)$$

where

$$x = \frac{V}{c}$$

$V$  = wind speed

and the constants  $c$  and  $K$  are functions of geographical location. Values of  $c$  and  $K$  are tabulated and available for 138 geographical locations throughout the United States (see Tables 2-1 and 2-2 in Reference 5). Seasonal variation of the mean wind speed frequency is included.

A third distribution, the Rayleigh distribution, which has been used for wind energy work, was applied for the analyses in this report. The Rayleigh probability density function is given by

$$f(x) = \frac{\pi}{2} \frac{V}{\bar{V}^2} \exp \left[ -\frac{\pi}{4} \left( \frac{V}{\bar{V}} \right)^2 \right] \quad (2-4)$$

where

$V$  = wind speed

$\bar{V}$  = average wind speed

The three distributions which have been used are compared in Figure 2-3 to experimental data for Boston, Massachusetts. The wind frequency in terms of hours/year/mph is shown as a function of wind speed for an average wind speed of 13.3 mph. It is seen that the Rayleigh distribution tends to emphasize the lower and higher wind speeds relative to the Boston data.

One of the applications of the high reliability SWECS will be for microwave repeater stations located in remote areas. Therefore, it was decided that a relatively low average wind speed be used which would be typical of a wind site location in the poorest wind season. The wind speed criteria selected is that the average wind speed,

$\bar{V} = 10$  mph. A comparison of the wind speed distribution in terms of time in hours/month/mph as a function of wind speed is given in Figure 2-4 for the three profiles used.

The NASA/Lewis wind speed distribution curve was specified in order to standardize wind energy calculations. The wind speed duration profile, which will be used in Phase II, is given by

$$H_z = 8766 \exp \left[ \frac{-\pi}{4.06} \left( \frac{V}{\bar{V}_z} \right)^{2.27} \right] \quad (2-5)$$

where

$H_z$  = time in hours that wind speed is equal to or exceeds the value,  $V$ .

$V$  = wind speed

$\bar{V}_z$  = mean wind speed at elevation  $z$

$z$  = elevation above ground level

### 2.3 TRADE-OFF STUDIES

Trade-off studies are normally conducted on a new SWECS design to determine the effect of different parameters on the machine performance, efficiency, cost, etc. The proposed 1-2 kW system was based on the Cycloturbine commercially manufactured by PEC. Since the existing proven design in the initial studies produced sufficient output, it was decided not to modify the structure in any significant manner. Therefore, studies of various blade lengths, turbine diameter, number of blades, etc., were not made. However, as a result of detailed analysis (Section 4) and performance tests (Section 5), it was decided that if the drive train (gearbox, coupling, and alternator) were less efficient than assumed, the existing Cycloturbine design with a 12-ft diameter might be marginal. As a result, the design diameter was changed to 15 feet. For a

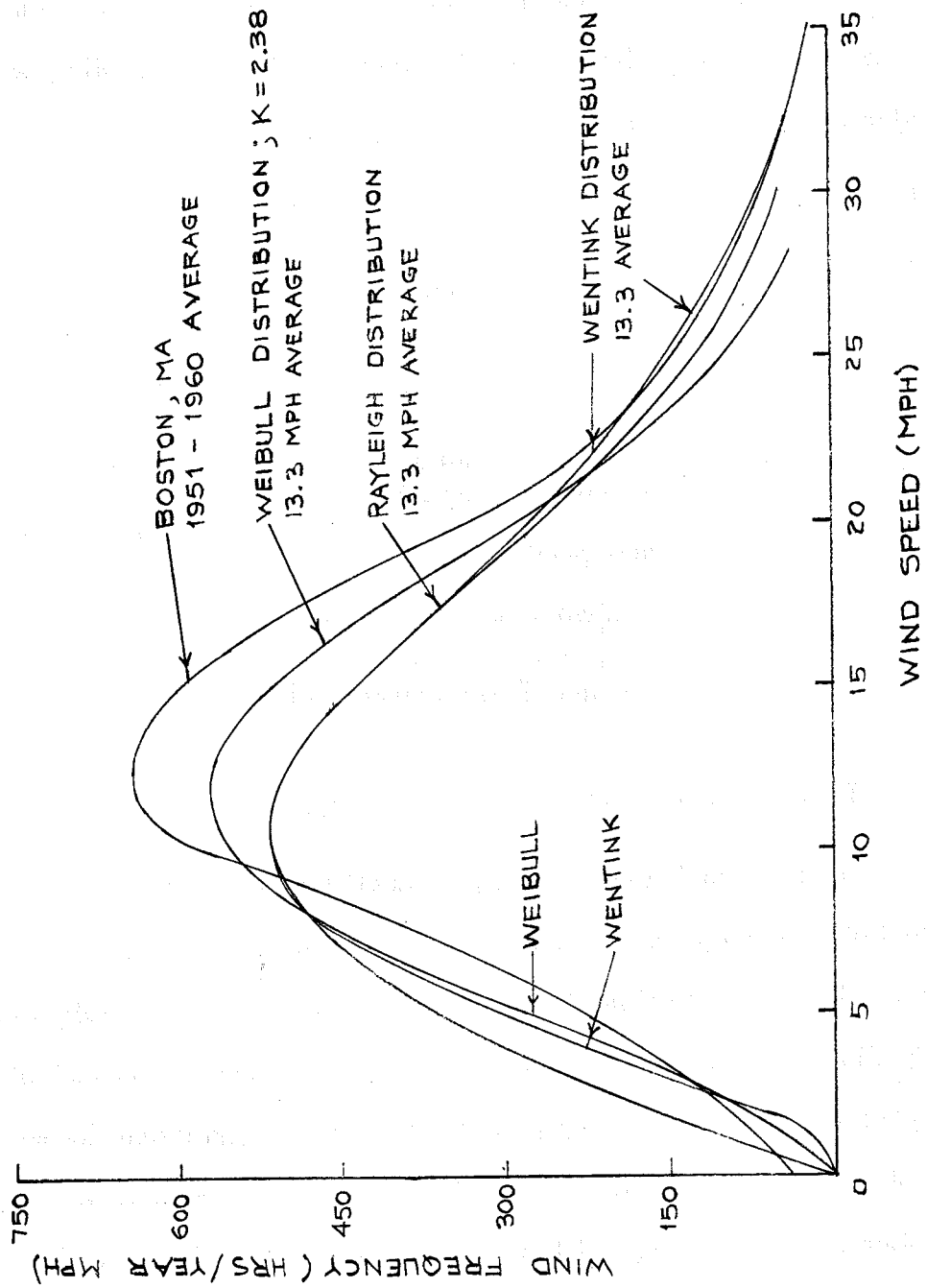


Figure 2-3. Wind Speed Distribution Comparison.

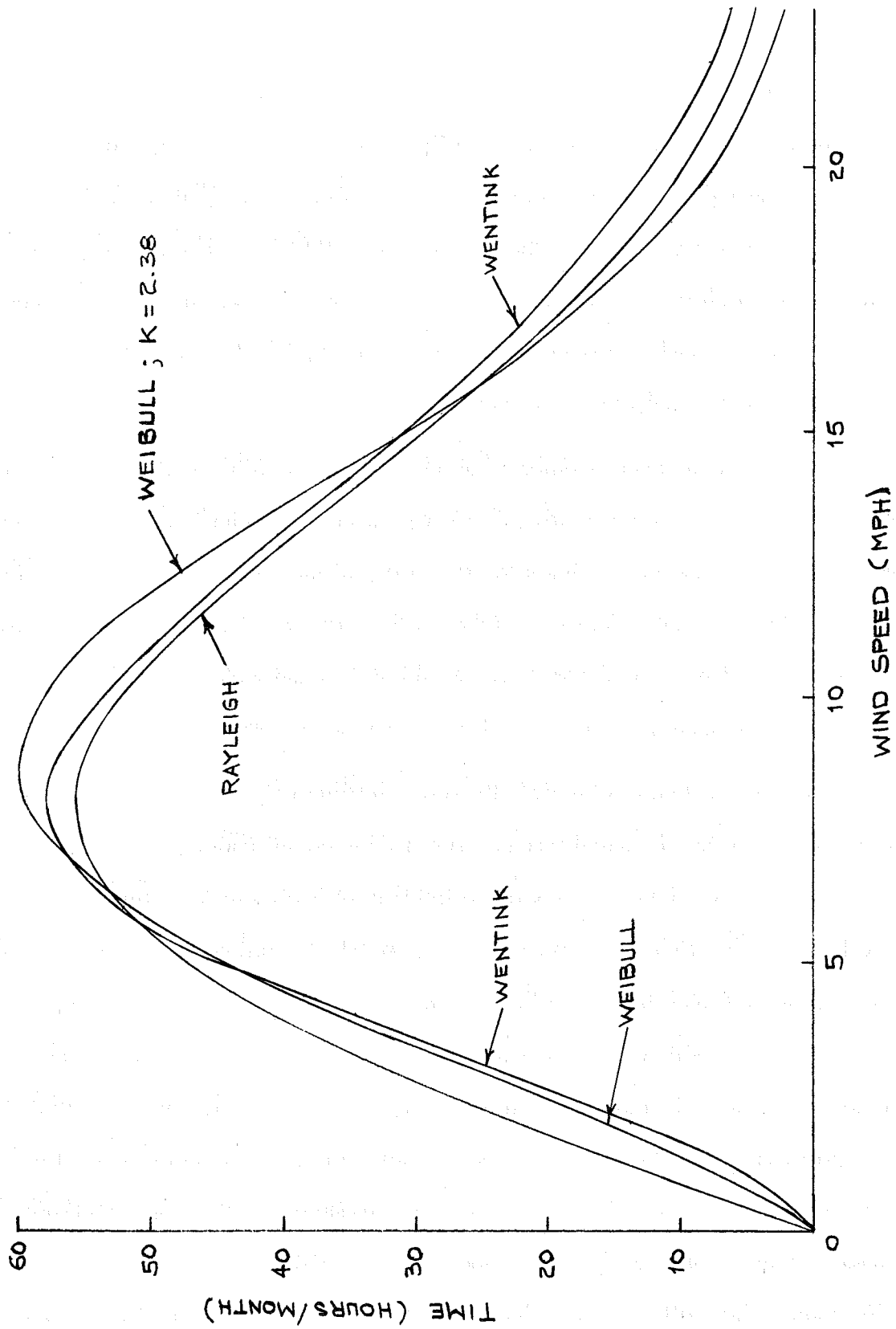


Figure 2-4. Wind Speed Distribution: 10 MPH Average.

vertical-axis machine, increasing the diameter (within the range of the proposed design) has the effect of decreasing the turbine solidity but increasing the tip speed ratio at which the maximum power coefficient occurs. Since as seen in Equation (4-23), the power coefficient is proportional to the tip speed ratio ( $\Omega R/V$ ) cubed but only proportional to the solidity, increasing the diameter is an effective manner of producing more power from the machine. As discussed in Section 4, the structural stress on the new size machine was analyzed.

Trade-off studies concentrated on the determination of the best size machine to build in terms of cost and reliability. A comparison of costs for both a 1-kW and a 2-kW machine was made to determine the feasibility of these power levels. Preliminary studies indicated that both machines could meet the cost goals for the thousandth unit but that the reliability of the 2-kW design would be less and probably would not meet the contract requirements.

In these preliminary studies, the reduced reliability for the 2-kW machine occurred largely in the electrical system. Primary factors influencing the electrical system reliability were the efficiency and reliability of available alternators and the availability of high reliability power rectifiers. A 1-kW alternator available through NPI was considered to be the best alternator in its class based on both efficiency (see Figure 3-26) and reliability. The alternator is a modification of a Maremont truck alternator proven to be reliable through long usage in a hostile environment. The SWECS application should be a milder environment. The NPI alternator uses a flux switching design thereby eliminating the need for commutators, slip rings and brushes. This simpler design is inherently more reliable than other available alternators in the 1-2 kW range. Thus, alternators in the 2-kW range with an output of 24V DC were not available with the efficiency and reliability required for the high-reliability SWECS

program. It was decided that the development of an alternator to produce 2-kW 24V DC would introduce undesirable uncertainties relative to reliability, performance, and schedule into the high-reliability program. Therefore, the NPI 1-kW alternator was selected as the best available component.

No particular problem was encountered for the 1-kW design with the available power diodes which were available in JAN TX quality (high reliability) for forward currents,  $I_f$ , through the diodes of up to 35 amps; however, the power rectifier proved to be the principal reliability driver for the electrical system. Each rectifier element must handle 80 percent of the full output current of 48 amps caused by the commutation characteristics of the chosen switched reluctance alternator.

After an extensive search, it was determined that silicon rectifiers in the range of 65 to 130 amperes forward current are not commercially available in high reliability versions. Two diodes were identified that came close to the system requirements. One of these is JAN1N3911 TX which is a silicon rectifier rated at 35 amps average forward current and a peak reverse voltage of 200 volts. The other is JAN1N3289 which is a silicon rectifier rated at an average forward current of 100 amperes and a peak reverse voltage of 200V. The 1N3911 did not have enough current capacity to convert the required power; therefore, if this device were selected, several diodes would have to be used in parallel with ballasting resistors or inductors to ensure equal current distribution. Although the 1N3289 is large enough to handle the required current with a single device, its quality factor is only 1/5th of the 1N3911. Thus, even though the 1N3289 is operating at stress levels of 1/3 the 1N3911, its reliability is less.

The reliability of the power diodes is illustrated at a stress level of 60 percent. The 1N3289 would be conducting 60 amperes and the 1N3911 21 amperes for the 1-kW design. If the reliability is calculated at 50°C with all other factors equal, the 1N3289 has a failure rate of 1.68 per million hours of operation while the 1N3911 exhibits 0.336 failures per million hours. Even if the stress on the 1N3289 were reduced to 21 percent so that it carried 21 amps, the same as the 1N3911, the 1N3289 would still exhibit 0.551 failures per million hours (see Reference 8). Thus, the better reliability of the 1N3911 must be traded off against the added complexity of paralleling several of these devices to reduce the stress level to an acceptable level to meet the upper temperature specification (Table 2-2).

In summary, the following factors for a 2-kW design influenced the decision to recommend a 1-kW machine:

Alternator:

- Limited availability of alternators producing 24V DC.
- Available machines inefficient.
- Available machines use slip rings and brushes which, for the specified application, are unreliable.
- Development of a 2-kW alternator to meet the contract goals was considered to introduce undesirable uncertainties relative to reliability, performance, and schedule.

Power Diodes:

- Available in JAN TX quality up to  $I_f = 35$  amps (about 70 amps required for 2-kW machine).
- Reliability data on power rectifiers above 50 amps scarce.
- Rectifiers for  $I_f < 35$  amps have a quality factor 5 times that of those for  $I_f > 35$  amps.
- Rectifier bridge for a 1-kW machine has a failure rate about 2.5 failures/ $10^6$  hours less than that for a 2-kW machine.

During the final design, cost analysis indicated that the projected cost/kW of the 1000<sup>th</sup> unit was excessive. Therefore, it was decided to reevaluate the possibility of a 2-kW machine in order to reduce the cost per kilowatt. Preliminary cost estimates for a 2-kW design indicated that this was a viable alternative. Two factors now made a 2-kW machine feasible, namely: 1) the final predicted reliability of the rotor allowed a relaxation of the electrical system reliability (in the alternator and power rectifier) without compromising the reliability goal of the machine; and 2) a 24V DC high reliability, 2-kW alternator was being developed by Maremont.

A detailed investigation of the 2-kW option revealed a number of uncertainties relative to the Maremont alternator. These included:

- 1) Availability - Development was delayed and first three models were to be delivered to another customer.
- 2) Cost - The cost of the thousandth unit had not been firmly established. In addition, each prototype unit will cost \$5,000.
- 3) Reliability - Failure rate of the alternator plus electronics for the rectifier and voltage regulator was estimated to be about six failures per million hours; however, this estimate could not be verified since neither circuitry nor component selection was available.
- 4) Electronics - The alternator was to be delivered with electronics mounted on it for the rectifier and voltage regulator circuits. However, the ASI team had a definite preference for locating electronics near the battery pack both for environmental protection and for having the regulator at the batteries rather than at the alternator.
- 5) Construction and Testing - Closely associated with availability was the fact that even though the alternators could be made available to ASI, it was quite likely that the delivery schedule could severely delay the high-reliability SWECS construction, checkout, testing, and delivery to Rocky Flats.

As a result of the uncertainties relative to the Maremont alternator, the ASI team considered modifying the 1-kW NPI alternator to produce 2-kW. Although it was felt that the modifications were technically feasible within reasonable costs and schedule delays, it was noted that the preliminary design required an alternator running speed of

4500 RPM. This speed introduced potential reliability and noise problems in the alternator as well as required that a complex transmission setup be used in order to achieve desired gear ratios. Finally, the reliability of the 2-kW electrical system, driven primarily by the power diodes, was estimated to have about 10.5 failures/ $10^6$  hours which was excessive.

In order to eliminate or circumvent the difficulties associated with an NPI 2-kW alternator, a compromise solution was sought. This involved relaxing the requirement on 2-kW of output. It was determined that a 1.8-kW NPI alternator with 1.7-kW of power delivered to the batteries was a viable alternative. Following is a list of improved features of the 1.7-kW version of the NPI alternator:

#### 1.7-kW NPI Alternator Features

- Meets cost/kilowatt goals.
- Meets reliability goals (electrical system failure rate estimated to be 6.5 failures/ $10^6$  hours).
- Reasonable running speed (about 3000 RPM).
- Standard gearbox transmission (25:1 ratio).
- Basic NPI alternator can be used as basis of design.

As a result of the consideration of the various alternatives, it was concluded that a 1.7-kW machine offers the best compromise for meeting the program goals of performance, reliability and cost. However, the use of a 1.7-kW alternator necessitated a resizing of the turbine and reevaluation of its performance, stress, and reliability. The electrical system would also have to be resized and component stresses and reliability determined. Since the 1-kW design was basically acceptable, it was decided by the Buyer not to incur the additional costs and schedule delays associated with a 1.7-kW machine redesign. Instead, the 1-kW was approved and additional effort made to improve the manufacturing costs of this machine (see Section 7).

A limited investigation was also made of a 2-bladed turbine. This was done since the results of the initial cost analysis indicated that the struts are a major cost item (see Section 7), and there are two per blade. However, a two-bladed Cycloturbine has stable positions relative to the wind in which a balance of forces is achieved preventing self-starting. Therefore, in order to ensure unassisted wind-driven startup, the Cycloturbine must have at least three blades. In terms of vibrational characteristics, three blades provide smoother operation than two. This effort was, therefore, curtailed, since the two-bladed Cycloturbine also necessitated a major redesign.

During the initial design phase, much attention was paid to optimizing the annual energy production of the wind turbine. An analytical model was developed which involved calculating the electrical power output of the wind turbine given an electrical load, wind speed, turbine area and  $C_p$  versus  $\Omega R/V$  (see Subsection 4.7 and Volume III). After the loads were calculated, turbine speed was modified until all loads matched to within a specified error limit. The analysis generated the energy production for an average wind speed regime. It was also used to pick an optimum gear train for hypothetical wind regimes. It could also provide information on power versus wind speed for various turbine sizes and generator loading schemes.

The effect of wind speed distribution on reliability was also analyzed. The turbine causes the power rectifier to convert power at varying stress levels for a fraction of the total time which is dependent on the wind regime. Therefore, the resultant reliability is dependent on the wind regime. A Rayleigh probability distribution was used for the calculations. As an example, for the 1N3289 power diode considered previously, the following results were obtained at a temperature of 85°C:

Average Wind Speed (MPH)	Failure Rate (Failures/10 <sup>6</sup> Hours)
5	3.5
10	5.0
15	12.0

The system voltage is a critical specification in the design. The low voltage specification requires relatively high currents to deliver the required power. Since losses in the generator output windings and in the electrical transmission line are proportional to the square of the current, doubling the system voltage while keeping all else constant would reduce the systems losses by almost 1/4. (There are some losses that are linear with current and would not be proportionately reduced.) A doubling of the system voltage would result in a significant improvement in the system reliability. This is because high quality rectifiers are not available in the required ranges for the present 24 volt design. The present rectifier could convert power at voltages up to 140V at no additional cost. A higher system voltage would also reduce the current in each element of the power rectifier.

## SECTION 3 CONFIGURATION AND CONSTRUCTION

The 1-kW high-reliability SWECS designed by the ASI team consists of two major subsystems, namely: 1) the rotor/transmission; and 2) the electrical system. The rotor is based on the Cycloturbine concept conceived and developed by Pinson Energy Corporation. The electrical system was designed by Natural Power, Inc. based on their 1-kW flux switching alternator. Each subsystem is discussed separately in this section.

### 3.1 CYCLOTURBINE

#### 3.1.1 CONFIGURATION

The general layout of the high reliability Cycloturbine is shown in Figure 3-1 with the associated nomenclature given in Figure 3-2.

##### 3.1.1.1 GENERAL CONSIDERATIONS

The design of the Cycloturbine was driven primarily by the Durability requirements of the "Key Design Specifications" (see Subsection 2.1). The Durability criterion calls for turbine survival in very extreme environmental conditions (Table 2-2). Equally as important as a design driver is the requirement that the turbine must operate totally automatically in a stand-alone condition for charging batteries at a remote location.

As noted in Section 2.3, three blades are required to ensure unassisted wind-driven start-up.

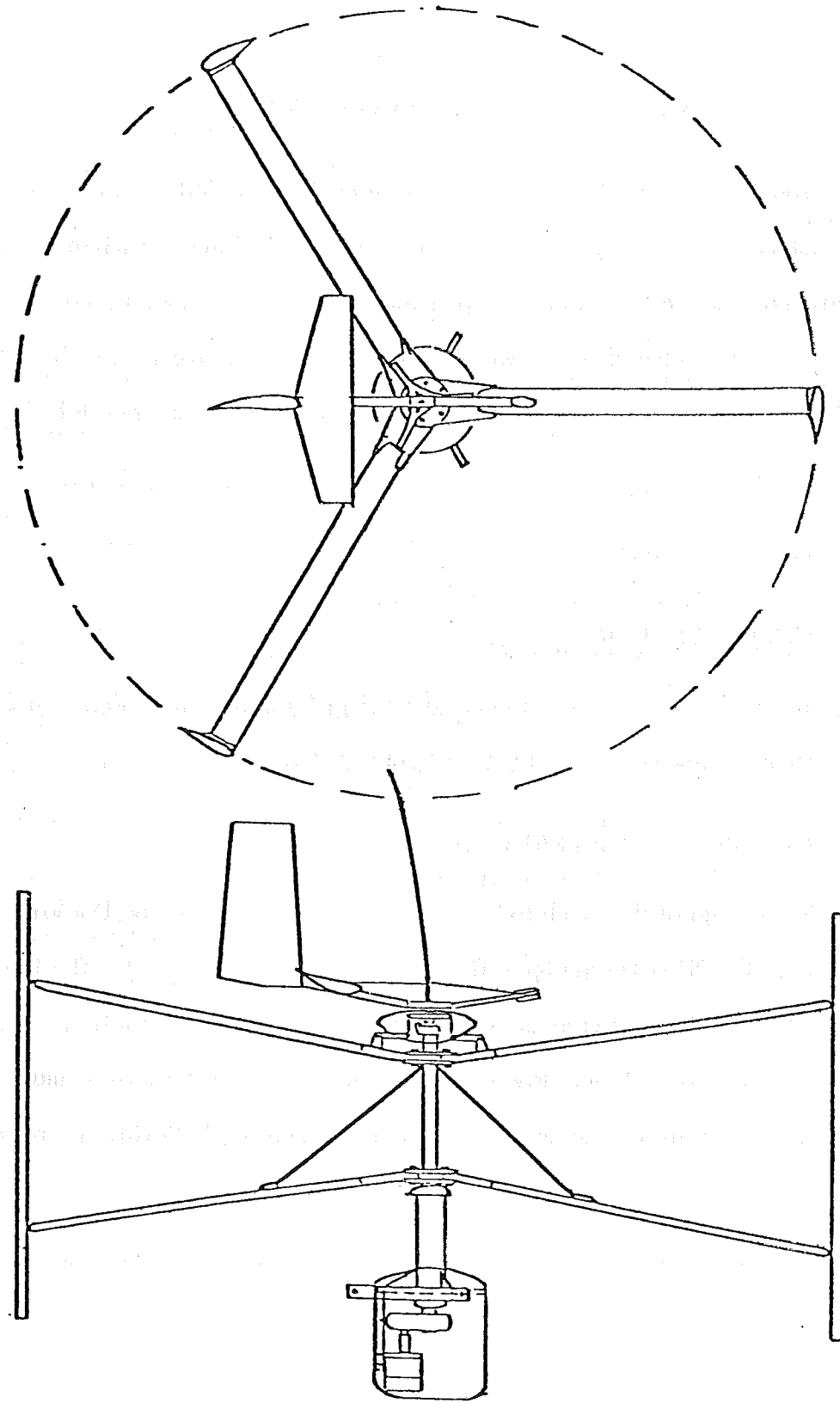


Figure 3-1. High-Reliability Cycloturbine Layout.

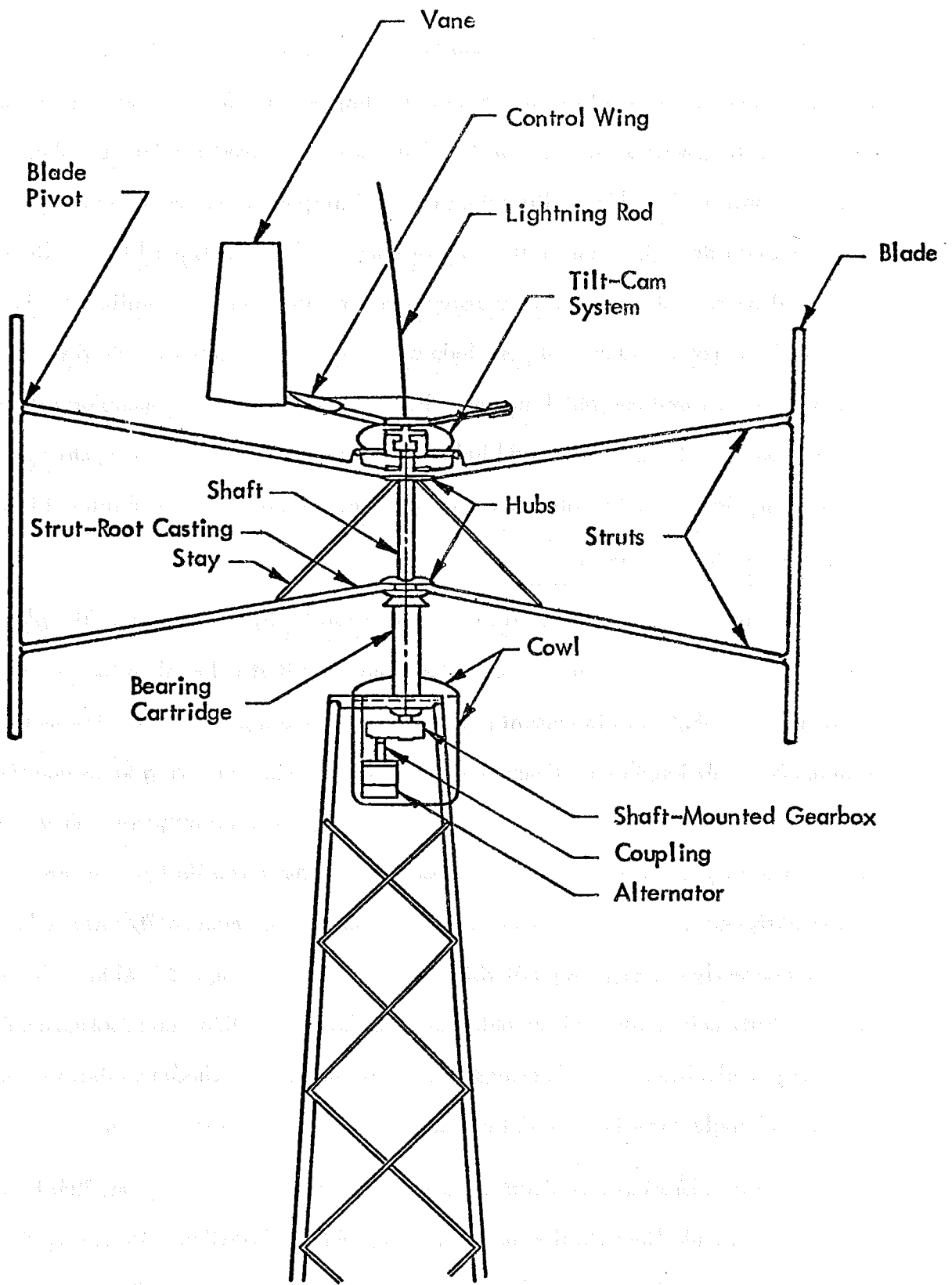


Figure 3-2. Cycloturbine Components.

Each blade is connected to the main shaft with two struts. The blade/strut attachment points are located in from the ends so that bending moments in the blade are minimized. Location of the pivots at the ends of the blade spar was considered because they are easier to construct but this configuration resulted in spar stresses approximately six times those obtained through optimum support placement. Three struts per blade, although a more rigid configuration, causes excessive aerodynamic drag and significantly increases the cost of the rotor. One strut per blade was also considered but required tapered mass and lift distributions which negated the simplicity and ease of manufacture of straight, untwisted, and untapered blades. Additionally, a single blade/strut pivot is more complicated structurally than two since the blades must be maintained in a vertical (spanwise) attitude.

The struts are connected to the main shaft by two hub plates. The plates are located on the shaft with a distance between them that is less than the distance between the blade/strut attachment point. The hub spacing was selected primarily to minimize shaft length and diameter which minimized main bearing loads and size (and, thereby, cost) and maintained a shaft first mode bending frequency above the aerodynamically induced excitation frequency. The turbine is designed to run significantly below critical shaft speeds. Experience with main shaft/tower vibrational coupling on early prototype Cycloturbines resulted in this design criterion. The angle that the struts make with the horizontal must not be greater than the misalignment capability of the blade pivot bearings. The hub spacing was chosen so that the struts make a  $10^{\circ}$  angle with the horizontal plane.

Consideration was given to connecting a strut pair to only one hub in order to reduce cost and eliminate the shaft bending problem altogether. However, the ice

loading specification (see Table 2-2) requires that the rotor withstand high vertical loading necessitating the need for support stays which must be connected above a hub. A single hub without stays would have to be heavy and bulky to carry the high vertical loads.

The bearing cartridge tube extends well above the tower attachment flanges in order to raise the rotor above the influence of the tower as much as feasible. In addition, the mounting of the transmission (gearbox) and generator inside a cowl is facilitated. The main bearings, which are of a flange-mounted type, cap both ends of the tube.

The control system for the high-reliability Cycloturbine has to permit automatic operation at remote locations. A tilt-cam mechanism which controls blade cyclic pitch amplitudes in a manner similar to a helicopter swash plate provides the required automatic features.

### 3.1.1.2 SELECTED CONFIGURATION

The general dimensions of the configuration selected to meet the performance criterion are shown in Figure 3-3 and the high-reliability Cycloturbine selected design is summarized in Table 3-1. The turbine has a diameter of fifteen (15) feet and a blade span of eight (8) feet providing a projected area of 120 square feet. At a turbine power coefficient of  $C_p = 0.4$ , the rotor will generate 1.96 kilowatts in the nominal wind speed of 9 m/sec. The rotor has an optimum tip speed ratio of approximately three (3) which results in a rotational speed of 112 RPM in a 9 m/sec wind.

The three blades, which are set 120 degrees apart, each have a one (1) foot chord which gives the rotor a solidity,  $\sigma$ , of 20 percent. Each blade is connected to a pair of struts with a distance of 8.667 feet between the blade/strut attachment points. The

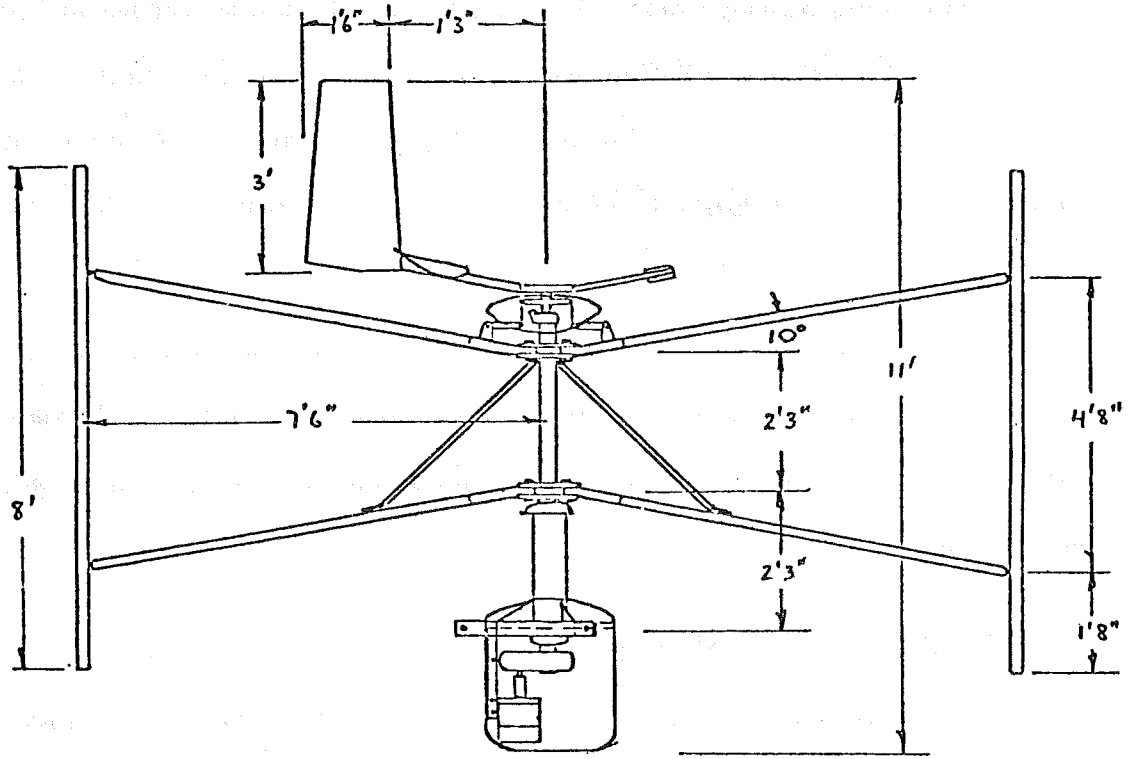


Figure 3-3. General Dimensions.

Table 3-1. High-Reliability Cycloturbine Selected Design.

Blades

Spar: Extruded D-Shape leading edge, 6061-T6 aluminum.  
Skin: Brake and roll-formed aluminum sheet for afterbody.  
Ribbing: Formed spanwise C-shape.  
Fastening: Rivet.  
Hinge: Welded bell crank TFE lined spherical ball bearing.

Struts (Two per Blade)

Structure and Skin: Wholly extruded shape with cast fittings welded to ends. Tension rods droop support.

Hub

Flame cut round steel discs, two per strut, two 1/2" hub bolts per strut, double shear strut-hub connection, sandwich construction.

Main Shaft

Steel DOM tubing, 3" OD, 1/4" wall, machined to main bearing bore at lower end and hubs welded.

Bearing Cartridge

Bearings: Medium duty, cartridge mounted construction.  
Cartridge: Steel weldment consisting of large OD tube and "ears" for fastening to tower and welded flanges for transmission, generator, and main bearing mounting.

Transmission

Off-shelf shaft-mounted, double reduction gearbox, speed increased ratio: 15:1.

Pitch Actuation System

Method: Mechanical, direct actuation. Construction consists of stainless steel tube links, rod end bearings, swivel assembly actuated by cam or crank mechanism.

Control System

Method: Aerodynamic control of cyclic pitch.  
Actuation: Aerodynamic surface on vane.

Corrosion Proofing

All aluminum and steel surfaces painted with DuPont Imron.

hub plates to which the root end of the struts are attached are 2.25 feet apart giving the struts an angle from horizontal of 10 degrees. Each bottom strut is supported by a stay rod.

The main shaft is seated in bearings mounted to the bearing cartridge tube. The tube has a triangular steel flange structure welded to it which affords mounting of the turbine to the tower. The distance between the lower hub and the tower attachment points is also 2.25 feet. The shaft-mounted gearbox, coupling and alternator are located below the tower attachment flange and are supported by steel brackets. These driven components are cowled with a molded cover.

The control system, which is seated atop the main shaft, consists of a tilting mechanism which actuates pull rods to control blade articulation. The axis of tilt direction is controlled by a 3 x 1.5-foot vane which reacts to wind direction. Tilting action is governed by a horizontal, highly cambered wing with four square feet of area mounted on the tail vane boom. The height of the rotor system, from the bottom of the cowling to the top of the vane is eleven (11) feet.

### 3.1.2 CONSTRUCTION

#### 3.1.2.1 GENERAL

Design of the components of the Cycloturbine was directed towards reducing time of their manufacture. Extruded shapes are used for the struts and blade leading edges. Castings and machine molded pieces are also used wherever possible to reduce labor hours in high volume production. The rotor is almost entirely aluminum in order to keep centrifugally induced loads low. Steel is used in the main shaft, hubs and bearing cartridge where high strength is needed and weight is less important.

Special attention was given to welds used in the construction, especially in the strut root area. There, the highly cyclic loads developed by the blades twice per revolution are absorbed partially by three pins instead of relying entirely on a weld of two dissimilar aluminum alloys, i.e., the forged strut extrusion and a casting. Highly weldable 6061-T6 aluminum is used throughout the turbine. Cast pieces are made of A356 alloys which has a high yield strength and is more weldable than most casting alloys.

All pins and bolts were checked to ensure a factor of safety greater than one in single shear. To enhance stress margins and reliability, pins and bolts were placed in double shear where space permitted. All stainless steel hardware is used throughout the turbine construction. Steel used in the structure is galvanized and the aluminum pieces are anodized following component fabrication for corrosion protection.

Considerable effort was expended in locating suitable control linkage bearings which have high load-bearing capacity and are maintenance free. Rod ends and spherical ball bearings were located that are lined with a Teflon fabric which eliminates the need for lubrication and has a significantly lower wear rate compared to ordinary spherical and rod-end bearings. This made it possible to eliminate service of bearings on the outboard ends of the struts - a difficult area to reach on top of a tower. All ball and roller bearings were chosen with the highest quality seals offered by a manufacturer. Mounted units were incorporated in the bearing cartridge structure to reduce machining costs.

The low temperature requirement was one of the most difficult design specifications to meet. The difficulty did not lie in the choice of metals since both aluminum and steel are negligibly affected in the temperature range specified. The Teflon fabric in the linkage system is also unaffected by the low temperature. However, the oils and greases in the gearbox, and ball and roller bearings are affected as are all rubber seals. Teflon was specified for the seals of the gearbox and bearings. These have not been

fully tested and evaluated as to their suitability. Silicone oil and silicone grease were found which meet the temperature specifications.

A flexible boot considered for the strut blade connection areas could not be used since it was not possible to find a suitable material which would be flexible at the low temperature specified. The boot was replaced by a sheet metal fairing which will prevent ice and blowing dust from entering the connection. The Teflon liner in the pivot bearings is largely unaffected by dust and grit. A more expensive all-metal coupling to connect the gearbox and alternator was chosen over a conventional elastomeric coupling for reason of meeting the temperature requirement.

The top areas of the blades are most vulnerable to direct lightning strikes which can burn holes in the metal. Therefore, a "cone of protection" was formed over the rotor by means of a long fiberglass-reinforced conductor mounted to the top of the tilt-cam assembly. The lightning will be attracted to the sharp point of the rod and directed down the main shaft, through the main bearings to the tower and ground. A lightning research laboratory consulted on this problem indicated that minimal bearing damage such as pitting is sustained by the high-voltage current passing through them.

The turbine is safe from hail damage. The blade skin on the afterbody is sheet but will not be damaged by the hail which falls nearly straight down. The same is true of the tail vane. The blade extruded leading edge will provide protection from hail strikes when the turbine is running. Horizontal flat areas facing skyward are heavy gauge metal, extrusions and castings. The wing, however, is a light gauge metal which could be damaged by severe hail. In the worst case, that is, complete loss of the wing, a limit cycle would be induced in the shutdown control in continuous high winds.

### 3.1.2.2 BLADES

In order to reduce bending loads resulting from the centrifugally magnified distributed mass of the blades, it is extremely important to keep the distributed

weight of the blades as low as possible. Blade construction options which were considered are given in Figure 3-4. Starting from the bottom, the stainless-sheet reinforced airfoil shell, although able to meet cost, weight and strength requirements, did not furnish sufficient structure to which attachment points could be fastened. The next option (with thin-wall aluminum tube) was considered vulnerable to hail damage besides having a fastening seam at the trailing edge. The blade with a brake-formed leading edge structure and built-up afterbody was considered difficult to fabricate.

The selected blade is constructed of an aluminum extruded leading edge and an aluminum sheet afterbody inside which is riveted a spanwise-sheet reinforcing rib (see Figure 3-5). The center of gravity is at the quarter chord and the flatwise moment of inertia is  $0.67 \text{ in}^4$ . Attachment tabs are welded to the extruded leading edge spar at an optimum distance apart to minimize bending stresses as shown in Figure 3-6. The total weight of one blade is 21 pounds or 2.625 lbs/ft. The blades are capped at both ends with end caps formed from epoxy resin.

### 3.1.2.3 STRUTS

There are six (6) struts per Cycloturbine which makes them a major cost item. Therefore, they must be especially inexpensive to construct. The struts should be as thin as possible at the outboard end to reduce aerodynamic drag. Additionally, they must be hollow to accommodate blade pitch control rods which move inside the top struts. Finally, they must be able to absorb the highly oscillating loads without danger of fatigue.

A suitable, lightweight construction is a built up A-frame with gusset attachment point at both ends as shown in Figure 3-7. This strut configuration, used in the commercially-available Cycloturbines, is labor intensive since each frame is aerodynamically faired with a riveted sheet aluminum shell.

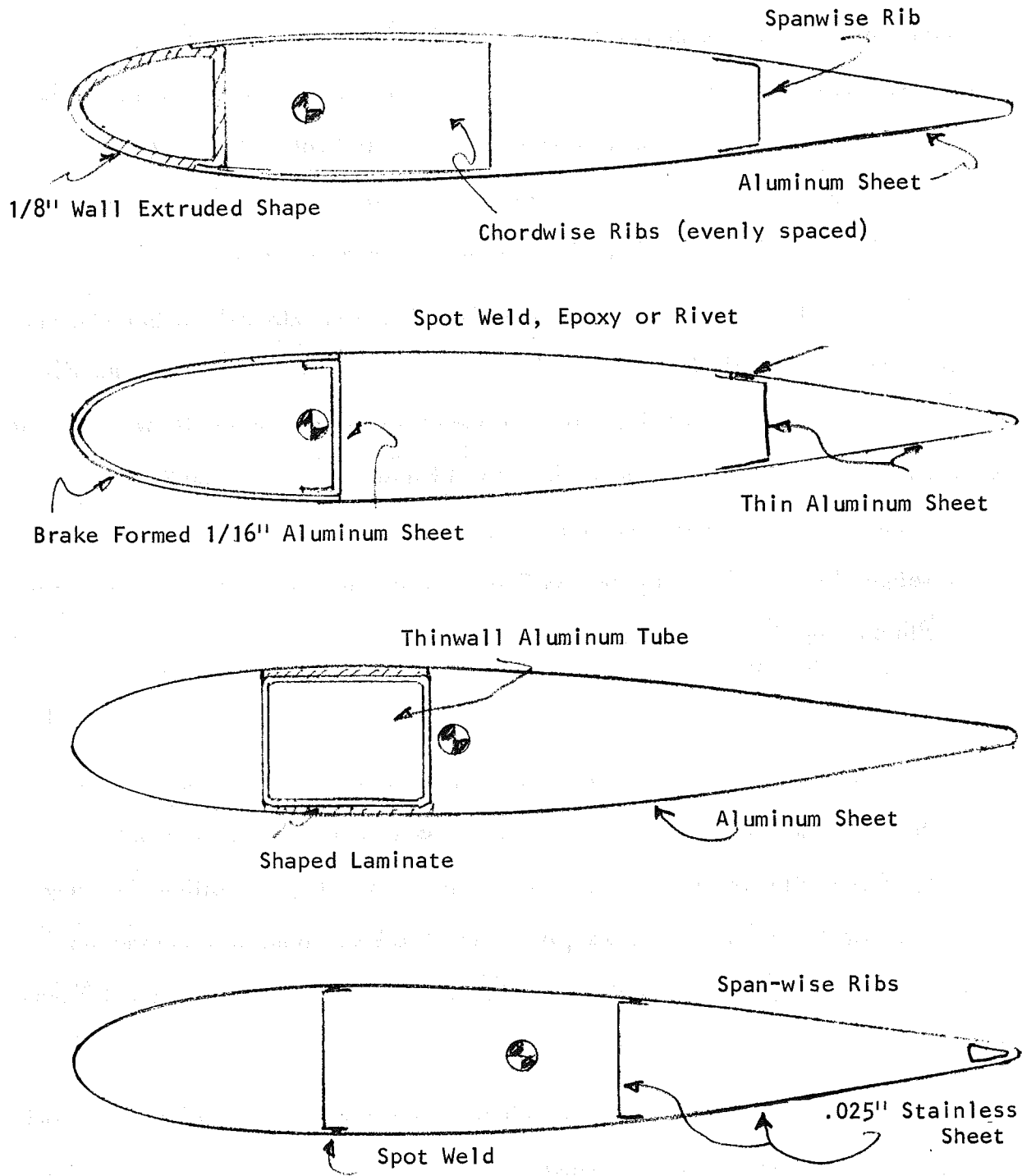


Figure 3-4. Blade Construction Options.

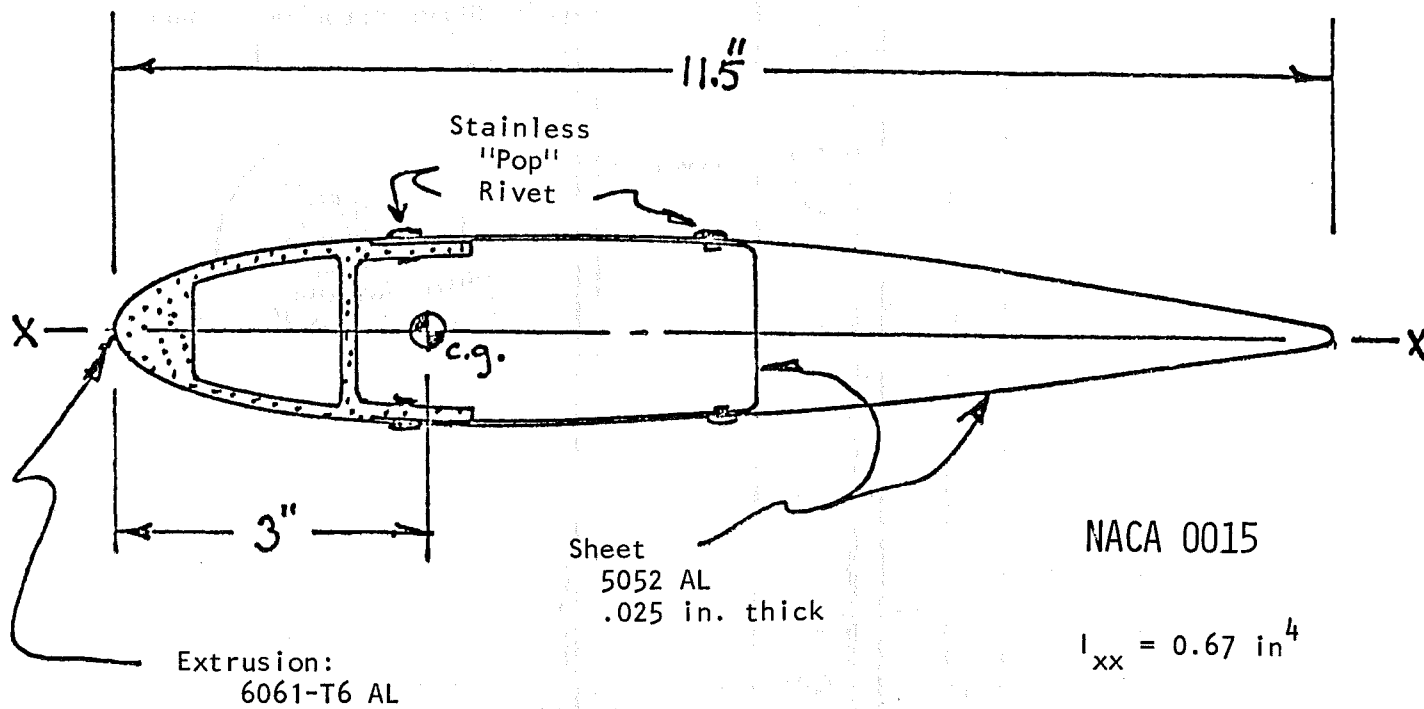


Figure 3-5. Blade Construction.

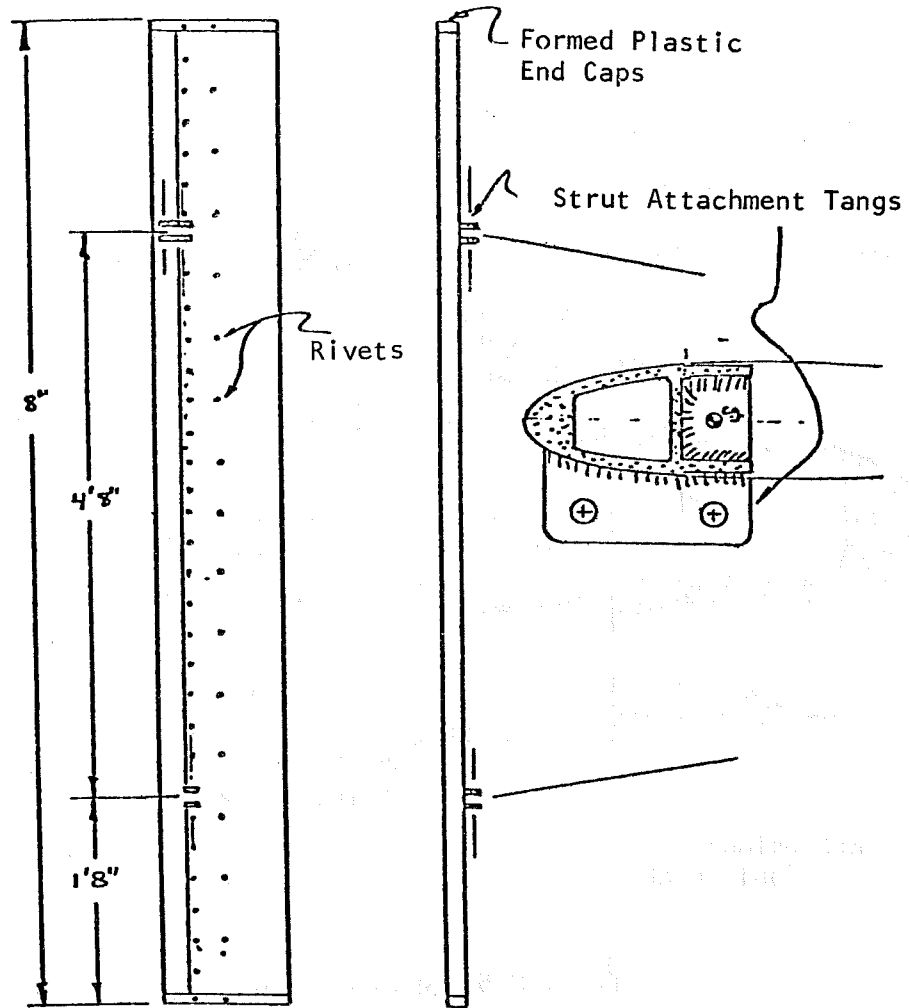
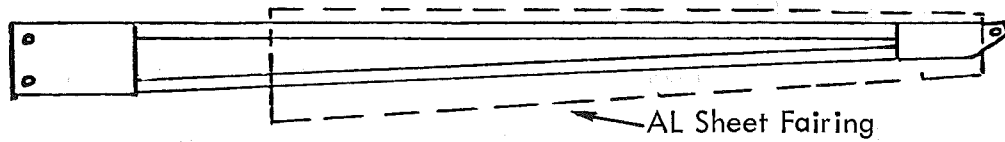
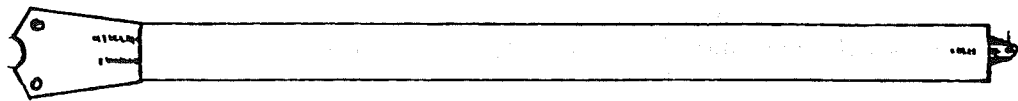


Figure 3-6. Blade Planform Detail.



a) Initial Design: A-Frame with Sheared Gusset Plates Welded to Ends.



b) Selected Design: Wholly Extruded Airfoil Shape with Castings Welded to Ends.

Figure 3-7. Strut Construction Methods Considered.

A six-inch NACA 0015 airfoil aluminum extrusion with a 0.9-inch maximum thickness is now commercially available and will be incorporated in the high-reliability Cycloturbine (Figure 3-7). The extrusion is hollow and has one web allowing a 7/16-inch diameter control rod to ride in Teflon bushings glued inside them. In the Reynolds number operating range of the Cycloturbine, the NACA 0015 airfoil has very low aerodynamic drag compared to other symmetric airfoils.

The strut root-hub connection had to be designed to withstand the highly oscillatory loads. A mechanical joint at the aluminum-to-steel juncture, and provisions for inserting the control rod inside of the extrusions must be made. Many design options were considered, several of which are shown in Figure 3-8. The option labeled #3 was found to be the most straightforward but the weld joint became the critical junction. Figures 3-9, 3-10 and 3-11 were design attempts to distribute the cyclic loads in shear through the welds and away from the sharp trailing edge of the extrusion. Although the design shown in Figure 3-11 is adequate, it was found to be cost prohibitive because the welding of a cast alloy to a forged one and heat-treating the entire piece to obtain a single temper is involved. The casting requires a complex mold which also increases the cost as does the need for two hub pairs.

Figure 3-12 shows the strut-to-hub attachment selected for the final design. Cast aluminum shapes are slid over the extrusion and welded at points about one foot apart. Holes are drilled through the casting and extrusion and press fit with a 3/4-inch stainless steel bushing. One-quarter inch galvanized steel plates are bent to shape and drilled with holes to fit the castings/extrusion holes and also those in the hub plate welded to the main shaft. Stainless steel sheet is used at the aluminum steel interfaces to prevent galvanic corrosion. This method of attachment avoids the need for involved heat treatment since the load is taken by the extrusion as well as the weld on the leading edge of the extrusion/casting interfaces. No weld is used on the trailing edge. Load is also carried by the steel at the locations on the top struts where the control rods enter

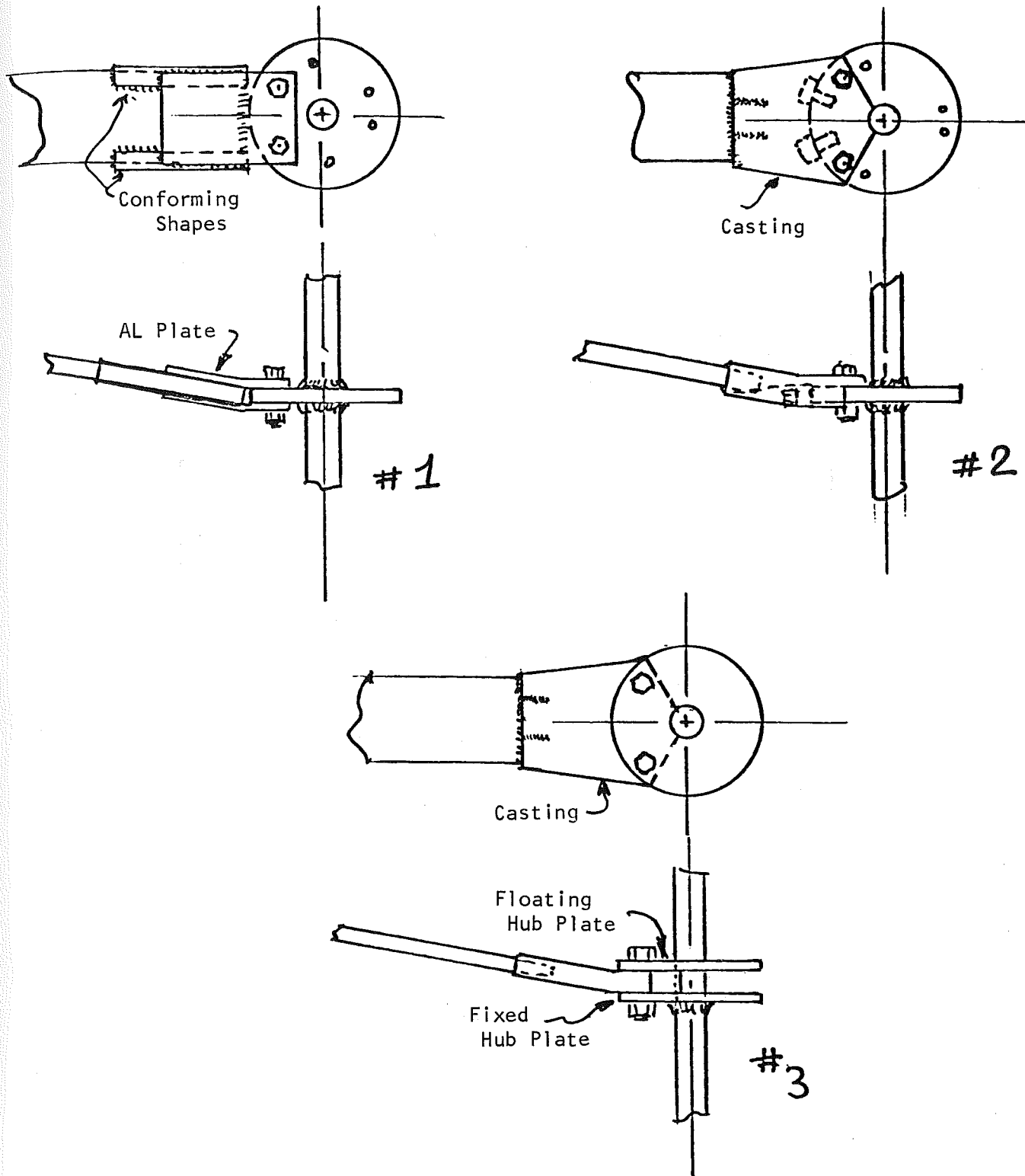


Figure 3-8. Hub - Strut Connection Options.

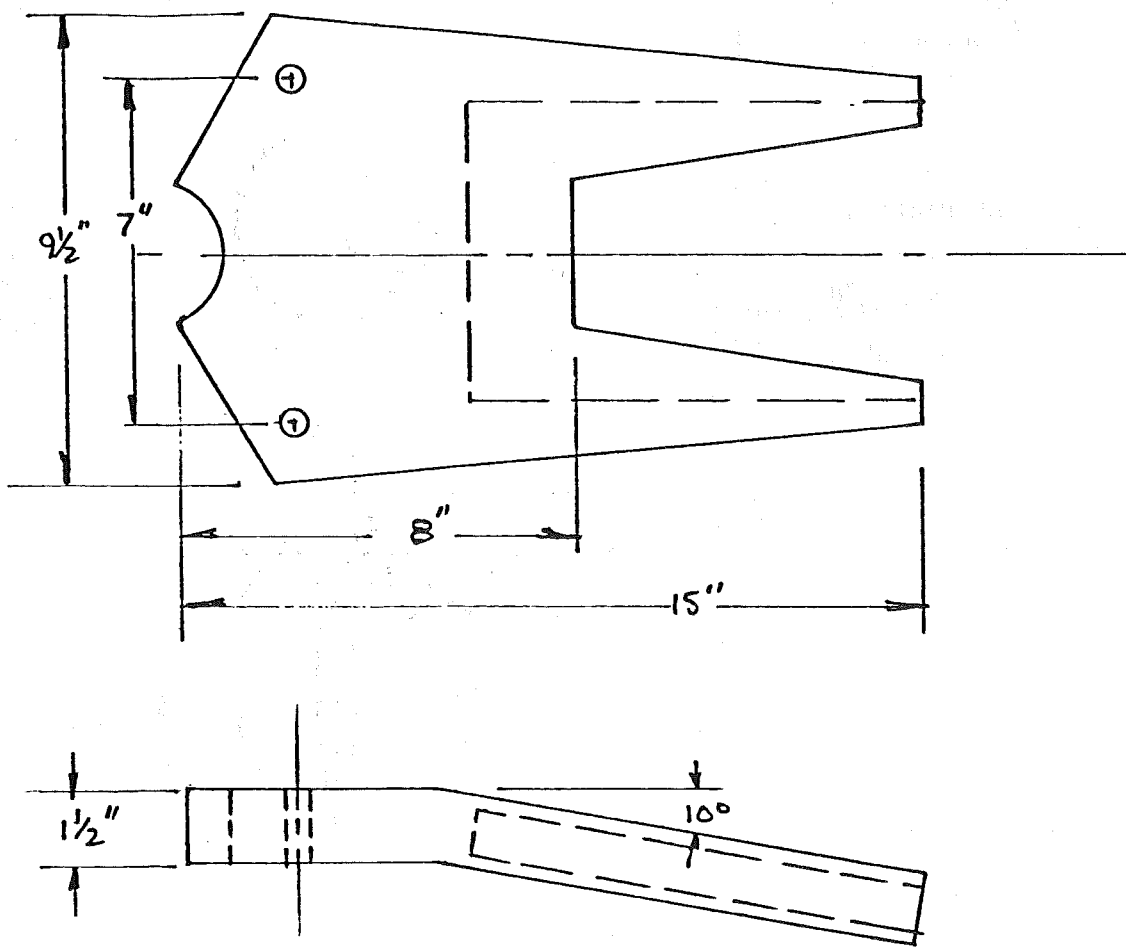


Figure 3-9. Strut Root Casting.

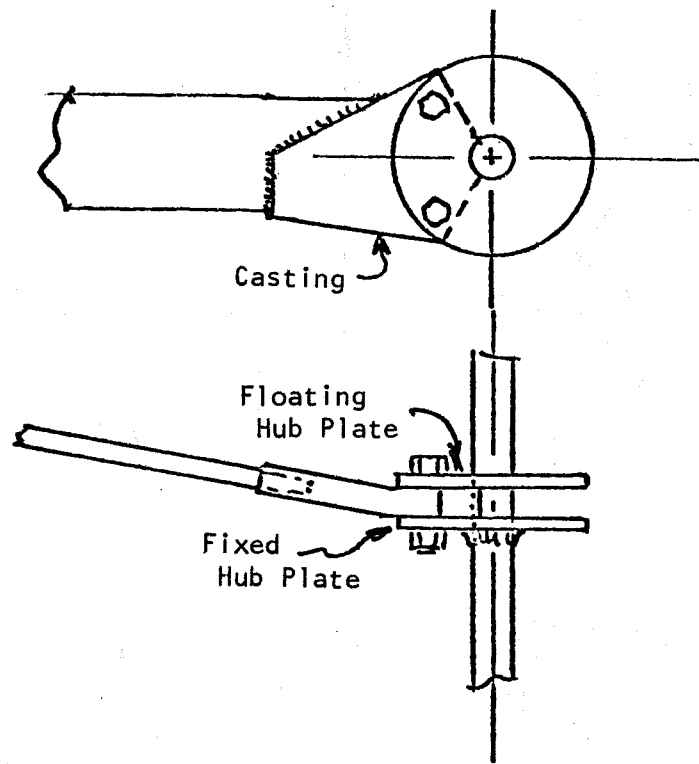
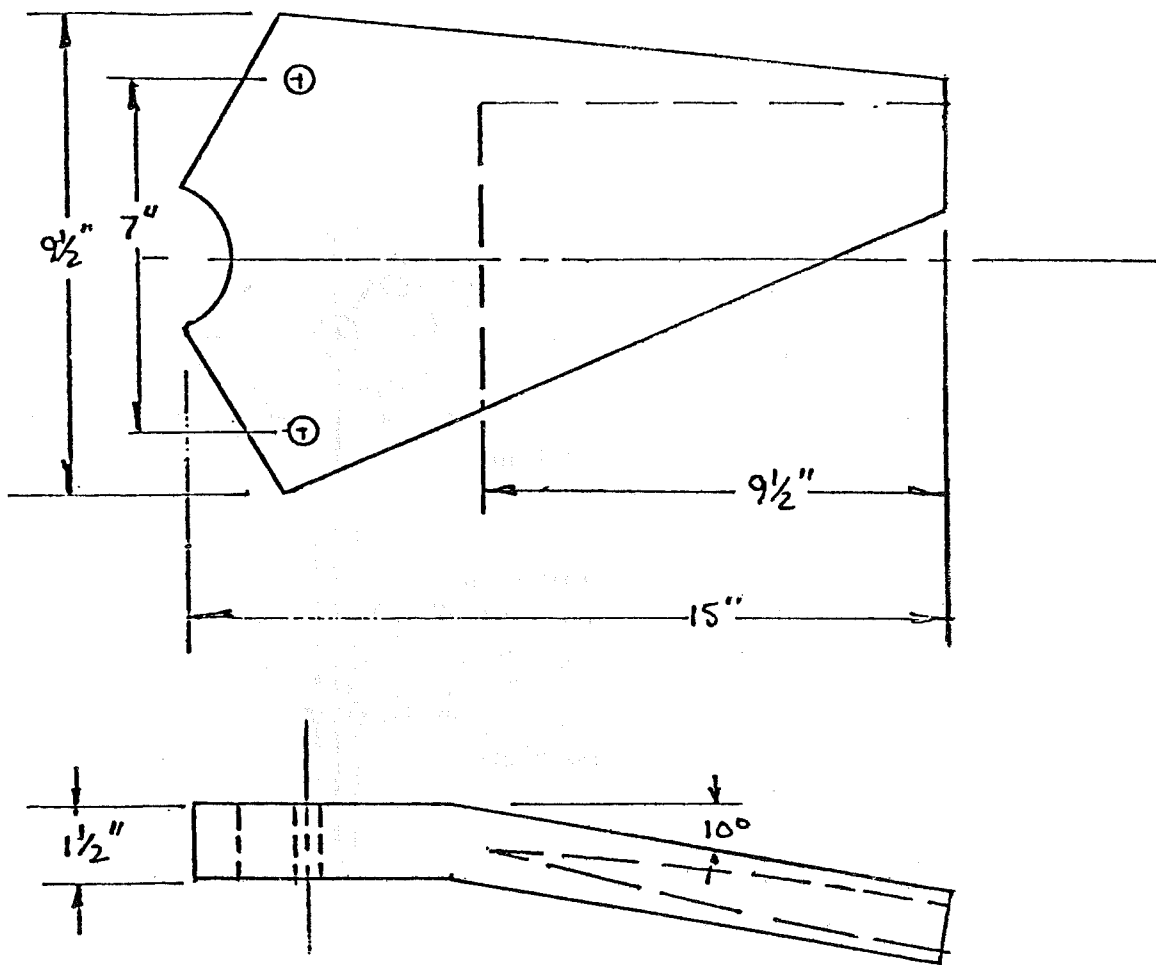
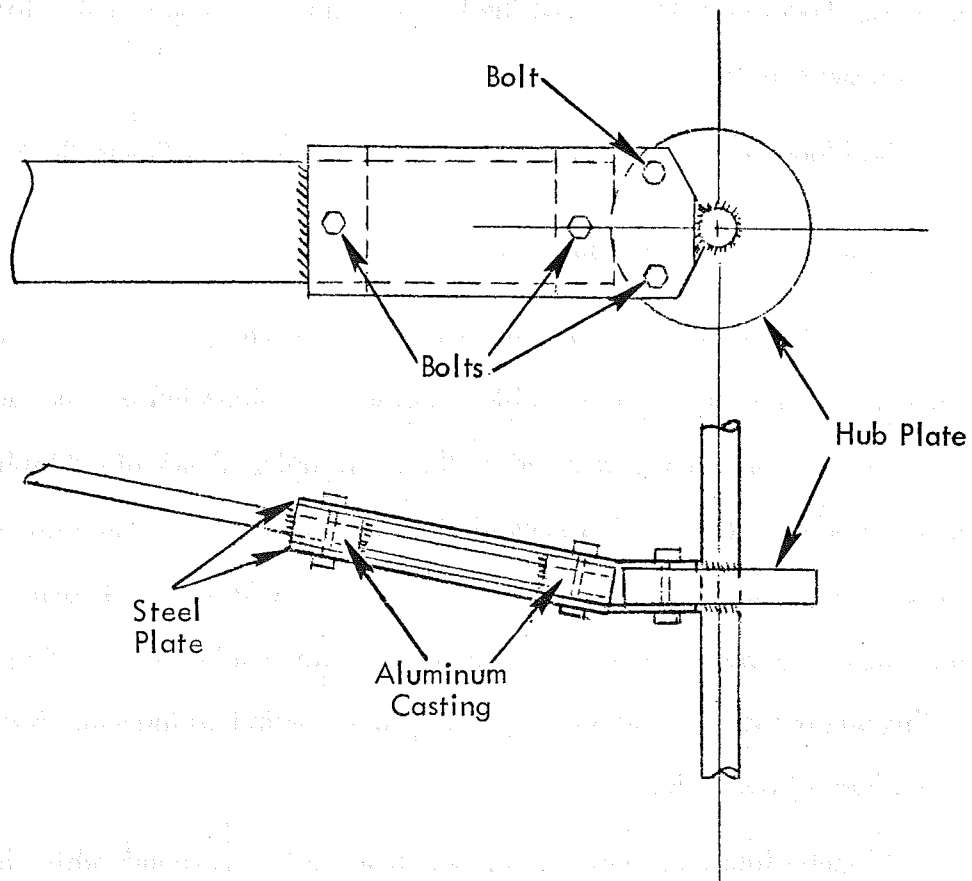


Figure 3-10. Hub - Strut Connection.



Material: Aluminum Casting Alloy A356

Figure 3-11. Strut Root Casting.



**Figure 3-12. Selected Hub - Strut Connection.**

the struts making for a simpler, less critical design. Finally, the castings remain small and cost is also reduced by using a single hub which are simple steel shapes instead of large castings. Location tolerances of the holes in the steel shapes and extrusions, however, become critical.

The blade-to-strut attachment design is illustrated in Figure 3-13.

#### 3.1.2.4 MAIN SHAFT AND HUB PLATES

In the design of the main shaft of the Cycloturbine, care must be taken to avoid runout, not only because of possible imbalance problems but also because the gearbox is suspended from the lower end of the main shaft. A machined bushing serves to adapt the gearbox. The bushing is welded to the shaft before machining and a keyway is cut. The top of the shaft, which is centerless ground to main bearing tolerances, is also machined to a specified inner diameter to fit the cam bearing housing. Mounting holes for this purpose are drilled and a relief between main bearing seats is also machined to facilitate ease of assembly.

The hub plates are one-inch thick, flame-cut steel rounds which have an inner diameter machined to shaft tolerances and strut mounting holes drilled. The plates are welded to the main shaft (see Figure 3-12).

#### 3.1.2.5 BEARING CARTRIDGE

The bearing cartridge/weldment shown in Figure 3-14 serves as the main structural component of the Cycloturbine rotor. All loads are transmitted to the tower from the two-sealed flange-mounted Sealmaster SFC main bearings to the weldment consisting of a 6-3/4-inch diameter steel support tube and three gusseted flanges welded to it with holes at the ends to allow bolting to towers. A structural framework bolts to the weldment which supports the alternator and gearbox. The weldment and frame are galvanized for corrosion protection.

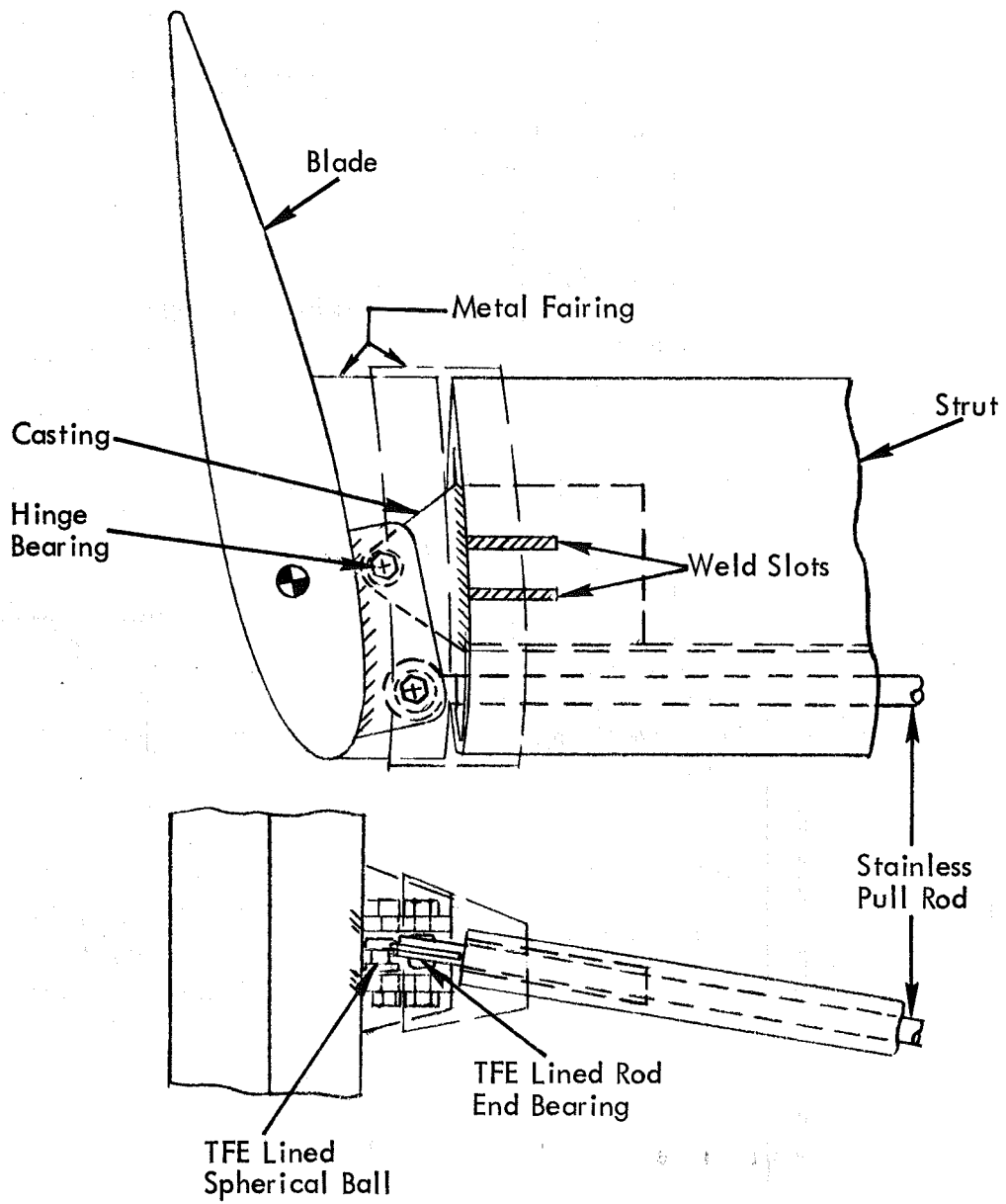


Figure 3-13. Blade/Strut Attachment Assembly.

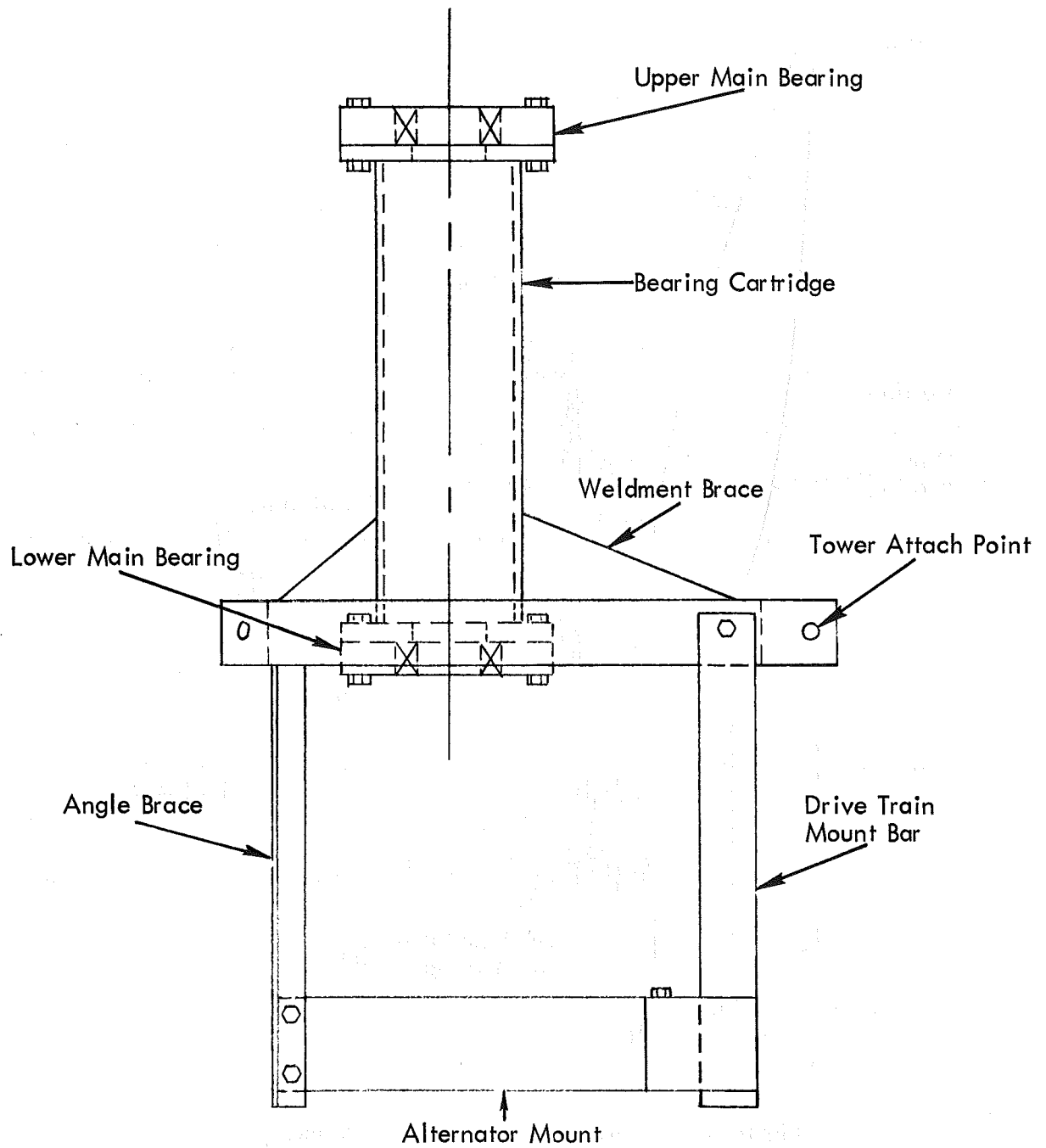


Figure 3-14. Bearing Cartridge/Weldment.

### 3.1.2.6 DRIVE SYSTEM

A Morse 115D15 shaft-mounted, double reduction gearbox was chosen as the transmission for the Cycloturbine after considering those illustrated in Figure 3-15. The two-stage transmission was preferred because of its simplicity and low cost. However, gear belts which could meet the temperature criteria (see Table 2-2) are not available. The direct drive system was not selected due to the unavailability of an off-the-shelf low speed alternator which could meet the reliability criteria (see Table 2-1). The Morse gearbox, shown in Figure 3-16, has a 14.971:1 increase ratio and has seals fitted to allow vertical-axis mounting. Silicone oil is used to meet the low-temperature specification. The gearbox also allows access to the bottom of the main shaft for attaching instrumentation.

An all stainless steel flexible coupling made by Heli-Cal Products Company (Figure 3-17) was chosen to connect the alternator to the gearbox.

### 3.1.2.7 CONTROL SYSTEM

The need for a fail-safe, reliable, and responsive control system is obvious. By controlling the angles of the blades, the system must allow the start-up, speed control, shut-down or stopping of the rotor. Experience by Pinson Energy Corporation has shown that it is undesirable to allow a vertical-axis rotor to operate in very high winds and at low tip speed ratios due to the abrupt high loadings from blade stalling.

Two control schemes were considered. One was the system used on the PEC Model C2E Cycloturbine which collectively pitches the constant amplitude, cyclically pitched blades trailing edge outboard. At high collective angles, the rotor will come to a stop and weathervane in a preferred orientation to ride out high winds. The action is controlled as centrifugally actuated forces overcome a weight in a balance to pitch the blades reducing tip speed ratios at higher wind speeds. At a predetermined RPM, the inertial forces activate a trip device which moves the cam to pitch the blades to a high collective pitch, thereby stopping the machine.

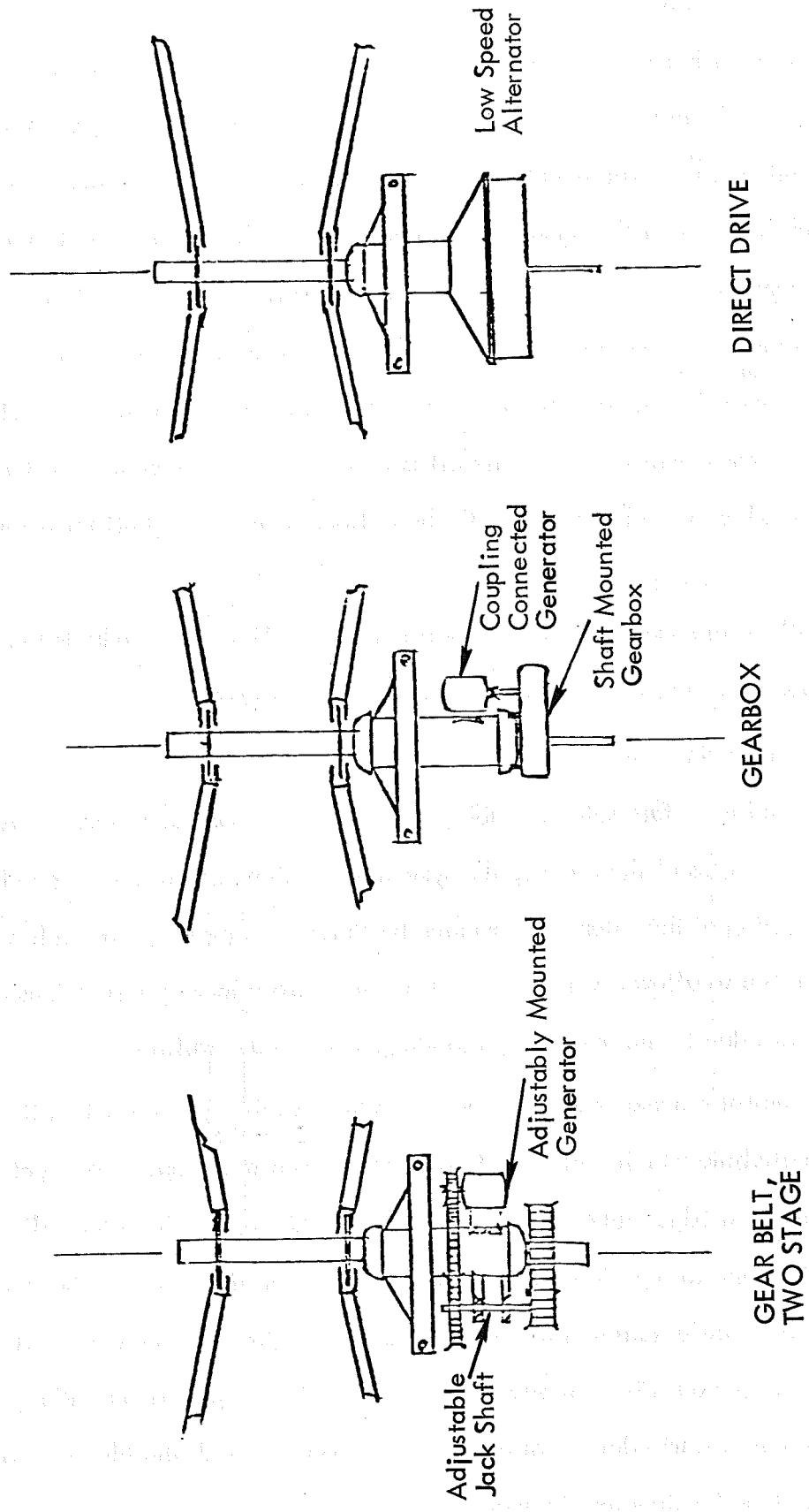
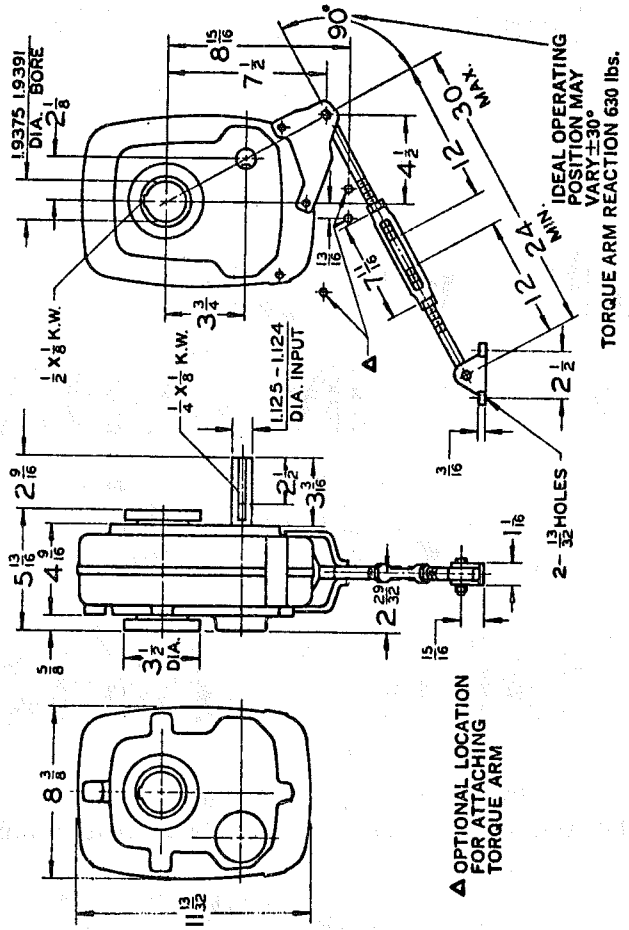
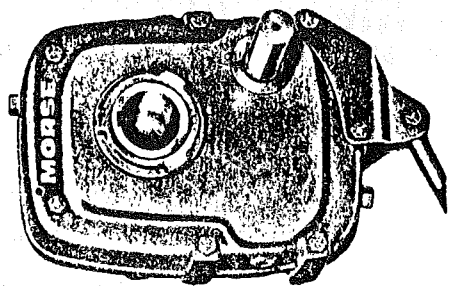


Figure 3-15. Considered Transmission Options.

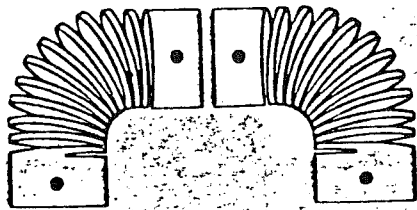


**Class I ratings for 115D15**

actual ratio: 14.971:1

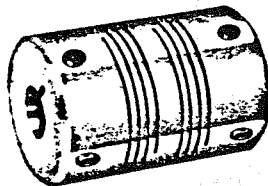
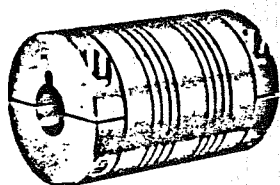
OUTPUT RPM	10	15	20	25	30	40	50	60	70	80	90	100	110	120	130	140
Input H.P.	0.80	1.20	1.60	2.00	2.40	3.20	3.76	4.32	4.88	5.44	6.00	6.33	6.67	7.00	7.33	7.67
Output Torque (In.-Lbs.)	4740	4740	4740	4740	4740	4740	4460	4270	4130	4030	3950	3750	3530	3460	3340	3240
Input O.H.L. (Lbs.) Middle of Shaft Extm.	945	854	769	708	661	593	549	516	489	466	447	432	420	408	402	388

Figure 3-16. Morse Double-Reduction Gearbox (Model 115D15, Morse Catalog SP-78, p. F-87, 1978).



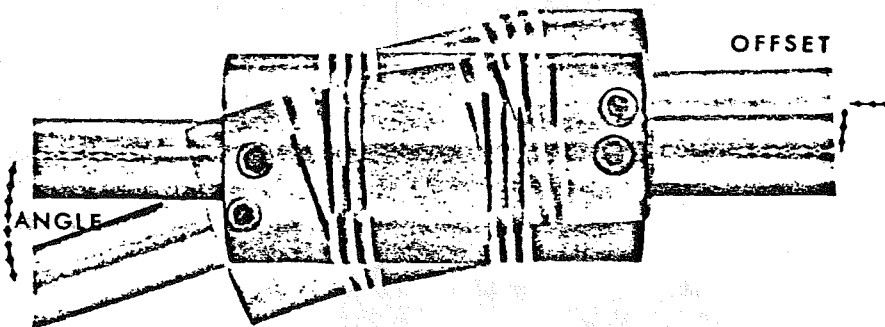
CONTINUOUS DUTY MOTOR COUPLING

# HELI-CAL<sup>®</sup>



## ONE PIECE ROTATING SHAFT FLEXIBLE COUPLINGS

Utilizing the endurance and high strength of either  
7075T6 Aluminum Alloy or 17-4 PH heat treated Stainless Steel



HELI-CAL Double-Flexing Shaft-Coupling compensates  
for all types of unavoidable or too  
costly shaft misalignment  
and unwanted stress

Figure 3-17. Heli-Cal Stainless Steel Flexible Coupling  
(Helical Announcement MC Series, Catalog  
#1-72, July 1977).

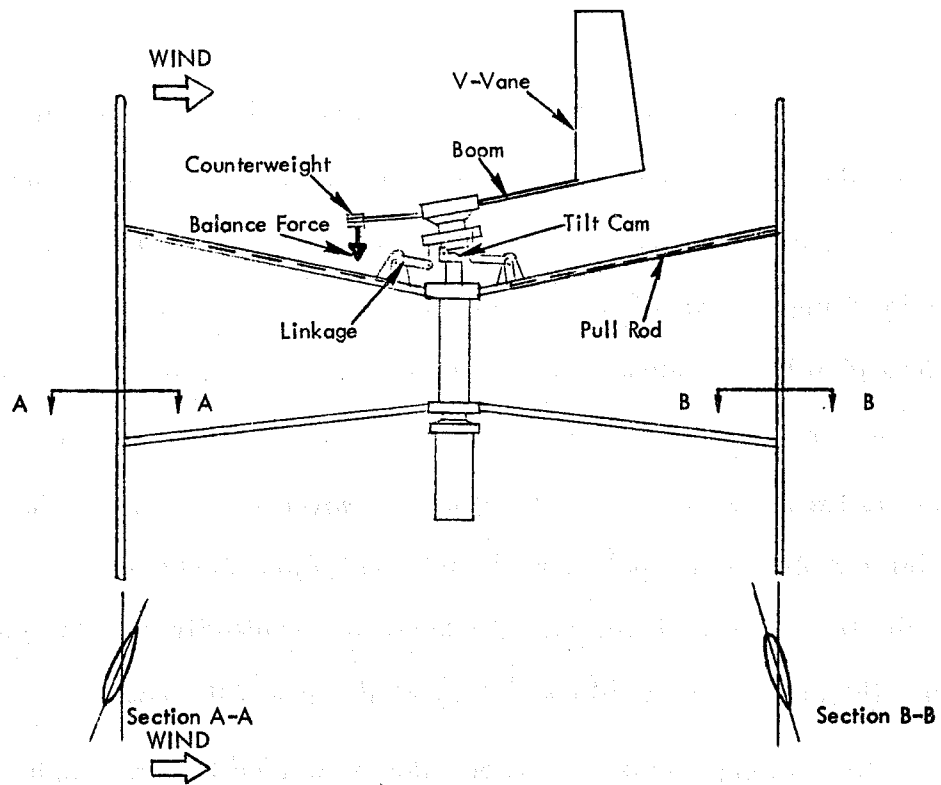
NG  
®

The second control scheme, a tilt-cam control system, was chosen for the high reliability design because it lends itself more readily to inherent automatic behavior, that is, with no need for auxiliary control devices. The tilt-cam system activates cyclic pitching by tilting a plane of linkage attachment points. These points connect to the blades through a link, L-lever, and a pull rod (see Figure 3-18). As the turbine rotates about the main shaft, the attachment points, through the link, impart the up-and-down motion (relative to the horizontal plane) to an L-lever which converts the vertical motion to a radial one through the pull rods which in turn rotate the blades about their hinge point. The tilted plane, therefore, introduces an eccentricity into the system which has the same effect as a mechanical cam. Hence, the name "tilt-cam".

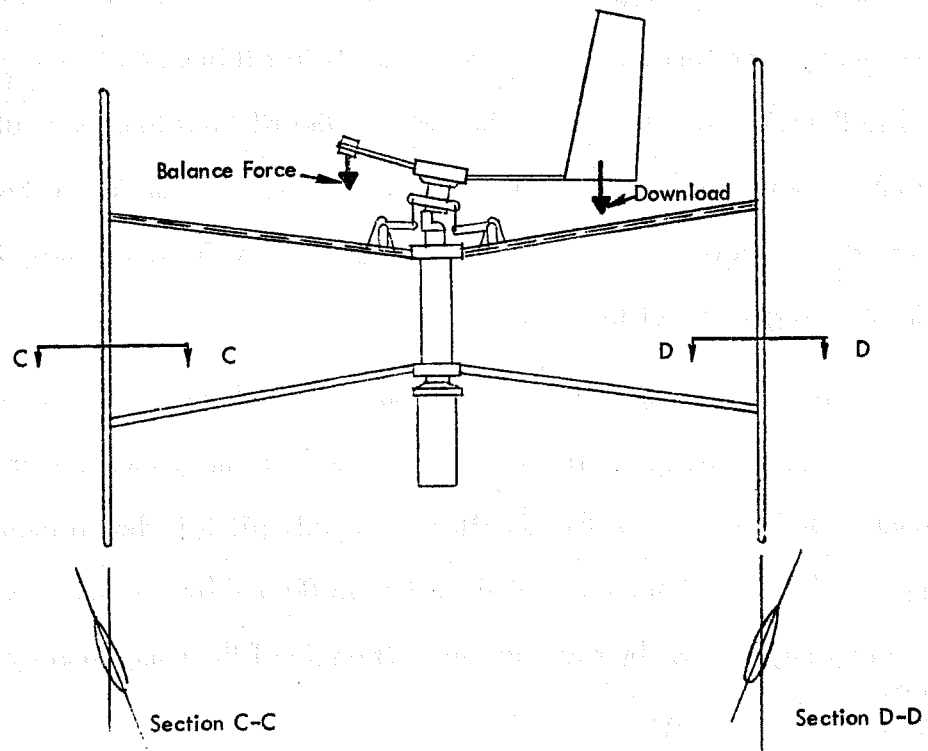
The tilting plane is a series of 3 flanges welded to a bearing housing allowing the linkage attachment points to rotate about a shaft. This shaft is mounted on a block supported by a hinge which allows the shaft to tilt back and forth in a plane parallel to the wind direction. The direction of the tilt axis (perpendicular to the wind direction) is controlled by a vertical vane on a boom. The entire "tilt-cam" assembly is supported on a shaft seated in bearings on top of the main shaft, thus, free to point in a direction regardless of the spinning rotor.

Since the linkages and pull rods on each blade are identical, as the tilt angle increases, the flanges "lift" the L-links one at a time, thus inducing cyclic pitch. The angular blade position or the amplitude of cyclic pitch is then a function of the tilt angle of the cam. Shut-down of the rotor is effected by slightly "reversing" the cyclic actuation, that is, by reversing the tilt angle of the cam, thereby, stalling the blades to stop the rotation.

The tilt angle is controlled by a balance of forces between a wing located on the vane boom and a counter weight on the other side of the pivot point as shown in Figure 3-18. Details of the tilt-cam mechanism and vane construction are shown



a) Start-Up and Operation.



b) Shutdown (Reverse Pitch).

Figure 3-18. Operation of Tilt-Cam Cyclic Pitch Control.

in Figures 3-19 and 3-20. It is anticipated that the weight of ice on the wing and vane will also actuate shut-down.

## 3.2 ELECTRICAL SYSTEM

### 3.2.1 GENERAL CONSIDERATIONS

The electrical system must be matched to the Cycloturbine performance characteristics in order to achieve the program objectives. This must be accomplished over environmental extremes including temperature, heavy salt spray, torrential rains, blowing sand and repeated lightning strikes, while meeting the reliability and cost goals for the wind turbine system. The low temperature requirement of  $-70^{\circ}\text{C}$  (see Table 2-2) implied that no existing, commercially available semiconductors could be used in this design as none were specified below  $-55^{\circ}\text{C}$ . An initial approach was to provide heat derived from the main battery pack to keep the semiconductors at or above  $-55^{\circ}\text{C}$ . Later it was possible to locate all semiconductors in the main control building with the battery pack. The semiconductors could still be heated, but this was deemed unnecessary as the battery pack would be inoperable at that temperature.

The low temperature requirement also presented problems in terms of bearing seals in the alternator and protective coatings for the alternator coils. The bearing lubricant also required careful consideration. The bearing seal problem was solved by using seals made of a Teflon, fiberglass composition. A silicone-based conformal coating with excellent thermal shock as well as high and low temperature characteristics was chosen for protecting the alternator coils. The lubrication for the bearings was selected to be a silicone-type grease.

The high temperature limit  $60^{\circ}\text{C}$  imposed limitations on the acceptable stress levels of the power semiconductors. The problem was handled by employing huge heat sinks and by keeping stress levels below 60 percent in all power semiconductors.

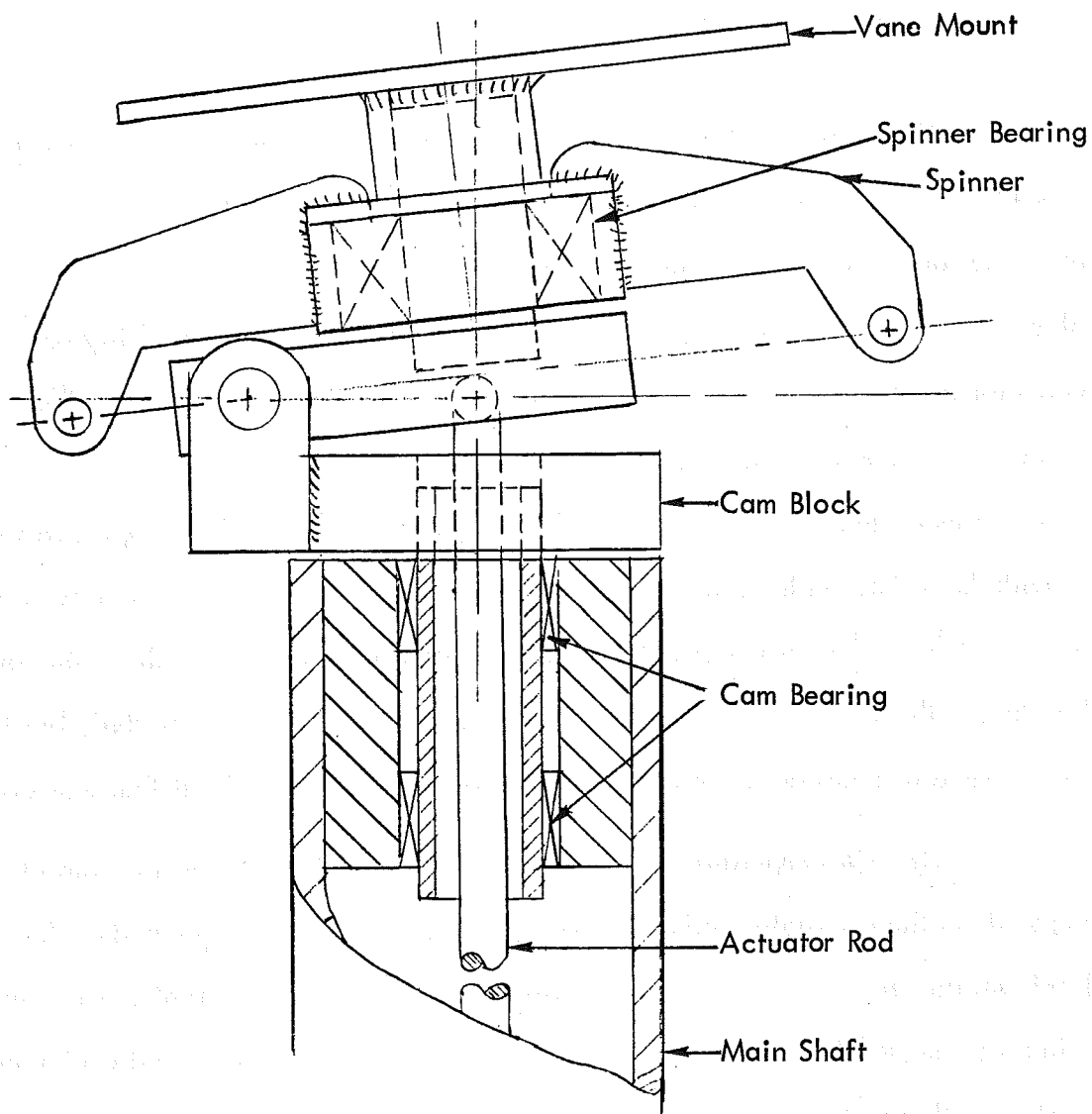


Figure 3-19. Tilt-Cam Detail.

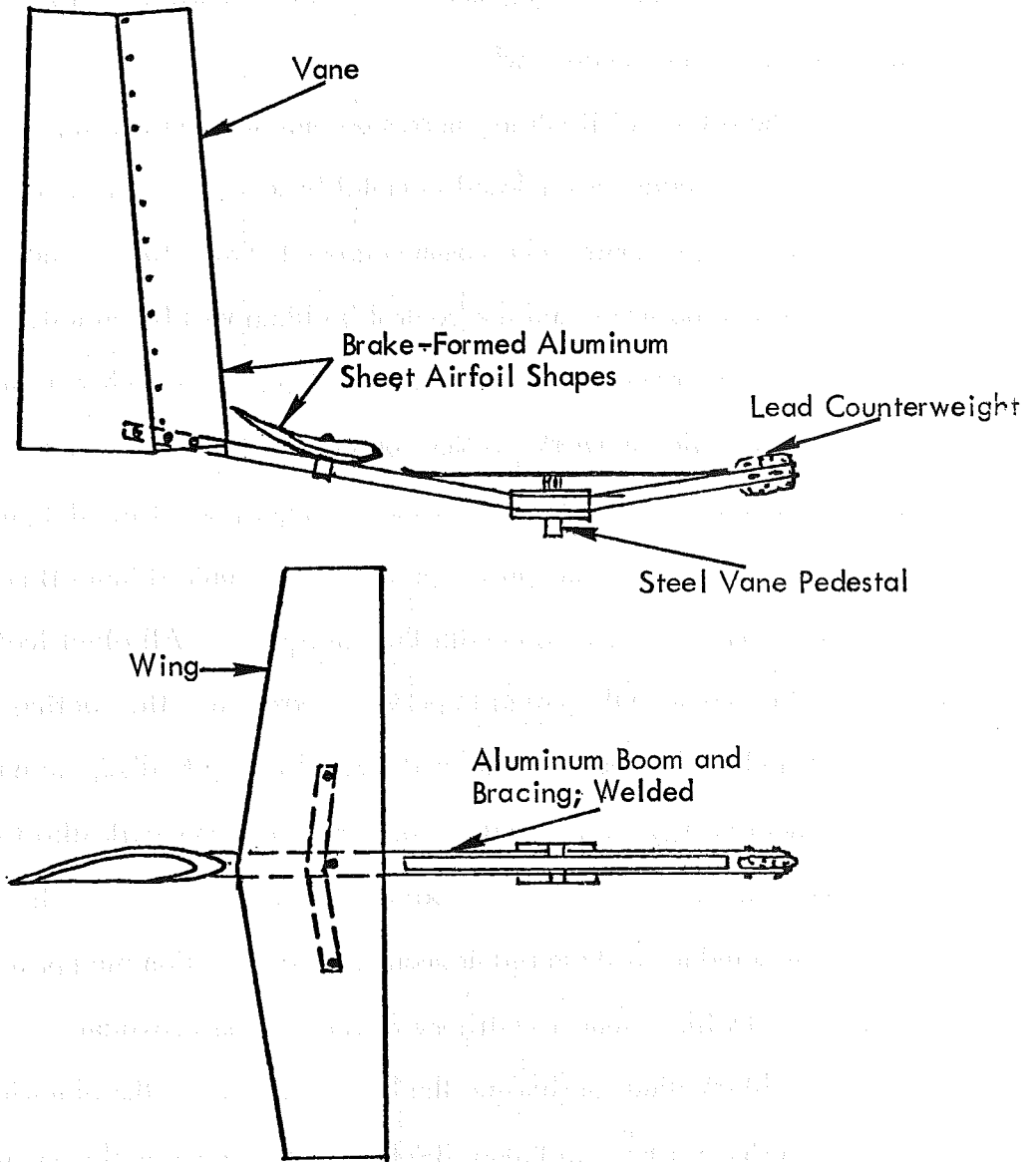


Figure 3-20. Vane and Wing Construction Details.

The torrential rain, snow, sleet, icing, hail and dust required that these be sealed out of all electrical equipment. This was accomplished by specifying liquid tight connectors, boxes and cowls.

The effects of lightning strikes are minimized by using the Faraday cage principle. All circuitry is enclosed in metal boxes. The system is bonded by the use of interconnecting conduit and a common ground wire. The ground wire and conduit running between the tower and the control building will be buried. The towers will be bonded with three ground wires, one on each leg, tied together at the bottom and grounded. Protection networks to limit and divert lightning-induced transients which may enter the electrical system constituted a major part of the design.

The corrosive atmosphere specification required that all metals be covered to prevent or limit their reaction with the atmosphere. All electrical components were covered with a conformal coating to prevent corrosion. The coatings for the alternator coils presented the biggest problem as it was necessary to dissipate a relatively large amount of heat energy from a small area. The alternator coils also traverse large temperature extremes, requiring a flexible coating; however, a silicone coating was secured that could meet these requirements. The steel lightning protection enclosures will be treated with a standard military finish to resist corrosion.

A block diagram showing the basic elements of the electrical system and their relationship is shown in Figure 3-21. The preliminary electrical design for a 1-kW SWECS is shown schematically in Figure 3-22. It included a three-phase alternator, two lightning protection networks, two dump loads, a voltage regulator, automatic battery equalization circuit and metering. The dump loads were located on the tower and in the control building (see Figure 3-23). The load on the tower was to provide the turbine with a backup load in the event the transmission line became severed in order to prevent overspeeding. The dump load in the control building was

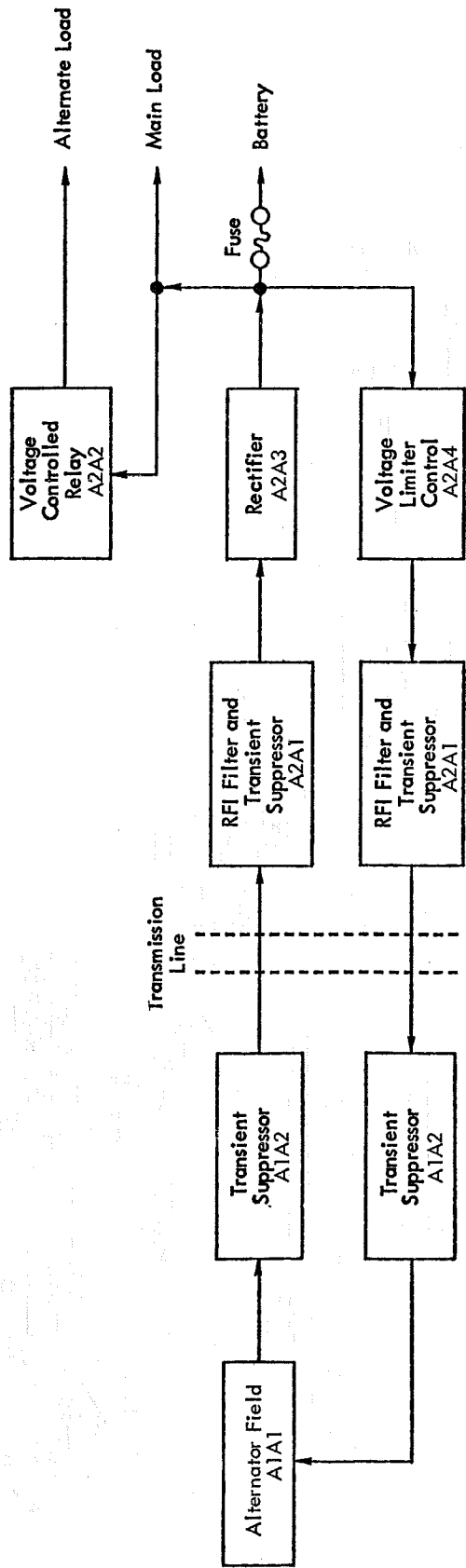


Figure 3-21. Electrical System Block Diagram.

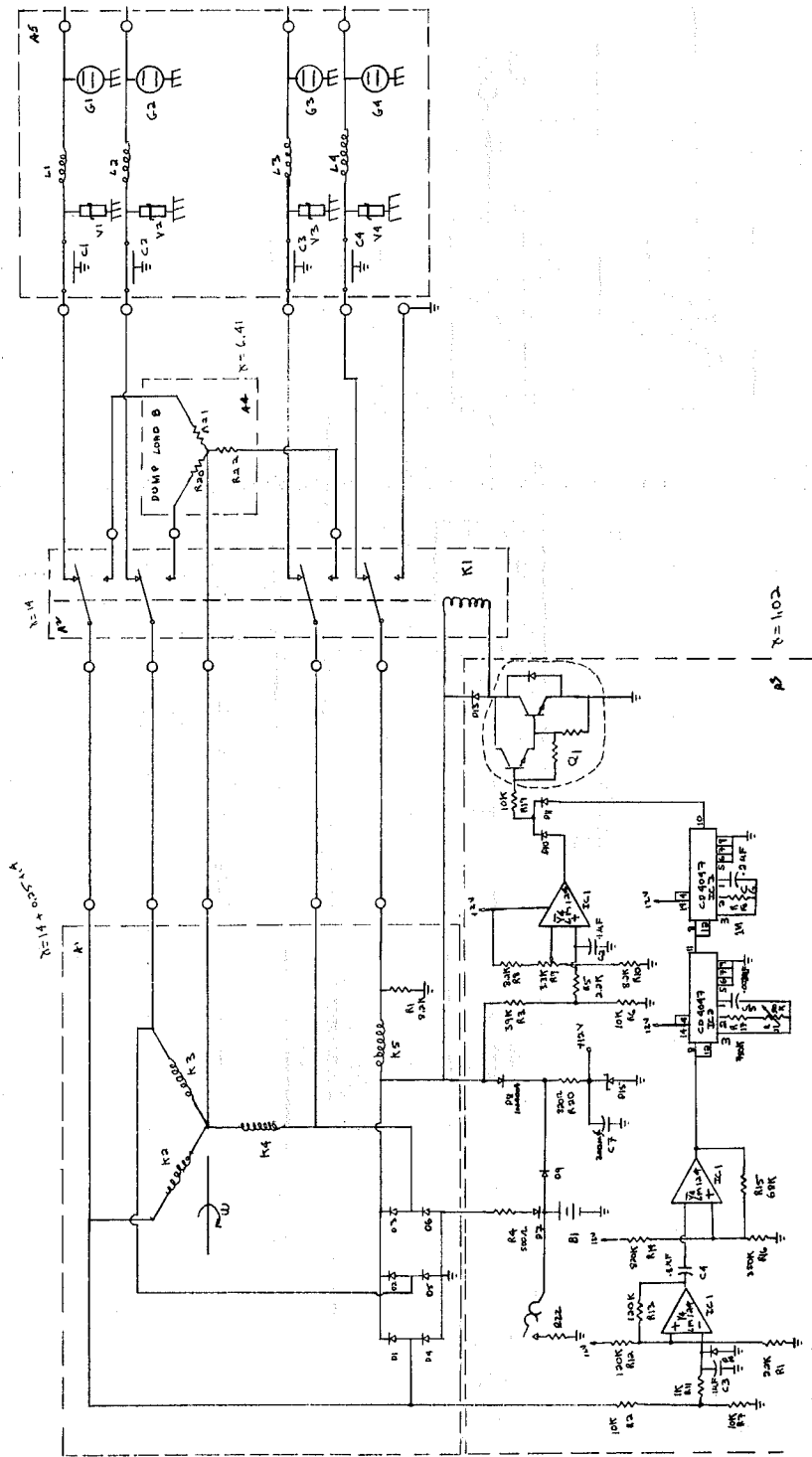


Figure 3-22. Preliminary Electrical System Circuit Diagram.



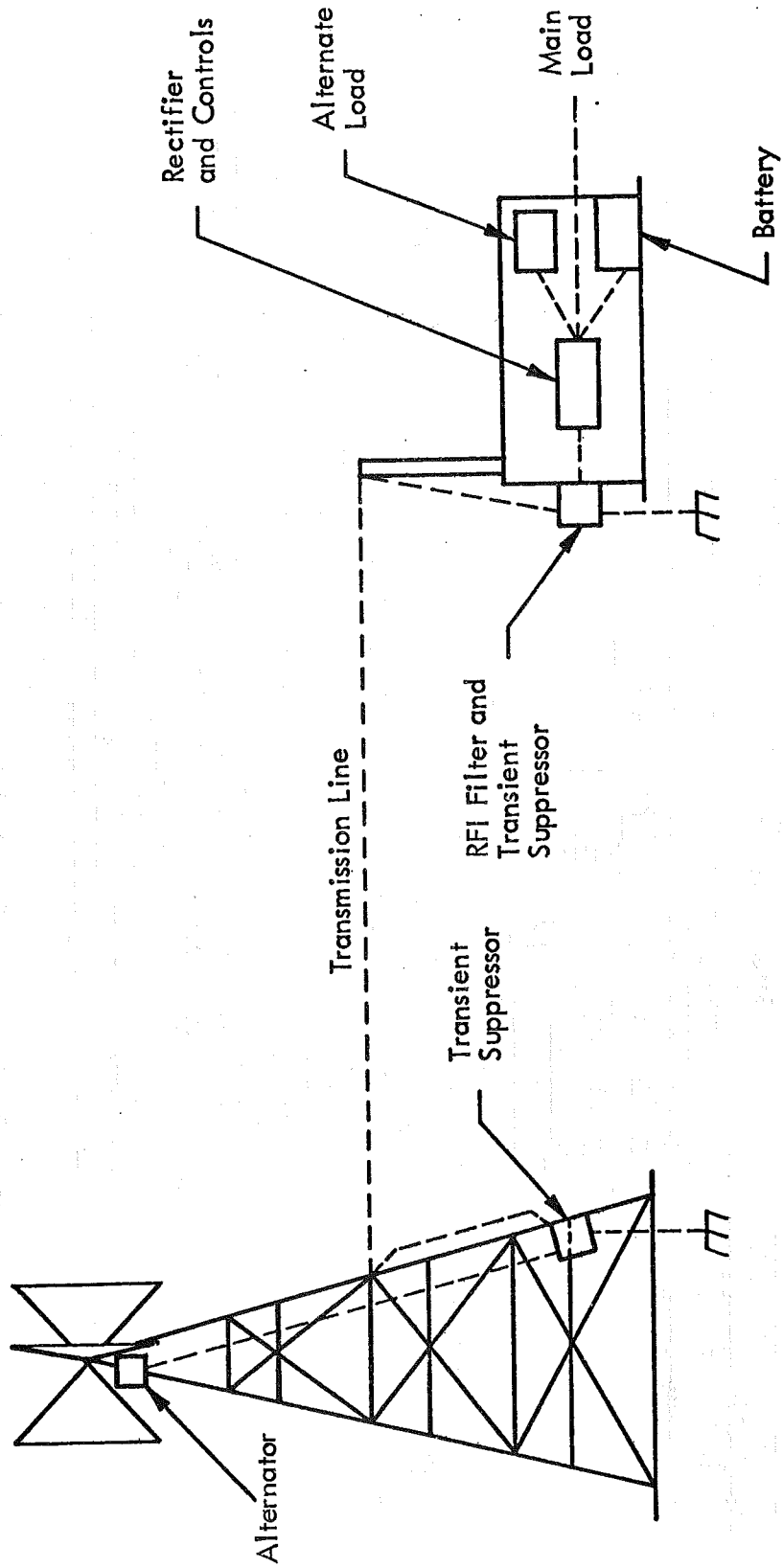


Figure 3-23. Typical System Configuration.

to provide the turbine with load when the battery pack became fully charged. The three-phase generator was of the switched reluctance type and converted the mechanical power from the rotor to electrical power. The voltage regulator was to control the battery voltage if the dump load in the control building failed. The lightning protection networks were identical and served to divert damaging energy from lightning strikes and other transients around the electrical system. The battery equalization network was designed to monitor the battery pack and periodically overcharge the battery to equalize all cells. Two meters were included to monitor generator and battery voltage, and the battery current.

The first cut at a reliability analysis indicated that the above systems had an MTBF that did not meet the contract specifications. The principal reliability drivers were the relay that activated the dump load on the tower, the metering and the charge equalization network. The tower dump load and charge equalizer had been included to enhance the reliability and capacity of the turbine and the battery pack but since they had high failure rates they were deleted. It was decided that since the SWECS was designed for remote applications, the metering could be deleted in favor of a test kit which could be carried in for inspections and tested in a calibration lab.

The system now consisted of an alternator, two lightning protection networks, a single dump load and a voltage regulator as shown schematically in Figure 3-24. The two lightning protection networks were located in separate steel boxes and the alternator in a cowl at the tower top (see Figure 3-23). All other circuitry was located in a third steel box in the control building. It was decided to include all semiconductors in the control building to isolate them from the vibration associated with the operation of the wind turbine, temperature extremes and lightning strikes.

This revised system could now meet the MTBF goal, but the total system could not meet the specified cost goal. The cost driver in the remaining circuitry was the

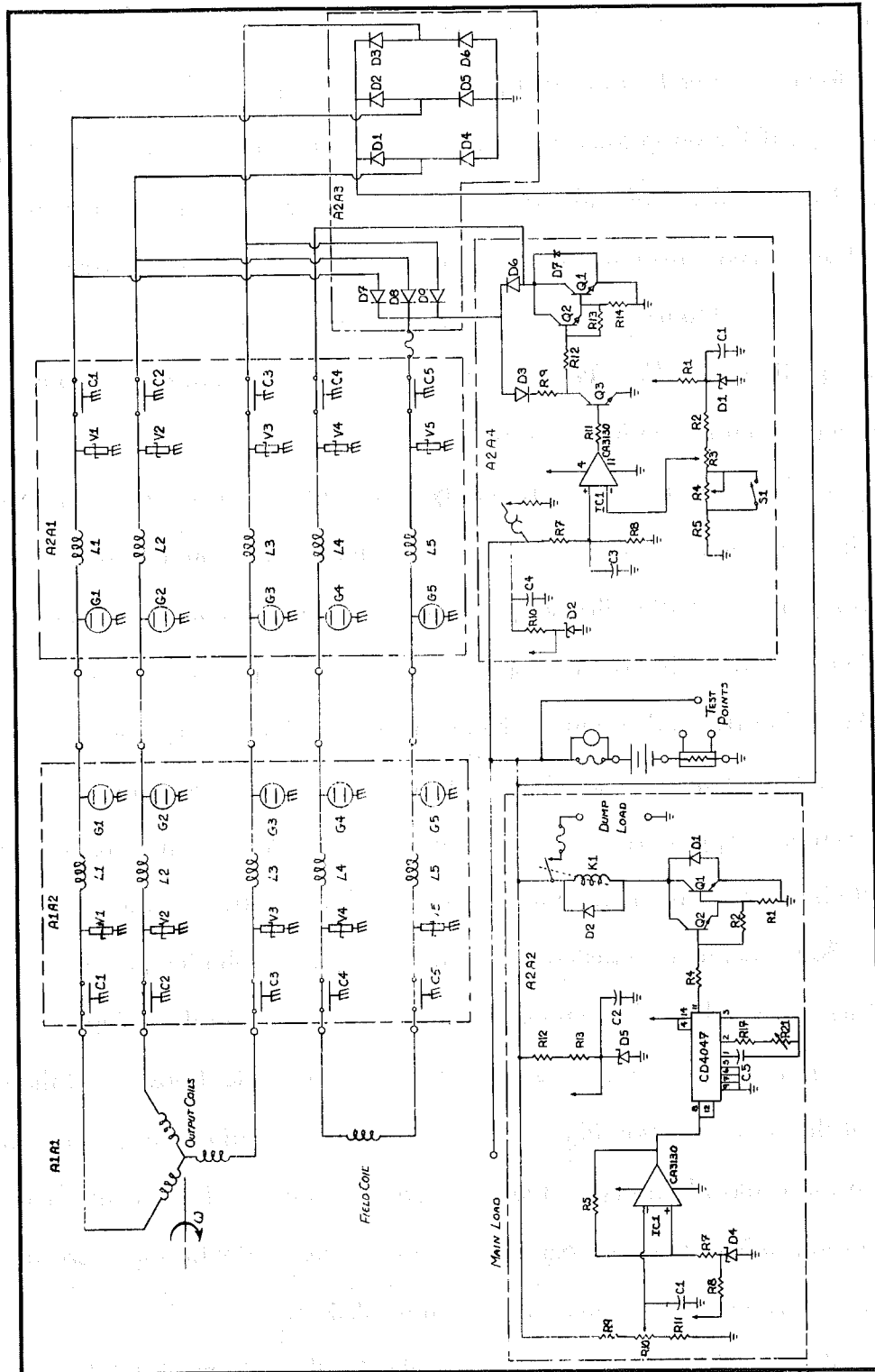


Figure 3-24. Revised Electrical System Circuit Diagram.

dump load. Therefore, a higher power level design was investigated. It was determined that higher power levels were unfeasible due to the unavailability of high quality power rectifiers. This unavailability resulted in unacceptable MTBFs (in excess of 9 failures per  $10^6$  hours of operation for power rectifier alone); therefore, a 1-kW power level design was adopted (see Subsection 2.3).

### 3.2.2 SELECTED DESIGN

The selected electrical system design for a 1-kW high-reliability SWECS is shown in Figure 3-25. It consists of the following subassemblies:

<u>Designation</u>	<u>Subassembly</u>
A1A1	Alternator
A1A2	Transient Suppressor (Tower)
A2A1	RFI Filter and Transient Suppressor (Control Building)
A2A2	Voltage Controlled Relay (Dump Load)
A2A3	Rectifier
A2A4	Voltage Limiter Control (Regulator)

#### 3.2.2.1 ALTERNATOR

The alternator is a three phase, wye-connected, eight pole, switched reluctance device (see Figure 3-26 and Table 3-2). Both the field coil and output coils are stationary. The flux is produced by a varying air gap. This configuration provides a simple design which has only one moving part (the rotor) and is efficient as the magnetic field responsible for producing the flux is unidirectional, thus minimizing eddy current losses. The alternator mechanism is internally insulated from its casing. The basic characteristics of the NPI alternator are compared to similar alternators in Figure 3-27.

A preliminary investigation of the alternator operation was made in order to develop an analytical model. It was determined that the theory to characterize

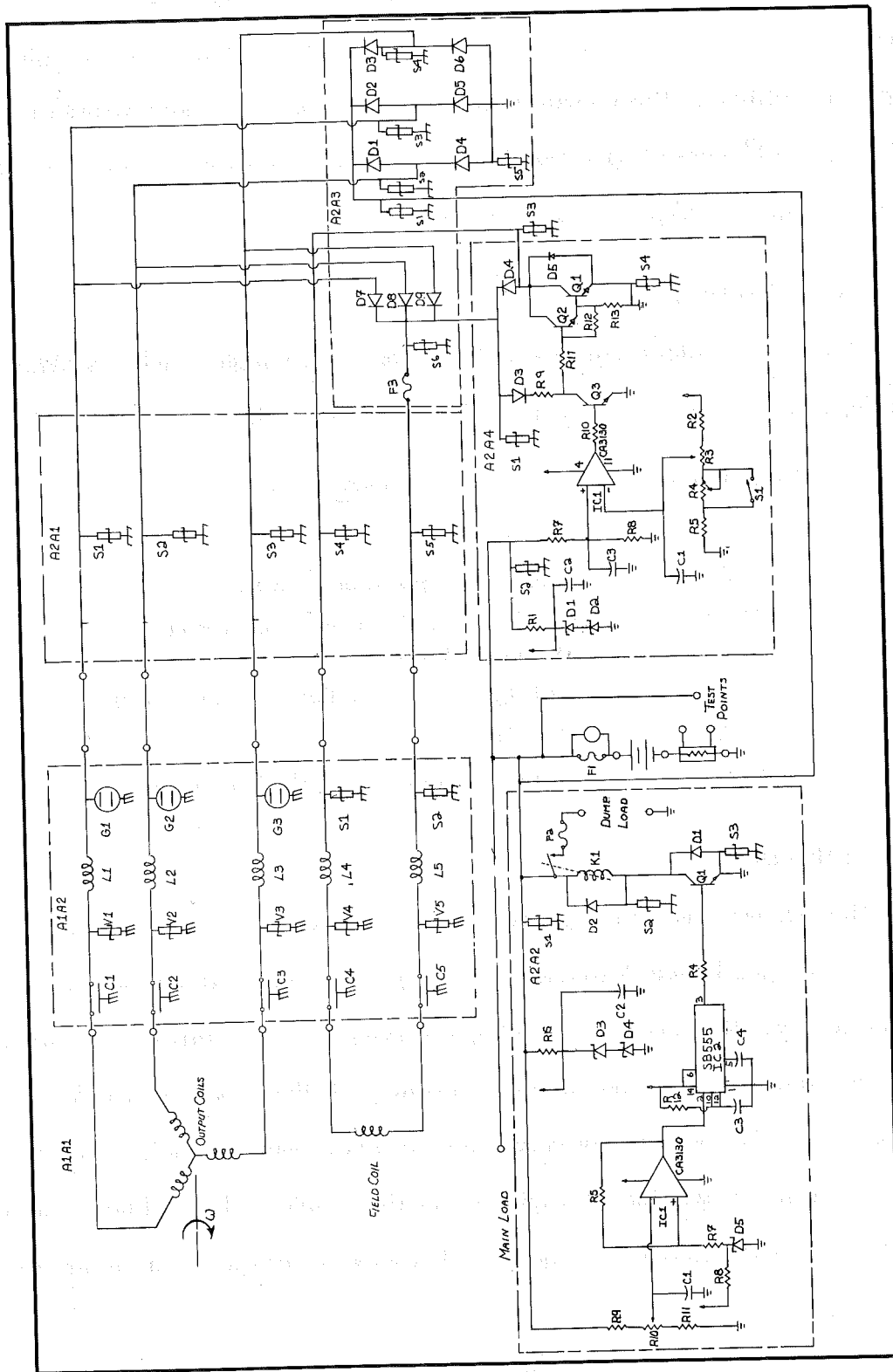
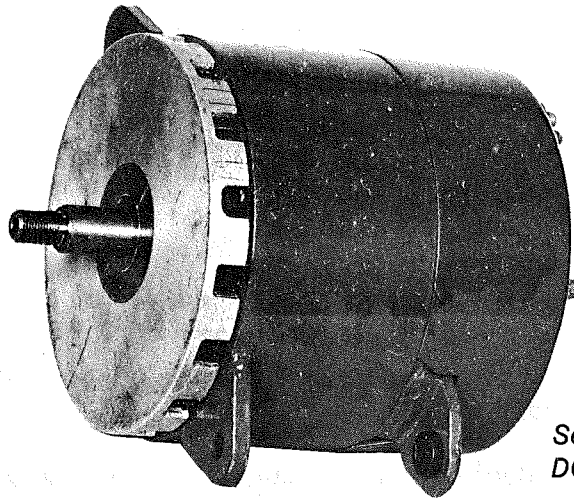
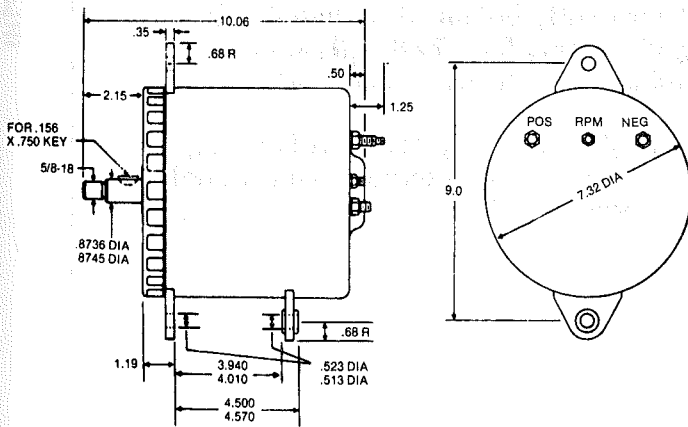


Figure 3-25. Selected Electrical System Circuit Diagram.



Series C25  
DC Alternator

OUTLINE DRAWING



CONSTRUCTION

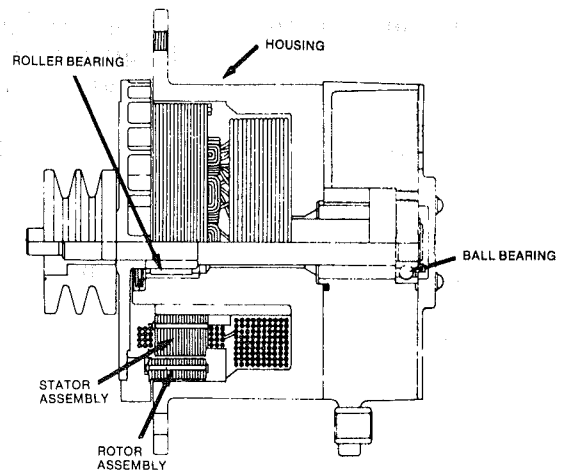
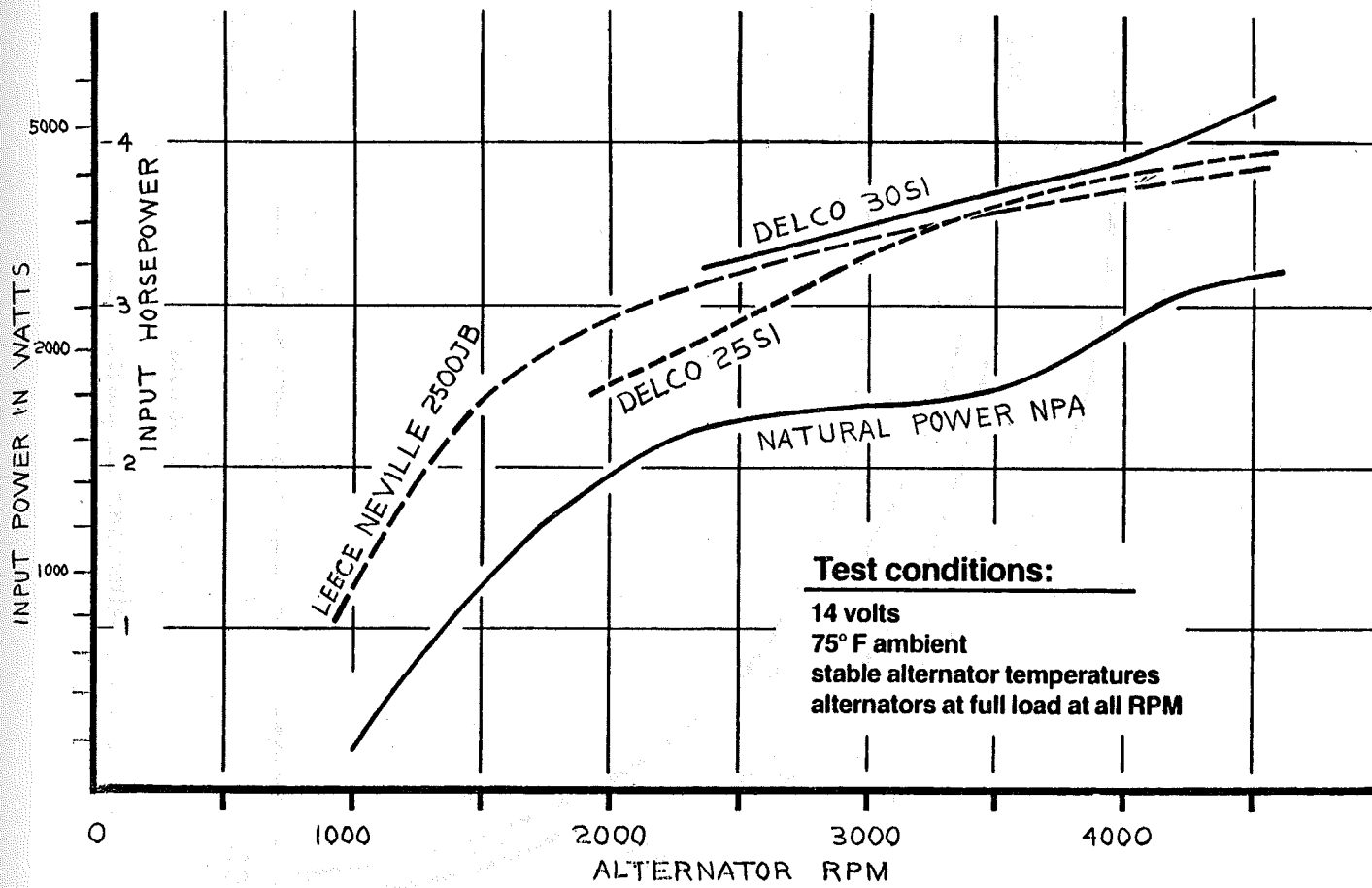


Figure 3-26, NPI 1-kW High-Reliability Alternator.

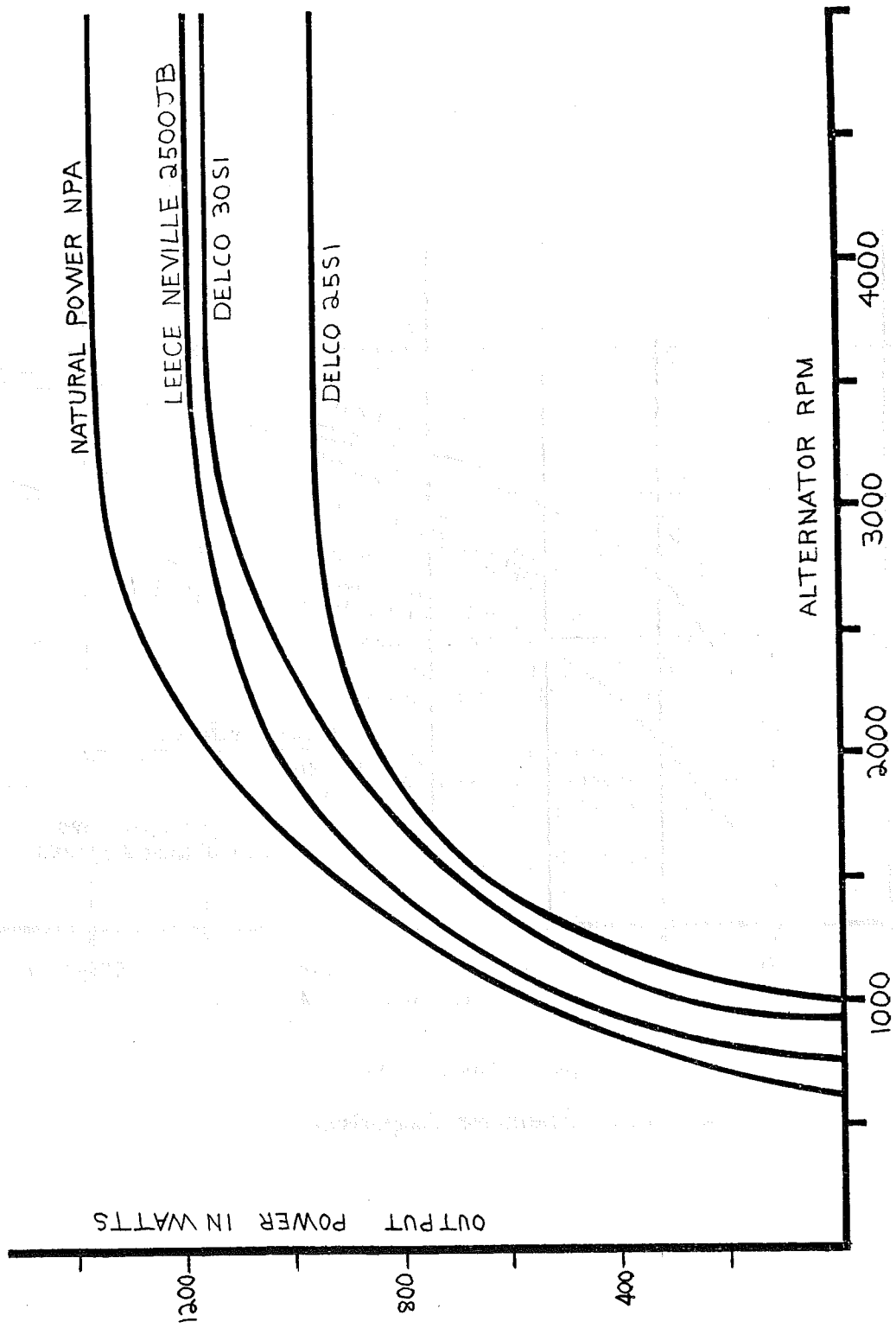
Table 3-2. NPI Alternator Specifications.

Specifications	Description
Output Voltage	24V DC.
Operating Range	700 RPM to 5,000 RPM normal (allowable operation to 10,000 RPM), either CW or CCW.
Temperature Range	-94° to +180°F.
Contaminants	Normal operation in adverse atmospheres such as salt and dust.
Housing	Steel with heavy-duty steel mounting ears.
Stator Coil Assembly	3-phase generating windings mounted on 12-tooth laminated stator core; generating and excitation windings remain stationary in the housing and are impregnated and sealed after assembly.
Low Inertia Rotor	Lightweight, dynamically balanced including cast aluminum integral cooling fan, 7/8" diameter shaft, and a flux-switching 8-tooth laminated stack.
Bearings	Heavy-duty front roller bearing, rear ball bearing, continuous 2.6 cu. in. grease reservoir, and a single Teflon double lip grease seal.
Weight	35 lbs.



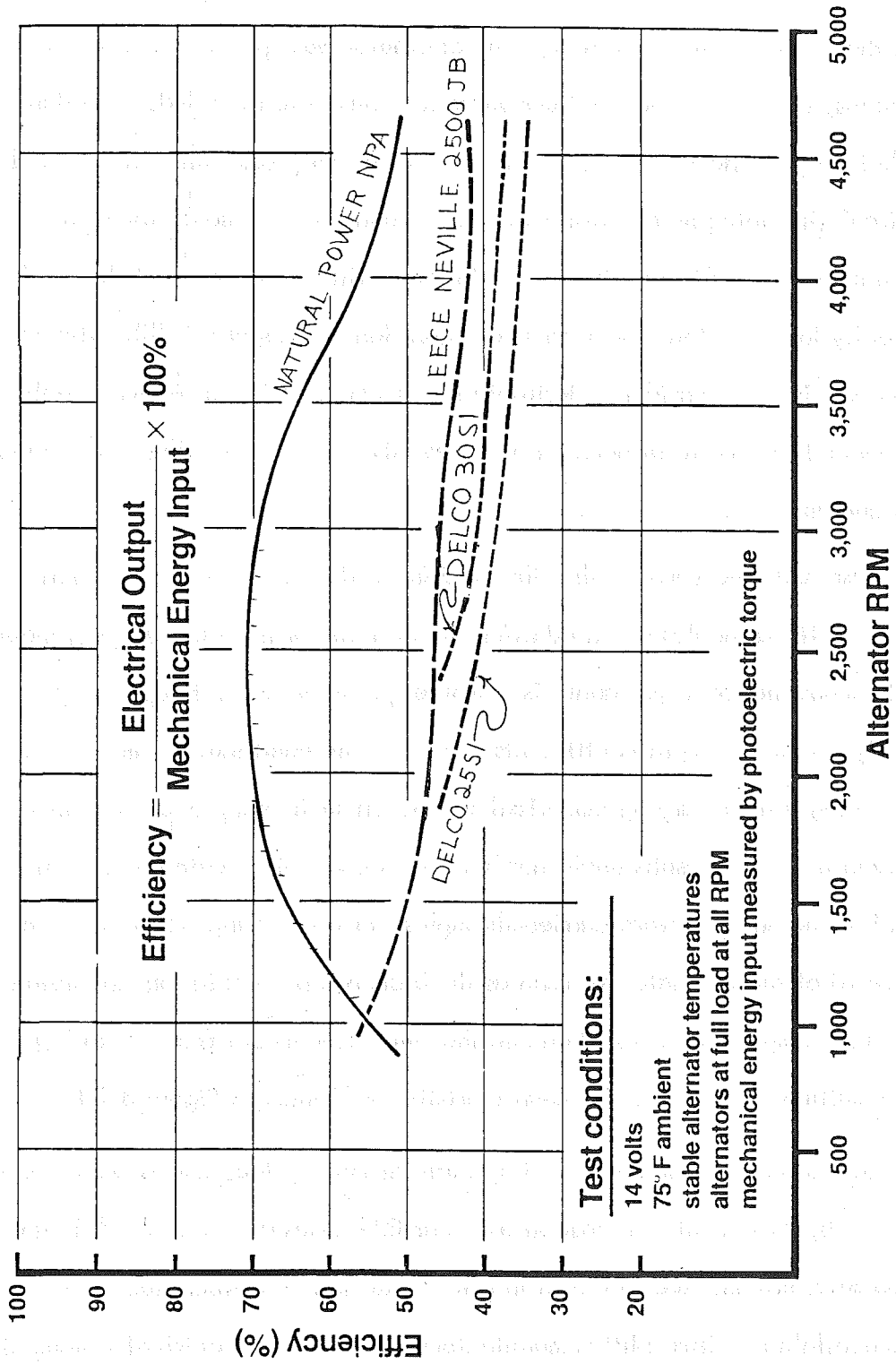
a) Horsepower Comparison

Figure 3-27. Alternator Comparison.



b) Power Curve Comparison

Figure 3-27. Alternator Comparison (Continued).



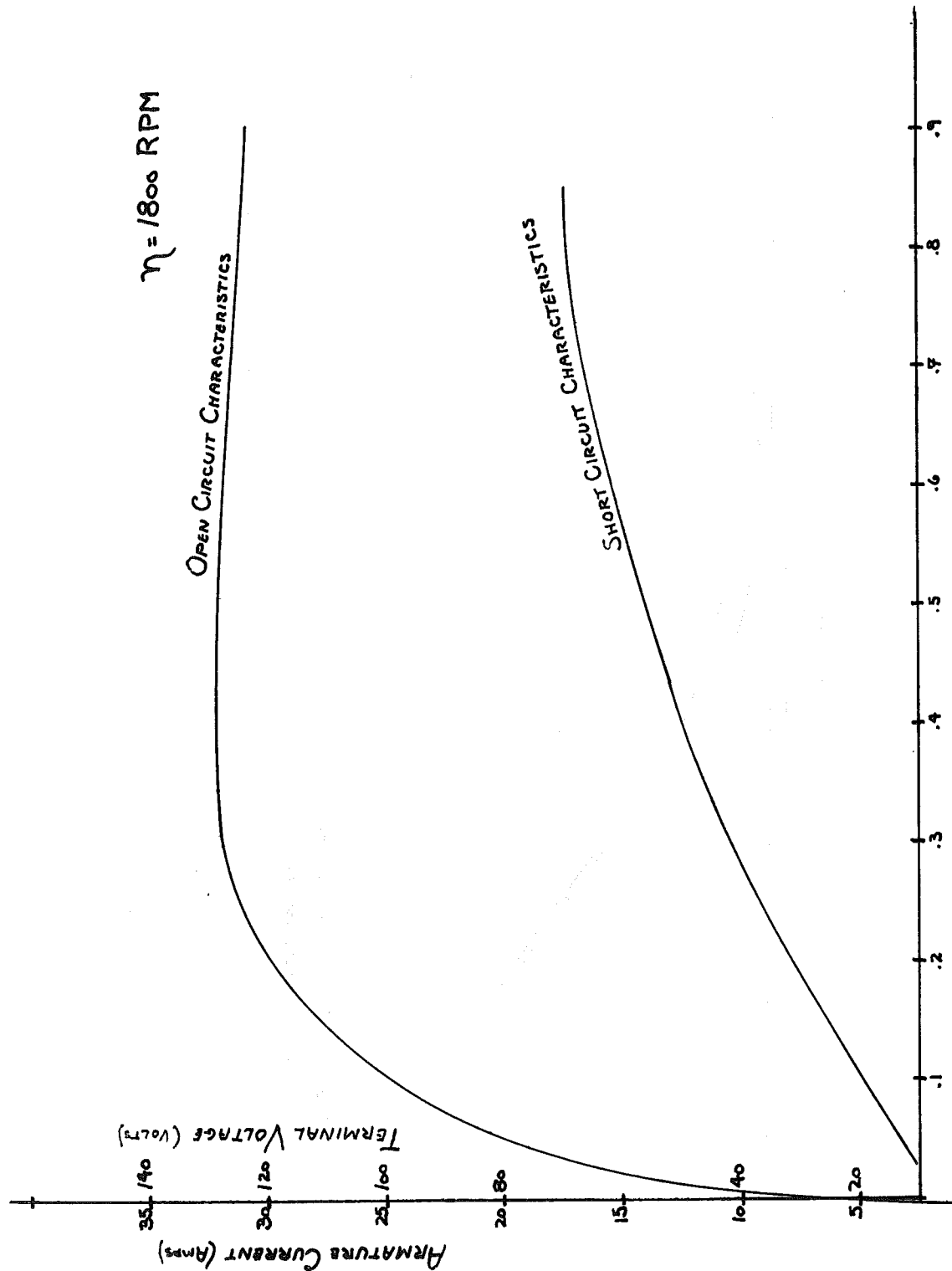
c) Efficiency Comparison

Figure 3-27. Alternator Comparison (Concluded).

the operation of this type of machine had little historical background and was not well developed. Tests were made to obtain basic characteristic data to provide additional insight into the nature of the alternator. The alternator was operated at various loads and shaft speeds, and the voltage and current waveforms were recorded. The data indicated that, as the alternator neared its maximum output, commutation occurred such that circulating interphase currents occurred when three or more diodes in the power rectifiers were simultaneously forward biased. This served to limit the maximum current capacity for the alternator in this configuration (see Figure 3-28). This current limiting characteristic is considered desirable for this application as it limits fault currents to about 120 percent of nominal and prevents excessive heating of the battery due to high charge rates.

These test data verified that the machine is dominated by nonlinearities which precluded linear analysis. In addition, the alternator has time-varying inductances which means that transient analysis computer programs are not applicable since they generally require constant coefficients. It was concluded that the machine must be analyzed using a time-varying numerical simulation such as a piece-wise linear analysis. Even then, the results might not bear good correlation with observed performance unless the analysis were carried through several modeling iterations. Therefore, a curve fit of the test data was used as the basis of all calculations involving the alternator. Comparison of test data and the simulation model is shown in Figure 3-29. The resulting computer model characteristics are shown in Figure 3-30.

The alternator is manufactured by Natural Power, Inc. and is wound on a frame produced by Maremont Corporation for their E95 series alternators. A large number of these alternators are in use in the field and limited information regarding failures was available. Since NPI is manufacturing a different electrical system, the data for the power rectifiers and voltage regulator were not useful; however, bearing



Field Current (Amps)

Figure 3-28. NPI Alternator Characteristics.

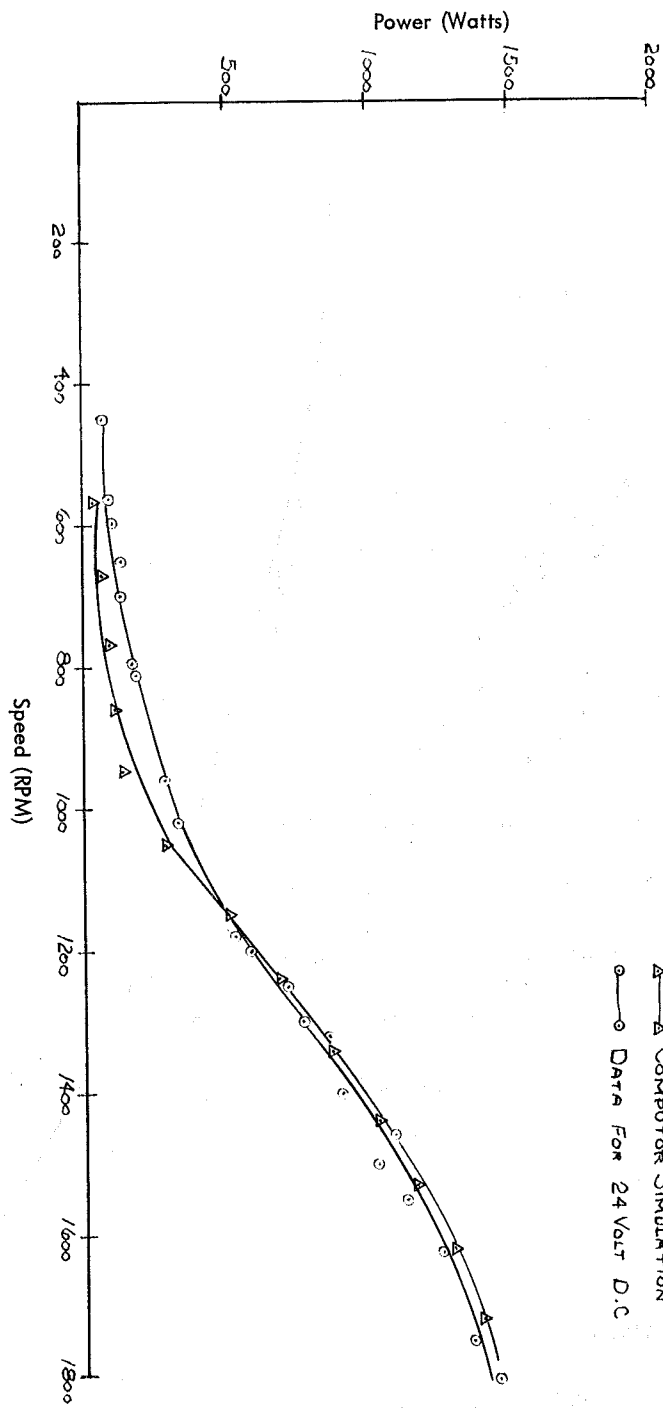
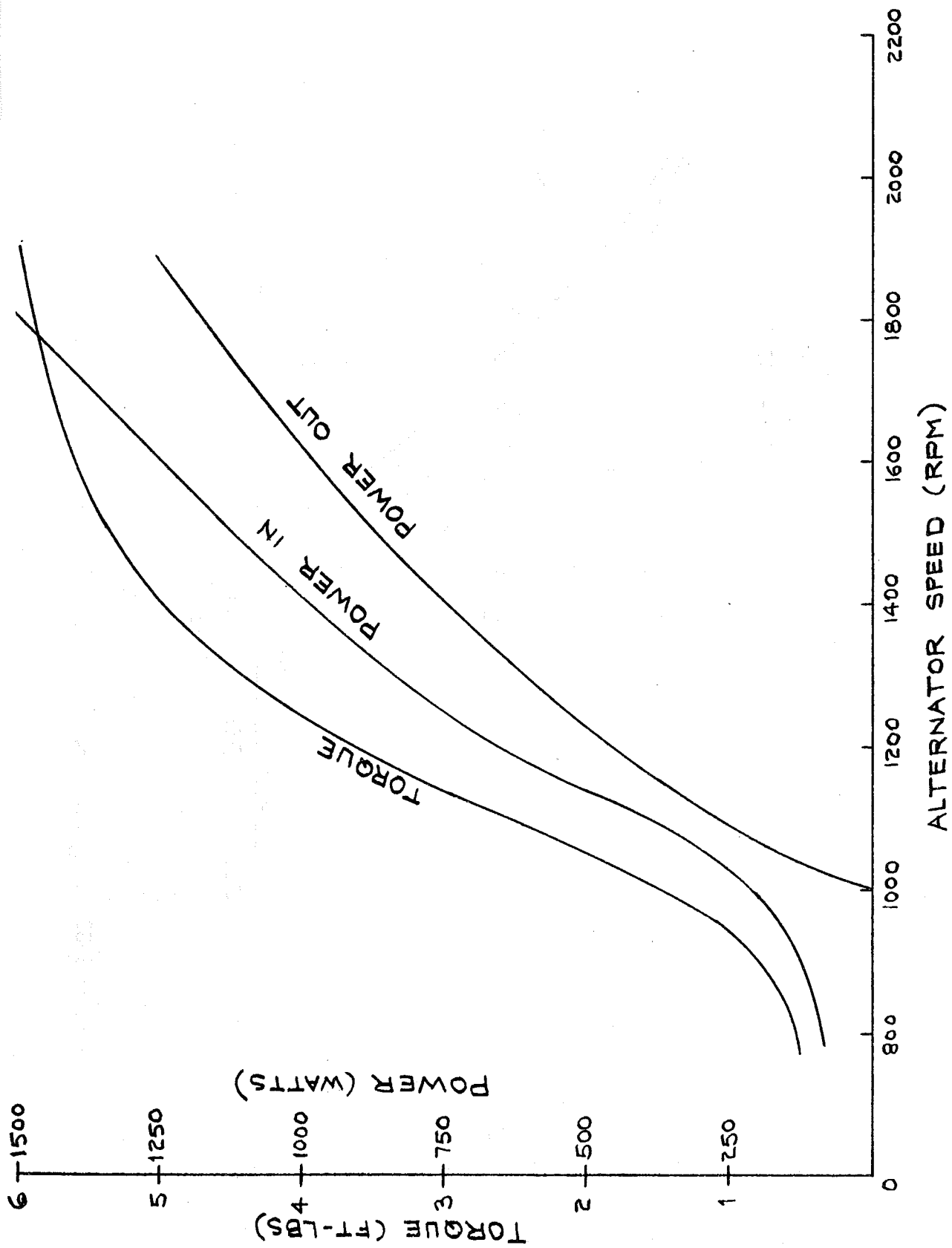
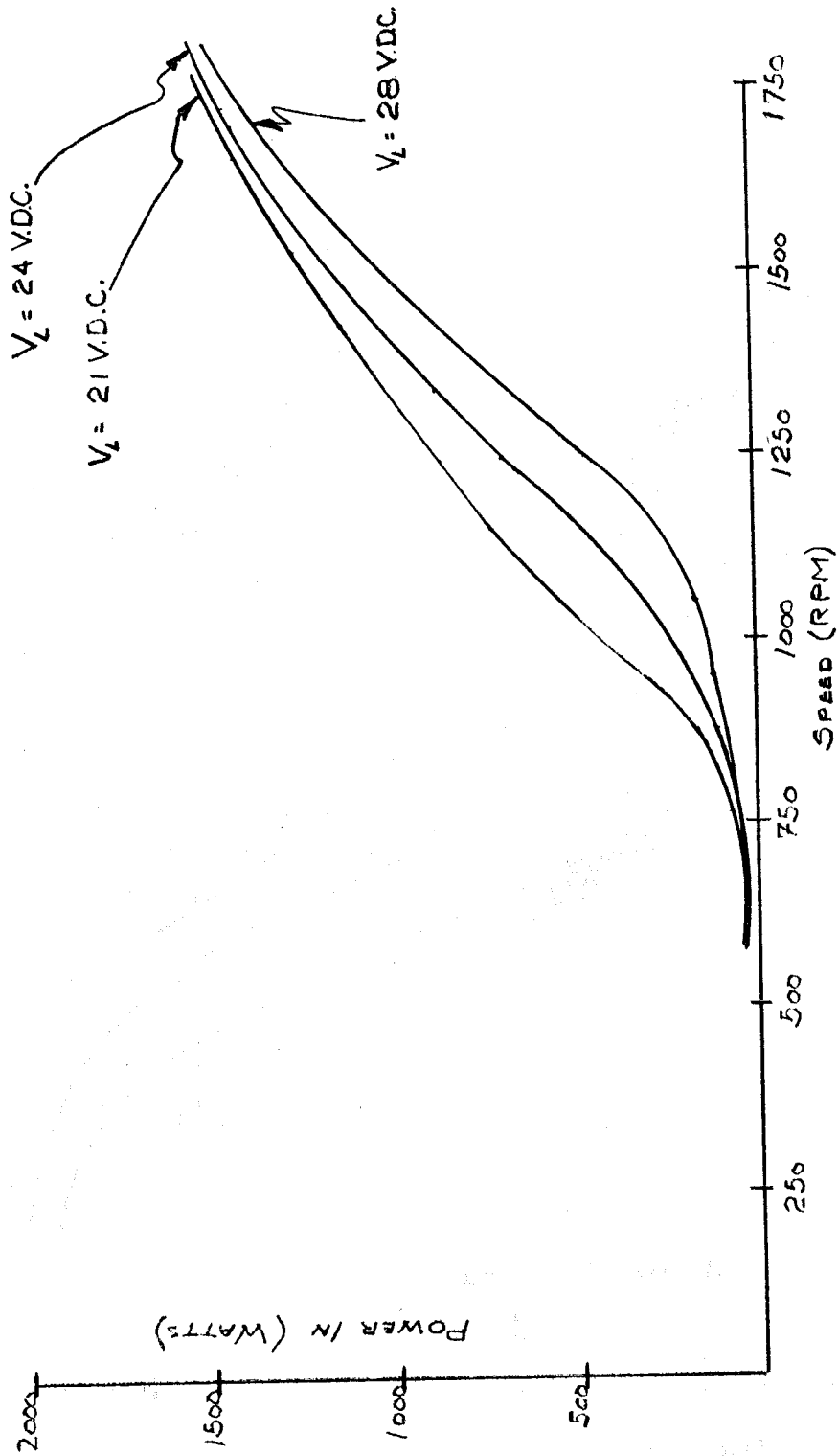


Figure 3-29. Comparison of 1-kW Alternator Test Data and Curve Fit.



a) Torque and Power

Figure 3-30. Computer Model Characteristics of 1-kW Alternator.



b) Performance

Figure 3-30. Computer Model Characteristics of 1-kW Alternator (Concluded).

data were applicable. It was determined that the forward bearing had an unacceptable MTBF for the SWECS application and, therefore, it was replaced with a higher quality bearing (see Subsection 6.3.3.1).

### 3.2.2.2 MAIN CONTROL BOX

The main control box contains the main power rectifier, voltage regulator, fusing and a connection panel and troubleshooting test points as shown in Figure 3-31.

It was decided to locate the main control panel in the control building to shelter it from temperature extremes. Also, the control panel and its associated electronics can be better protected from lightning by locating it on the ground and it would not be subjected to vibration from the SWECS operation.

The power rectifier consists of six rectifiers to convert the three phase AC power from the alternator to DC (components D1 to D6 in subassembly A2A3 of Figure 3-25). The output of the rectifier is 1250 watts at 48 amps. Each rectifier element must handle 80 percent of the full output current due to the commutation characteristics of the chosen switched reluctance alternator. The power rectifier proved to be the principal reliability driver for the electrical system (see discussion in Subsection 2.3). In addition, if a 25°C temperature rise over ambient is assumed for the power rectifier, then the stress level must be kept at or below 60 percent for the device to operate at an ambient of 60°C without the device overheating. As a result of numerous calculations relative to reliability, stress level and cost, it was concluded that the best solution for a maximum power conversion of 1300 watts was six 1N3289 diodes, as this would be a simple and least expensive approach even though the reliability was somewhat lower than other configurations.

The voltage regulator is included to monitor the battery voltage and reduce the power output of the alternator should it sense the battery is approaching full charge.

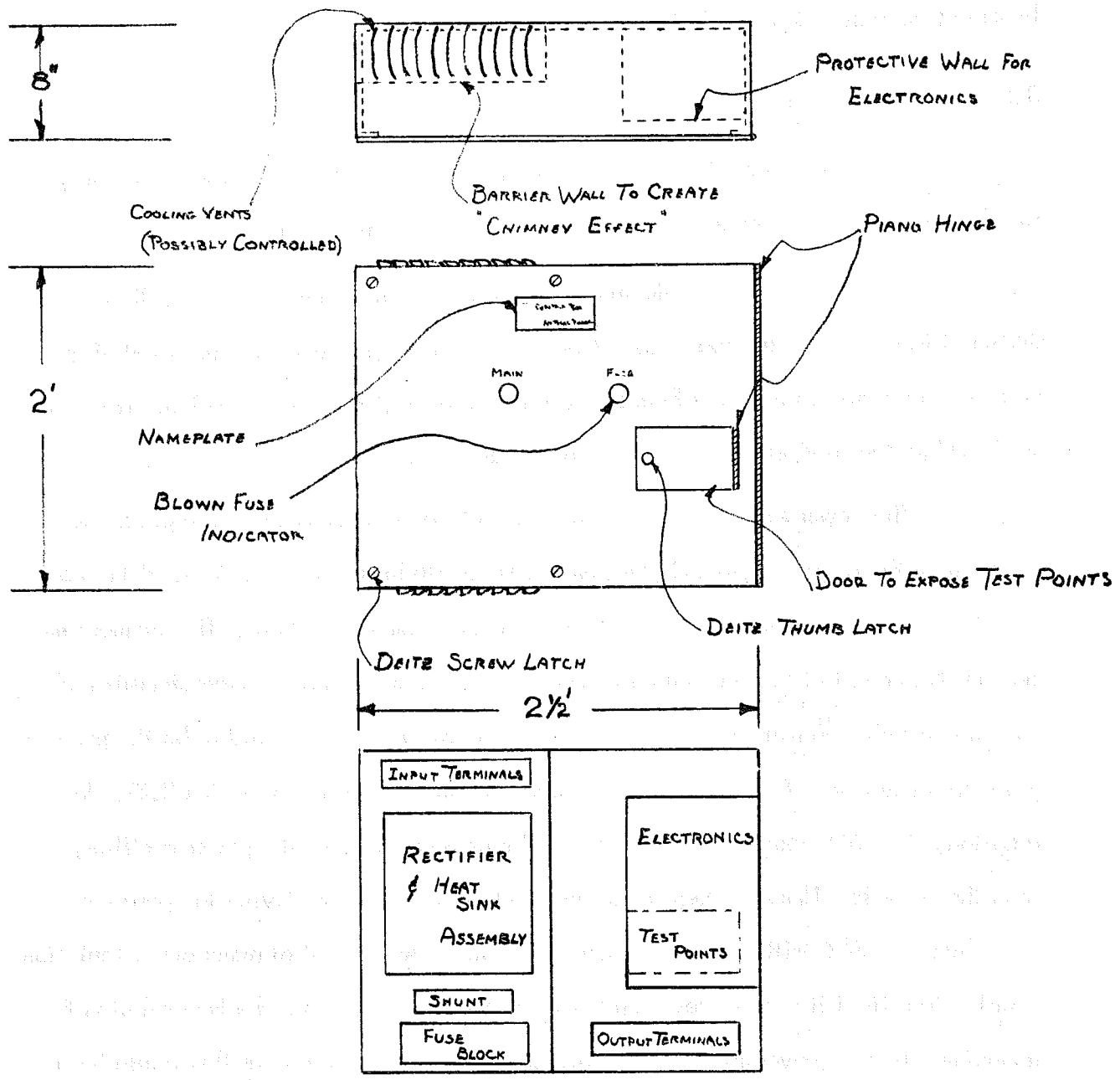


Figure 3-31. Main Control Box Layout.

It does this by varying the average current to the field of the alternator. The field coil of the alternator has a very large inductance which resists instantaneous changes in current. The voltage regulator senses the battery voltage which, if it exceeds its limit of 26.4V DC in its normal mode or 28V DC in the equalizer overcharge mode, it turns the field current off completely; that is, the alternator is no longer supplying power and the turbine is running unloaded.

The circuit is arranged so that a current may circulate through diode rectifier D4 in Subassembly A2A4 (Figure 3-25), even when the pass transistors Q1 and Q2 are cut off until all the energy stored in the coil is dissipated. Thus, the pass transistor is operated in a switching mode allowing an efficient and cool running design. The alternator current will then fall off with a time constant dictated by the inductance and resistance of the field coil. It is thereby possible to control the voltage at the battery pack with a fairly simple circuit.

Since the battery voltage needs to be precisely regulated and not the generator voltage, the regulator is mounted near the battery in the control building so that voltage drops in the transmission line (which are dependent on the charge rate) are not "seen" by the voltage regulator. A voltage regulator mounted atop the tower will begin reducing battery voltage before the battery is fully charged thus spilling valuable energy.

The regulator is configured so that the field circuit is always completed and is only turned off when an overvoltage condition is experienced. This could allow a few extra weeks of operation should part of the regulator fail before a repair crew could remedy the situation. It is also designed so that the machine will self excite. The field circuit has a separate power supply (diode rectifiers D7 to D9 in Subassembly A2A3, Figure 3-25), and is independent of the battery. The system will self excite even when the battery is low and requires only a few milliamperes of stand-by current.

The dump load ensures the wind turbine operates under load. Its main function is to activate an auxiliary load when it senses the battery voltage above a preset level. The auxiliary load could be a resistance heater to help heat the battery pack in the winter or a secondary battery pack to power a secondary transmitter. The dump load also provides the wind turbine with full load even though the battery pack may be fully charged. This will help to reduce cycling of the turbine overspeed control. In order to avoid switching discontinuities, the alternator remains connected to the batteries even when the dump load circuit is operative.

As shown in Figure 3-25, a current shunt is included in the main control box to attach a meter to monitor battery current and a plug to monitor battery voltage. In addition, there are three fuses all mounted on extractors. These serve dual purposes as switches. It was felt imperative to protect workers from the high energy in the battery pack should a short circuit occur in the battery system and also to provide a means of completely shutting the system down electrically without climbing the tower. They are included for the above reason even though they reduce the reliability of the system.

### 3.2.2.3 TRANSIENT SUPPRESSION

Since the SWECS will likely be installed in locations where lightning strikes are probable, protection of the electrical and mechanical systems is vital. Indirect strikes in the near area probably present the greatest hazard to the machine. This is because high voltage gradients may be generated by lightning seeking the path of least resistance to ground, which may cause high potential differences between different parts of the machine, i.e., tower and control building. The resultant currents are not as intense as those generated by a direct strike, but they are more likely as lightning energy may be brought into the area along tree roots and streams. Direct

strikes have a much higher energy content, but are less likely. In the event of a direct strike, the bolt will be attracted to a lightning rod atop the turbine. There will also be a cable connecting the frame of the wind turbine to a ground rod at the tower base. No sliprings have been included to bypass bearings in the turbine itself.

Due to the transient nature of the lightning strike, inductance is the dominant circuit element in the system including the tower and the rotor. While it is possible to provide the lightning with a very low resistance path to ground, the inductance of the path may not be much different than that through a bearing and through the tower structure to ground. However, a solid ground is provided since it is relatively simple and will help to prevent damage to tower joints.

The initial design had two identical transient suppression networks for lightning protection. One was placed near the alternator on the tower (Figure 3-23). This was to deter lightning-induced energy from entering the alternator. The second was placed near the transmission cable entrance to the control building. The unit placed near the control building was to deter unwanted energy from entering the control building. The circuitry also included a low pass filter to prevent radio frequency interference from the power system.

The circuitry consisted of a through-pass capacitor, a metal oxide varistor (MOV), an inductor and a spark gap (see Figure 3-22). The inductor appears as a high impedance to waveforms with fast rise times. The energy thus diverted was then directed through a spark gap to ground. The spark gap was used as it provides a low impedance to ground after it has fired and has a high current capacity. The MOV clamped the other terminal at a safe voltage while the inductor and capacitor formed a low pass filter to prevent RFI during normal operation. The capacitor also helped to clamp the protected side of the assembly (alternator and main control box) at a safe voltage as the capacitor will not allow a rapid change in voltage across its terminals.

The transient suppression networks were modified after a review of the design at a high voltage test laboratory. The basic design of the alternator protection was satisfactory; however, the spark gaps were replaced with thyrite surge suppressors for the control building lightning protection. This was to provide slightly faster clamping action. All semiconductor circuitry was provided with silicon-type surge suppressors wherever cables enter the main control box and for each input to the voltage regulator and dump load circuit boards. Also, since the inductance of the cable connecting the main control box to the lightning protection network for the main control building was larger than the lumped inductor in that network, the inductor was deleted. Finally, all equipment is housed in steel boxes with phosphor bronze gaskets to act as a shield for the magnetic field associated with strong electric currents.

## SECTION 4

### ANALYSIS

A broad base of design knowledge exists for the classical horizontal-axis wind machine gained through refinement of applicable propeller theory, extensive development effort, and testing of units in the field. However, the design and analysis techniques developed for these machines are not directly applicable to the vertical-axis wind machine because of basic differences in configuration. Theoretical investigations of the aerodynamic and performance characteristics of the vertical-axis Darrieus wind machine have been made (References 9 and 10) and wind tunnel tests have been conducted to verify and to supplement the analyses (Reference 11); but these results and techniques are also of limited use because of differences in configuration.

The vertical-axis Cycloturbine is a relatively new concept which differs from the Darrieus rotor in that its blades are straight and do not remain at a fixed angle, but follow a preset schedule of pitch angle change. These conditions have necessitated the development of an aerodynamic analysis specially designed for the Cycloturbine configuration. This analysis is described in this section with particular application to the Cycloturbine performance and structural loads and stresses. In addition, analysis of certain aspects of the Cycloturbine dynamics is also described. A list of symbols is included as Appendix A.

Initially, all analyses were developed using the approximation that the turbine blades operate at small angles, and that the blade aerodynamics could be described with a constant lift curve slope and a constant drag coefficient. These assumptions allowed closed form solutions to be obtained which facilitated insight into the physical nature of the results. The intent of the analyses had been to make calculations at selected design points; however, it was found to be convenient to computerize the analyses. This permitted far more extensive calculations to be made.

Subsequently, the analyses were modified to include a more accurate representation of drag coefficient, that is, as a function of angle of attack. Lift was also described as a function of angle of attack, and because the analyses were done numerically, the small angle approximation was no longer used (although it was proven to be valid).

#### 4.1 BLADE LOADING

The aerodynamic forces generated on a blade element are the lift and drag. Consider a vertical-axis, constant radius turbine blade rotating with velocity  $\Omega$  about its axis at point O as shown in Figure 4-1. The blade lift, neglecting unsteady non-circulatory and wake effects, is

$$L = \frac{1}{2} \rho U^2 C_L c l \quad (4-1)$$

where

$\rho$  = air density

$U$  = relative wind speed

$C_L$  = blade lift coefficient

$c$  = blade chord

$l$  = blade length

Similarly, the blade profile drag is

$$D = \frac{1}{2} \rho U^2 C_D c l \quad (4-2)$$

where  $C_D$  is the blade drag coefficient.

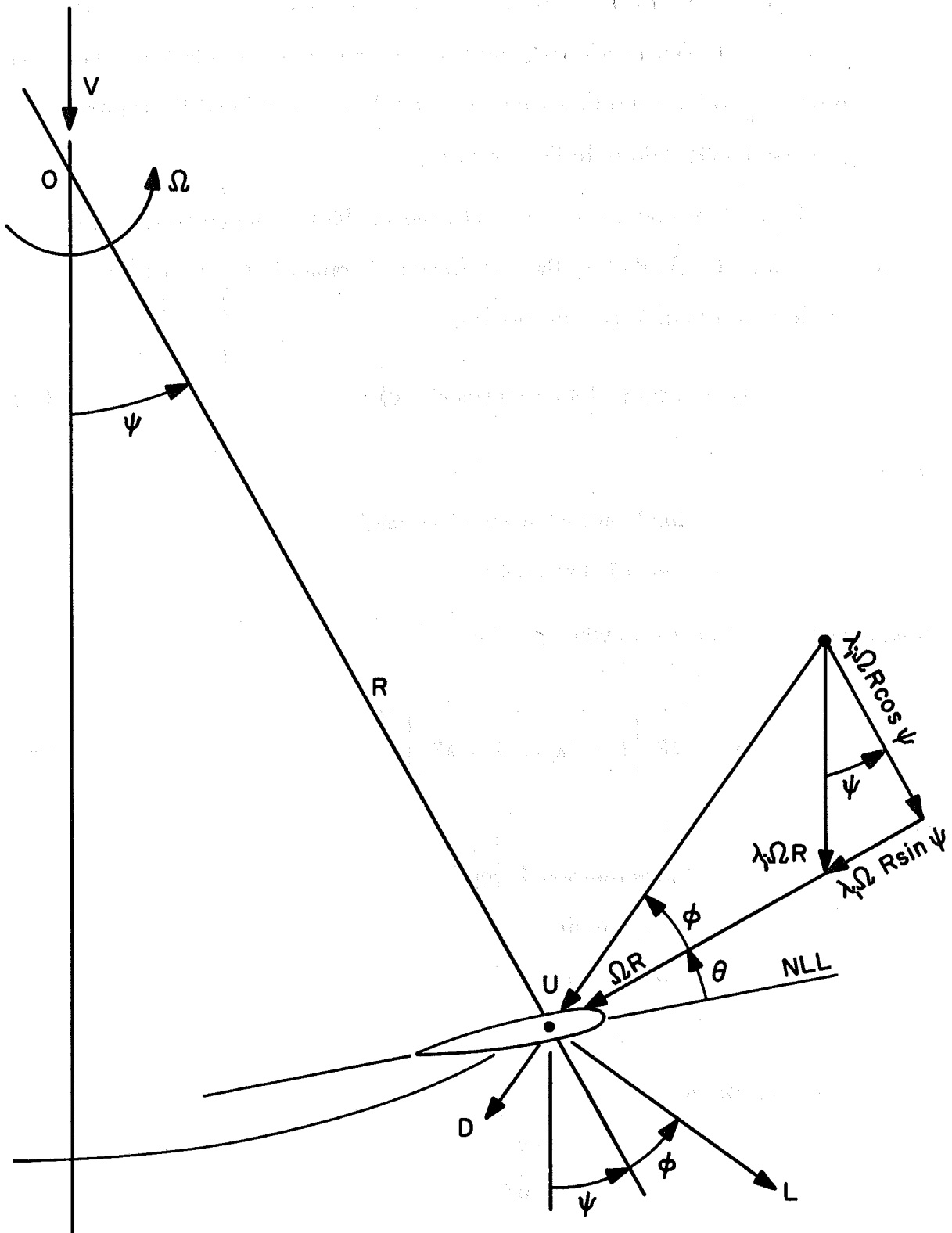


Figure 4-1. Turbine and Blade Geometry.

Both  $C_L$  and  $C_D$  are functions of the blade angle of attack,  $\alpha$ . These functions for the NACA 0015 airfoil (Reference 12) are shown in Figures 4-2 and 4-3. It is seen that  $C_L$  is largely a linear function of  $\alpha$  between -12 and 12 degrees, but that  $C_D$  varies greatly with  $\alpha$  in the same range.

The loads of interest for the blades are the forces tangent and perpendicular to the no-lift line (NLL), that is, the chordwise and normal forces on the blade element. The blade chordwise force is (see Figure 4-1)

$$C = L \sin(\theta + \phi) - D \cos(\theta + \phi) \quad (4-3)$$

where

$\theta$  = blade instantaneous pitch angle

$\phi$  = blade inflow angle

From Figure 4-1, the relative wind speed is

$$U = \Omega R \left[ 1 + 2\lambda_i \sin \psi + \lambda_i^2 \right]^{1/2} \quad (4-4)$$

where

$\Omega$  = blade rotational speed

$R$  = turbine radius

$\lambda_i$  = inflow ratio

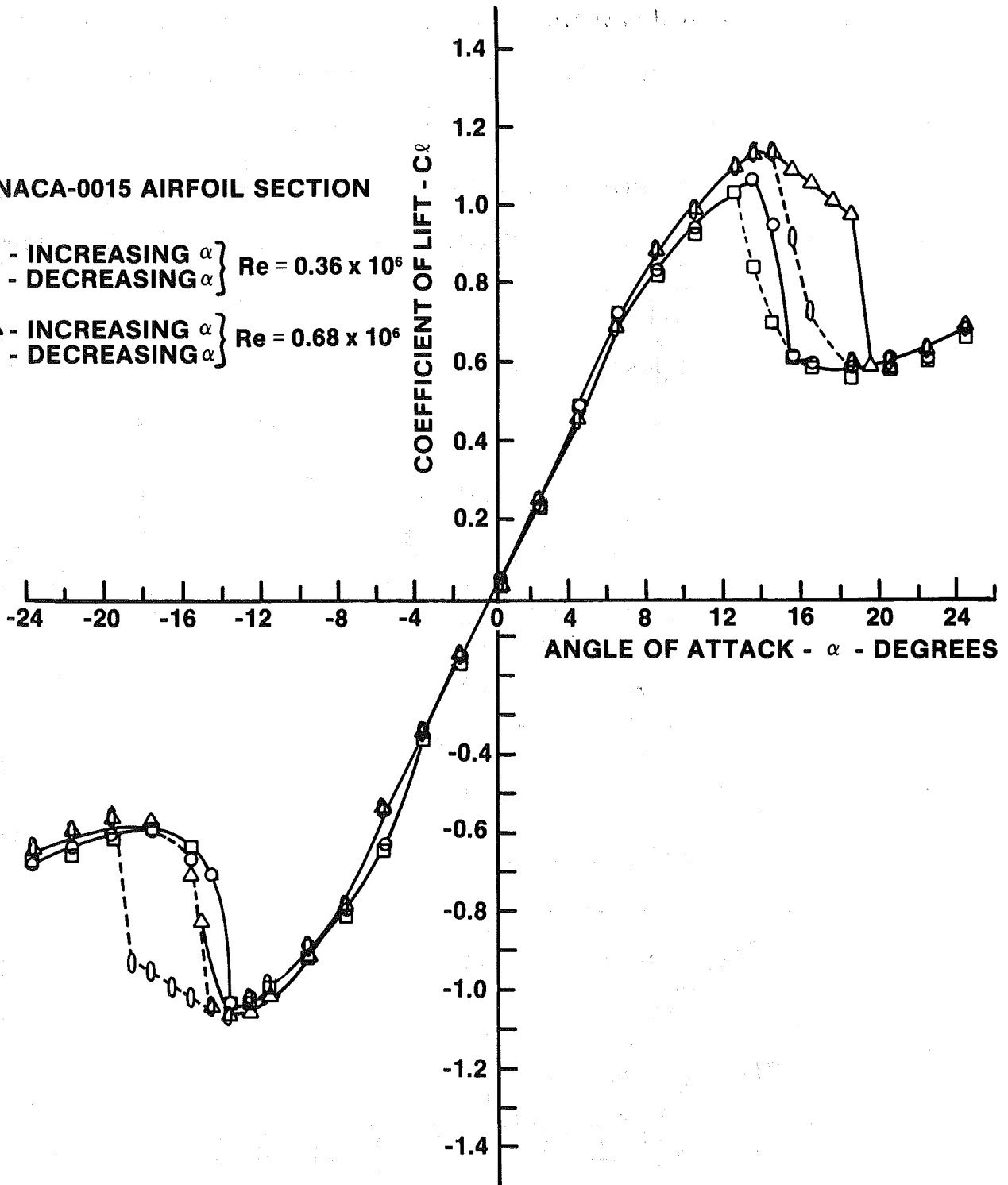
$\psi$  = azimuth angle

and the blade inflow angle,  $\phi$ , is

$$\phi = \tan^{-1} \frac{\lambda_i \cos \psi}{1 + \lambda_i \sin \psi} \quad (4-5)$$

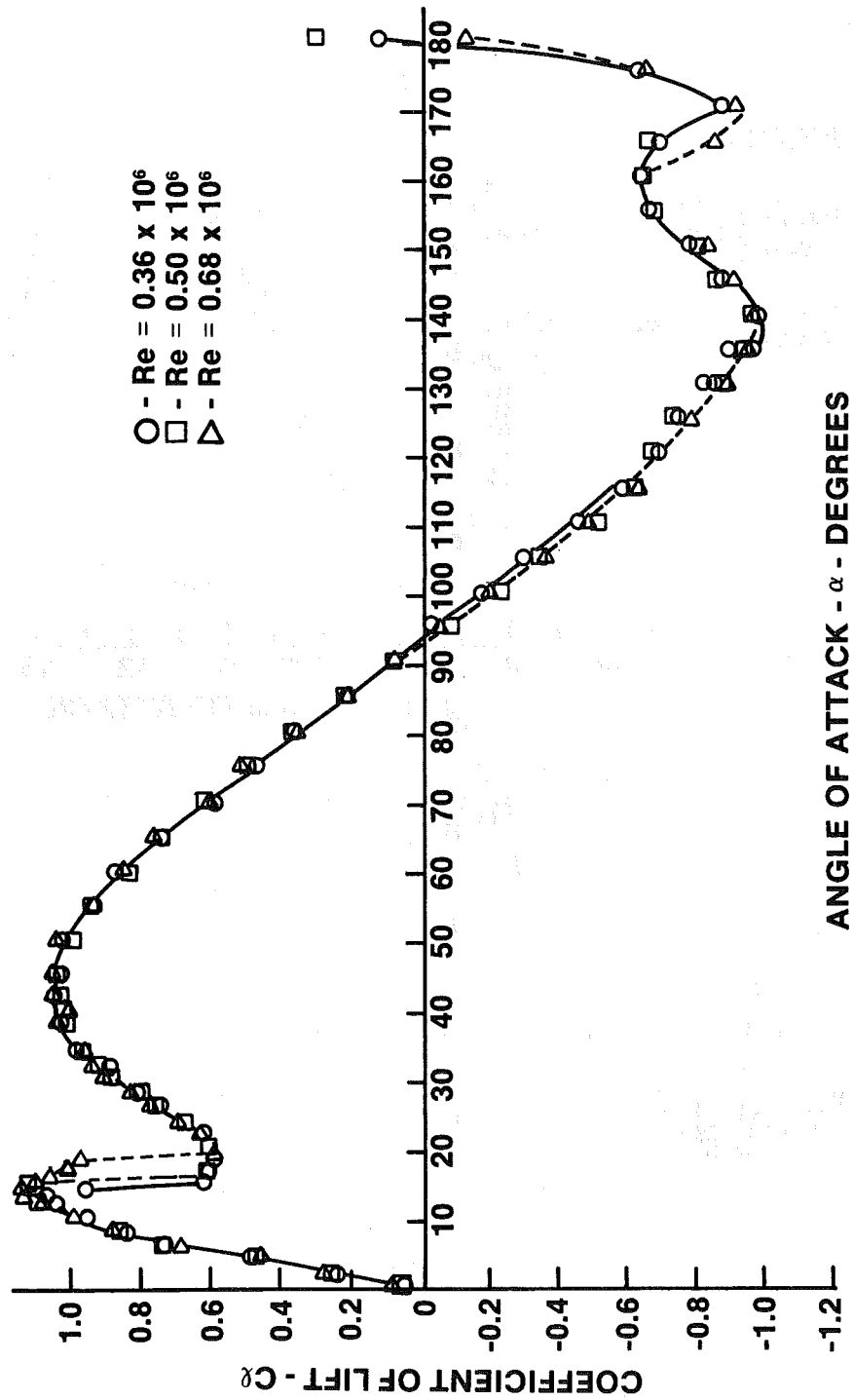
NACA-0015 AIRFOIL SECTION

- - INCREASING  $\alpha$  }  $Re = 0.36 \times 10^6$
- - DECREASING  $\alpha$  }
- △ - INCREASING  $\alpha$  }  $Re = 0.68 \times 10^6$
- ◊ - DECREASING  $\alpha$  }



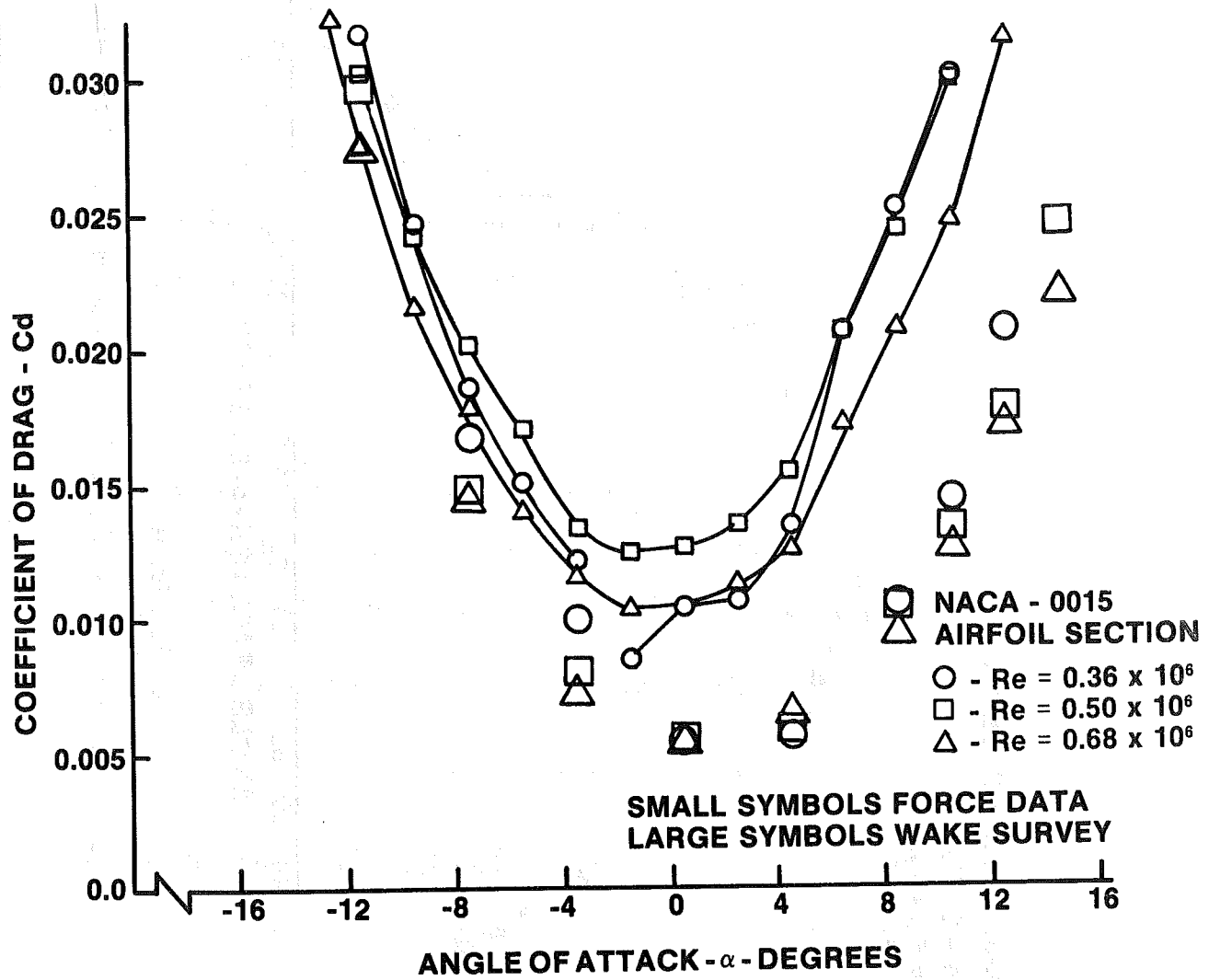
a) Normal Operating Range

Figure 4-2. Section Lift Coefficient for NACA 0015 Airfoil (Reference 12).



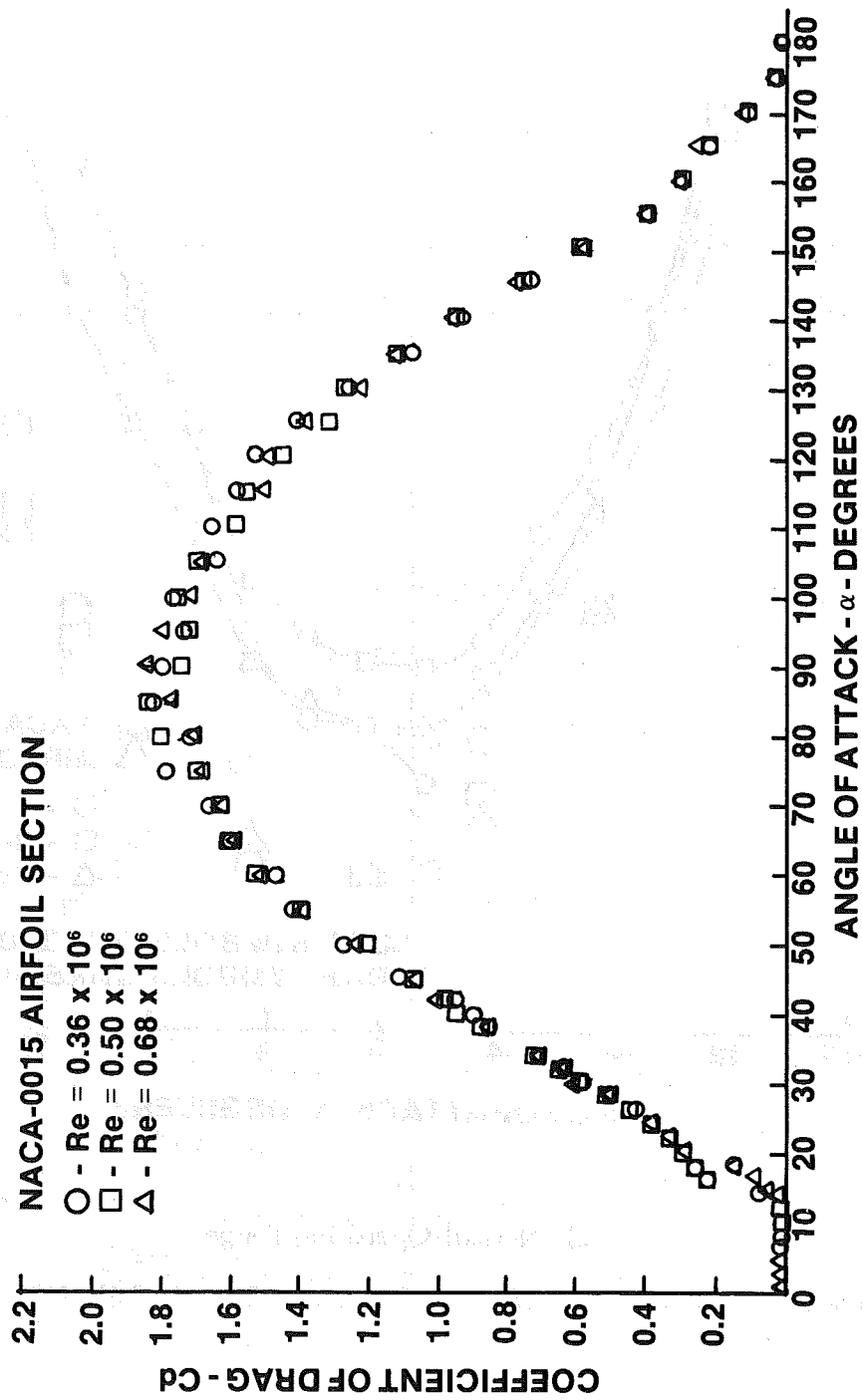
b) Full Range

Figure 4-2. Section Lift Coefficient for NACA 0015 Airfoil (Reference 12) (Concluded).



a) Normal Operating Range

Figure 4-3. Section Drag Coefficient for NACA 0015 Airfoil (Reference 12).



b) Full Range

Figure 4-3. Section Drag Coefficient for NACA 0015 Airfoil (Reference 12) (Concluded).

The pitch angle,  $\theta$ , is a controlled parameter. If  $\theta$  is sinusoidal as shown in Figure 4-4, then it can be expressed as

$$\theta = \theta_o + \theta_{1c} \cos \psi \quad (4-6)$$

where the collective pitch,  $\theta_o$ , and cyclic pitch,  $\theta_{1c}$  are fixed values.

Thus, the chordwise force,  $C$ , in addition to being a function of the airfoil type, the blade geometry, the air density, turbine radius and rotational speed is also a function of azimuth angle, and inflow ratio. The inflow ratio,  $\lambda_i$ , is given by

$$\lambda_i = \frac{V - v}{\Omega R} \quad (4-7)$$

where  $V$  is the wind speed and  $v$  is the inflow velocity which, as shown in Subsection 4.2, is a function of the turbine solidity. A typical history of the blade chordwise force for the Cycloturbine over one rotational cycle is shown in Figure 4-5a.

The blade normal force is (see Figure 4-1)

$$N = L \cos (\theta + \phi) + D \sin (\theta + \phi) \quad (4-8)$$

for which Equations (4-4), (4-5), (4-6) and (4-7) apply. A typical history of the blade normal force for the Cycloturbine over one rotational cycle is shown in Figure 4-5b.

To provide a general understanding of the operation of the Cycloturbine, the aerodynamic loading, i.e., normal force,  $\frac{dN}{d\ell}$ , and chordwise force,  $\frac{dC}{d\ell}$ , and the blade pitch schedule for a 12-ft Cycloturbine at various azimuth positions and various operating conditions (see Table 2-3) are presented in Figure 4-6. These results were obtained using Equations (4-3) and (4-8). The oscillatory blade aerodynamics at normal operating condition,  $V = 20$  mph, are shown in Figure 4-6a.

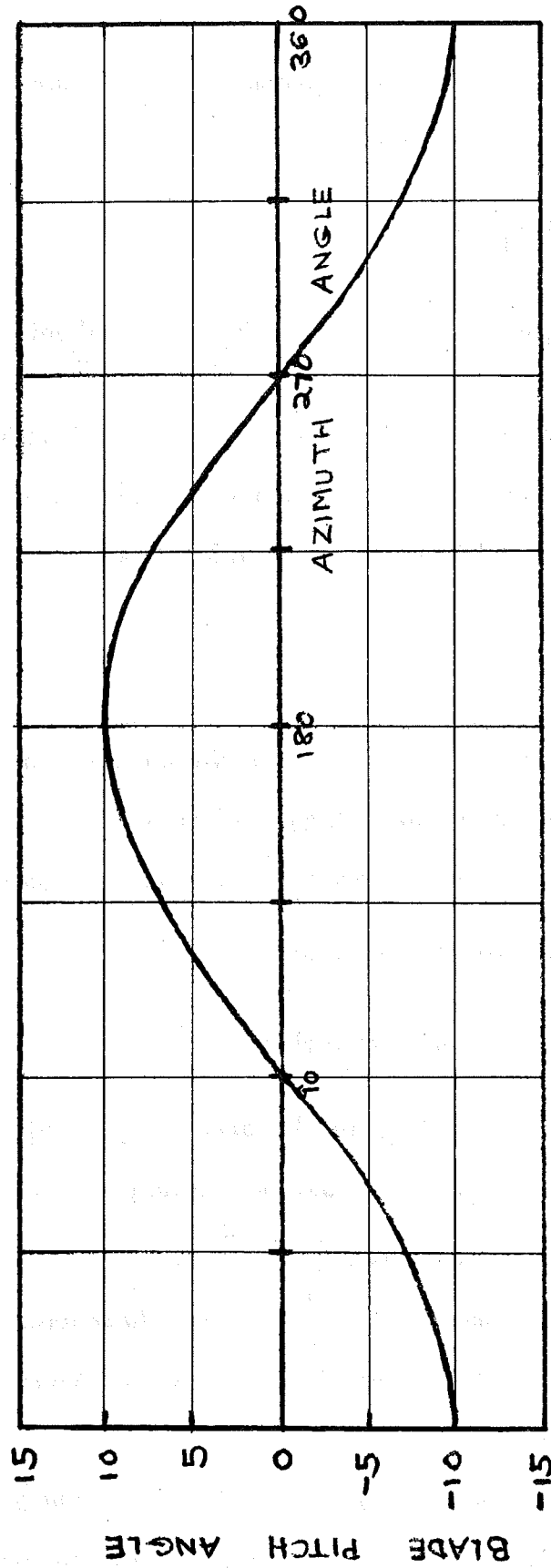
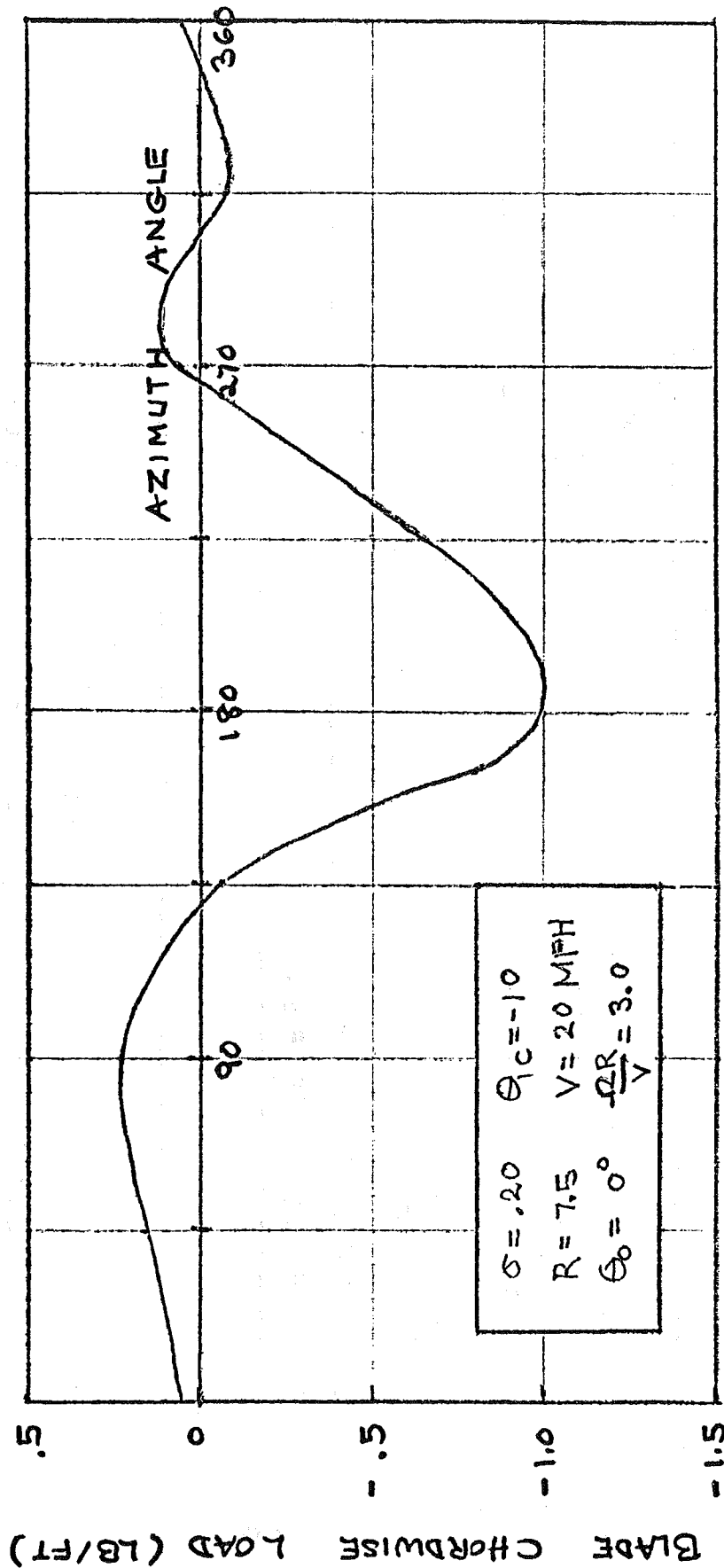
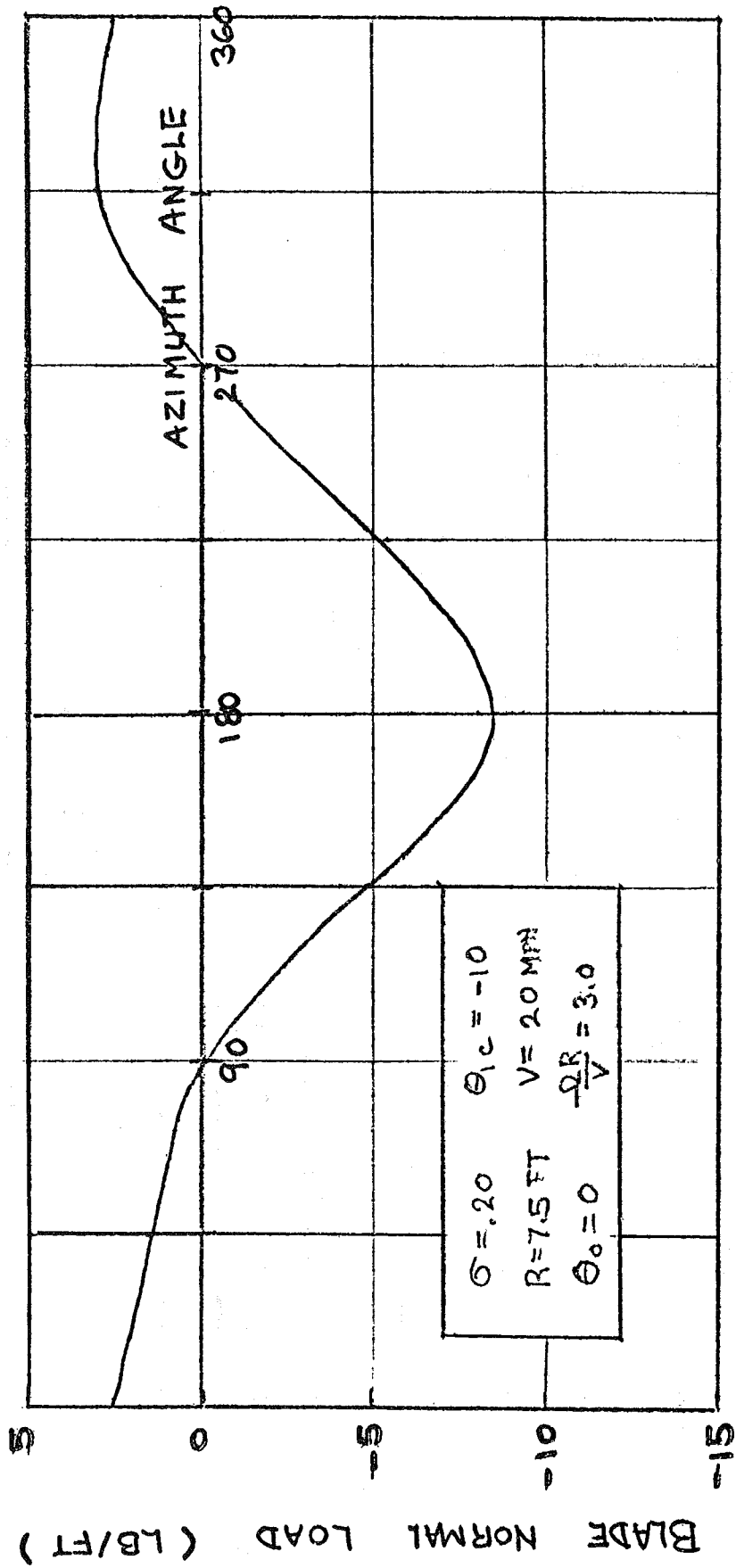


Figure 4-4. Sinusoidal Blade Pitch Schedule.



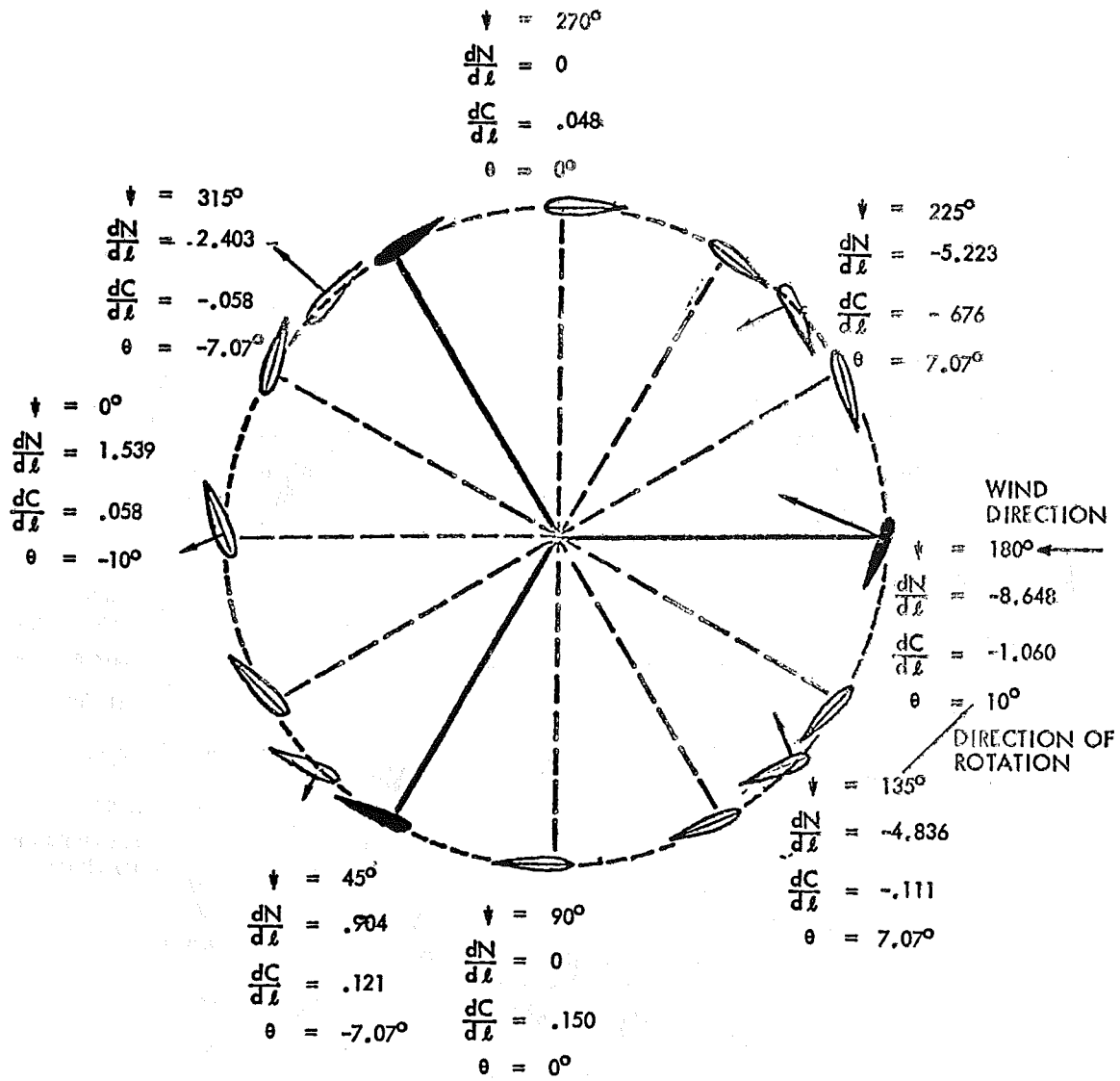
a) Chordwise

Figure 4-5. Blade Aerodynamic Load: 15-Ft Cycloturbine.



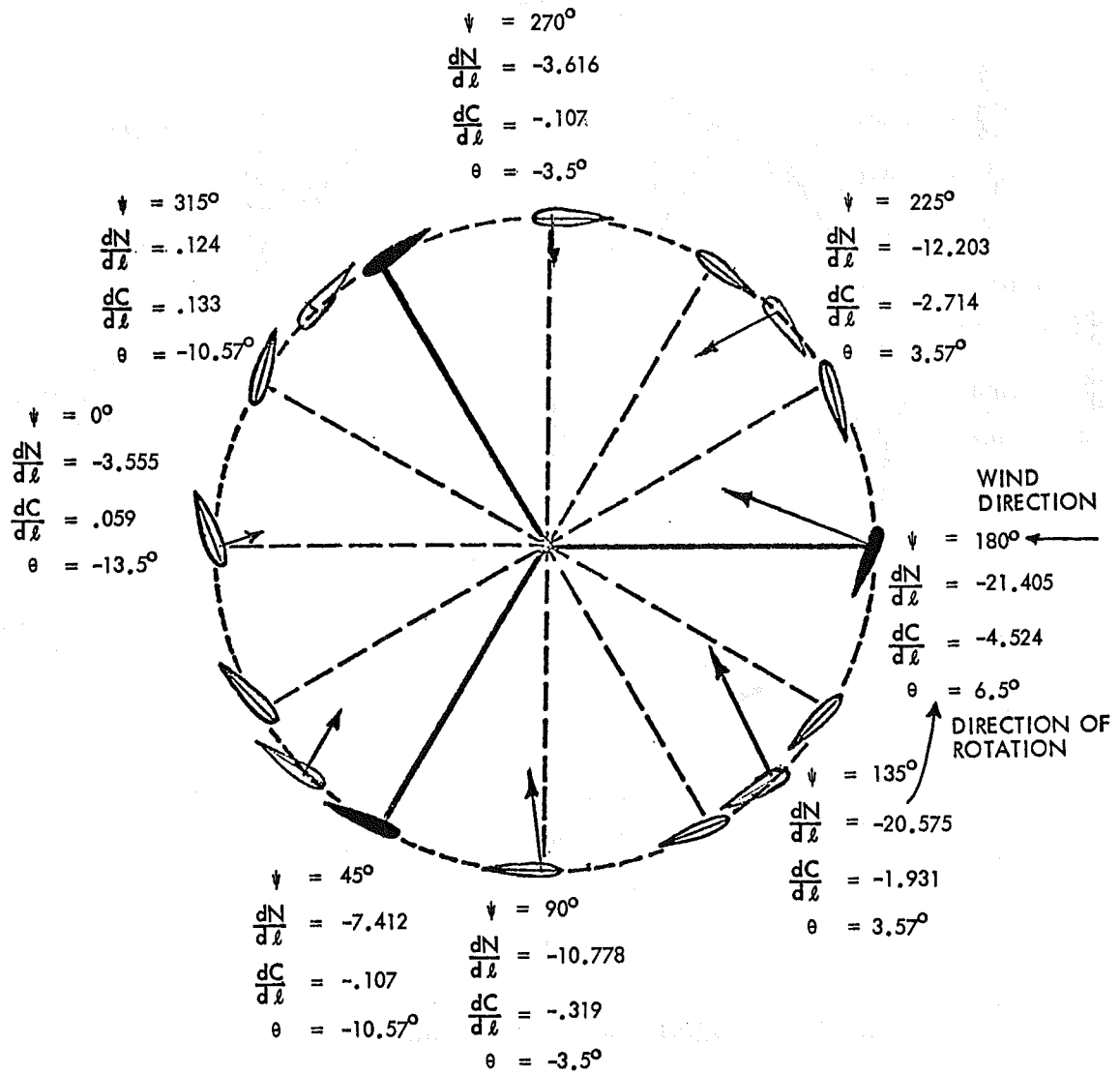
b) Normal

Figure 4-5. Blade Aerodynamic Load: 15-Ft Cycloturbine (Concluded).



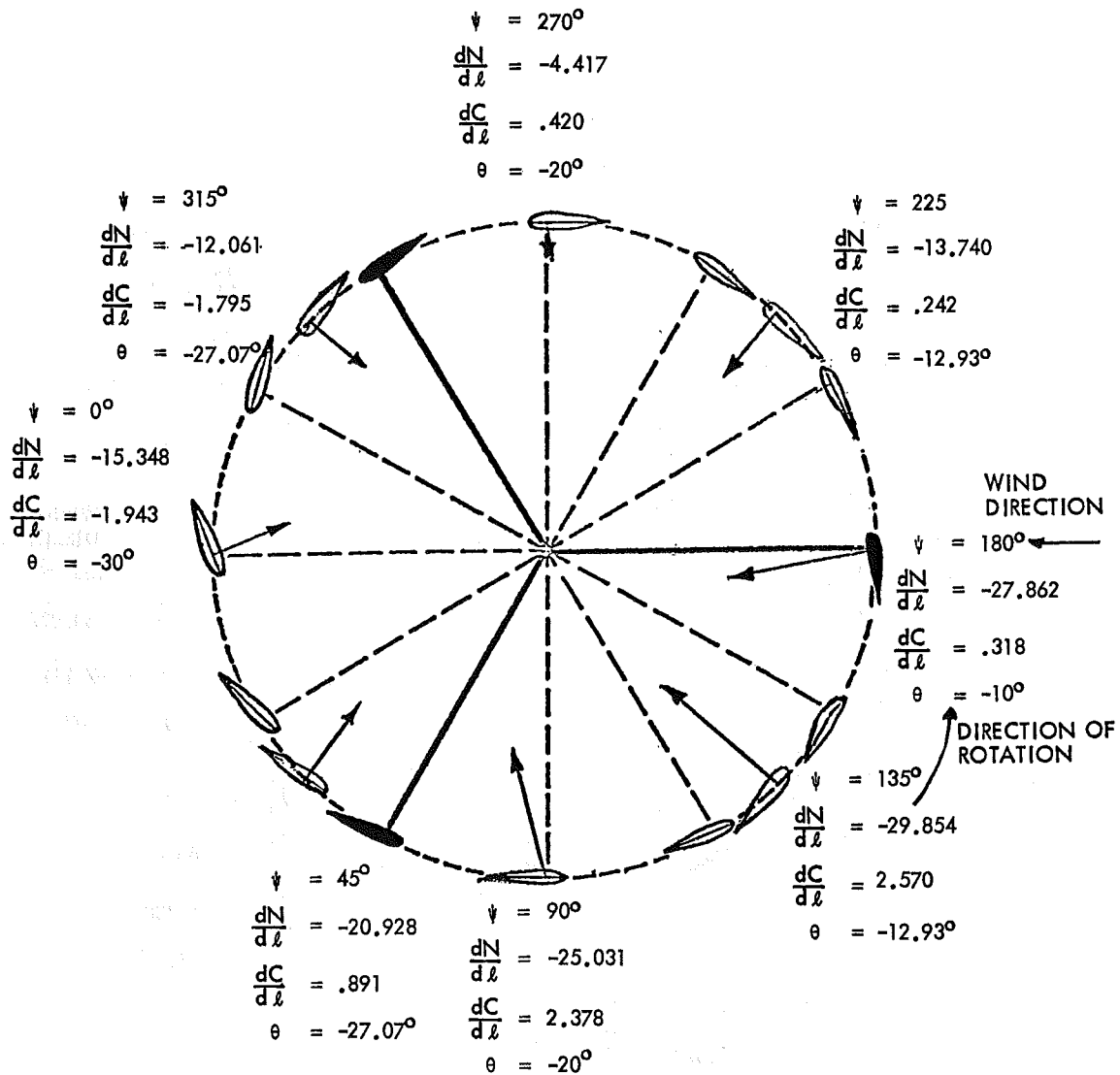
a)  $V = 20$  MPH, Normal Operating Condition

Figure 4-6. Representation of the Operation of Cycloturbine C2E.



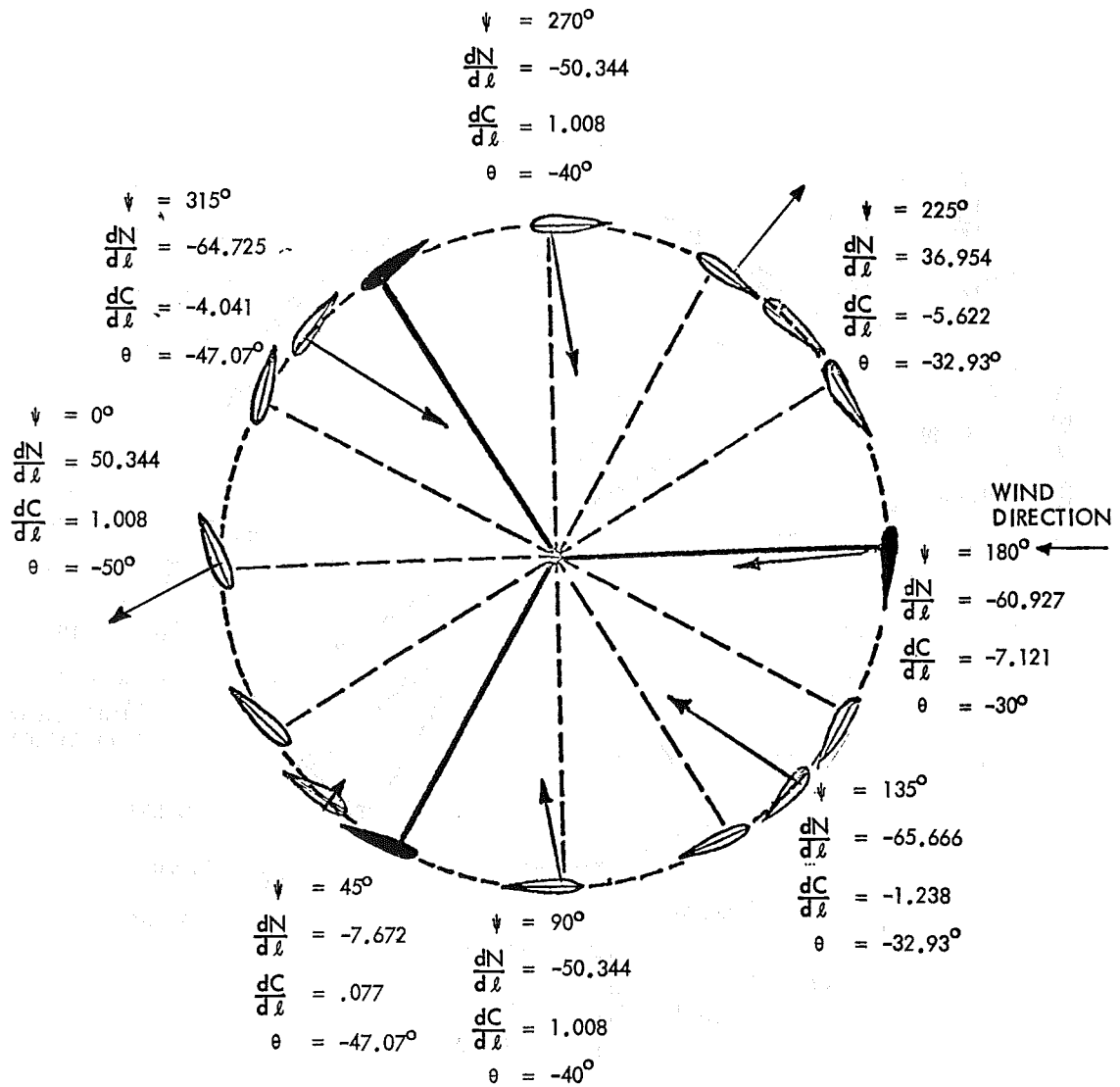
b)  $V = 28$  MPH, Turbine RPM Limited

Figure 4-6. Representation of the Operation of Cycloturbine C2E (Continued).



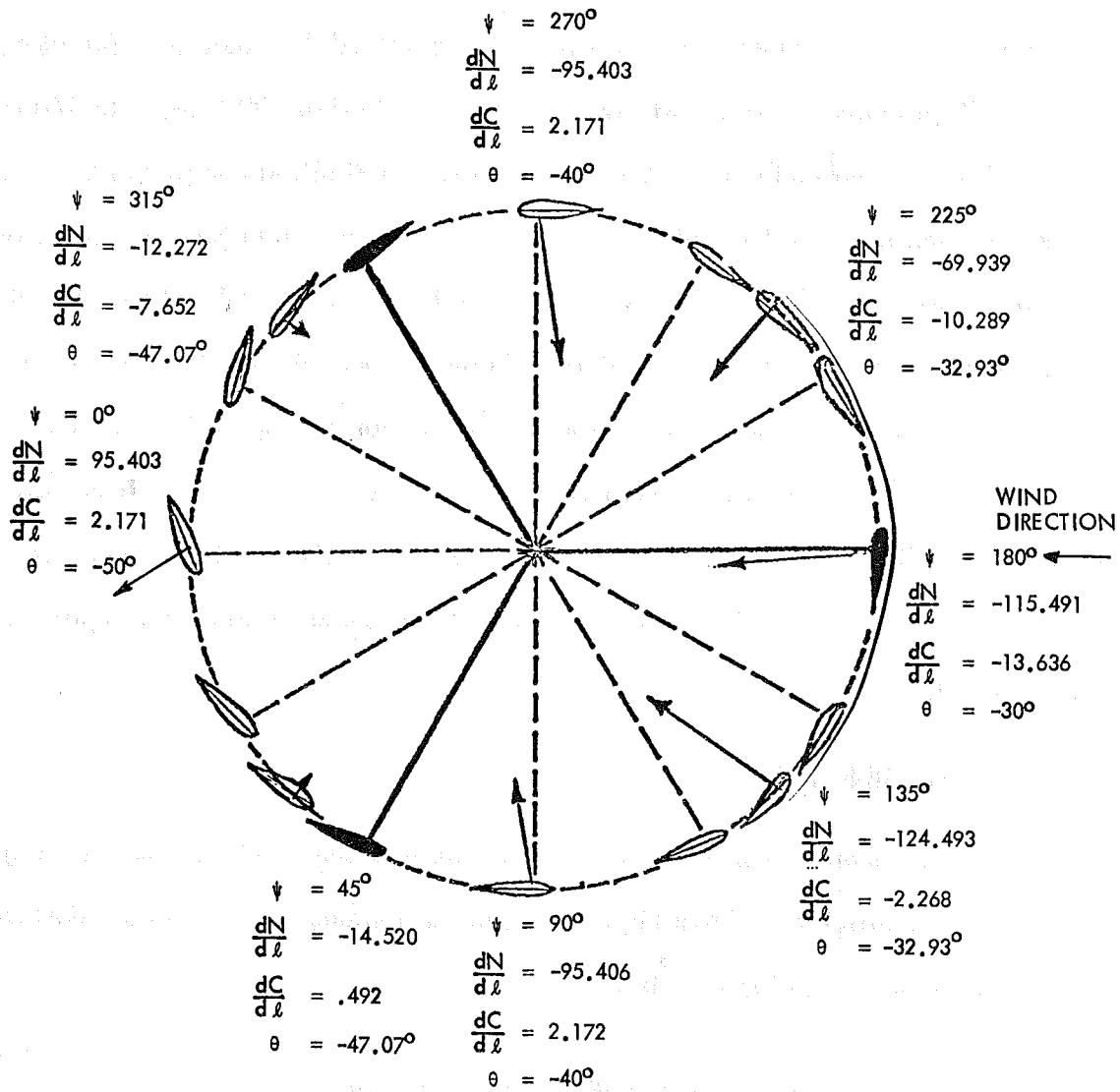
c)  $V = 40$  MPH, Stalled Condition

Figure 4-6. Representation of the Operation of Cycloturbine C2E (Continued).



d)  $V = 120$  MPH, Stopped Rotor

Figure 4-6. Representation of the Operation of Cycloturbine C2E (Continued).



e)  $V = 165$  MPH, Stopped Rotor

Figure 4-6. Representation of the Operation of Cycloturbine C2E (Concluded).

For this case, the blades are pitched cyclically from  $10^\circ$  trailing-edge inboard upwind ( $\psi = 180^\circ$ ) to  $10^\circ$  trailing-edge outboard downwind ( $\psi = 0^\circ$ ). This cyclic pitch capability allows the Cycloturbine to be self-starting. It is seen that the peak blade loading, i.e., the power stroke of the Cycloturbine, occurred upwind at azimuth position,  $\psi = 180^\circ$ . Note that the blade normal force is defined to be positive acting outward and the chordwise force is positive acting toward the blade leading edge. Figure 4-6b presents similar results for the turbine limited at 200 RPM. The blade cyclic pitch also makes the rotor aerodynamically self-limiting and prevents overspeed of the Cycloturbine. In the stalled condition, that is,  $V = 40$  mph, the blades are pitched  $45^\circ$  trailing-edge outboard by the collective pitch control system. Results for the stalled rotor are given in Figure 4-6c. In high winds, the blades are pivoted to the position of least wind resistance. The blade loadings for a stopped rotor in high winds at 120 and 165 mph are presented in Figures 4-6d and 4-6e respectively. It is seen that, for these conditions, large normal loads can result depending on the blade position (operational experience indicates one blade tends to remain in the upwind position approximately as shown).

#### 4.2 TURBINE INFLOW

The mean inflow ratio,  $\lambda_0$ , for the turbine can be approximated using the turbine drag coefficient. From Figure 4-1, the instantaneous force in the downwind direction due to one turbine blade is

$$\Delta H = L \cos(\psi + \phi) + D \sin(\psi + \phi) \quad (4-9)$$

In order to obtain a closed form solution, it is assumed that  $\theta$  is small, the lift curve slope is a constant,  $a$ , and the drag coefficient is a constant,  $C_{D_0}$ .

Then for all blades, the mean drag force based on the mean inflow is

$$\begin{aligned}
 H = \frac{1}{2} \rho (\Omega R)^2 c_l \frac{b}{2\pi} \int_0^{2\pi} & \left[ a \theta \cos \psi (1 + \lambda_o \sin \psi)^2 \right. \\
 & + a \lambda_o \cos^2 \psi (1 + \lambda_o \sin \psi) - a \theta \lambda_o \sin \psi \cos \psi (1 + \lambda_o \sin \psi) \\
 & - a \lambda_o^2 \sin \psi \cos^2 \psi + C_{D_o} \sin \psi (1 + \lambda_o \sin \psi)^2 \\
 & \left. + C_{D_o} \lambda_o \cos^2 \psi (1 + \lambda_o \sin \psi) \right] d\psi \quad (4-10)
 \end{aligned}$$

where  $U \approx \Omega R (1 + \lambda_o \sin \psi)$  is used in approximating the profile drag term.

Then defining the turbine drag coefficient as

$$C_H = \frac{H}{\frac{1}{2} \rho V^2 (2R\ell)} \quad (4-11)$$

Equation (4-10) becomes

$$C_H = \sigma \left( \frac{\Omega R}{V} \right)^2 \left[ \frac{a}{2} (\theta_{1c} + \lambda_o) + \frac{3}{2} \lambda_o C_{D_o} \right] \quad (4-12)$$

Note that Equation (4-12) is independent of  $\theta_o$ .

If it is assumed that the flow through the turbine is a one-dimensional stream tube, the drag force can also be expressed by momentum theory as

$$H = 2 \rho (2R\ell) (V - v) v \quad (4-13)$$

or, by applying Equations (4-7) and (4-11),

$$C_H = 4\lambda_o \left[ \left( \frac{\Omega R}{V} \right) - \left( \frac{\Omega R}{V} \right)^2 \lambda_o \right] \quad (4-14)$$

Equating Equations (4-12) and (4-14) results in

$$\lambda_o^2 - \left[ \left( \frac{V}{\Omega R} \right) - \frac{\sigma}{8} (\alpha + 3C_{D_o}) \right] \lambda_o + \frac{\sigma \alpha}{8} \theta_{1c} = 0 \quad (4-15)$$

Thus, the inflow ratio is given by

$$\lambda_o = \frac{K}{2} + \left[ \left( \frac{K}{2} \right)^2 - \frac{\sigma \alpha}{8} \theta_{1c} \right]^{1/2} \quad (4-16)$$

where

$$K = \frac{V}{\Omega R} - \frac{\sigma}{8} (\alpha + 3C_{D_o})$$

and

$$\sigma = \text{turbine solidity} = \frac{bc}{2R}$$

$$b = \text{number of blades}$$

The mean inflow velocity,  $v_o$ , is related to  $\lambda_o$  using Equation (4-7) as

$$\lambda_o = \frac{V - v_o}{\Omega R} \quad (4-17)$$

The inflow ratio undergoes harmonic variation as the turbine rotates. Assuming the variation is sinusoidal (such as used for the pitch angle), then

$$\lambda_i = \lambda_o + \lambda_{1c} \cos \psi \quad (4-18)$$

where  $\lambda_{1c}$  is the magnitude of the harmonic variation.

Application of momentum theory shows that the induced velocity in the fully developed wake is twice that at the actuator disk. Results from detailed wake studies (e.g., Reference 13) also confirmed this. Therefore, for the Cycloturbine it is assumed that the turbine induced velocity ("blockage"),  $v$ , is zero at the most upwind part of the path swept by the blade; of magnitude  $v_o$  (see Equation (4-17)) at the plane perpendicular to the incident wind and passing through the rotor center; and of magnitude  $2v_o$  at the most downwind point of the path swept by the blade (i.e., the fully developed wake). Then as the blade sweeps through its orbit, it will encounter an apparent variation of inflow given by

$$\lambda_{1c} = -\frac{v_o}{\Omega R} \quad (4-19)$$

#### 4.3 TURBINE POWER COEFFICIENT

The mean power generated by the turbine is

$$P = \Omega R \frac{b}{2\pi} \int_0^{2\pi} (L \sin \phi - D \cos \phi) d\psi \quad (4-20)$$

where  $b$  is the number of blades and the inflow angle,  $\phi$ , is given by Equation (4-5).

Substituting Equations (4-1), (4-2) and (4-4) into (4-20) yields

$$P = \frac{1}{2} \rho (\Omega R)^3 bc \ell \frac{1}{2\pi} \int_0^{2\pi} \left[ (1 + 2\lambda_i \sin \psi + \lambda_i^2) (C_L \sin \phi - C_D \cos \phi) \right] d\psi \quad (4-21)$$

Then, defining the turbine power coefficient as

$$C_P = \frac{P}{\frac{1}{2} \rho V^3 (2R\ell)} \quad (4-22)$$

Equation (4-21) becomes

$$C_P = \sigma \left( \frac{\Omega R}{V} \right)^3 \frac{1}{2\pi} \int_0^{2\pi} (1 + 2\lambda_i \sin \psi + \lambda_i^2) (C_L \sin \phi - C_D \cos \phi) d\psi \quad (4-23)$$

where  $\sigma$  is the turbine solidity and  $\Omega R/V$  is the tip speed ratio.

#### 4.3.1 DYNAMIC STALL

The stall characteristics of an airfoil undergoing a rapidly changing angle-of-attack differ substantially from the familiar static stall at constant angle-of-attack. This stall condition, referred to as dynamic stall, can cause a large increase in blade torsional loads and vibration levels. Since the Cycloturbine blades cycle through an angle-of-attack change during each revolution, dynamic stall needs to be evaluated for the 1-kW design.

The primary characteristics of dynamic stall are its occurrence at an angle-of-attack greater than the stall angle, followed by the shedding of vorticity from the leading and trailing edges (References 14 to 16). The unsteady aerodynamic forces

due to this vorticity passing over the upper surface of the airfoil produce a lift and nosedown moment, with peak values much greater than the corresponding static stall loads. Theoretical calculations and experimental data in Figure 4-7 show the increased loads.

Normal aerodynamic loads on the blade are affected by the rate of change of angle-of-attack,  $\dot{\alpha}$  as shown in Figure 4-8 by the velocity parameter,  $\dot{\alpha} c/U$ . For the conditions considered, it is readily apparent that the maximum aerodynamic load due to dynamic stall is about 3 times the magnitude predicted without dynamic stall effects.

The velocity parameter,  $\dot{\alpha} c/U$ , is obtained as follows for the Cycloturbine. The blade element angle-of-attack is

$$\alpha(\psi) = \theta(\psi) + \phi(\psi) \quad (4-24)$$

Therefore, the velocity parameter is

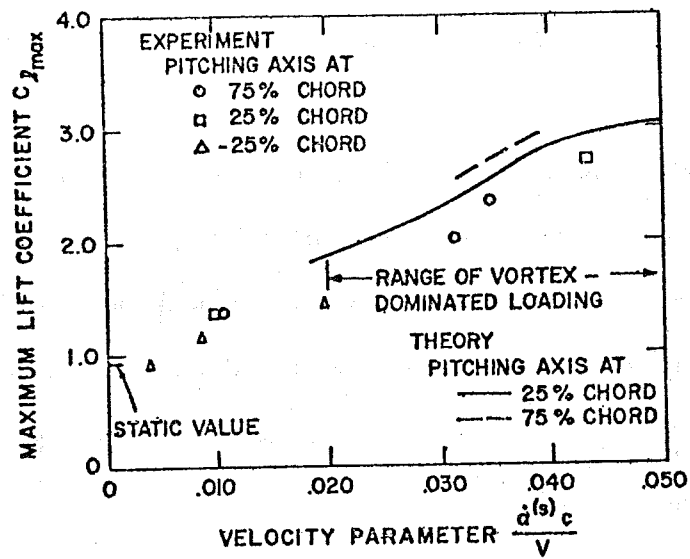
$$\frac{\dot{\alpha} c}{U} = \left[ \frac{\dot{\theta}(\psi)}{\Omega} + \frac{\dot{\phi}(\psi)}{\Omega} \right] \frac{\Omega R}{U} \frac{c}{R} \quad (4-25)$$

where, from Equations (4-5), (4-6) and (4-18), and applying Equation (4-4),

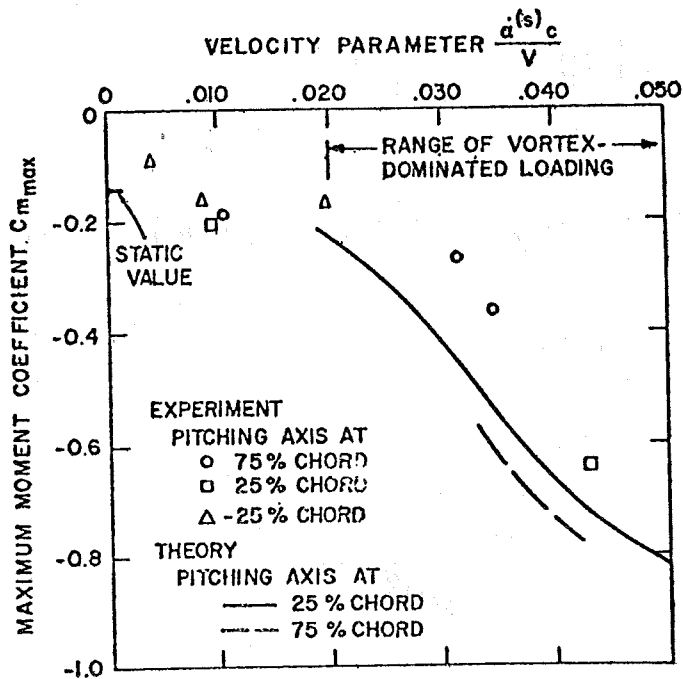
$$\frac{\dot{\theta}(\psi)}{\Omega} = -\lambda_{1c} \sin \psi$$

$$\frac{\dot{\phi}(\psi)}{\Omega} = \frac{-\lambda_i \sin \psi + \frac{\dot{\lambda}_i}{\Omega} \cos \psi - \lambda_i^2}{(U/\Omega R)^2}$$

$$\frac{\dot{\lambda}_i}{\Omega} = -\lambda_{1c} \sin \psi$$



a) Maximum Lift Coefficient



b) Maximum Moment Coefficient

Figure 4-7. Effect of Dynamic Stall Velocity Parameter,  $\frac{\dot{\alpha}c}{U}$  (Reference 14).

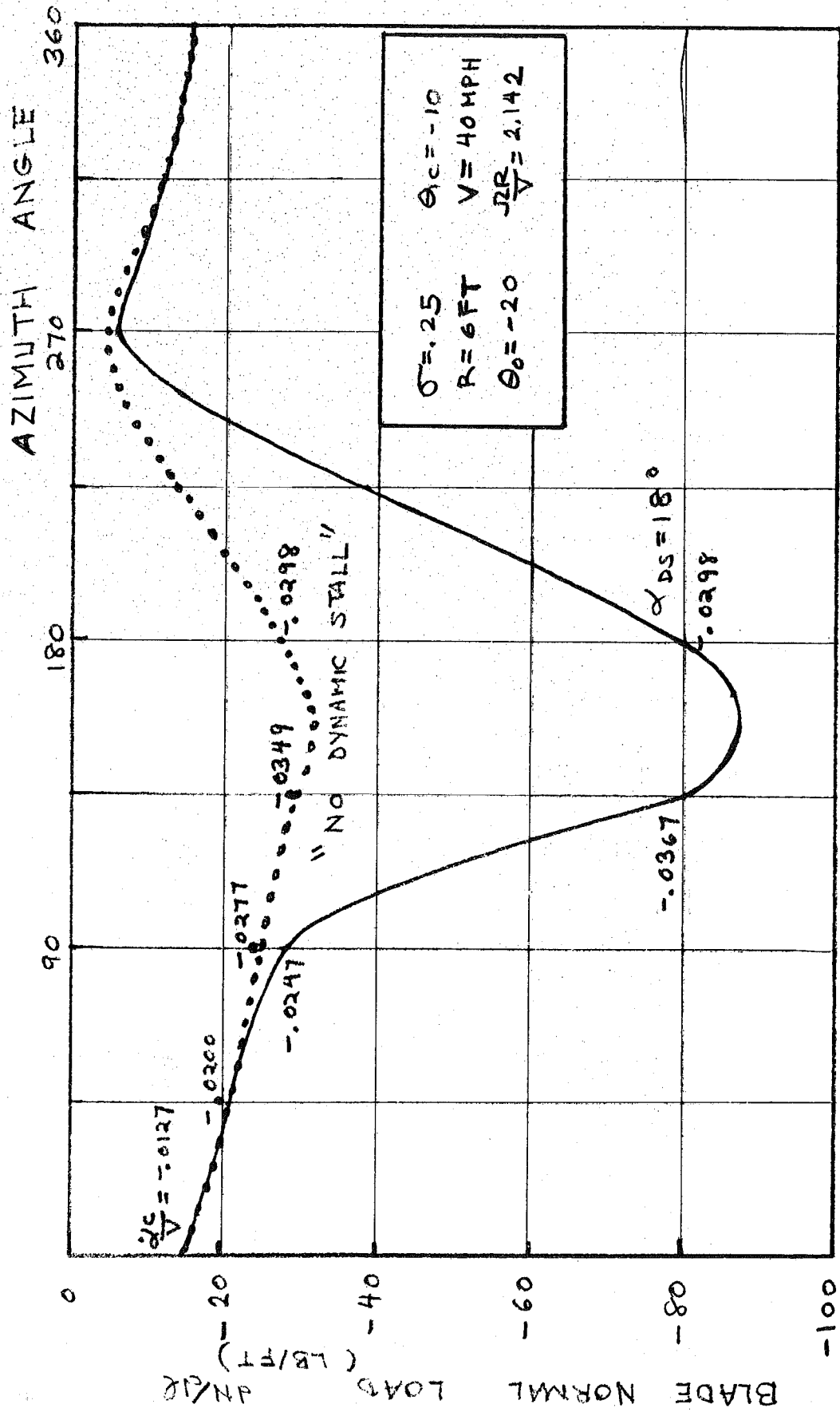


Figure 4-8. Effect of Dynamic Stall on Blade Normal Aerodynamic Load.

Finally, Equation (4-25) becomes,

$$\frac{\dot{\alpha}c}{U} = \left[ \frac{\dot{\theta}/\Omega}{U/\Omega R} + \frac{\frac{\dot{\lambda}_i}{\Omega} \cos \psi - \lambda_i \sin \psi - \lambda_i^2}{(U/\Omega R)^3} \right] \frac{c}{R} \quad (4-26)$$

The effect of dynamic stall on the performance of the Cycloturbine has been predicted (see Volume III) and is shown in Figure 4-9. The dynamic stall angle,  $\alpha_{DS}$ , while not affecting the peak value of power coefficient,  $C_p$ , does affect the power at lower values of tip speed ratio. However, at these tip speed ratios, the large increase in blade drag associated with the dynamic stall tends to stop the machine. Thus, the increased torsional loads are of primary concern. The exact value of  $\alpha_{DS}$  is not known and must be obtained from wind tunnel tests. It usually occurs in the range from  $15^\circ$  to  $20^\circ$ ; for the present analysis a value of  $\alpha_{DS} = 18^\circ$  has been used.

#### 4.3.2 ADDITIONAL DRAG EFFECT

The analysis of Subsection 4.1 included drag on the turbine blades which is the primary source of drag. Additional drag to account for the Cycloturbine struts, interference, etc., has been included in the analysis. This is represented by

$$C_D = C_D(\alpha) + C_{D_a} \quad (4-27)$$

where  $C_{D_a}$  is the additional drag coefficient.

Estimates of the order of magnitude of  $C_{D_a}$  were made using the struts alone as the basis of the calculations. Two-dimensional airfoil theory was used to obtain the drag on a single strut (see Equation (4-2)). It was assumed that the strut is an NACA 0015 airfoil at zero angle of attack. Strut drag for various wind speeds is shown in Table 4-1.

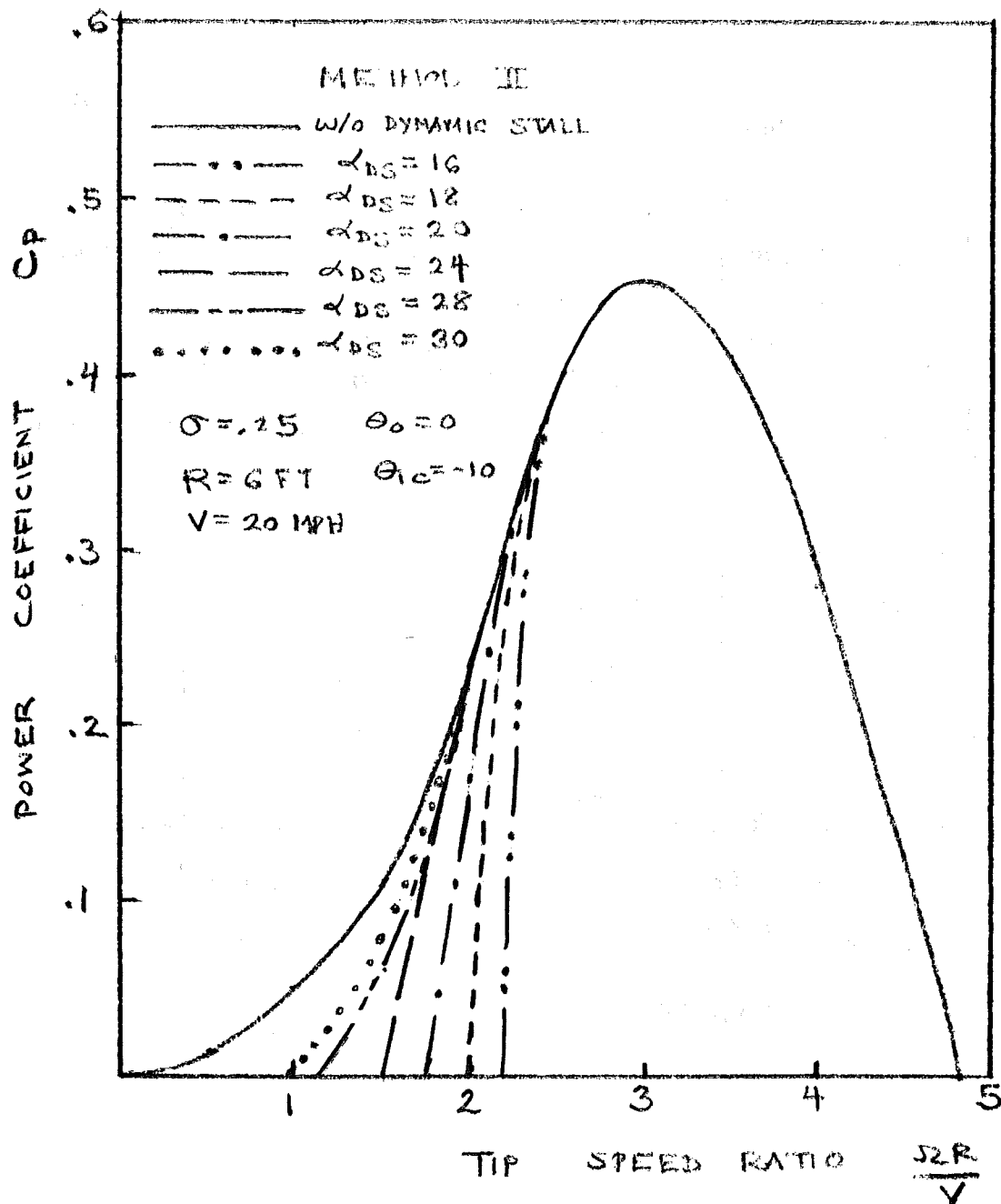


Figure 4-9. Effect of Dynamic Stall on Turbine Power Coefficient.

Table 4-1, Calculation of Strut Drag.

WIND SPEED (MPH)	STRUT DRAG (LB)	
	COMPUTER*	AIRFOIL THEORY**
5	.0063	.0024
10	.0253	.0096
15	.0569	.0216
20	.1013	.0384
25	.1582	.0600
30	.1770	.0864
35	.1939	.1176
40	.2065	.1536

\*  $C_{D_a} = 0.005$

\*\* NACA 0015 Airfoil

Various values of  $C_{D_a}$  were chosen and the total drag on the machine calculated by the computer program. The difference between this value and that for  $C_{D_a} = 0$  (blades only) was assumed to represent the drag on the six struts. The drag per strut calculated in this manner is shown in Table 4-1 for  $C_{D_a} = .005$ . It is seen from Table 4-1 that the drag per strut estimated by both methods is of the same order of magnitude with the computer value being higher. This is the desired result since the value of  $C_{D_a}$  used in the computer analysis must represent not only the drag of the struts but all the additional drag of the machine except for the blades.

The power coefficient of the 15-ft Cycloturbine is shown in Figure 4-10, both with and without the additional drag term. The effect of the additional drag on both peak power coefficient and runaway speed is evident. The value  $C_{D_a} = .005$  was used for the Cycloturbine analysis since it provided good correlation with experimental data (see Subsection 5.1.1.2).

#### 4.3.3 EFFECT OF WIND SHIFT

A sudden shift in wind direction is an important consideration for horizontal-axis machines; however, for a vertical-axis configuration it is not expected to be important. To verify this, calculations were performed for wind shifts of up to  $30^\circ$ .

The primary effect in the analysis is seen in the cyclic schedule for pitch angle. Thus, Equation (4-6) becomes

$$\theta = \theta_o + \theta_{1c} \cos(\psi + \Delta\psi)$$

where  $\Delta\psi$  is the change in azimuth angle due to the change in wind direction, that is, it is the wind shift angle. A positive wind shift angle is a clockwise rotation of the wind vector when viewing the machine from above.

Results of the calculations for a positive and a negative shift of  $30^\circ$  are shown in Table 4-2. It is seen that the wind shift actually increases the peak power coefficient and causes it to occur at a higher tip speed ratio. This would be a steady

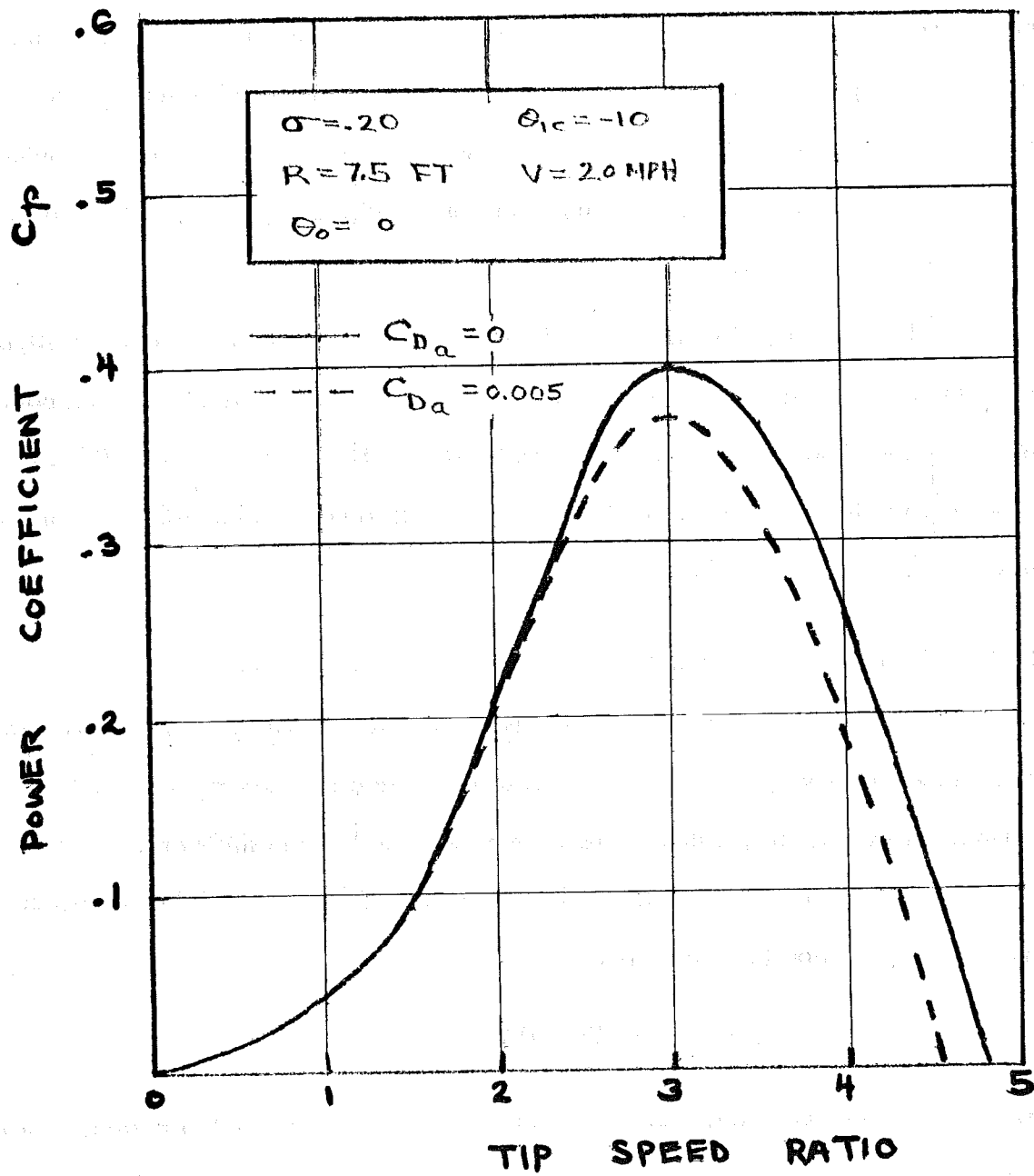


Figure 4-10. Effect of Additional Drag on the Power Coefficient for 15-ft Cycloturbine.

Table 4-2. Effect of Wind Direction Shift on Turbine Power Coefficient.

$\frac{\Omega R}{V}$	$C_p$		
	No Wind Shift	Wind Shift of 30°	Wind Shift of -30°
.5	.0123	.0141	.0098
1.0	.0443	.0298	.0299
1.5	.0961	.0746	.0619
2.0	.2112	.2044	.1439
2.5	.3462	.2488	.4004
3.0	.4024	.3843	.4837
3.5	.3653	.4295	.4993
4.0	.2563	.3963	.4458
4.5	.1075	.3242	.3422
5.0	-.0761	.2086	.2105

NOTE:

- $\sigma = .20$
- $R = 7.5\text{-ft}$
- $V = 20\text{ mph}$
- $\theta_o = 0^\circ$
- $\theta_{1c} = -10^\circ$

state effect. However, in the instantaneous change considered, tip speed ratio would remain constant so that a positive wind shift would decrease the power and a negative shift would increase the power output. Any torque produced would change the RPM of the machine until the no wind shift condition is again reached.

#### 4.4 GUSTS

The complex problem of random turbulent air disturbances is commonly treated in the form of response to discrete gusts (e.g., Reference 17). The discrete gust is often represented as being sinusoidal in nature. For the Cycloturbine analysis, the gust not only affects the wind speed,  $V$ , but also modifies the inflow ratio,  $\lambda_i$ . Thus, for the sinusoidal gust, the inflow ratio becomes

$$\lambda_i = \lambda_o + \lambda_{1c} \cos \Omega t + \frac{v_G}{\Omega R} \cos \omega t \quad (4-28)$$

where

$v_G$  = velocity amplitude of a discrete gust

$\omega$  = gust frequency

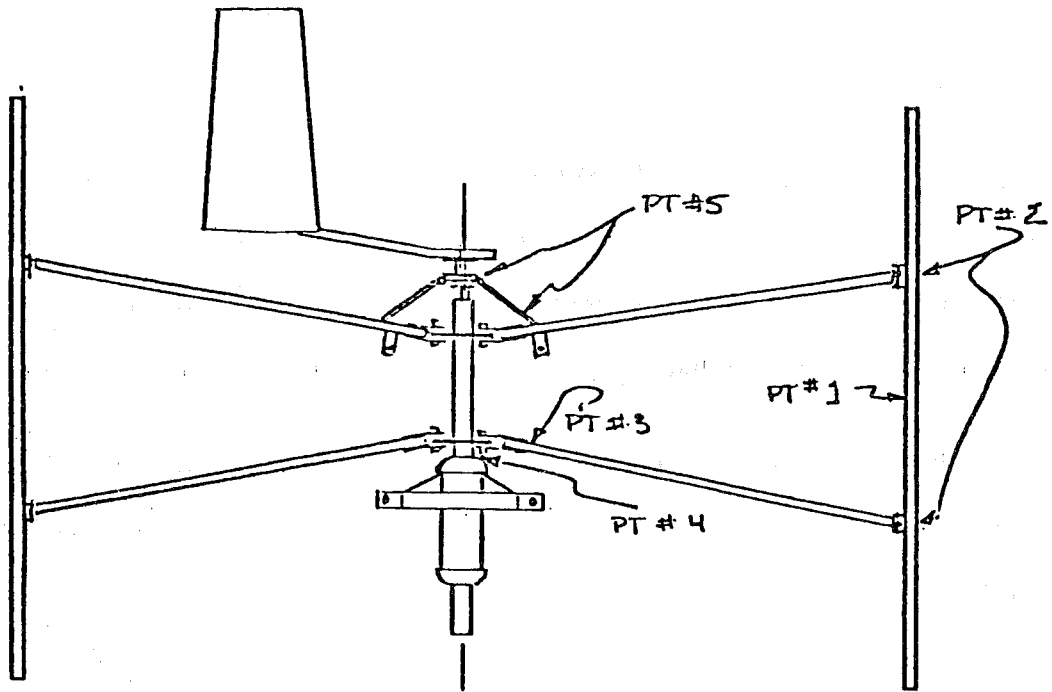
Typically,  $\frac{\omega}{\Omega} \sim 0.1$  for the Cycloturbine so that the effect of gusts can be approximated by letting  $\omega = 0$ , that is,

$$\lambda = \lambda_o + \lambda_{1c} \cos \Omega t + \frac{v_G}{\Omega R} \quad (4-29)$$

Thus, the gust is represented as a sharp-edged gust which has been shown in the aircraft industry to yield a more conservative result.

#### 4.5 STRUCTURAL LOADS

Five areas of the Cycloturbine are analyzed for critical stress. These areas which are shown in Figure 4-11 are: 1) blade spar center; 2) blade/strut connection; 3) strut root; 4) main shaft at the main bearings; and 5) pitch actuation system.



- PT #1 Blade Center
- PT #2 Blade/Strut Attachment
- PT #3 Strut Root
- PT #4 Shaft Root
- PT #5 Pitch Actuation System

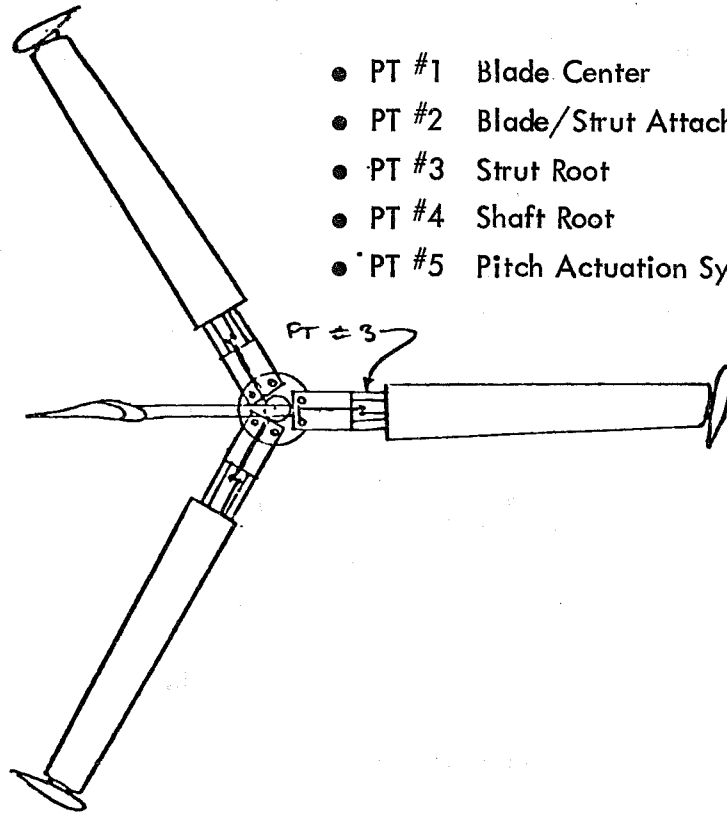


Figure 4-11. Critical Load Points.

## 4.5.1 STRESS ANALYSIS

### 4.5.1.1 BLADE STRESSES

The blade is subjected to both centrifugal and aerodynamic loads as depicted in Figure 4-12. The aerodynamic loads,  $w_a = \frac{dN}{dl}$ , (see Equation (4-8)), are oscillatory in nature. They are superimposed on a mean centrifugal load which is a function of the blade distributed weights,  $w_1$  and  $w_2$ .

The bending moments caused by the aerodynamic and centrifugal loads are shown in Figure 4-12. The bending moment at the blade spar center due to centrifugal loading is

$$M_{c_1} = M_{cc} + w_1 a \left[ \frac{L_s l_s}{2} - \frac{L_s^2}{8} \right] + w_2 l_c l_s a \quad (4-30)$$

and that at the blade/strut connection is

$$M_{c_2} = M_{cc} + \frac{1}{2} w_1 l_s^2 a + w_2 l_c l_s a \quad (4-31)$$

where

$$M_{cc} = \frac{1}{2} w_2 l_c^2 a \text{ is the moment on the tip caps}$$

$$w_1 = \text{distributed weight of spar, ribs, and skin}$$

$$w_2 = \text{distributed weight of the skin of tip caps}$$

$$l_c = \text{length of tip cap}$$

$$l_s = \text{distance between end of spar and strut connection}$$

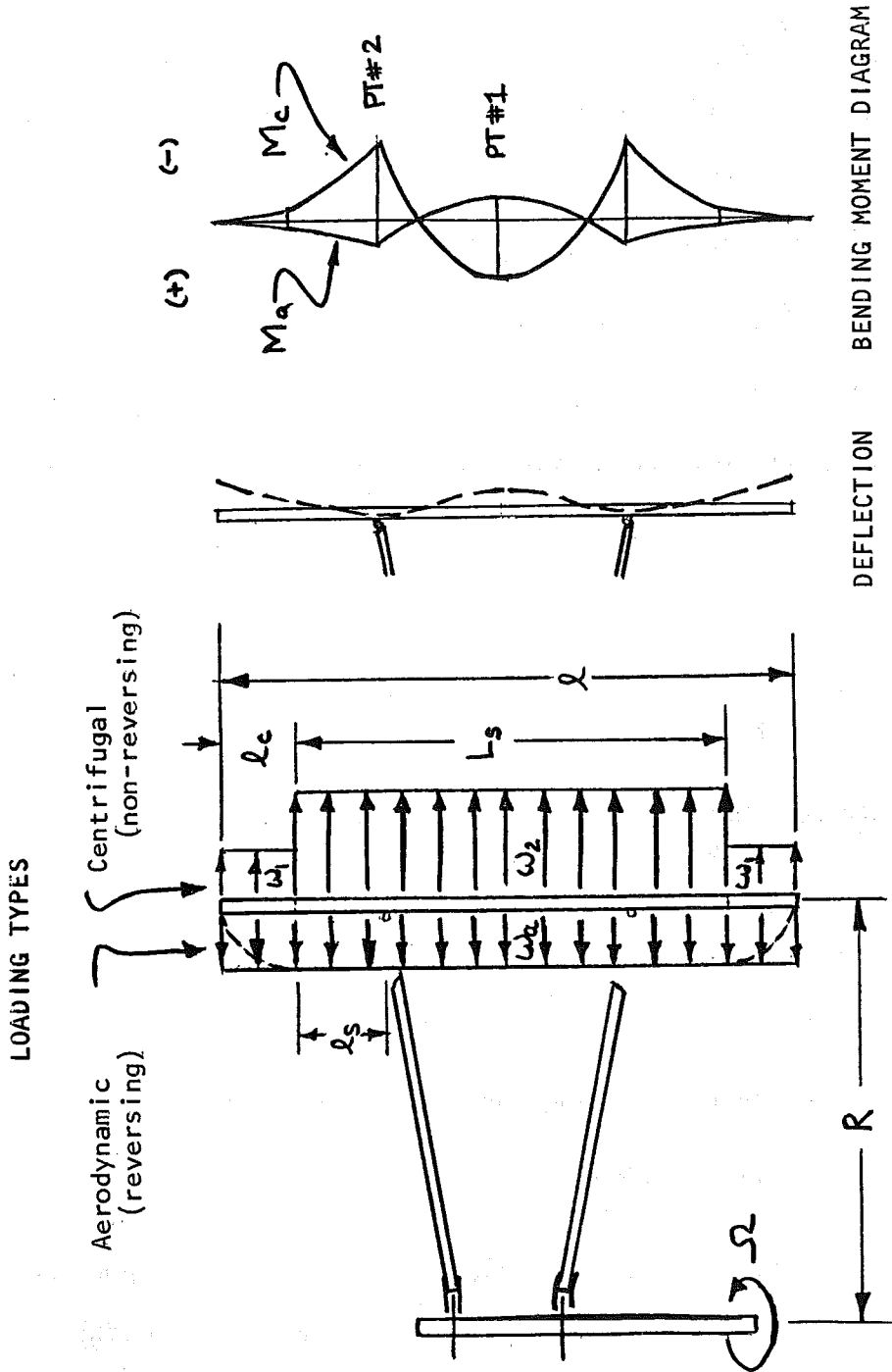


Figure 4-12. Blade Load Distribution and Bending Moments.

$L_s$  = length of spar

$$a = \frac{V_B^2}{Rg}$$

$$V_B = \Omega R$$

$g$  = acceleration of gravity

$\Omega$  = blade rotational speed

$R$  = turbine radius

The aerodynamic bending moment at the blade spar center is

$$M_{a_1}(\psi) = w_a(\psi) \left[ \frac{l l_t}{2} - \frac{l^2}{8} \right] \quad (4-32)$$

and that at the blade/strut connection is

$$M_{a_2}(\psi) = \frac{1}{2} w_a(\psi) l_t^2 \quad (4-33)$$

where

$w_a$  = distributed aerodynamic normal load

$l_t$  = distance from blade end to strut connection =  $l_s + l_c$

$L$  = total blade length

Thus, the total bending moments,  $M_1$  and  $M_2$ , at the blade spar center and the blade/strut connection, respectively, are (from Equations (4-30 to 4-33)),

$$M_1 = M_{c_1} + M_{a_1}(\psi) = \frac{1}{2} w_2 \alpha l_c (l_c + 2l_s) - \frac{1}{8} w_1 \alpha L_s (L_s - 4l_s) + \frac{1}{2} w_a l \left[ l_t - \frac{L}{4} \right] \quad (4-34)$$

$$M_2 = M_{c_2} + M_{a_2}(\psi) = \frac{1}{2} w_2 \alpha l_c (l_c + 2l_s) + \frac{1}{2} w_1 \alpha l_s^2 + \frac{1}{2} w_a l_t^2 \quad (4-35)$$

Finally, the stress is given by

$$S_i = \frac{M_i \bar{y}}{I_{cc}} \quad (4-36)$$

where

$\bar{y}$  = distance from chord line to outer fiber

$I_{cc}$  = inertia of spar

It is useful for life calculations to keep the aerodynamic and centrifugal moment separated so that oscillatory and mean stresses can be easily plotted on a Soderberg Diagram (see Subsection 2.2.3.1). Therefore, using Equations (4-34) and (4-35) in Equation (4-36), the stresses at the blade spar center and the blade/strut connection can be found from

$$S_1 = S_{a_1}(\psi) + S_{c_1} \quad (4-37)$$

$$S_2 = S_{a_2}(\psi) + S_{c_2} \quad (4-38)$$

Stresses for the blade spar center and for the blade/strut connection at the Cycloturbine nominal operating condition are shown in Figures 4-13 and 4-14, respectively. The stresses caused by the oscillating aerodynamic load is shown in Figures 4-13a and 4-14a, whereas the mean centrifugal stress as well as the total stresses are shown in Figures 4-13b and 4-14b.

#### 4.5.1.2 STRUT ROOT STRESS

Stress at the strut root is a combination of a radial stress caused by a reaction to the blade aerodynamic and centrifugal loads transferred through the blade/strut connection (see Subsection 4.5.1.1), centrifugal loads on the strut, and an in-plane bending stress induced by oscillating aerodynamic drag loads on the strut.

The radial loads acting on the strut root are shown in Figure 4-15. Referring to Figure 4-15a, the strut radial load caused by the reaction at the blade/strut connection is

$$F(\psi) = \frac{(2w_2 \ell_c + w_1 L_s) \alpha + w_a(\psi) \ell}{2 \cos \xi} \quad (4-39)$$

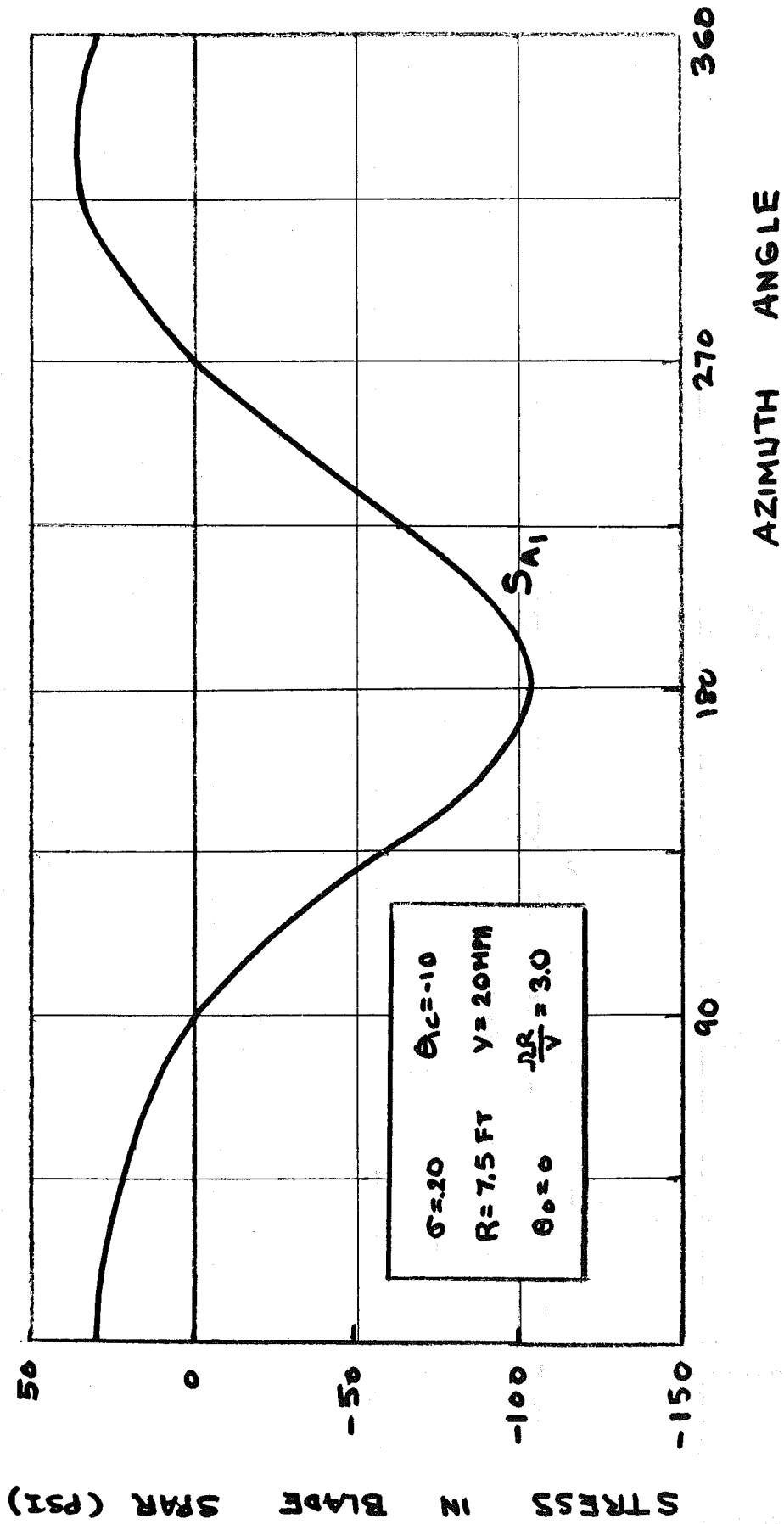
Centrifugal loading at the strut root due to the radially distributed weight of the strut is given by

$$D = \frac{w_s (R^2 - r^2) \Omega^2}{2g} \quad (4-40)$$

where

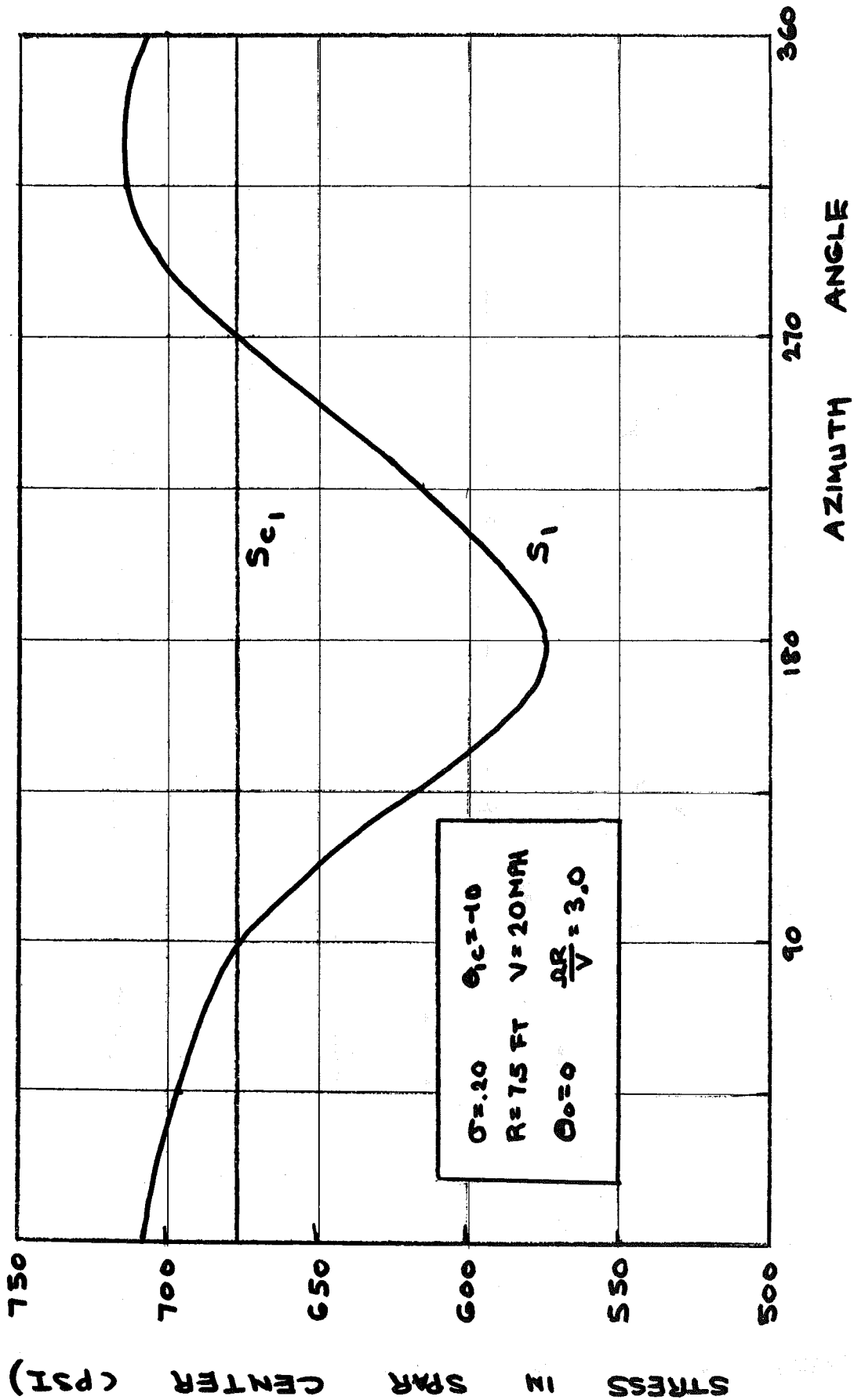
$w_s$  = distributed weight of strut

$R$  = radius of turbine



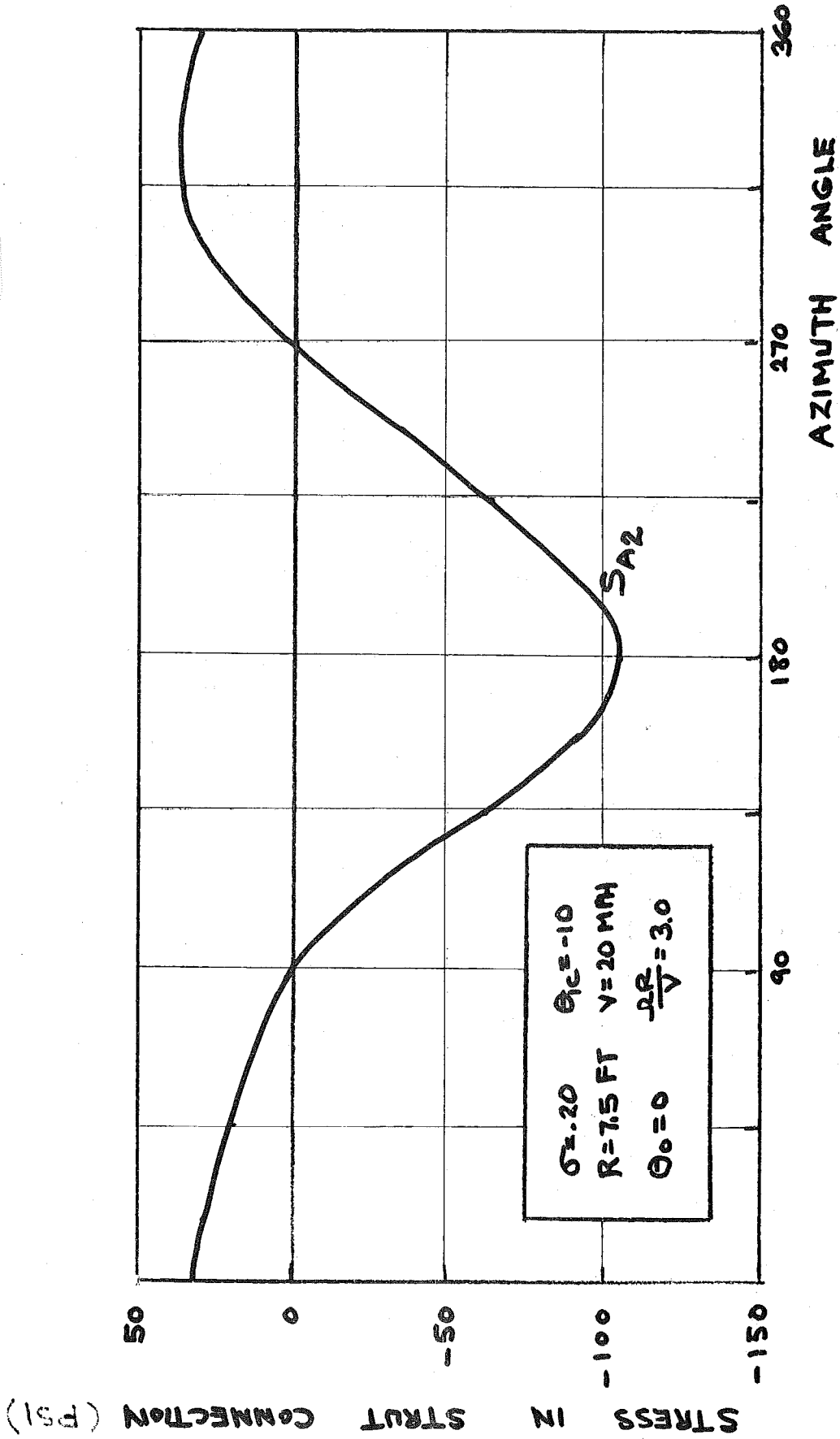
a) Aerodynamic

Figure 4-13, Stress at Blade Spar Center: Nominal Operating Condition.



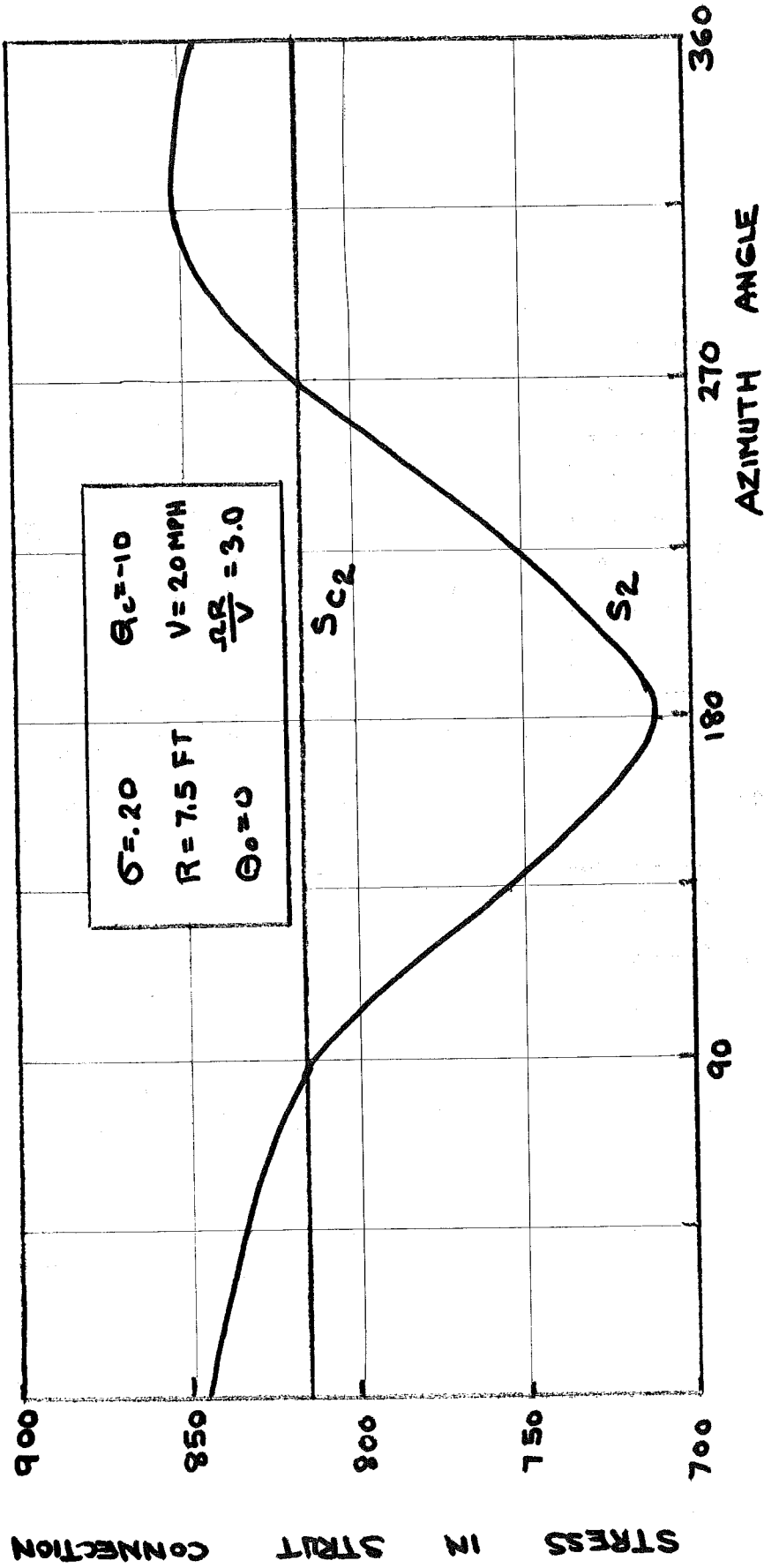
b) Centrifugal and Total

Figure 4-13. Stress at Blade Spar Center: Nominal Operating Condition (Concluded).



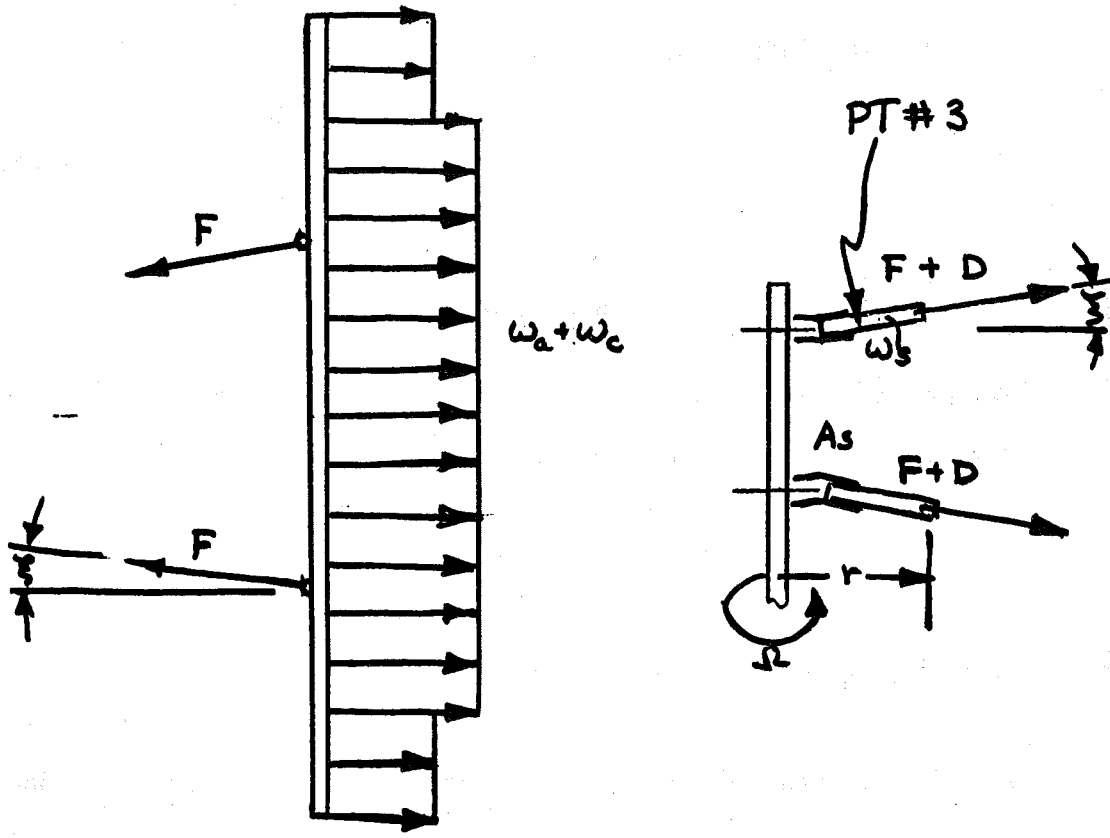
a) Aerodynamic

Figure 4-14. Stress at Blade/Strut Connection: Nominal Operating Condition.



b) Centrifugal and Total

Figure 4-14. Stress at Blade/Strut Connection: Nominal Operating Condition (Concluded).



a) Blade/Strut Connection

b) Strut Root

Figure 4-15. Strut Radial Loading.

$r$  = radial station on strut from shaft center

$\Omega$  = angular velocity

Thus, the total radial load at a radial station,  $r$ , on the strut is  $F + D$  (see Figure 4-15b).

Note that  $F$  has an oscillatory component caused by the blade aerodynamics. The strut root stress in the radial direction is given by

$$S_{c_3}(\psi) = \frac{F(\psi) + D}{A_s} \quad (4-41)$$

where  $A_s$  is the material cross-sectional area of strut root.

The strut root stresses of primary concern are due to oscillatory in-plane aerodynamic loads of the blades. This tangential force (shown in Figure 4-16) is

$$T(\psi) = \left[ \frac{dN}{dl} \sin \theta + \frac{dC}{dl} \cos \theta \right] l \quad (4-42)$$

where  $C$  and  $N$  are given by Equations (4-3) and (4-8), respectively. Considering the strut as a cantilever beam with an oscillatory point force at the end, the resulting bending moment at a distance  $r$  from the axis of rotation is (for one of a pair of struts)

$$M_s(\psi) = \frac{1}{2} (R - r) T(\psi) \quad (4-43)$$

The stress due to this moment is

$$S_{a_3}(\psi) = M_s \frac{\bar{x}_{cc}}{I_{xx}} \quad (4-44)$$

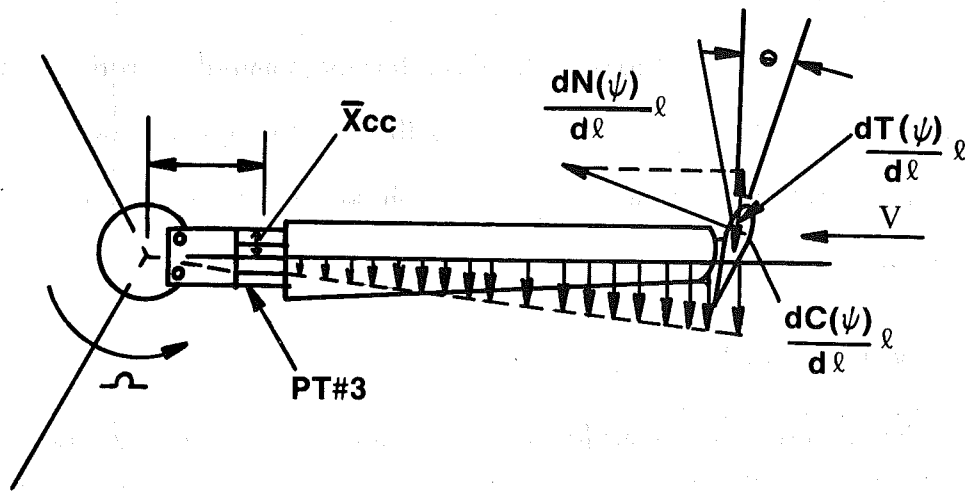


Figure 4-16. Strut Tangential Loading.

where

$\bar{x}_{cc}$  = distance from hub center to outer fibers of the strut

$I_{xx}$  = inertia of the strut

The total strut radial stress can be written as

$$S_3 = S_{c3} + S_{a3} \quad (4-45)$$

Again, it is necessary to keep the mean (centrifugal) and oscillatory (in-plane aerodynamic) stresses separated so that the Soderberg Diagram can be used.

Stresses for the strut root at the Cycloturbine nominal operating condition are shown in Figure 4-17. The stress caused by the oscillating aerodynamic load is shown in Figure 4-17a and the mean centrifugal stress and the total stress on the strut root are shown in Figure 4-17b.

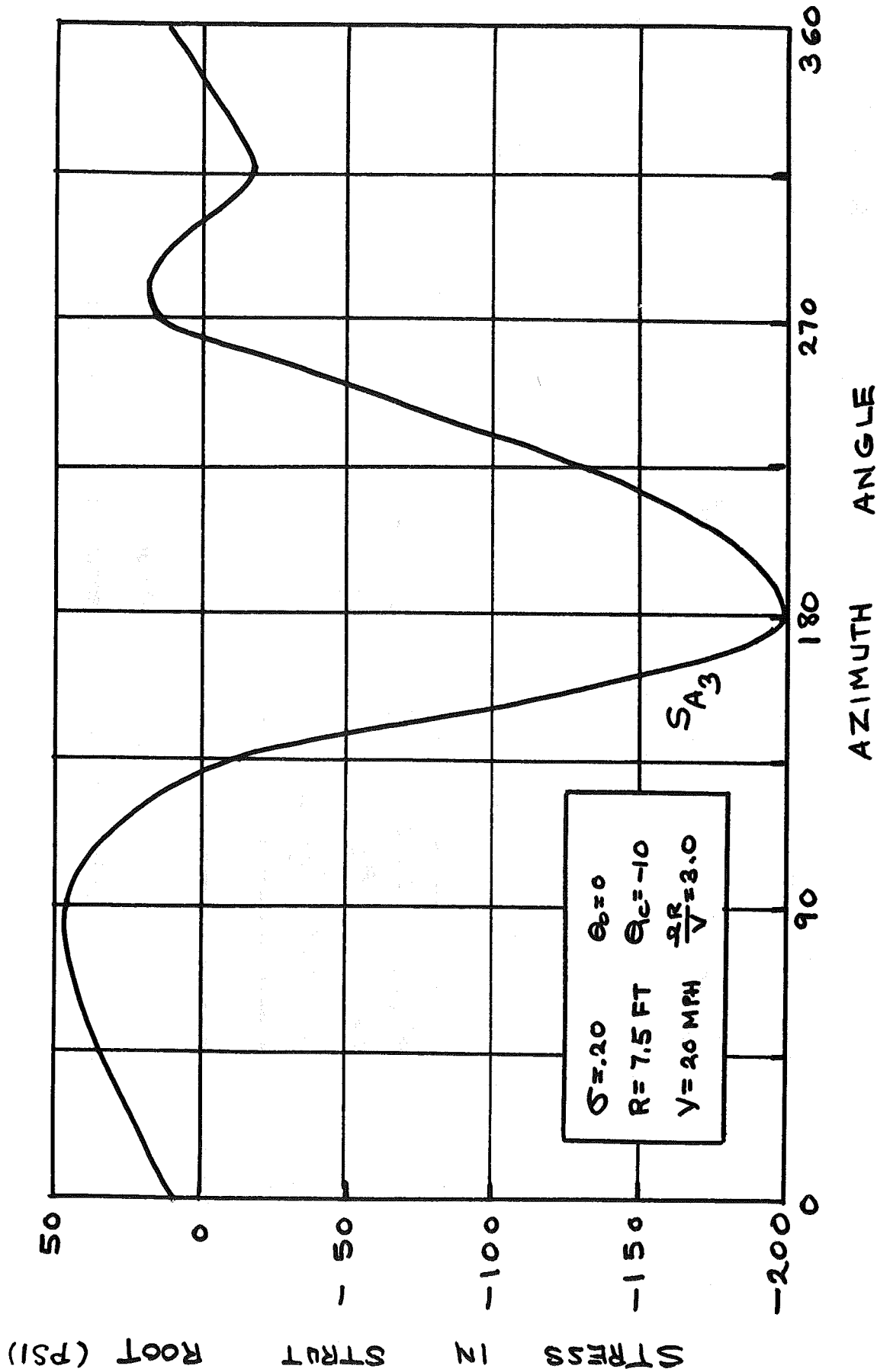
#### 4.5.1.3 MAIN SHAFT STRESS

The main shaft is a cantilever beam subjected to oscillatory loads from the aerodynamic action of the blades. The centrifugal loads contribution from the three blades cancel. As shown in Figure 4-18,  $A(\psi)$  represents the aerodynamic load due to all three blades. The bearing loads are

$$B_1(\psi) = A(\psi) \left[ 2 + \frac{(a+b)}{c} \right] \quad (4-46)$$

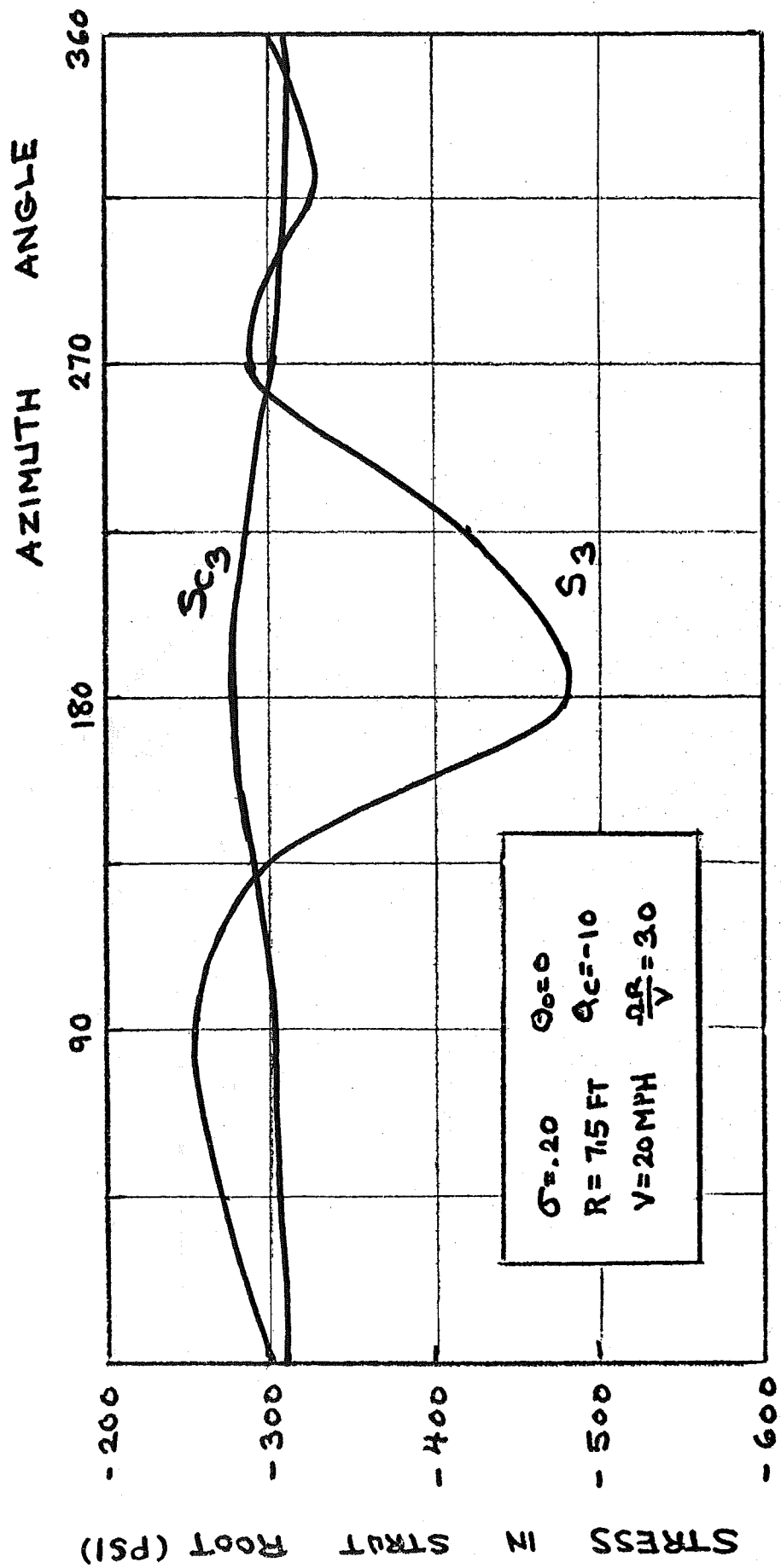
$$B_2(\psi) = \frac{A(\psi) (a+b)}{c} \quad (4-47)$$

where  $a$ ,  $b$ , and  $c$  are shaft dimensions shown in Figure 4-18.



a) Aerodynamic

Figure 4-17. Strut Root Stress: Nominal Operating Condition.



b) Centrifugal and Total

Figure 4-17. Strut Root Stress: Nominal Operating Condition (Concluded).

### TOTAL AERODYNAMIC LOADING

$$\Sigma A(\psi)$$

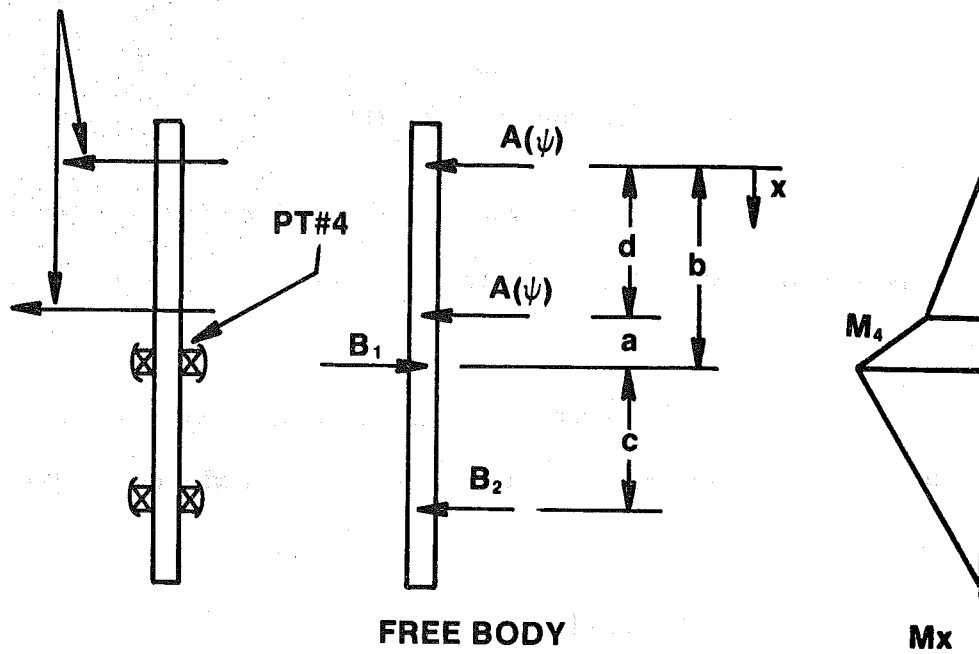


Figure 4-18. Main Bearing and Shaft Loading.

The largest bending moment on the main shaft which occurs at bearing  $B_1$ , is given by

$$M_4 = A(\psi) (d + 2a) \quad (4-48)$$

with the resulting stress given by

$$S_4 = \frac{M_4 \bar{z}}{I_{ss}} \quad (4-49)$$

where

$\bar{z}$  = shaft radius

$I_{ss}$  = shaft polar moment of inertia

The main shaft stress caused by moment,  $M_4$ , at the Cycloturbine nominal operating condition is shown in Figure 4-19. Note that the 3/rev aerodynamic loading is clearly seen.

Torsional loads at the bearings due to friction are assumed to be negligible. Thus, the aerodynamic torque on the turbine causes it to turn with no resistive moment on the shaft.

#### 4.5.1.4 PITCH ACTUATION CONTROL LOADS

Pitch actuation of the blades is effected by means of a cam device (see Section 3.1.2.7) which causes relative changes in pull rod linkage lengths between the cam and the blades. The loads in the pull rods are of several types. It is assumed that the blade pitch actuation is sinusoidal so that inertia forces on the actuation system can be determined by applying simple harmonic motion. The actuation system is also subjected to centrifugal loads and to blade aerodynamic loads. Therefore, the total force on the pull rod is

$$F_p(\psi, \alpha) = F_{P_i}(\psi) + F_{P_c} + F_{P_B}(\psi, \alpha) \quad (4-50)$$

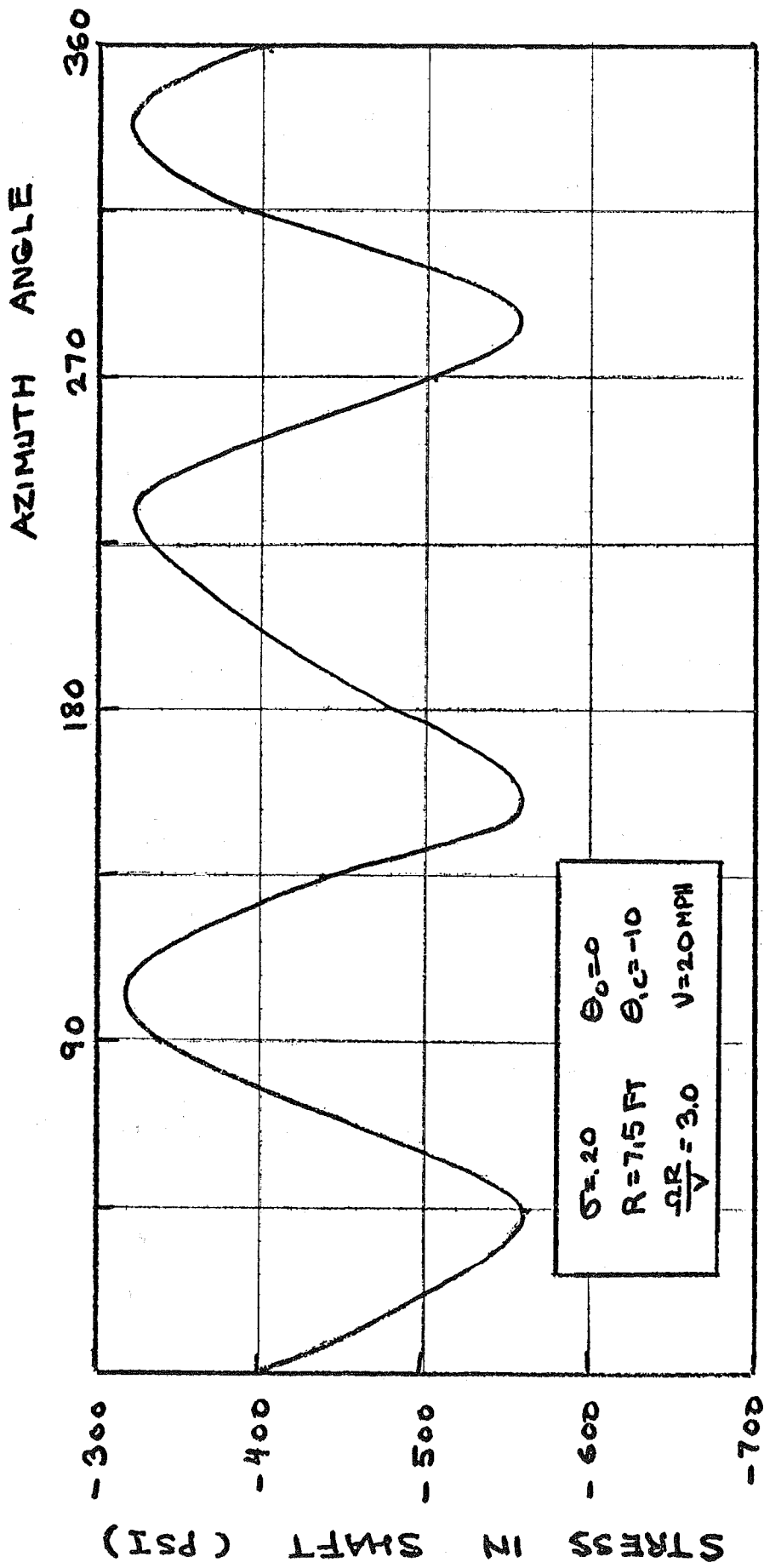


Figure 4-19. Main Shaft Stress: Nominal Operating Condition.

where  $F_{p_i}(\psi)$  is the pull rod oscillatory inertia force,  $F_{p_c}$  is the force on the pull rod due to centrifugal acceleration and  $F_{p_b}$  is the force on the pull rod caused by the blade. These forces are discussed in the following subsections.

### Blade Loads

Control system loads induced by the blades can be separated into inertial, centrifugal, and aerodynamic loads. The inertial load is caused by the rotation of the blade about its pivot or hinge point as it goes through its pitch schedule. The centrifugal load is a result of the blade center of mass being displaced tangentially relative to the hinge point. This load is not present if the blade pivot is located at the center of mass. The aerodynamic loads were discussed in Subsection 4.1. The moments,  $M_{H_p}$ , on the blade/pitch actuation system, illustrated in Figure 4-20, are

$$M_{H_p}(\psi, \alpha) = M_{H_i}(\psi) + M_{H_c}(\psi) + M_{H_a}(\psi, \alpha) \quad (4-51)$$

where  $M_{H_i}$  is the inertial moment about the blade pivot point,  $M_{H_c}$  is moment due to the centrifugal force and  $M_{H_a}$  is the aerodynamic moment on the blade. Forces due to Coriolis effects were negligible.

The inertial moment about the blade pivot is

$$M_{H_i} = I_B \ddot{\theta}(\psi) \quad (4-52)$$

where  $I_B$  is the blade moment of inertia relative to the pivot. For a given blade cross-section,  $I_B$  can be found by

$$I_B = \sum m_i r_i^2 \quad (4-53)$$

where  $m_i$  is a mass element distributed a distance  $r_i$  away from the pivot. Since the pitch schedule can be written as

$$\theta(\psi) = \theta_{1c} \cos(\Omega t - \psi_y) \quad (4-54)$$

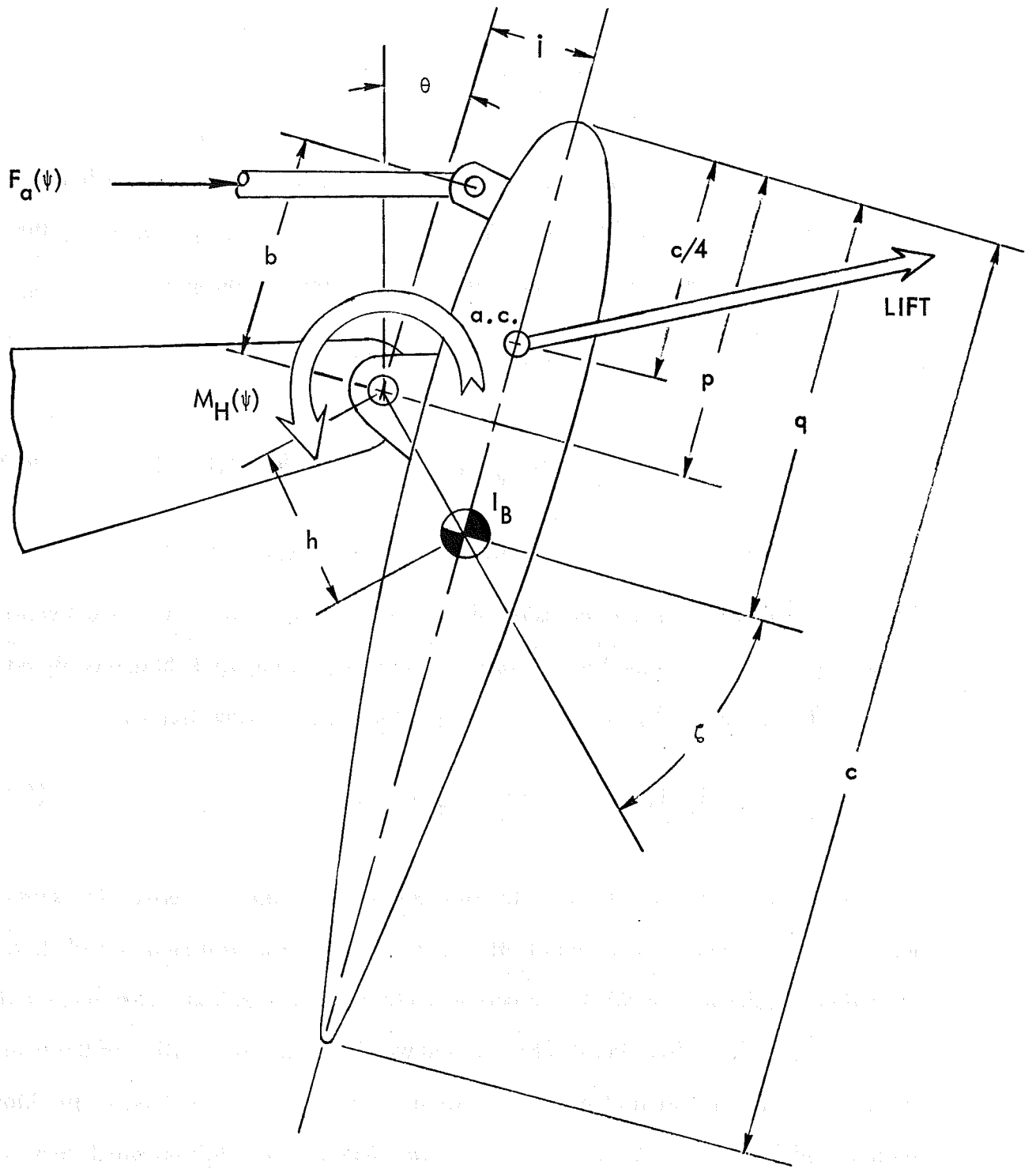


Figure 4-20. Blade/Pitch Actuation System.

the pitch acceleration is

$$\ddot{\theta}(\psi) = -\Omega^2 \theta_{1c} \cos(\Omega t - \psi_y) \quad (4-55)$$

The centrifugal moment,  $M_{H_c}(\psi)$ , about the pivot point is oscillatory tangentially because of the blade pitching motion and, thereby, induces an oscillatory moment about the blade pivot. From Figure 4-20, it can be seen that

$$\begin{aligned} M_{H_c}(\psi) &= w_b a h \sin[\theta(\psi) + \zeta] \\ &= w_b a \sqrt{(q-p)^2 + j^2} \sin[\theta(\psi) + \zeta] \end{aligned} \quad (4-56)$$

where  $w_b$  is the weight of the blade and  $a$  is the centrifugal acceleration in g's.

The aerodynamic forces act through the aerodynamic center (a.c.) which is about at 25 percent of the blade chord,  $c$ . Referring to Figure 4-20 and applying Equations (4-3) and (4-8), the aerodynamic pitching moment is written as

$$M_{H_a}(\psi, \alpha) = N(p - a_c) + jC \quad (4-57)$$

where  $a_c$  is the location of the aerodynamic center in percent of chord. The center moves aft as function of the angle of attack,  $\alpha$ . As  $\alpha$  increases from near stall to a "flat plate" position ( $\alpha = 90^\circ$ ), the aerodynamic center moves from  $.25c$  to approximately  $.5c$ . A table function can be inserted which defines the position of the aerodynamic center as function of  $\alpha$ . The position is related to the aerodynamic pitching moment,  $M(\alpha)$ , about the quarter chord of a two dimensional airfoil on which there is existing data for the NACA series. It is important to know the position of the

aerodynamic center, especially for highly stalled operation in high winds where oscillating forces are the most severe.

Moments about the blade pivot at the Cycloturbine nominal operating condition are shown in Figure 4-21. Figure 4-21a shows the inertial moment,  $M_{H_i}$  (Equation (4-52)), and the centrifugal moment,  $M_{H_c}$  (Equation (4-56)), whereas Figure 4-21b shows the aerodynamic moment,  $M_{H_a}$  (Equation (4-57)), and the total of all three moments,  $M_{H_p}$  (Equation (4-51)).

#### Pull Rod Loads

From Figure 4-20, the force exerted by the blade on the pull rod,  $F_{p_B}(\psi, \alpha)$ , can be written as

$$F_{p_B}(\psi, \alpha) = M_{H_p}(\psi, \alpha) \left[ \frac{1}{b} \right] \cos \theta(\psi) \quad (4-58)$$

Also, the side force which the pull rod retainer system (sliders) must withstand is

$$F_{p_s}(\psi, \alpha) = M_{H_p}(\psi, \alpha) \left[ \frac{1}{b} \right] \sin \theta(\psi) . \quad (4-59)$$

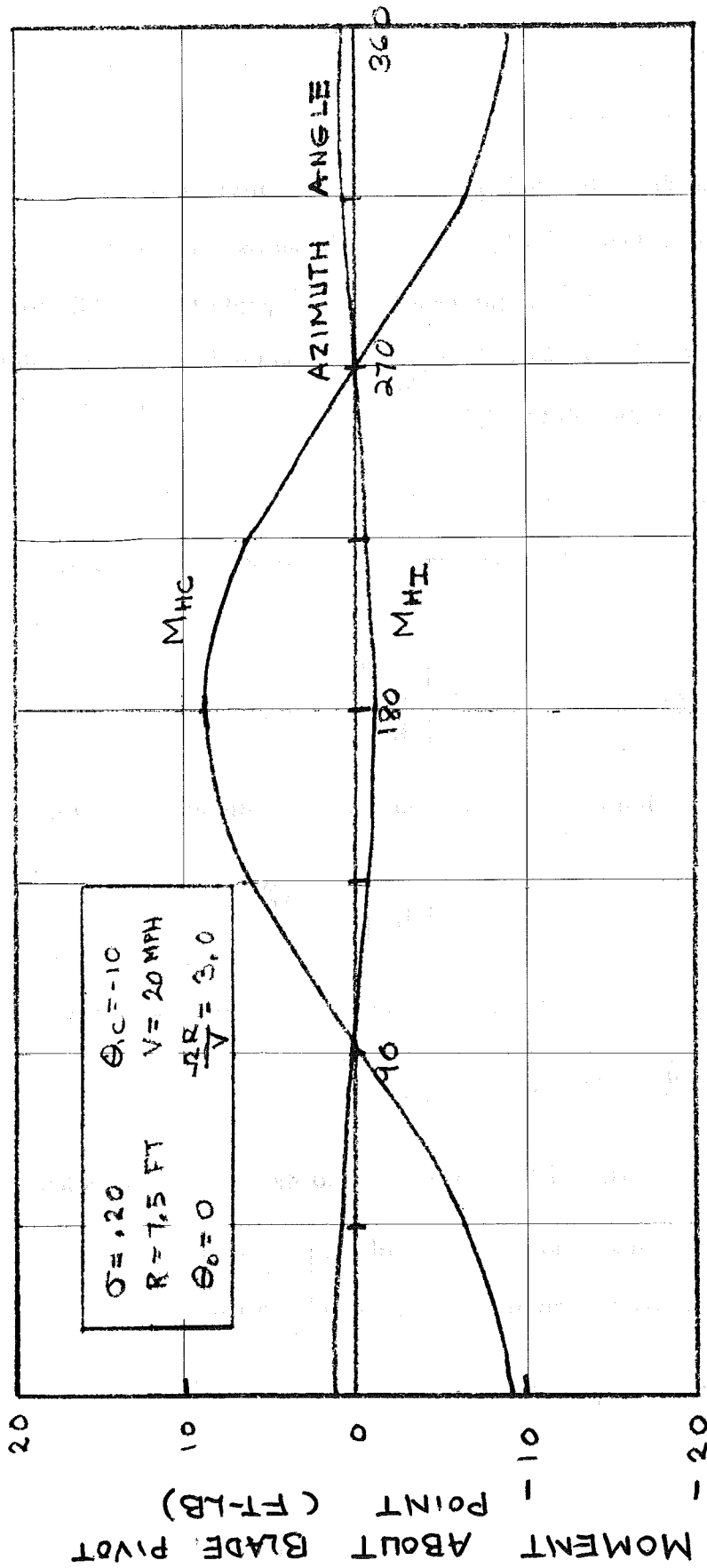
From Newton's second law, the oscillating inertial force of the pull rod is

$$F_{p_i}(\psi) = m_p a_{p_i}(\psi) \quad (4-60)$$

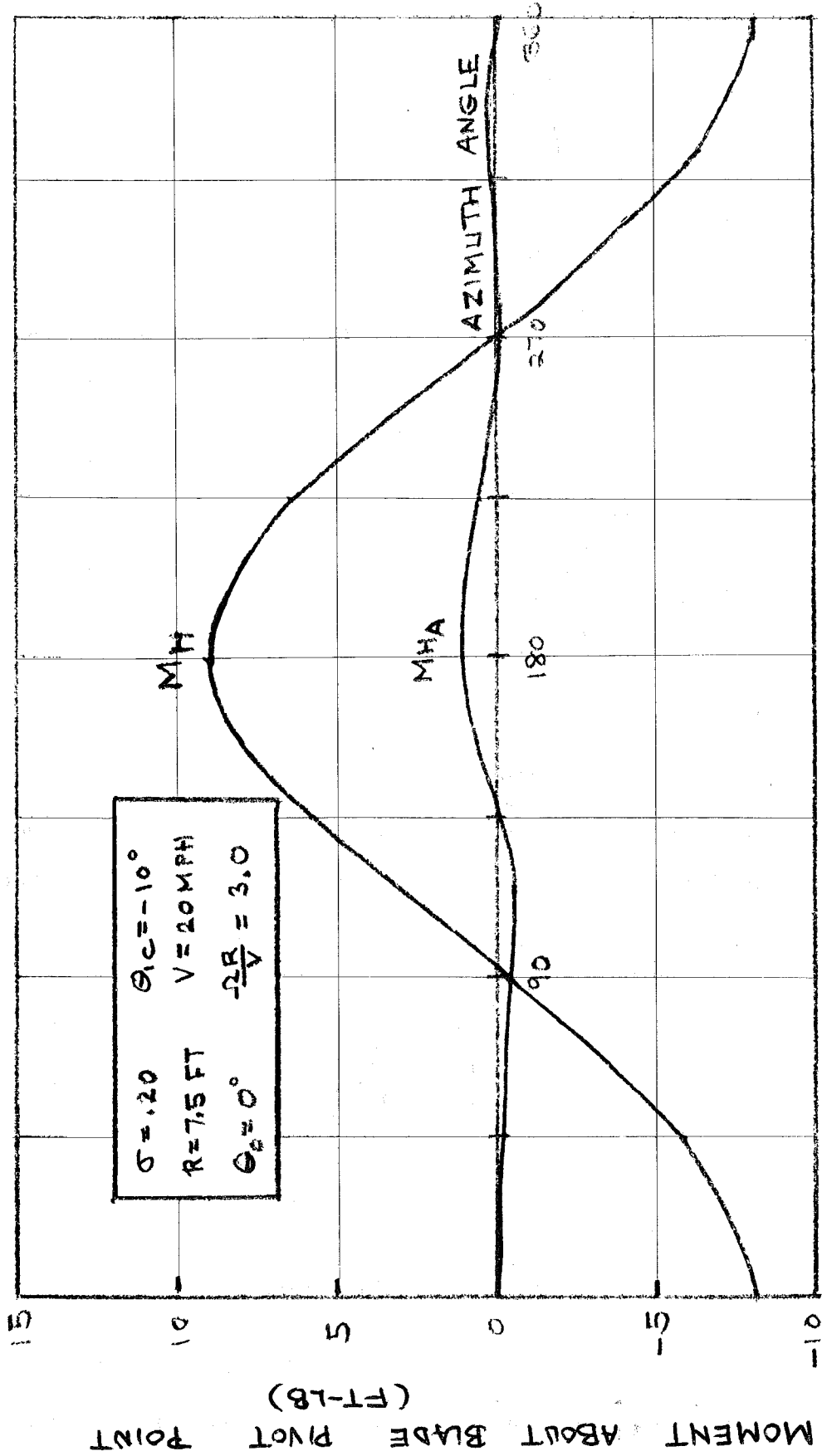
where  $a_{p_i}$  is the acceleration of the pull rod due to the tilt-cam eccentricity.

The relative change in length,  $e$ , of the pull rod linkage induced by the cam eccentricity at a given azimuth angle,  $\psi$ , can be written as

$$e(\psi) = E \cos(\Omega t - \psi_y) \quad (4-61)$$



a) Inertial and Centrifugal  
 Figure 4-21. Moment About Blade Pivot: Nominal Operating Condition.



b) Aerodynamic and Total

Figure 4-21. Moment About Blade Pivot: Nominal Operating Condition (Concluded).

where

$$\psi = \Omega t$$

$$E = \text{eccentricity}$$

$$\Omega = \text{angular velocity}$$

$$\psi_y = \text{phase angle}$$

Differentiating Equation (4-61) twice, the acceleration of the pull rod is obtained

$$a_{P_i}(\psi) = -\Omega^2 E \cos(\Omega t - \psi_y) \quad (4-62)$$

Thus, Equation (4-60) becomes

$$F_{P_i}(\psi) = \frac{w_p}{g} \Omega^2 E \cos(\Omega t - \psi_y) \quad (4-63)$$

where  $w_p$  is the weight of pull rod.

This oscillatory force is superimposed on a mean centrifugally activated force. Small forces due to radial position change are neglected. The force due to centrifugal acceleration of the pull rod is obtained by integrating over the radial length, so that

$$F_{P_c} = \frac{w_p}{2g} \Omega^2 \left[ \frac{R^2 - r_o^2}{R - r_o} \right] \quad (4-64)$$

where

$$R = \text{turbine radius}$$

$$r_o = \text{distance between cam center and pull rod}$$

The total force on the pull rod root given by Equation (4-50) at the Cycloturbine nominal operating condition as a result of the total blade moment shown in Figure 4-21b is given in Figure 4-22.

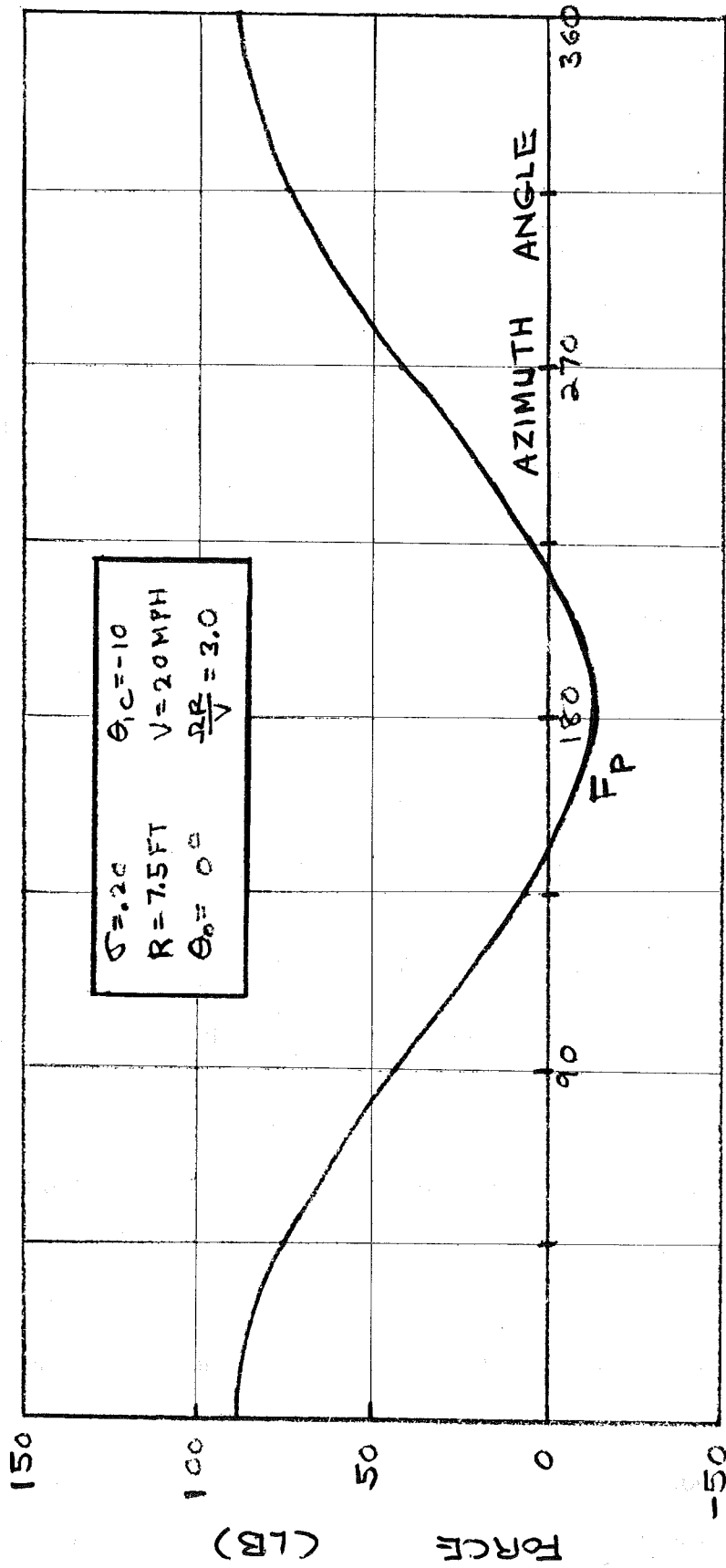


Figure 4-22. Force on the Pull Rod Root: Nominal Operating Condition.

#### 4.5.2 MAXIMUM OPERATIONAL STRESSES

The total stresses for the 15-ft Cycloturbine in its nominal operating condition, i.e.,  $V = 20$  mph, are shown in Figures 4-13, 4-14, 4-17, 4-19, and 4-22. The variation in the stresses with azimuth angle shows that the stresses are cyclic but not sinusoidal. Peak stresses can be determined from plots such as these. This has been done for the stresses at the five critical points over the operational range of 5 mph to 40 mph. The maximum stresses are shown as a function of wind speed in Figure 4-23 for the rotor critical points and in Figure 4-24 for the pitch actuation system.

The criticality of the stresses is determined by comparing the operational stress to the yield stress for the material used in the rotor components. The yield stresses for the Cycloturbine components are listed in Table 4-3. It is seen that the maximum stresses are conservative for the normal operational range and conditions to be encountered.

Table 4-3. Cycloturbine Yield Stresses.

Material	Component	Yield Stress
Aluminum 6061-T6	Blade and Strut	30,000 psi (bending)
DOM Steel	Shaft	60,000 psi (bending)
Stainless 304	Pull Rod	95,000 psi (tension)

The oscillatory nature of the stresses, however, introduces the possibility of fatigue problems. In order to evaluate the severity of the fatigue condition, the Soderberg diagram has been used (see Subsection 2.2.3.1). In this diagram, experimental fatigue data for various materials are used to establish an operational boundary. The calculated oscillatory stresses are plotted in the diagram as a function of the mean

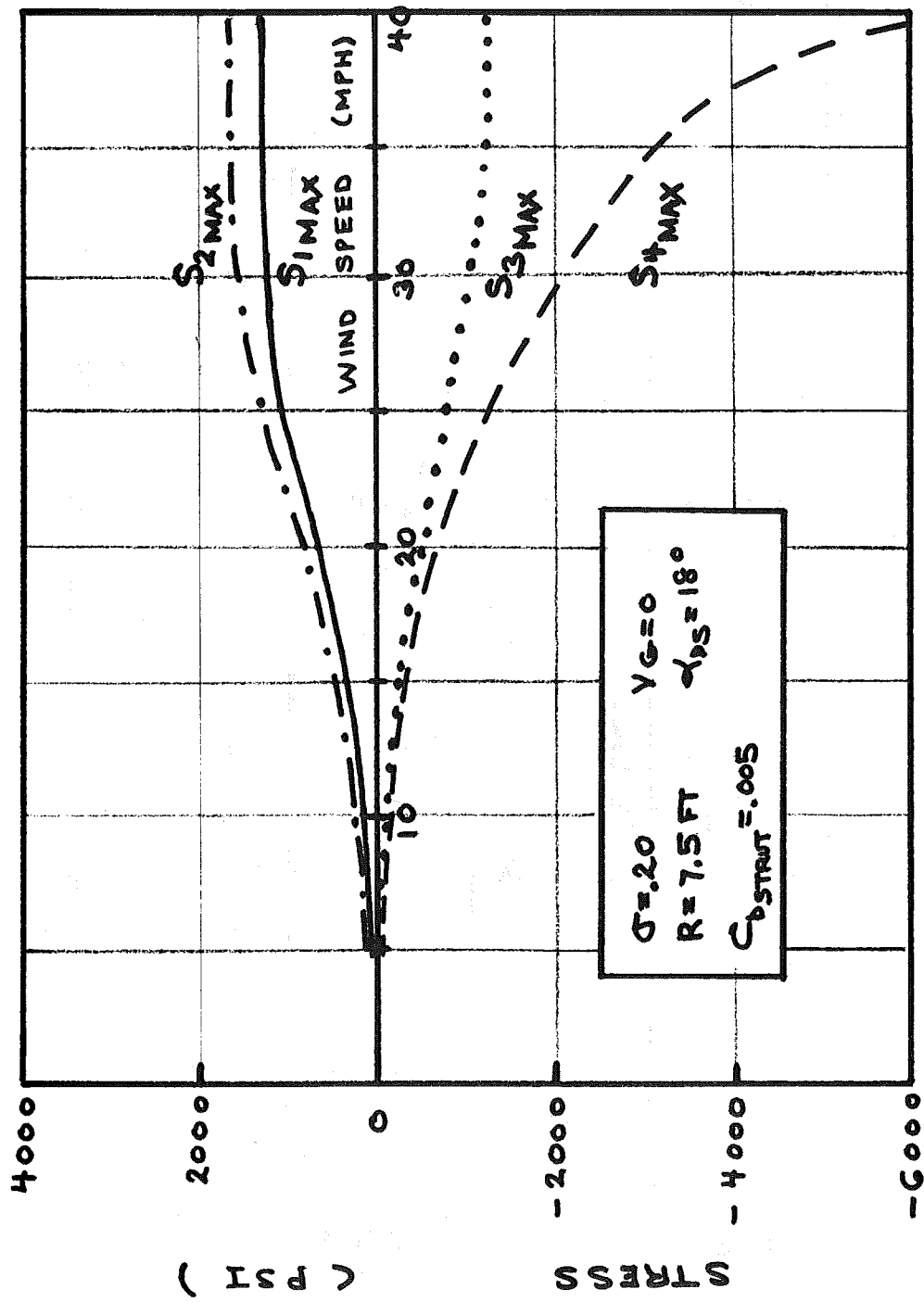


Figure 4-23. Maximum Operational Stresses: Blade Center Spar, S1; Blade/Strut Connection, S2; Strut Root, S3; and Main Shaft, S4.

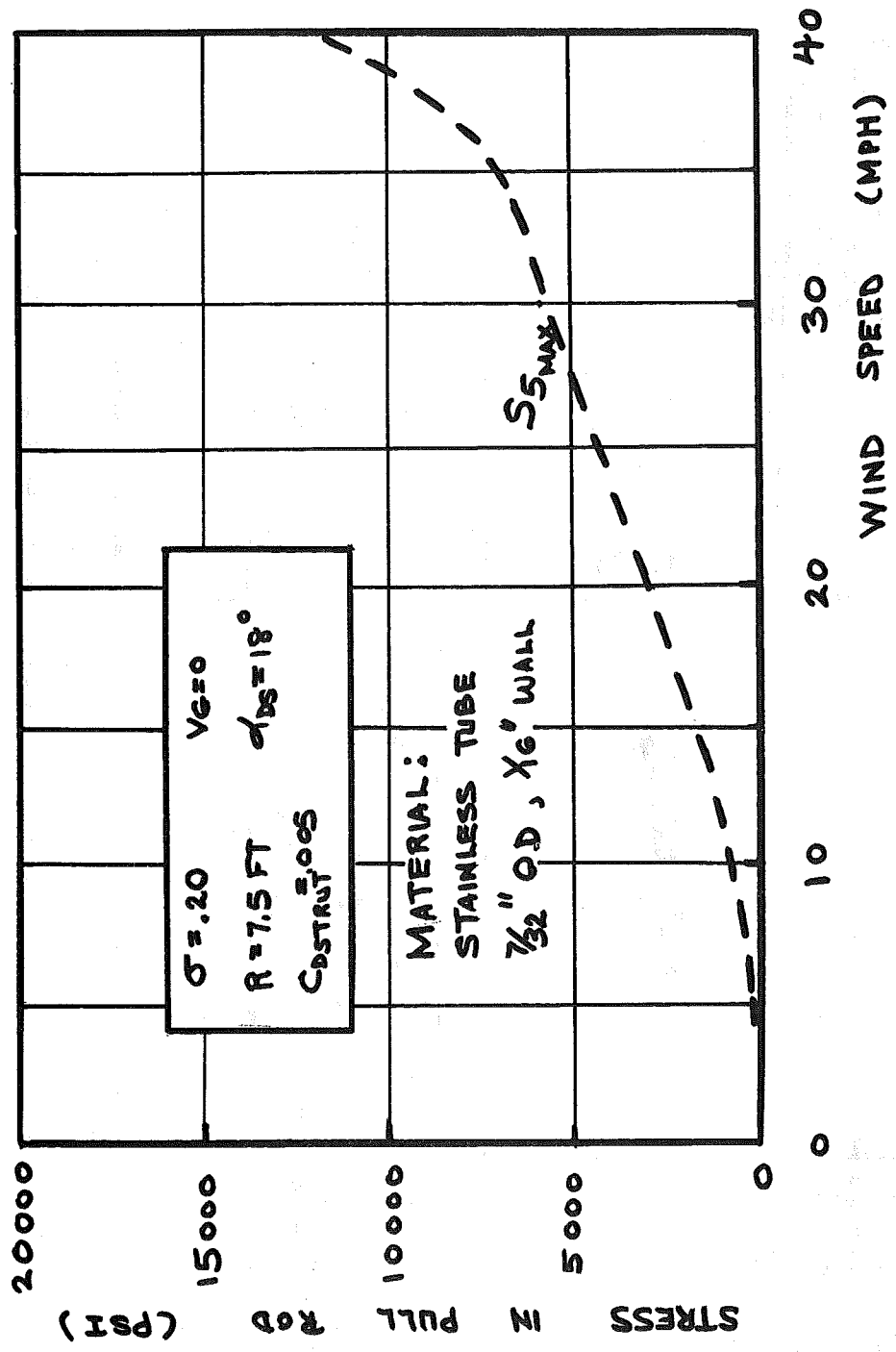


Figure 4-24. Maximum Operational Stress: Pull Rod Root,  $S_5$ .

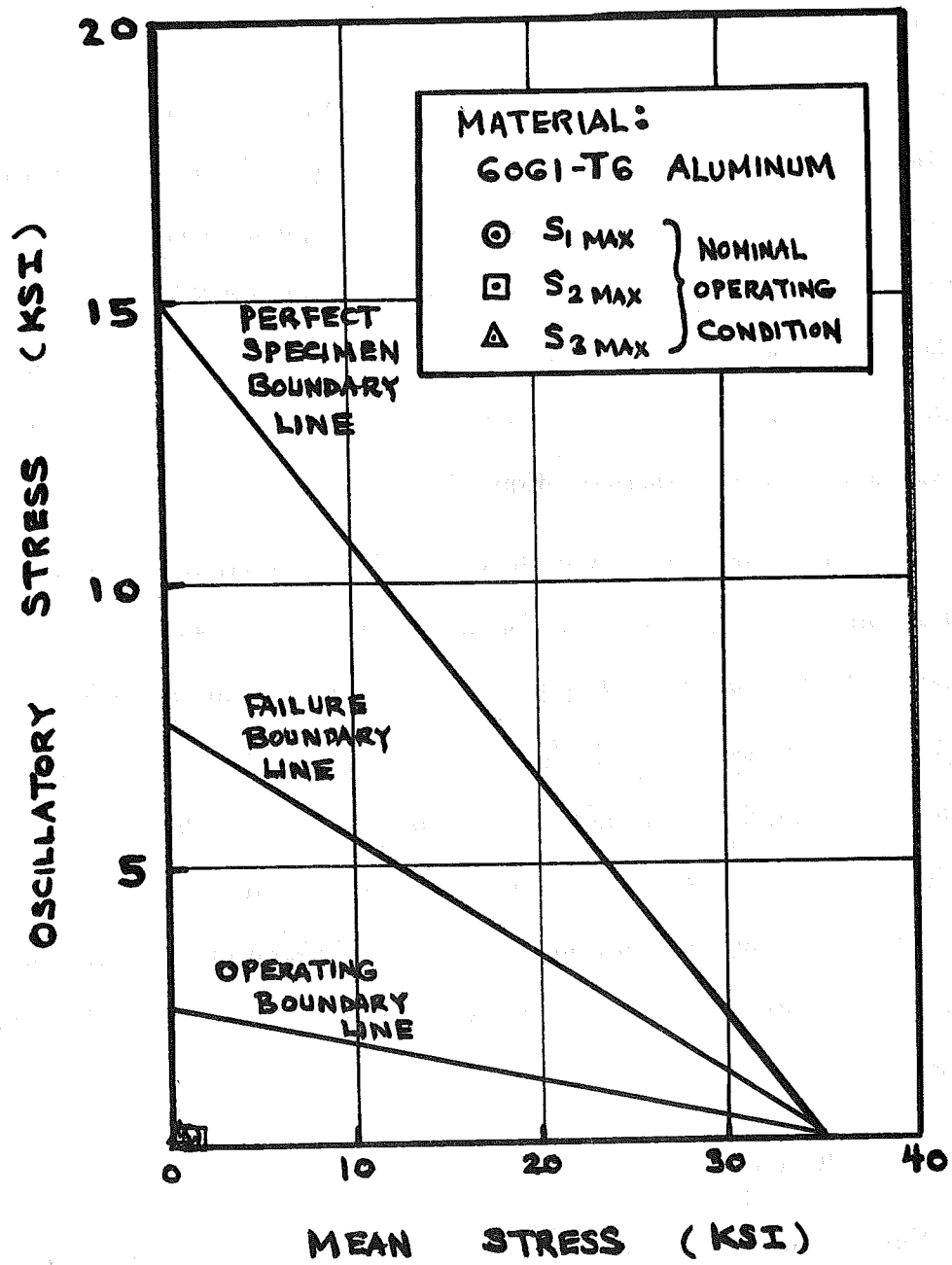
stress. If the calculated stresses lie below the operational boundary, this is considered adequate substantiation for unlimited fatigue life. The Soderberg diagram is recommended for use in design because it is on the safe side of the test results and is, therefore, considered to be conservative. The maximum stresses at the nominal operating condition are shown on the Soderberg diagram in Figure 4-25. The aerodynamic stress is plotted as the oscillatory stress and the centrifugal stress is plotted as the mean stress. The aluminum component stresses are shown in Figure 4-25a and the steel shaft stress is shown in Figure 4-25b. As seen in these figures, the nominal operational stresses lie well below the Operating Boundary Line, and, therefore, these components can be considered to have unlimited fatigue life.

At 40 mph, the shutdown mechanism of the Cycloturbine is aerodynamically activated and the rotor stops rotating. The maximum stresses generated on the stopped rotor in the wind speed range of 40 mph to 120 mph are shown in Figure 4-26.

Figure 4-26a shows the stresses at the blade spar center, the blade/strut connection, and the strut root, and the main shaft stress is shown in Figure 4-26b. Pull rod root stress is given in Figure 4-26c where the tension stress is for a blade on the upwind side of the turbine and the compression stress is for a blade on the downwind side of the turbine. Comparison of the stresses to the yield stresses (see Table 4-3) shows that they are not critical.

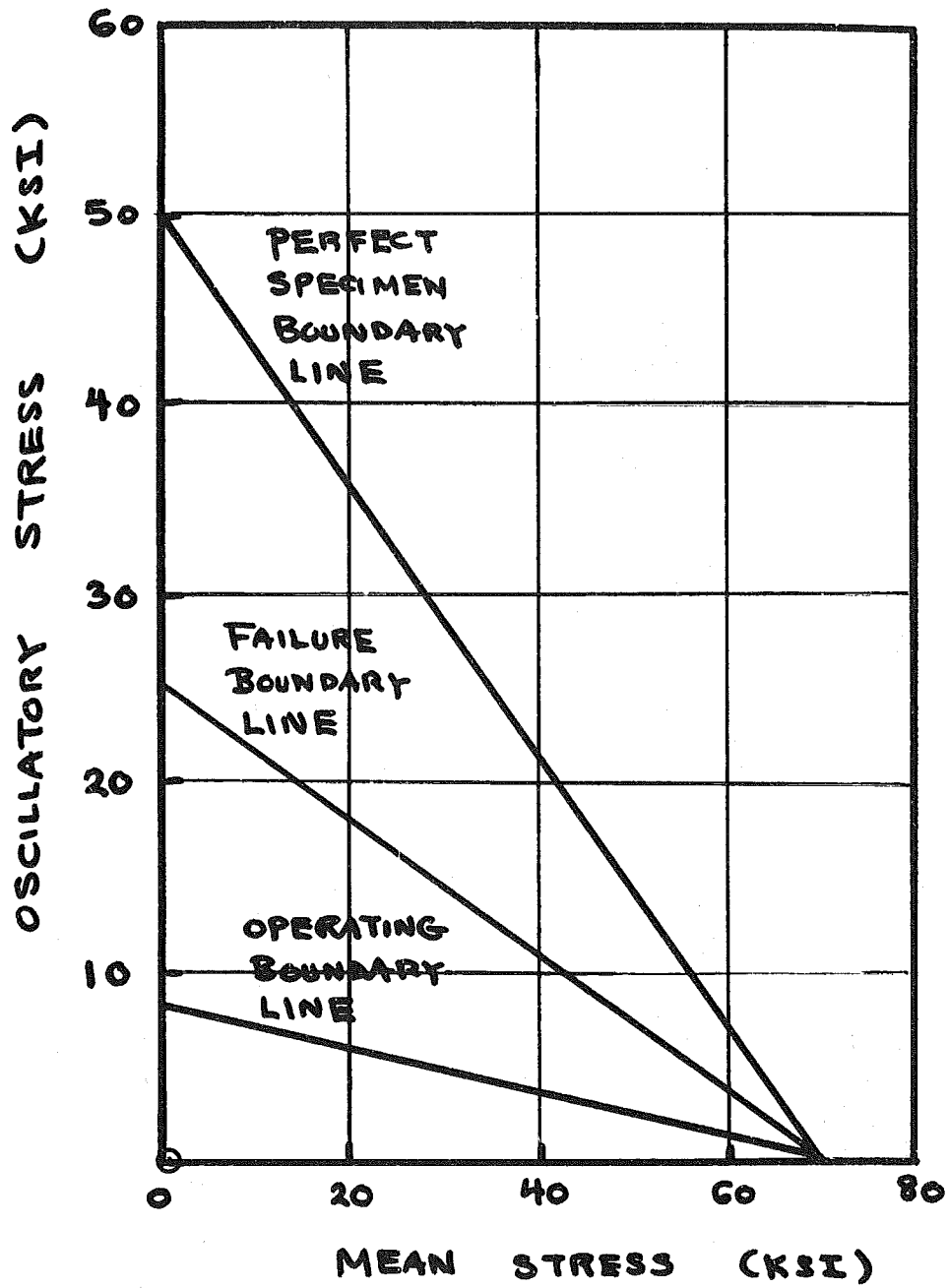
#### 4.5.3 MAXIMUM STRESSES DUE TO GUSTS

The gust analysis of Subsection 4.4 was used to determine the aerodynamic loads on both the operating and stopped rotor, and the subsequent maximum stresses. The effect of a sharp-edged gust on the maximum stress is shown in Figure 4-27 for two different wind speeds, namely, nominal wind speed of 20 mph and the maximum operating wind speed of 40 mph. The blade spar center stress and the blade/strut connection



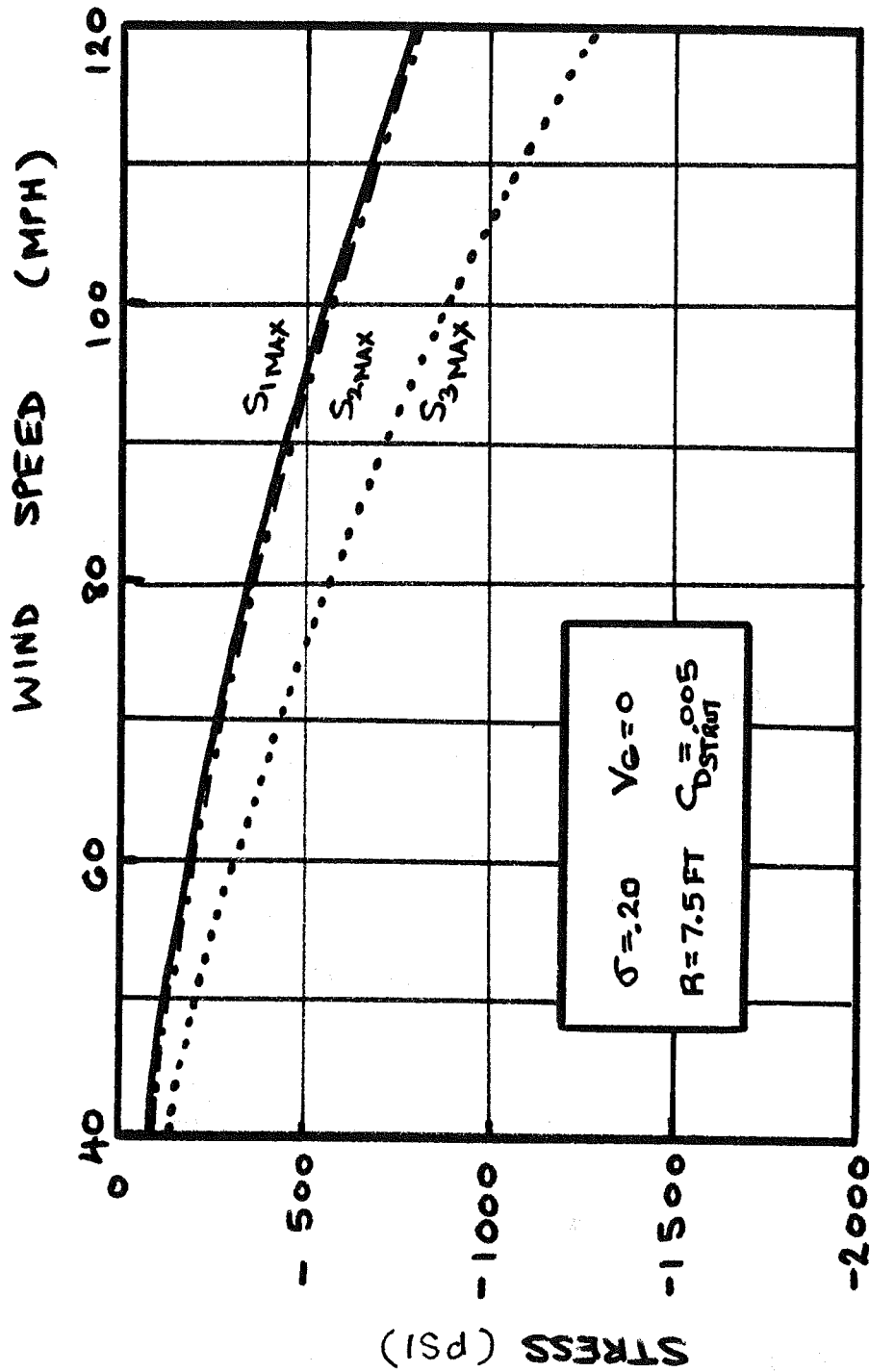
a) 6061-T6 Aluminum

Figure 4-25. Soderberg Diagram: Nominal Operating Condition.



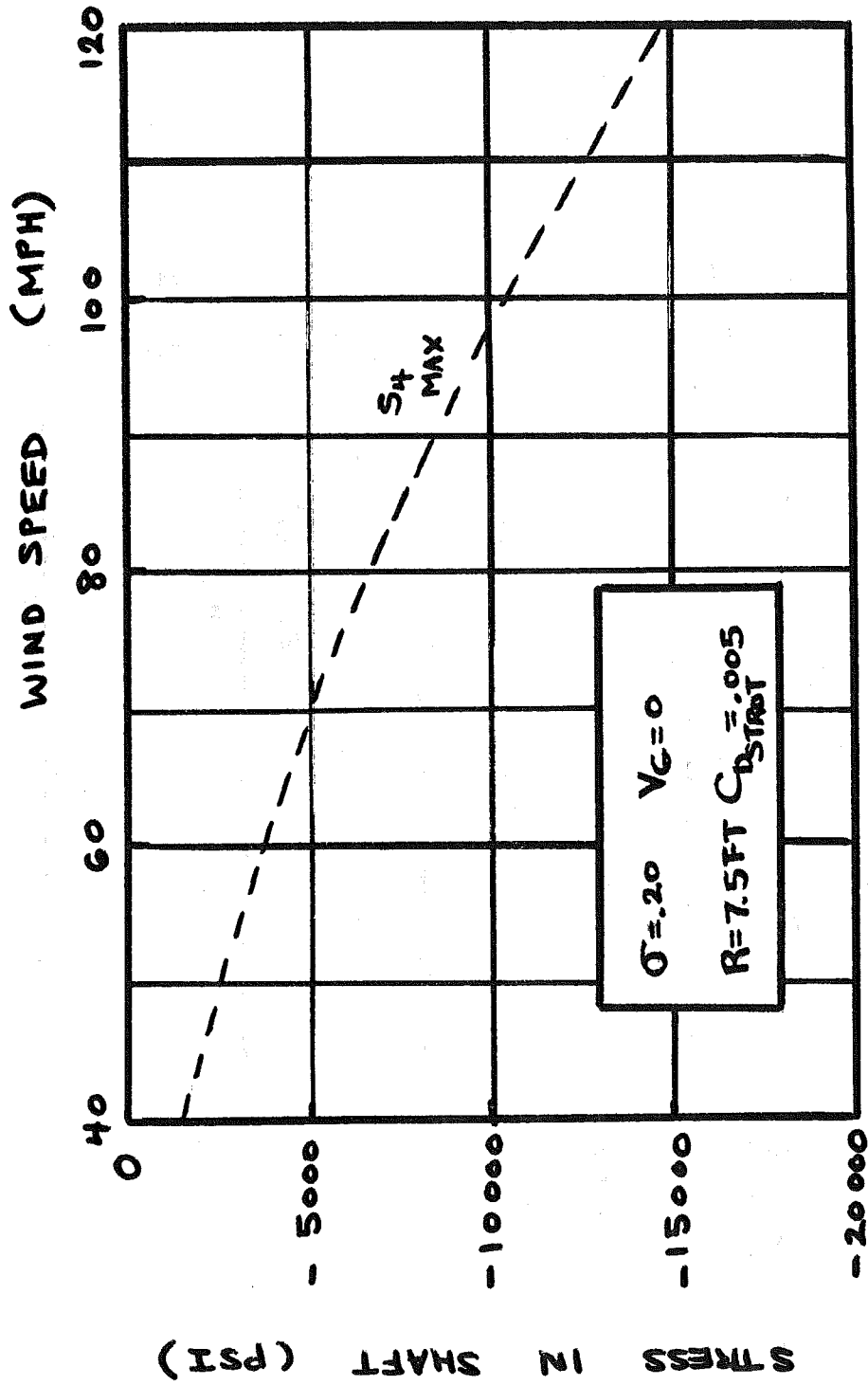
b) Steel

Figure 4-25. Soderberg Diagram: Nominal Operating Condition (Concluded).



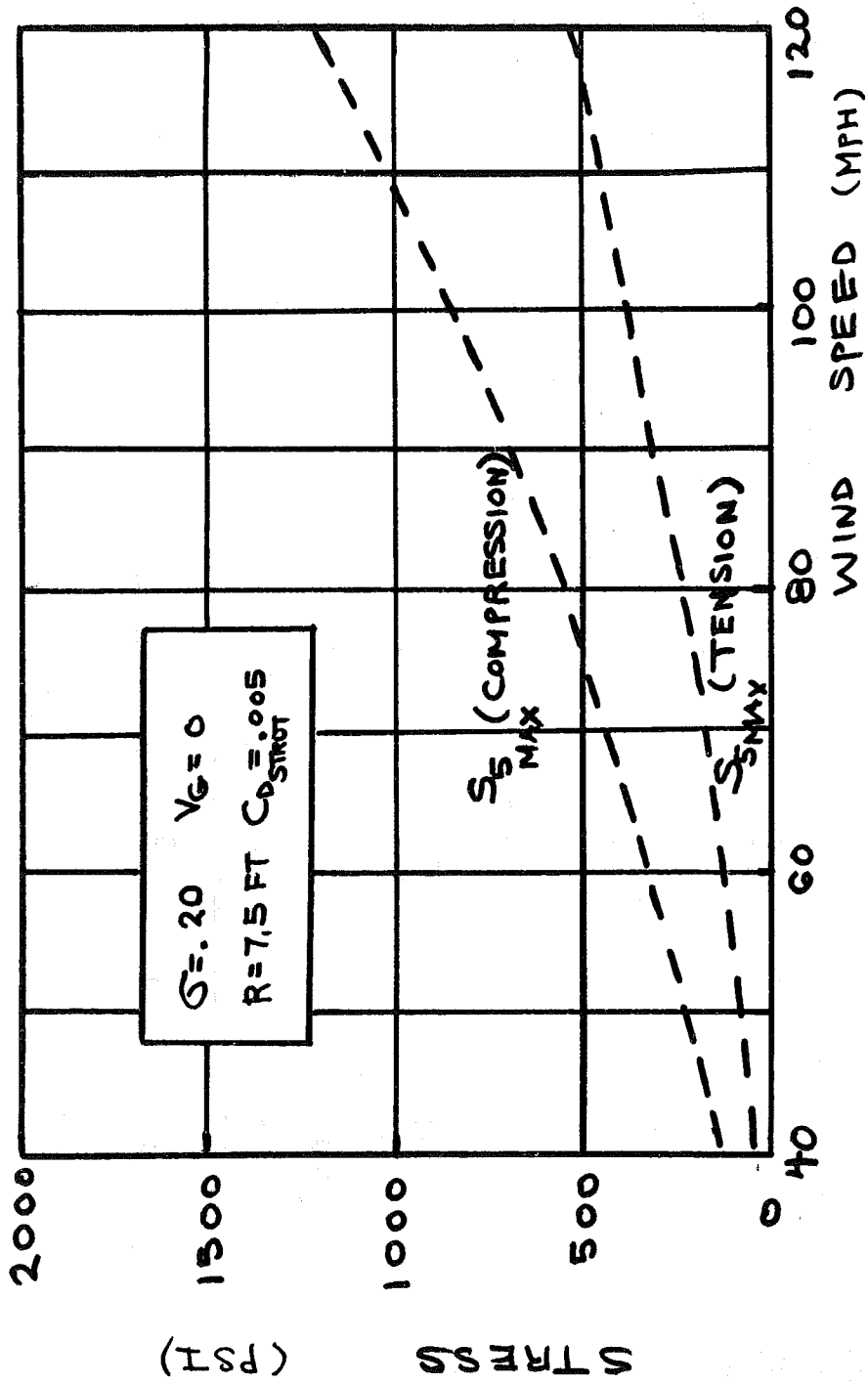
a) Blade Spar Center, Blade/Strut Connection, and Strut Root

Figure 4-26. Maximum Stresses on Stopped Rotor.



b) Main Shaft

Figure 4-26. Maximum Stresses on Stopped Rotor (Continued).



c) Pull Rod Root

Figure 4-26. Maximum Stresses on Stopped Rotor (Concluded).

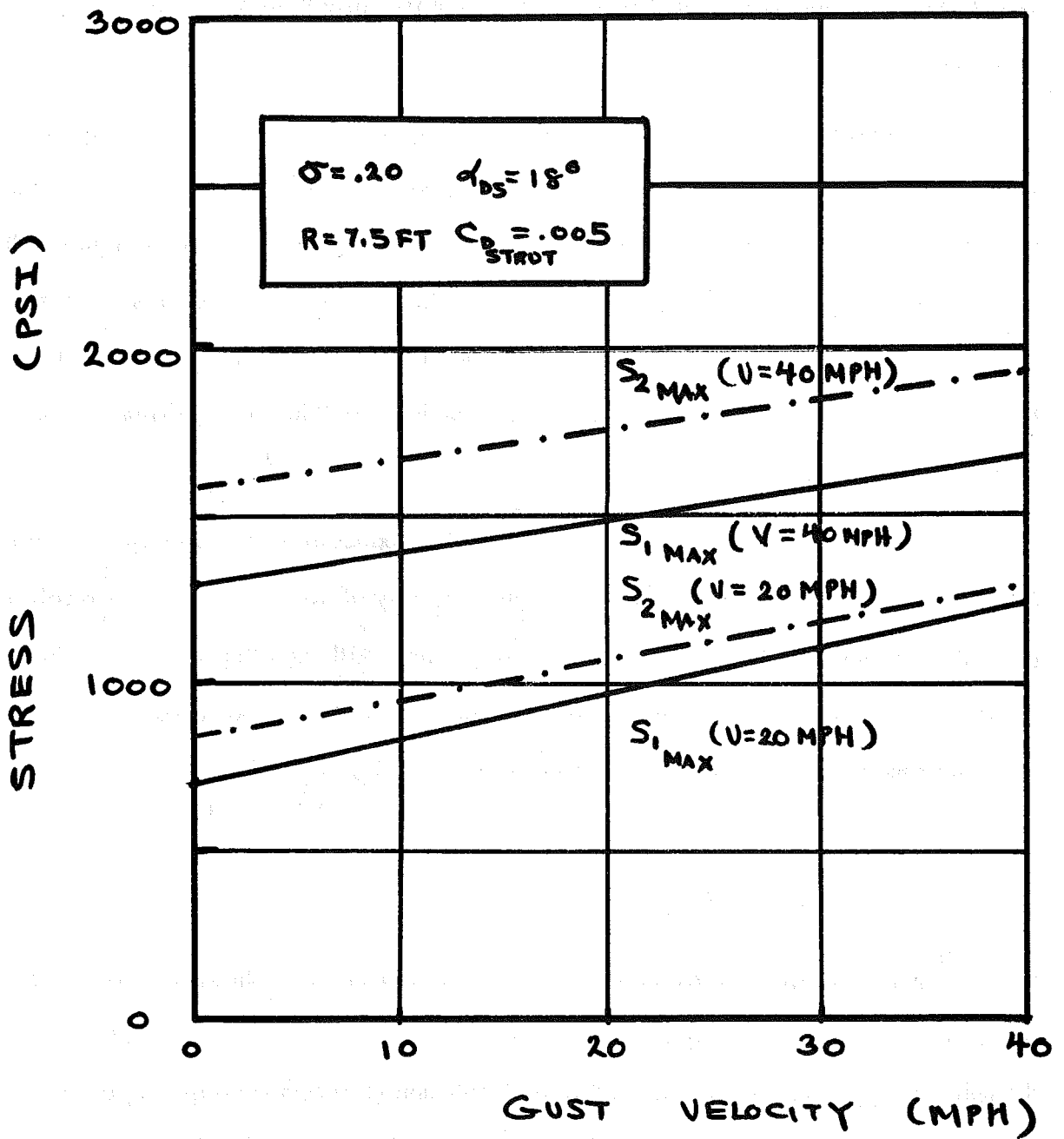
stress are shown in Figure 4-27a for gust velocities up to 40 mph and the strut root stress and mainshaft stress are shown in Figure 4-27b. Although none of the stresses are critical (see Table 4-3), the main shaft stress increases significantly with both wind speed and gust velocity.

Similar data are shown in Figure 4-28 for the worst case gust velocity of 40 mph. The maximum rotor stresses are shown in Figure 4-28a as a function of wind speed prior to the gust, and the pull rod root stress is presented in like manner in Figure 4-28b. As seen in the table on each figure, the effect of the gust input was to reduce the tip speed ratio  $\Omega R/U$  instantaneously while the rpm of the rotor remained unaffected. The range of resultant tip speed ratios caused the rotor to be running in the dynamic stall regime.

The gust analysis was also applied to the stopped rotor for wind speeds before gust of up to 120 mph with a superimposed gust velocity of 40 mph. The stress results are presented in Figure 4-29 for all of the critical points. Although the stresses are significantly higher than those without the effect of the gust, none approach the corresponding yield stresses (see Table 4-3). The margin of safety, MS, defined by

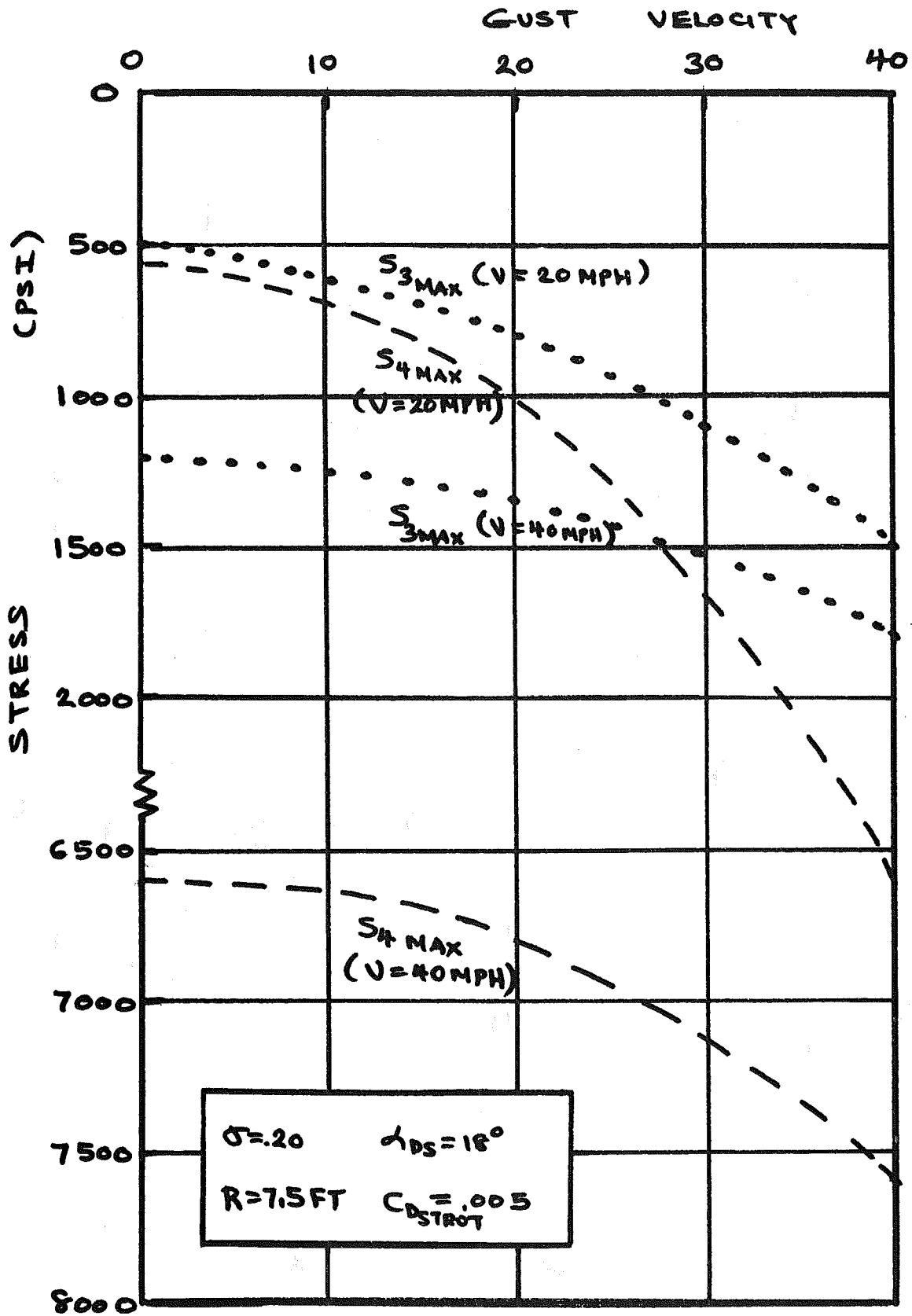
$$MS = \frac{F - f}{f}$$

where  $F$  is the allowable stress and  $f$  is the calculated stress, is shown for the critical areas in a 120-mph wind in Table 4-4. Note that the stresses at 120 mph with the 40 mph gust approach the design condition of 165 mph (120 mph wind speed plus a 45 mph gust velocity). The margin of safety of the critical areas for the 165 mph design condition are presented in Table 4-4.



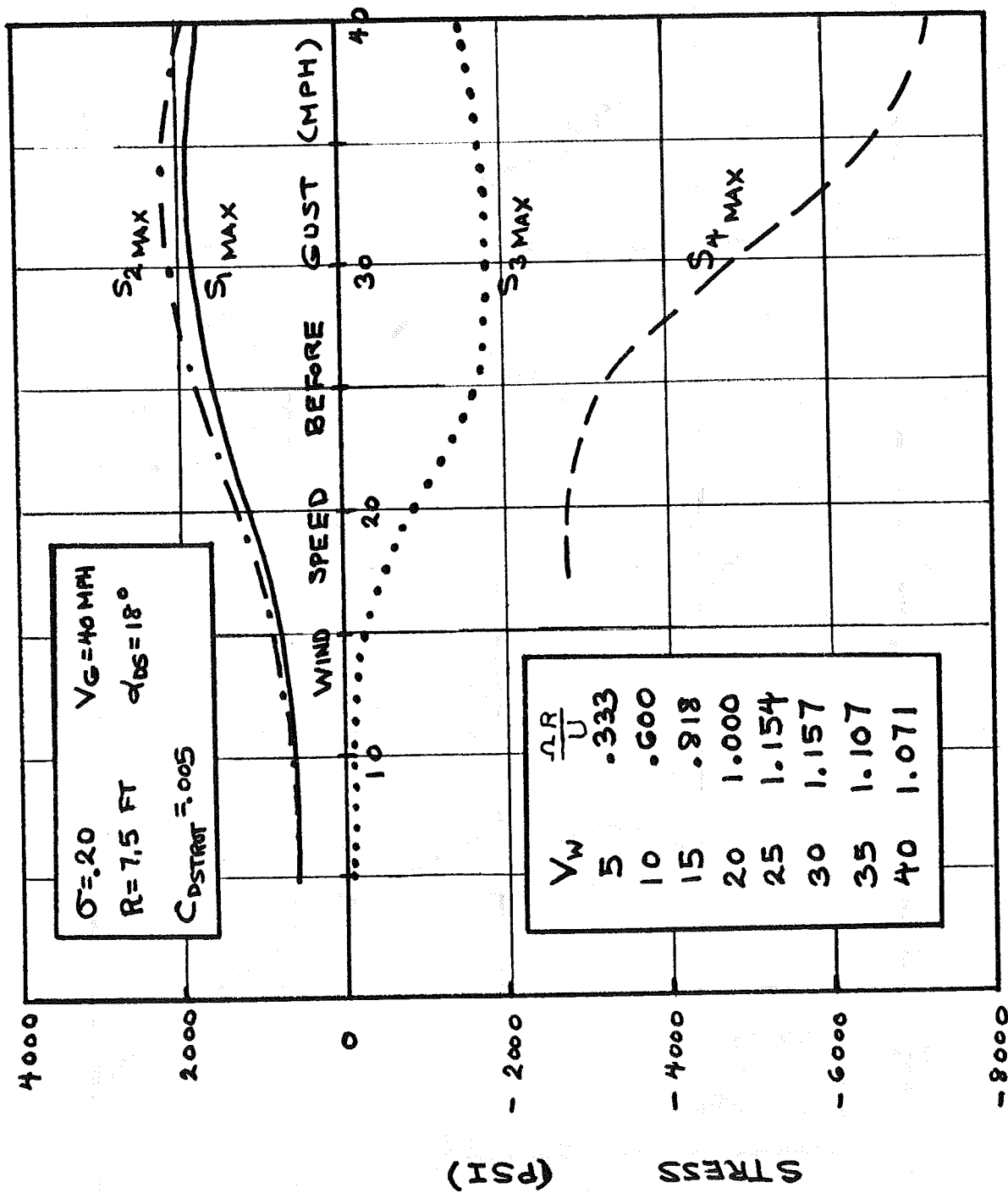
a) Blade Spar Center and Blade/Strut Connection

Figure 4-27, Effect of Sharp-Edged Gust.



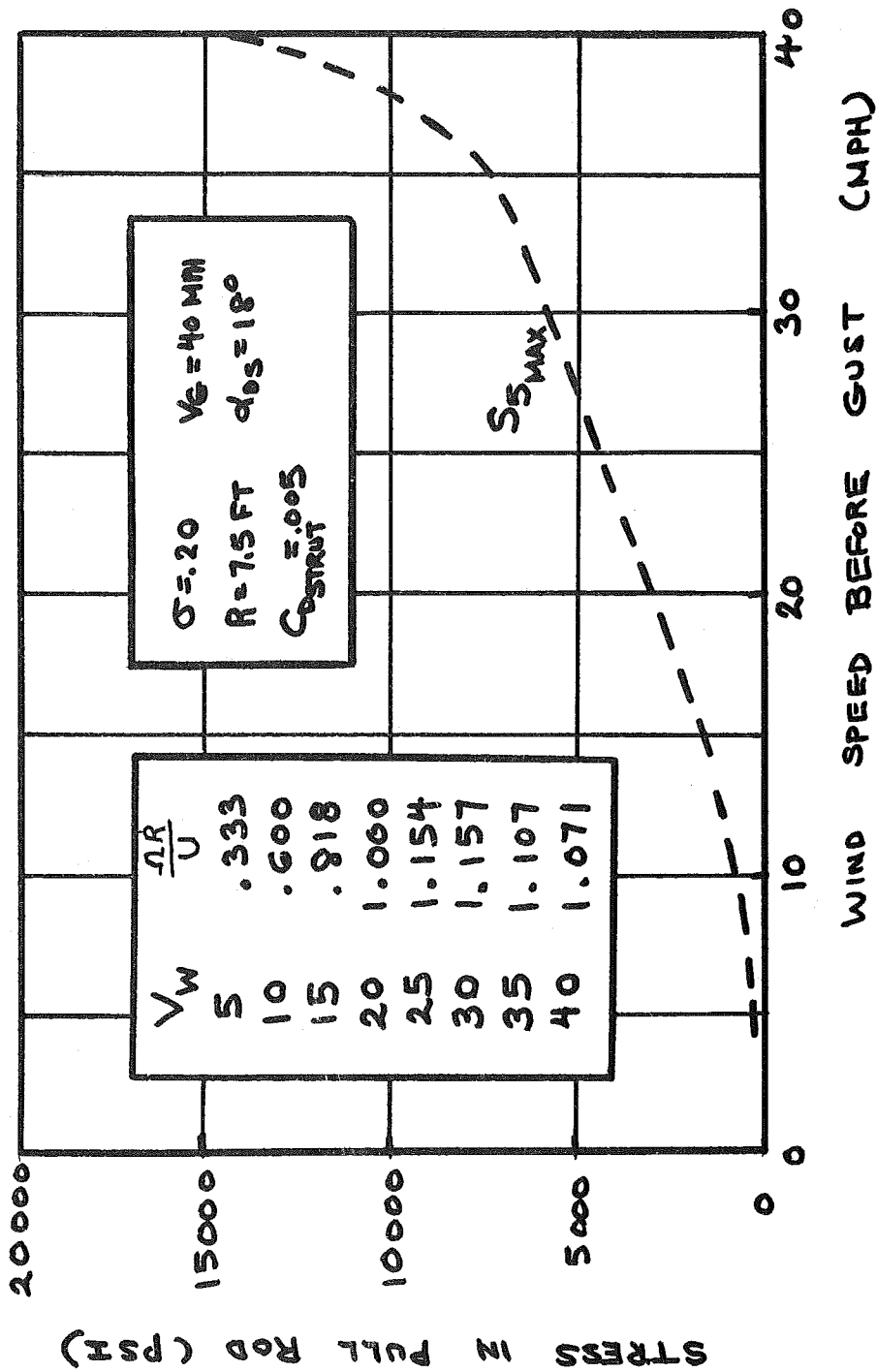
b) Strut Root and Main Shaft

Figure 4-27. Effect of Sharp-Edged Gust (Concluded).



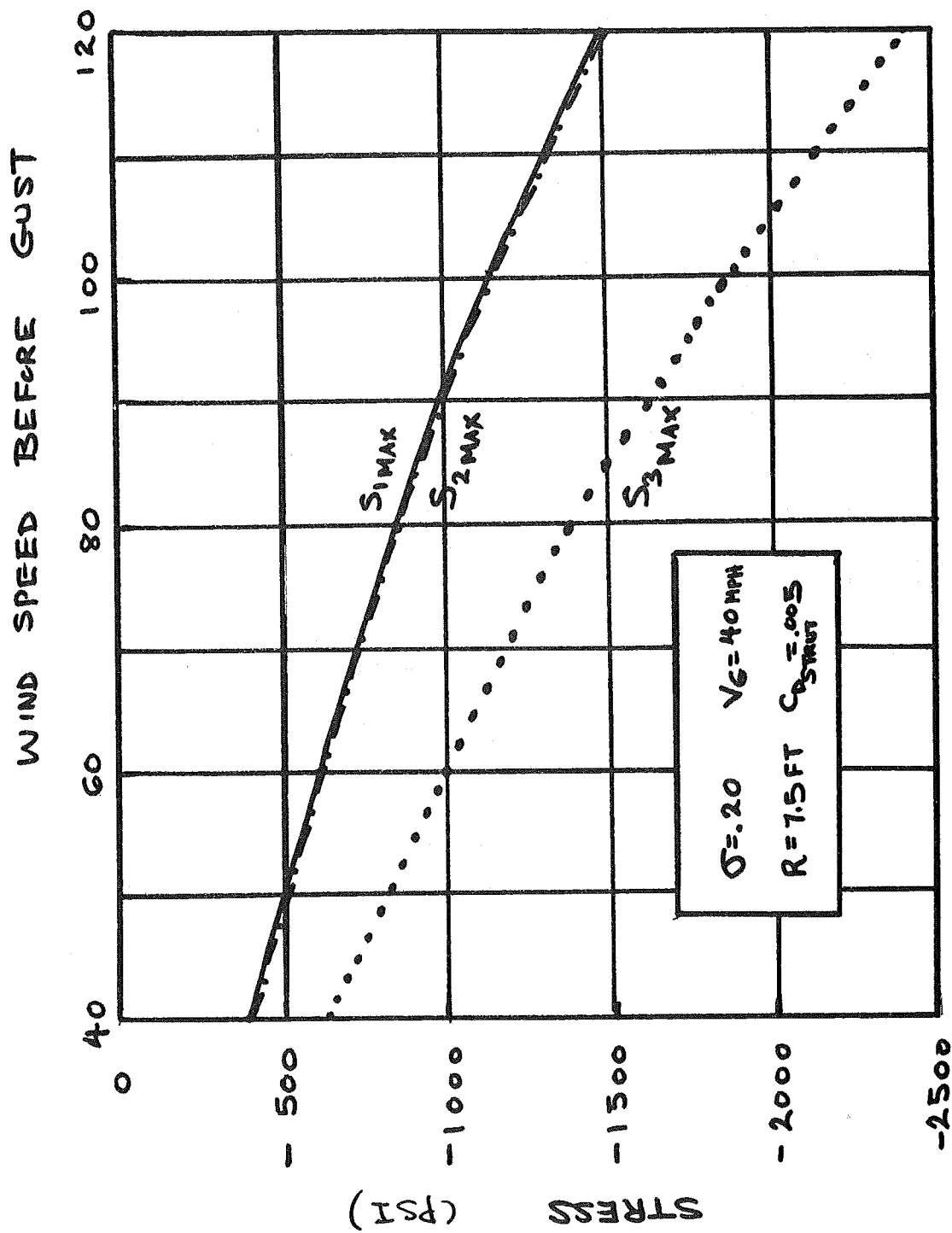
a) Rotor Critical Points

Figure 4-28. Maximum Operational Stresses Due to Gusts.



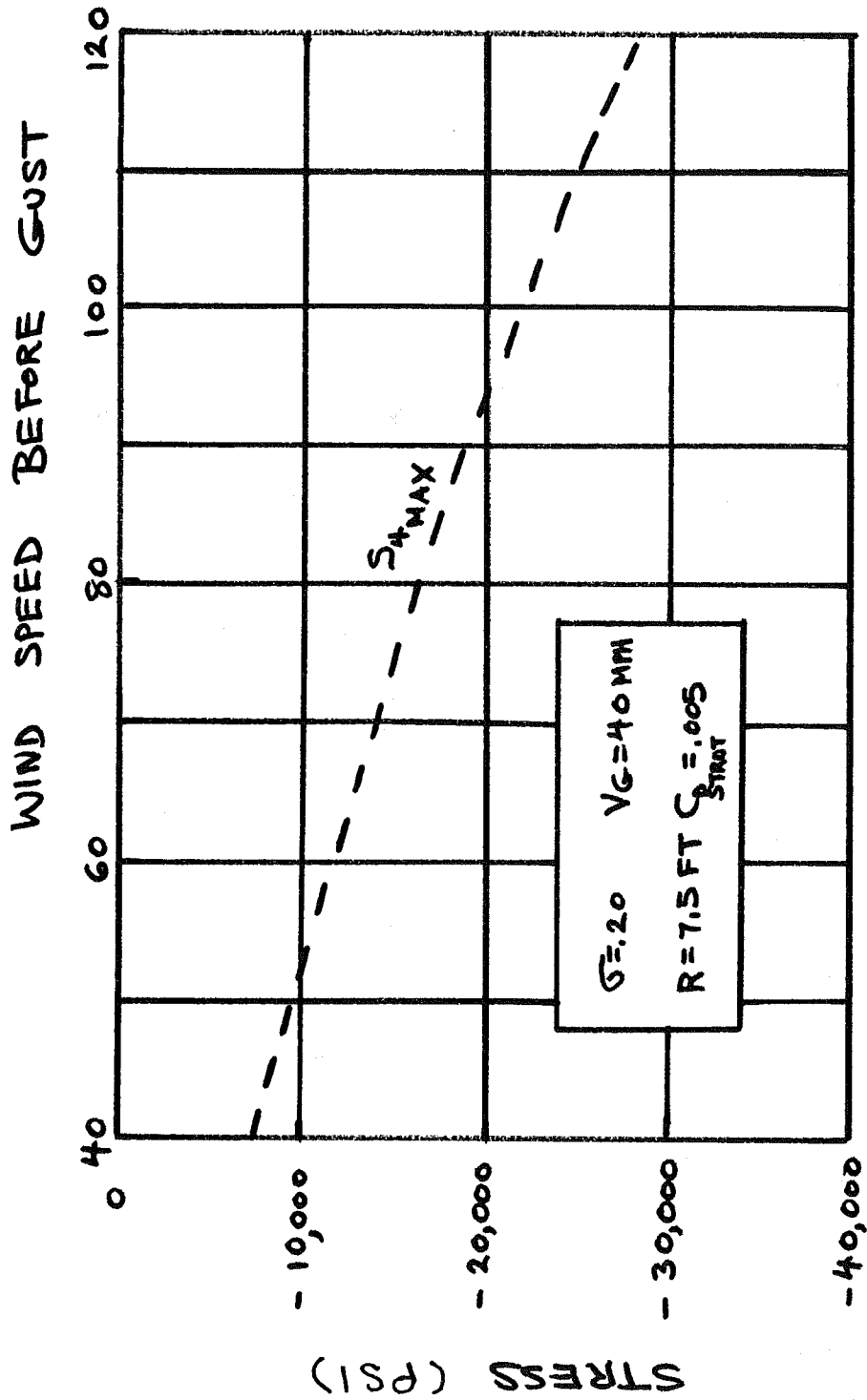
b) Pull Rod Roof

Figure 4-28. Maximum Operational Stresses Due to Gusts (Concluded).



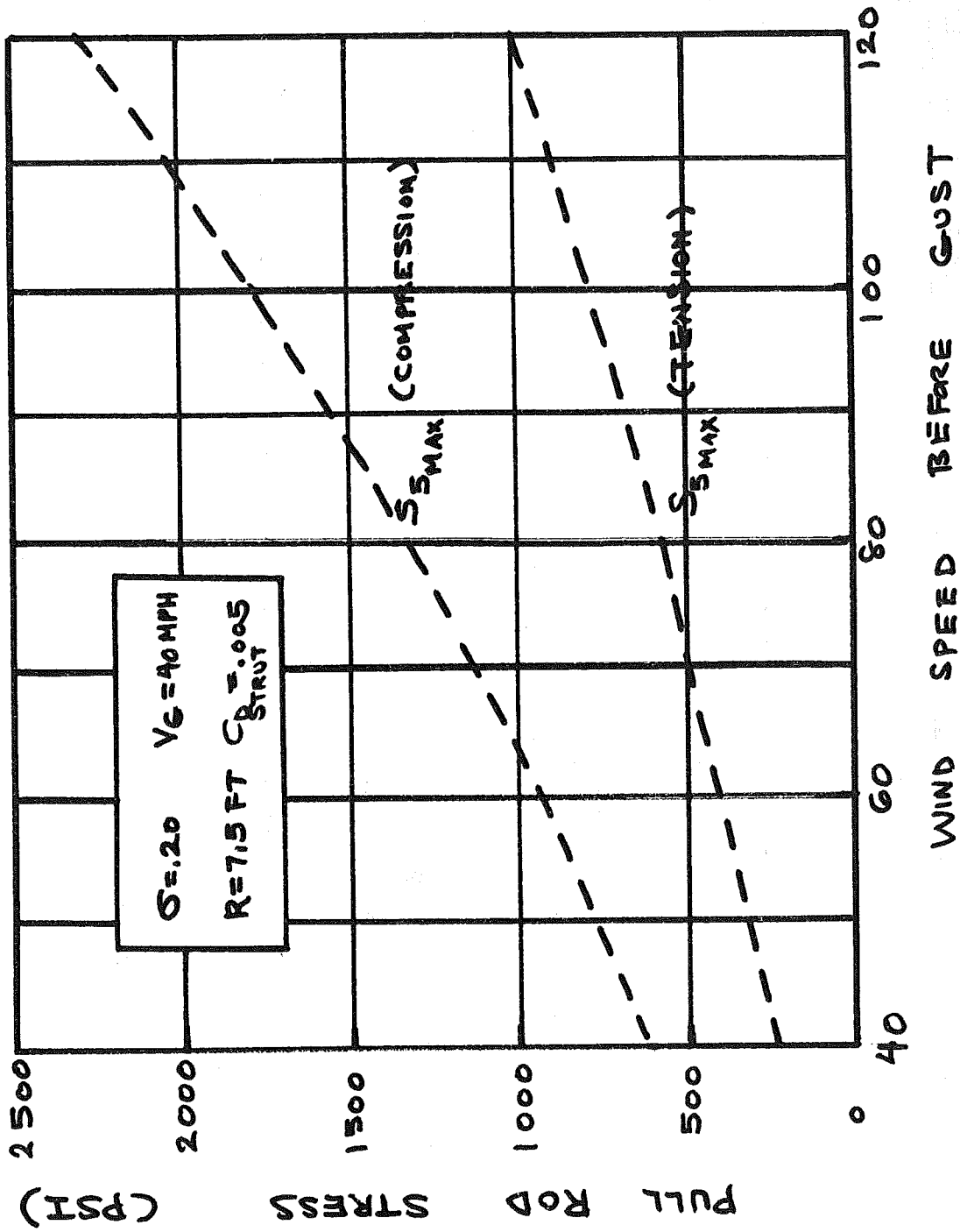
a) Blade Spar Center, Blade/Strut Connection, and Strut Root

Figure 4-29. Maximum Stresses on Stopped Rotor Due to Gusts.



b) Main Shaft

Figure 4-29. Maximum Stresses on Stopped Rotor Due to Gusts (Continued).



c) Pull Rod Root

Figure 4-29. Maximum Stresses on Stopped Rotor Due to Gusts (Concluded).

Table 4-4. Cycloturbine Margins of Safety.

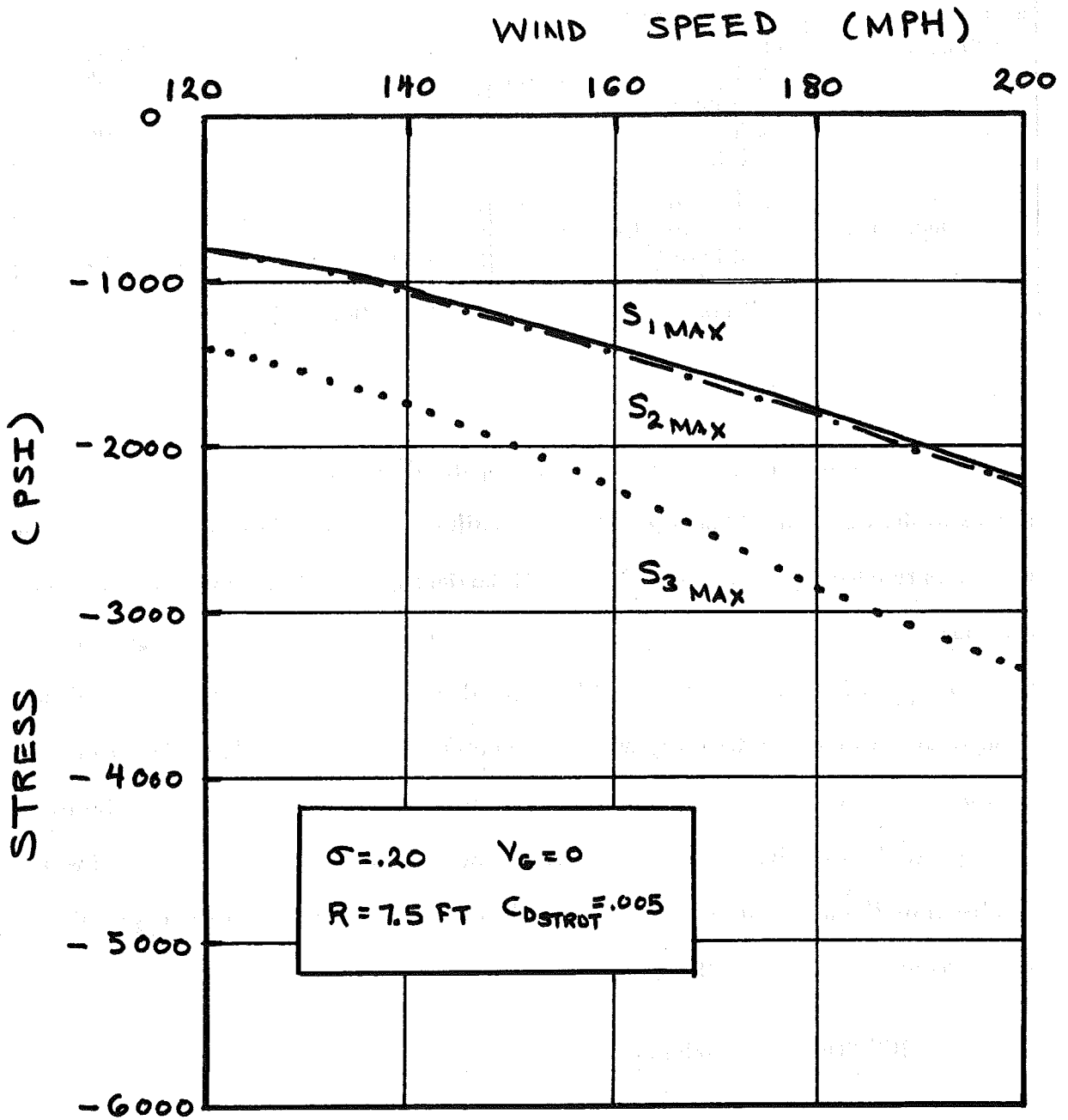
Wind Condition	Critical Area	Stress (psi)	Margin of Safety
120 mph	Blade Center	1070	27.04
	Blade/Strut Connection	1085	26.65
	Strut Root	1740	16.24
	Main Shaft	20,320	1.95
	Pull Rod	525 (tension)	179.95
120 mph + 45 mph gust	Blade Center	1490	19.13
	Blade/Strut Connection	1510	18.87
	Strut Root	2420	11.40
	Main Shaft	28,225	1.13
	Pull Rod	992 (tension)	94.77

#### 4.5.4 FAILURE ANALYSIS

A failure analysis was conducted for the five critical areas for basic wind speeds in the range of 120 mph to 200 mph. Failure was defined as the point at which any stress reaches its yield value. Resultant maximum stresses for a no-gust condition are shown in Figure 4-30. Comparison to the yield stresses of Table 4-3 shows that none of the critical areas exceed yield for speeds to 200 mph. The application of a 45 mph gust velocity to the basic wind speed produced higher stresses as shown in Figure 4-31. As seen in Figure 4-31b, the mainshaft stress reaches yield at a basic wind speed of 195 mph. It should be noted, however, that the basic high speed wind condition of 120 mph wind velocity plus a 45 mph gust velocity is easily met by the Cycloturbine (see Table 4-4).

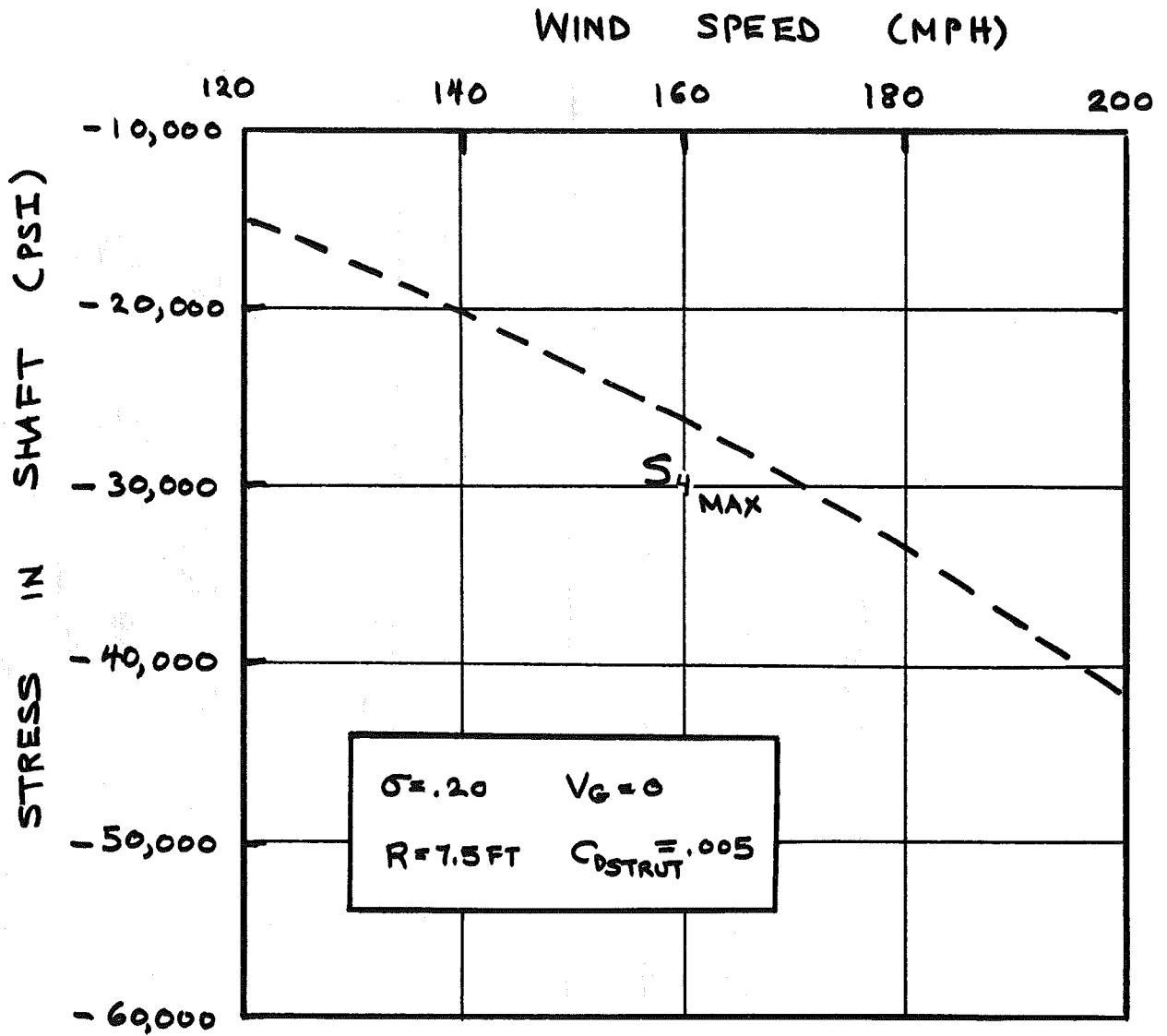
#### 4.5.5 ICE BUILDUP STRESSES

One of the requirements of the high-reliability Cycloturbine is that it have the capability to withstand ice buildup to 2.5 inches on the rotor system. Extreme icing on the rotor is a complex problem which depends on wind speed, temperature, geometry of the surface, droplet size, etc. Icing may cause a significant reduction in blade lift, overall performance may be seriously degraded, and uneven ice buildup may cause rotor imbalance.



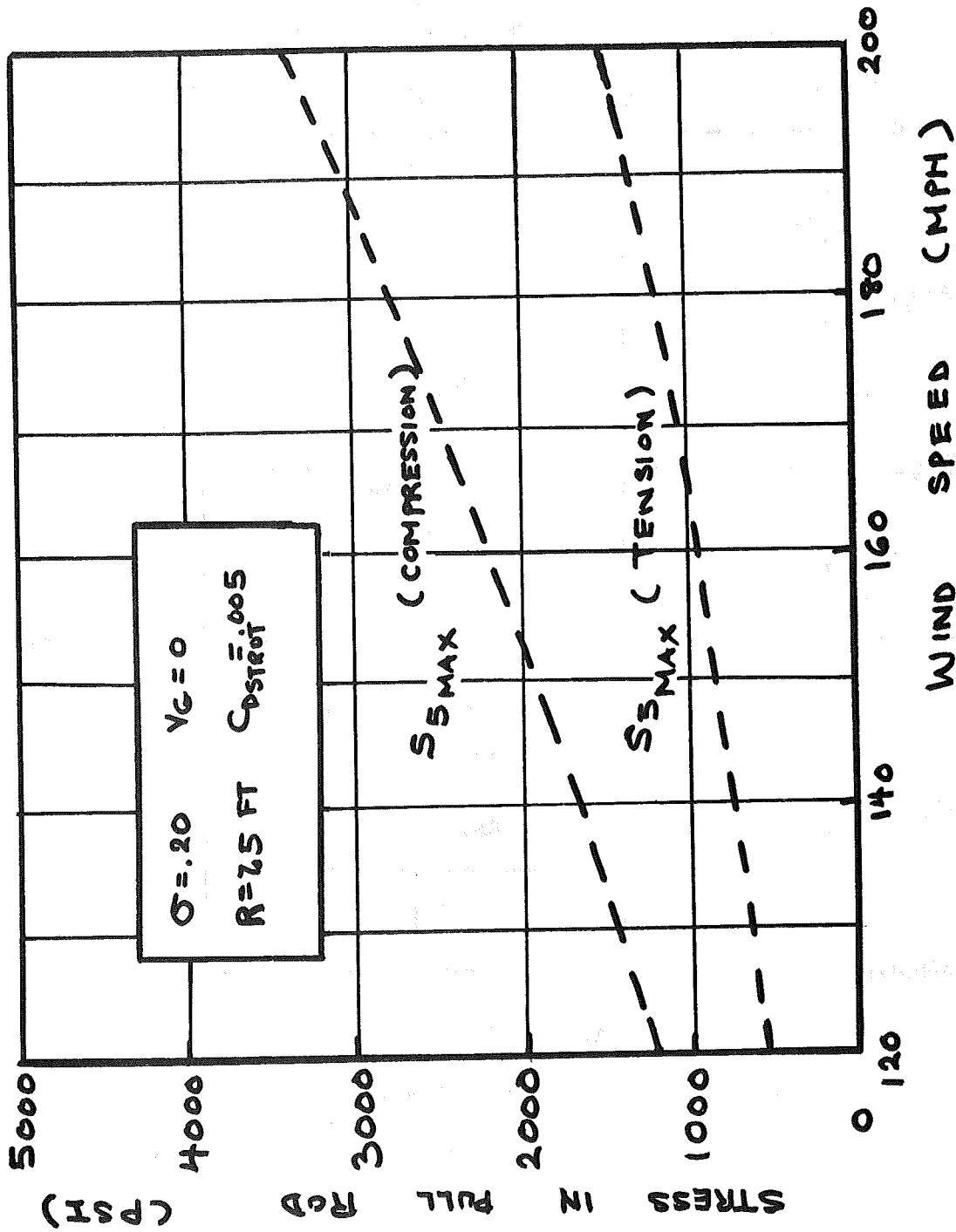
a) Blade Spar Center, Blade/Strut Connection, and Strut Root

Figure 4-30. Failure Analysis.



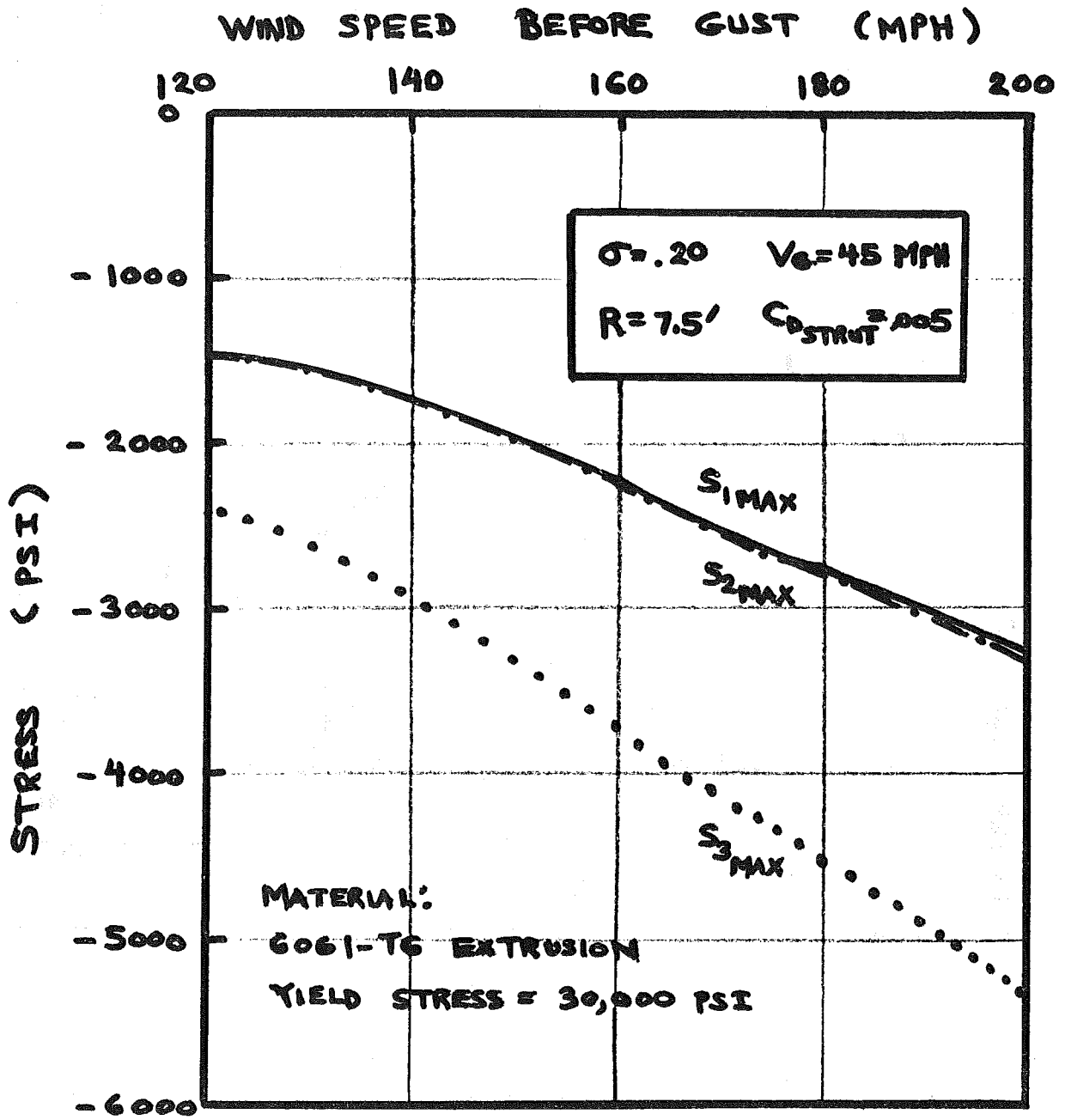
b) Main Shaft

Figure 4-30. Failure Analysis (Continued).



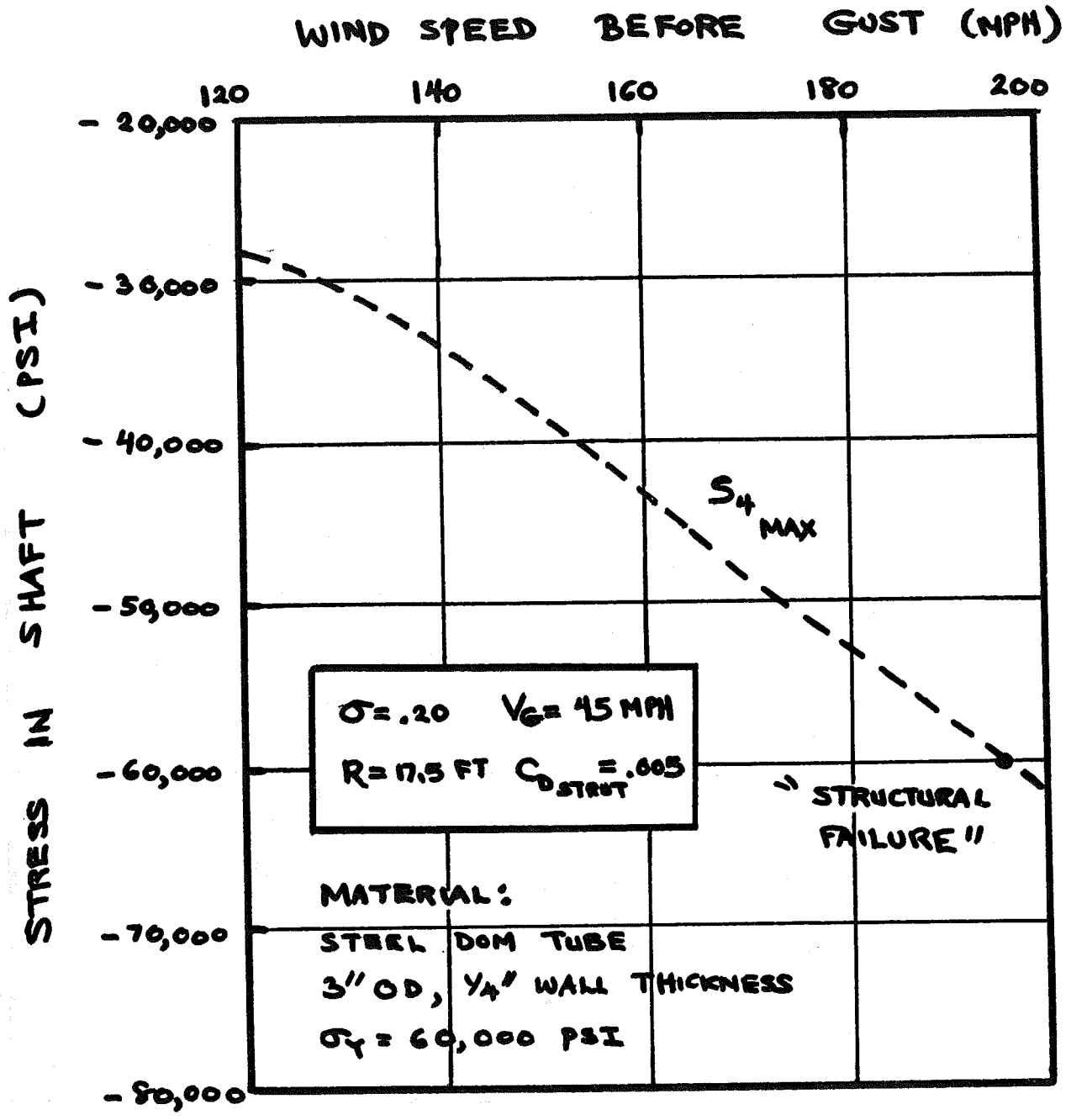
c) Pull Rod Root

Figure 4-30. Failure Analysis (Concluded).



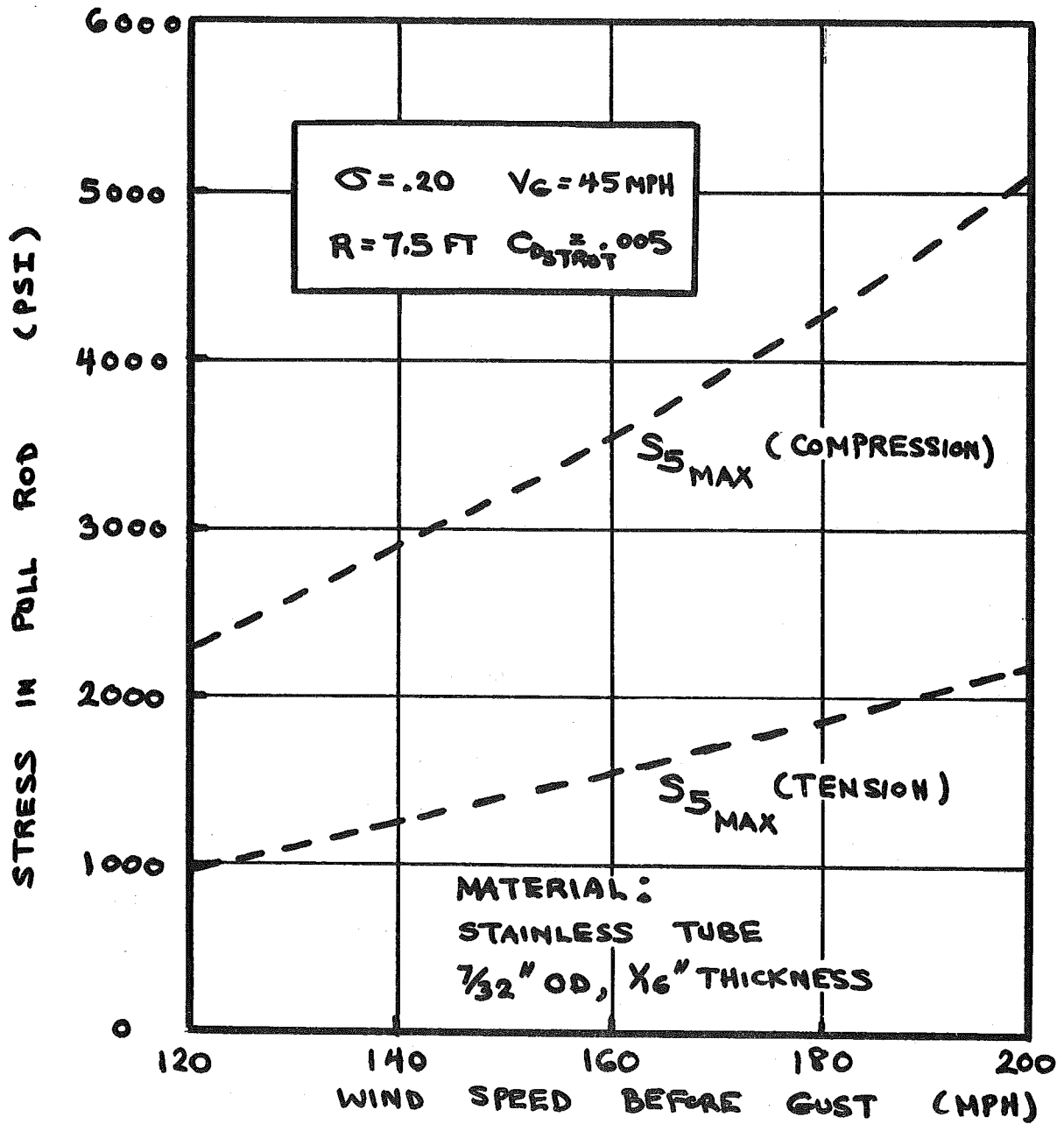
a) Blade Spar Center, Blade/Strut Connection, and Strut Root

Figure 4-31. Failure Analysis with Gust.



b) Main Shaft

Figure 4-31. Failure Analysis with Gust (Continued).



c) Pull Rod Root

Figure 4-31. Failure Analysis with Gust (Concluded).

Analysis of icing on the rotor was limited to the buildup of clear ice which contributes large amounts of added weight on the rotor and, therefore, increases stress on the structure. It was assumed that the ice built up evenly on the rotor as illustrated in Figure 4-32. The increase in blade weight due to ice buildup is given in Table 4-5 which shows that 2.5 inches of ice increases the weight of each rotor blade by 190 lbs. The effect of ice buildup on the rotor stresses is shown in Figure 4-33 for the nominal wind speed of 20 mph and the stalled rotor condition at 40 mph. It is seen that the blade stresses ( $S_1$  and  $S_2$ ) are increased by factors of about 10 and 20 for the 20 mph and 40 mph conditions, respectively. In both cases, the resultant stresses are below the yield stress of 30,000 psi. Stresses for a wind speed of 120 mph and for a total speed of 165 mph (120 mph + 45 mph gust) are summarized in Table 4-6.

Table 4-5. Ice Accumulation on Blades.\*

Ice Thickness (Inch)	Weight of Ice per Blade** (Lb)	Running Load (Lb/Ft)
0.5	38	4.75
1.0	76	9.50
1.5	114	14.26
2.0	152	19.01
2.5	190	23.76

\*Uniform clear ice formation on rotor system.

\*\*Ice density,  $\rho_i = 0.033 \text{ lb/in}^3$ .

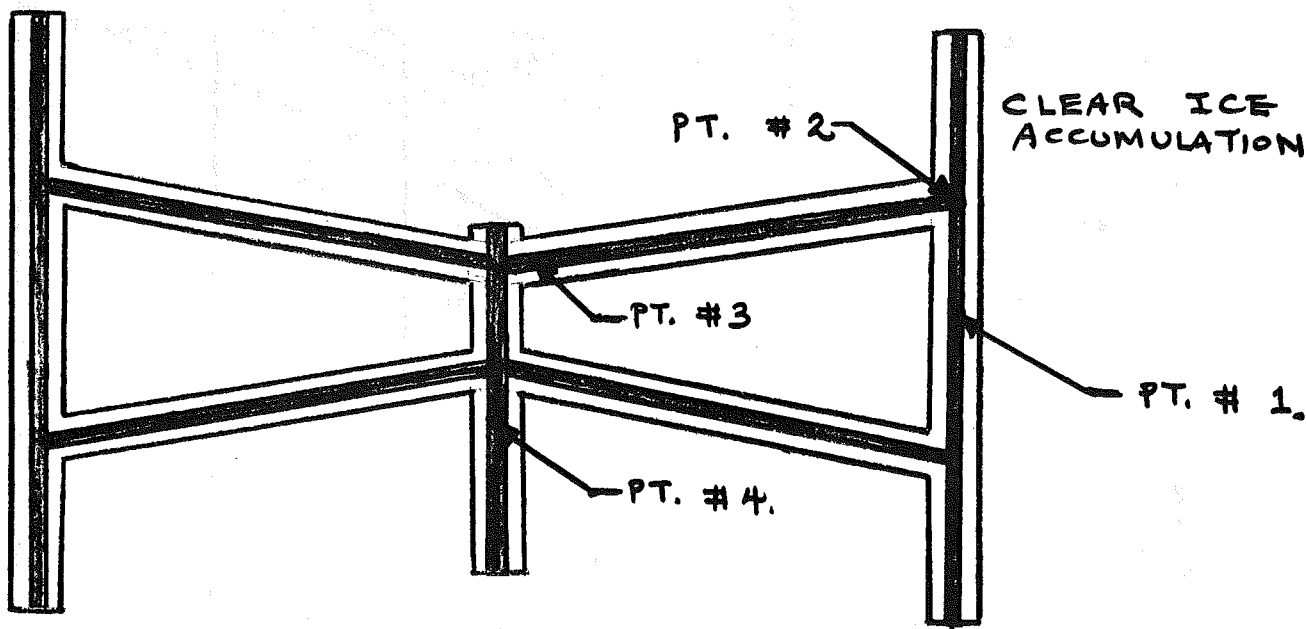
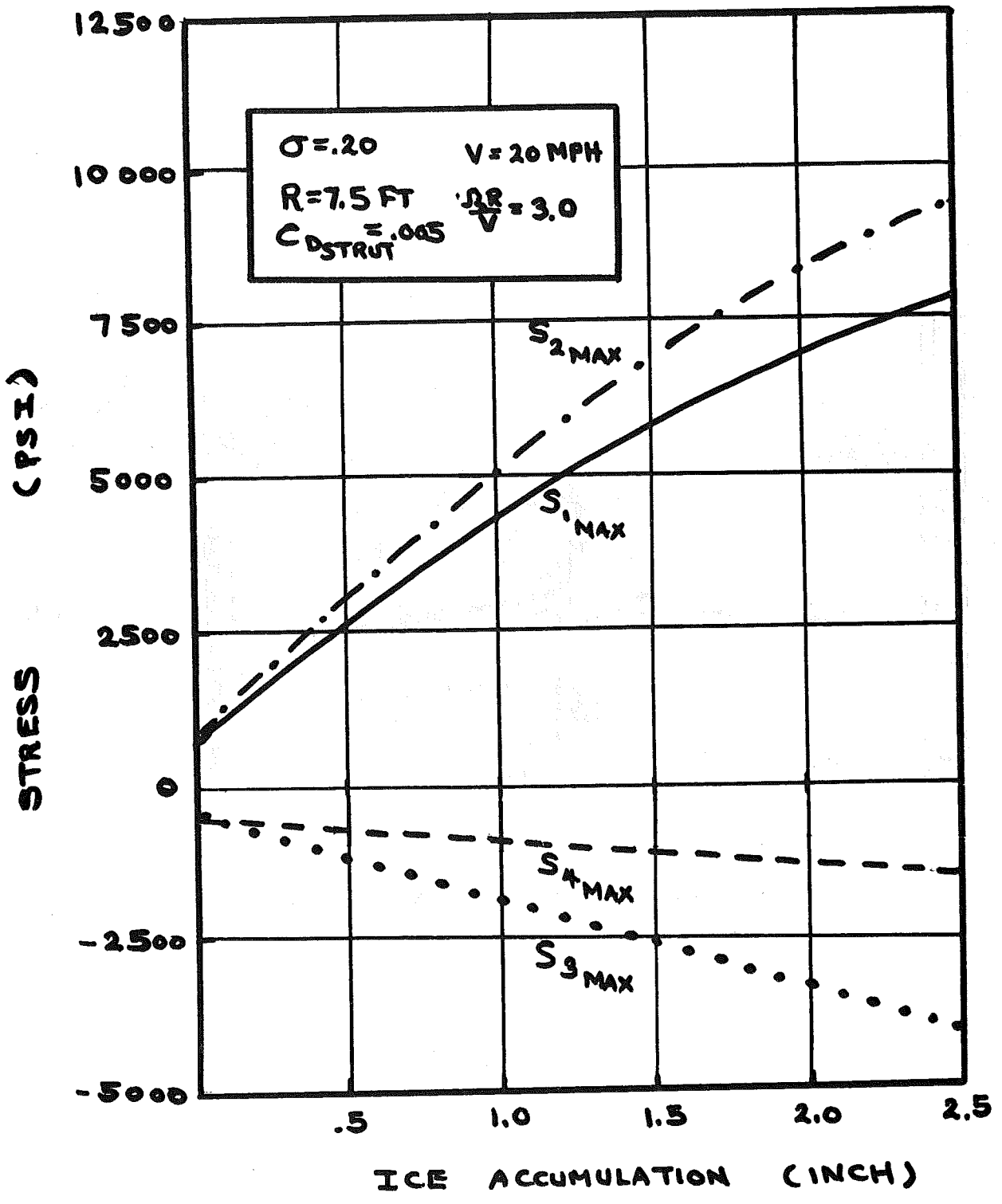
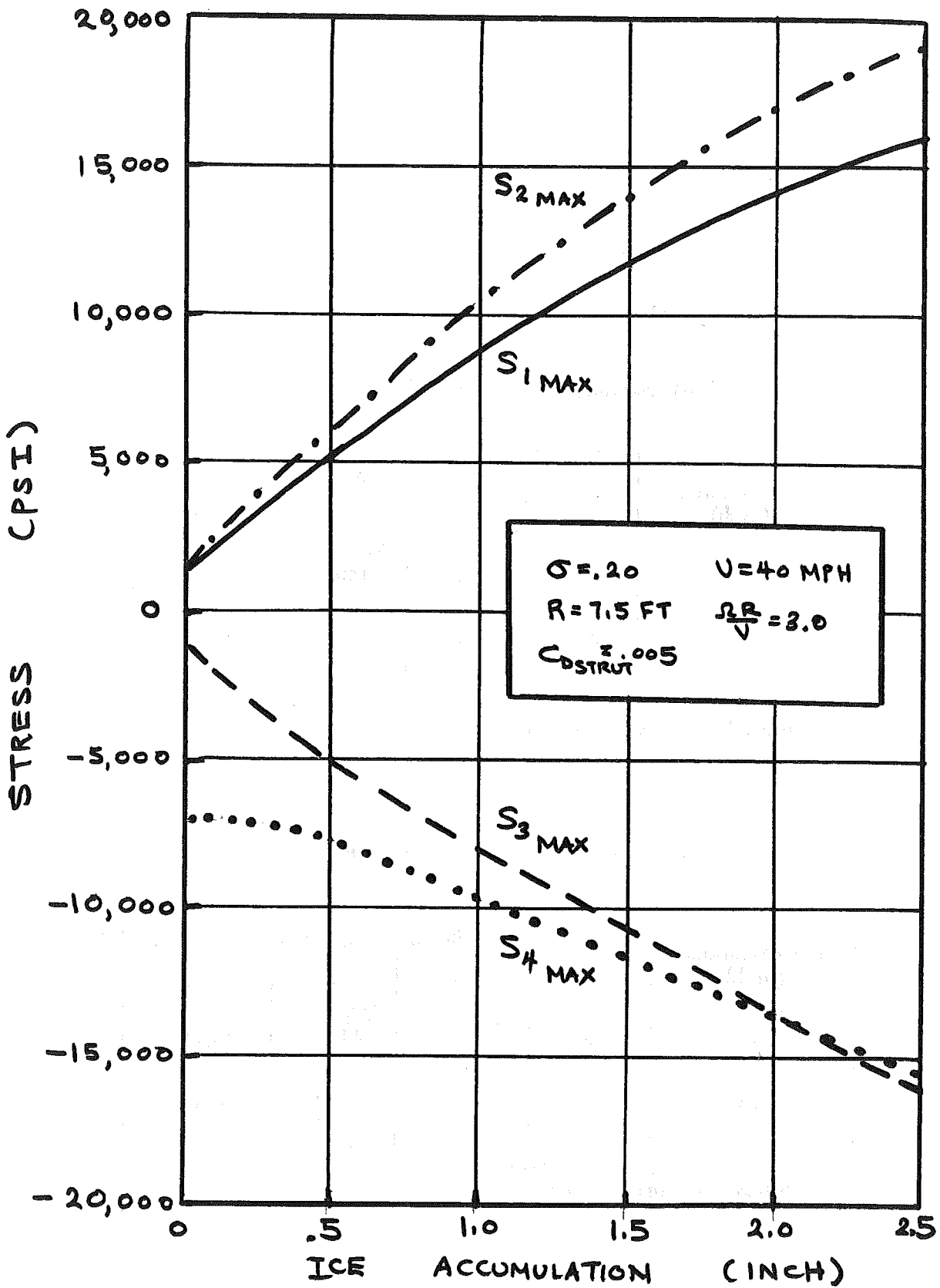


Figure 4-32. Uniform Ice Buildup on Rotor System.



a) Nominal Operating Condition (20 MPH)  
 Figure 4-33. Effect of Clear Ice Accumulation.



b) Stalled Condition (40 MPH)

Figure 4-33. Effect of Clear Ice Accumulation (Concluded).

Table 4-6. Effect of Ice on Stresses at High Wind Speeds.

a) Maximum Wind Speed (120 mph)

Ice Thickness (Inch)	Maximum Stresses (psi)			
	S <sub>1</sub>	S <sub>2</sub>	S <sub>3</sub>	S <sub>4</sub>
0	800	800	1400	15,000
2.5	740*	750*	1180*	9,880*

\*Ice takes up part of loads.

b) V = 165 mph (120 mph + 45 mph Gust)

Ice Thickness (Inch)	Maximum Stresses (psi)			
	S <sub>1</sub>	S <sub>2</sub>	S <sub>3</sub>	S <sub>4</sub>
0	1490	1510	2420	28,200
2.5	1395*	1415*	2330*	18,685*

\*Ice takes up part of loads.

## 4.6 DYNAMICS ANALYSIS

Analysis of the Cycloturbine dynamics was performed to determine: 1) the aeroelastic effects of blade dynamics on the structural loads and on flutter phenomena; and 2) the dynamic response of the combined Cycloturbine/tower system.

### 4.6.1 AEROELASTIC ANALYSIS

The rotating, constant-radius (i.e., straight prior to elastic deflection) turbine blade is shown in Figure 4-34. The bending moment,  $M$ , at station,  $x$ , from one end is given by

$$M(x) = \int_x^{\bar{l}/2} \{ [R + y(\xi)] \Omega^2 - \dot{y}'(\xi) \} m(\xi) (\xi - x) d\xi - H \left[ y \left( \frac{\bar{l}}{2} \right) - y(x) \right] \quad (4-66)$$

where

$\Omega$  = turbine rotational speed

$m(\xi)$  = blade mass at  $\xi$  per unit of  $x$ -distance

$H$  = constant blade tension force component parallel to axis of rotation

$\bar{l}$  = distance between the two blade supports

$R$  = turbine radius

$y$  = blade deflection

Note that the blade ends are essentially hollow fairings which can be neglected in the analysis.

The analysis technique follows that of Reference 18 except that structural bending stiffness is retained. If it is assumed that the blade is deflected under steady centrifugal loading,  $\Omega^2 m R$ , in the following shape (let  $k = 1$ )

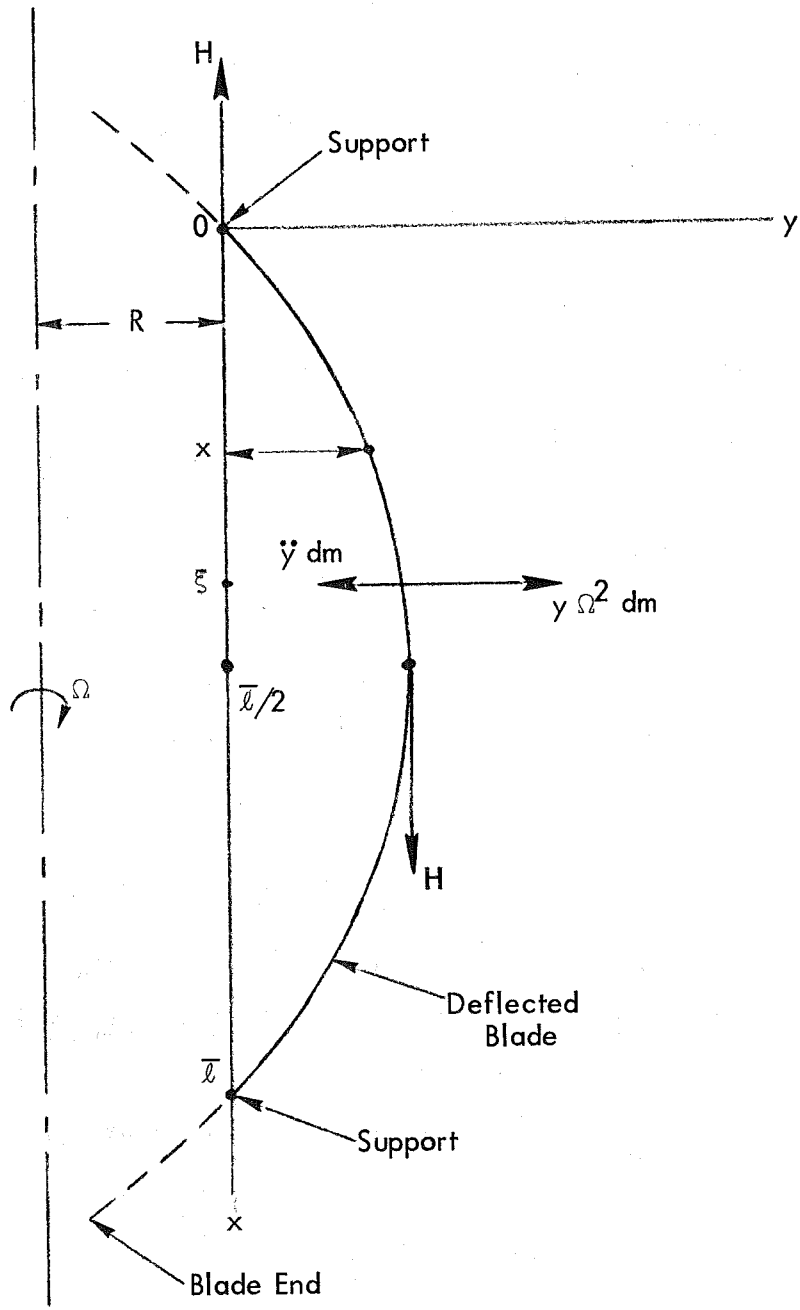


Figure 4-34. Elastic Blade Geometry.

$$y_k = \bar{y} \sin \frac{k\pi}{\bar{l}} x \quad (4-67)$$

then it can be shown that the blade tension is

$$H = \Omega^2 m \left( \frac{\bar{l}}{\pi} \right)^2 \quad (4-68)$$

and the blade frequencies in bending are given by

$$\omega_k^2 = \left[ \frac{EI}{m} \left( \frac{k\pi}{\bar{l}} \right)^4 + (k^2 - 1) \Omega^2 \right] \quad (4-69)$$

The first term represents the natural frequency of the blade on the stopped rotor and the second term provides the effect of centrifugal stiffening. It can be shown that Equation (4-69) applies to either normal or chordwise bending modes. The corresponding mode shapes are given by Equation (4-67).

The blade bending frequencies are important to the dynamic response of the blades to airloads. The blade dynamic amplification factor for either normal or chordwise bending in the  $k$ th mode in response to the  $n$ th harmonic airload is given by

$$A_{kn} = \frac{1}{\left\{ \left[ 1 - \left( \frac{n}{v_k} \right)^2 \right]^2 + \left[ \frac{nm_g}{v_k^2} \right]^2 \right\}^{1/2}} \quad (4-70)$$

where

$$v_k = \frac{\omega_k}{\Omega}, \text{ the nondimensional natural frequency of the } k\text{th mode}$$

$$m \cdot g = \text{damping coefficient of any mode; } = \frac{\gamma}{2} C(\phi), \text{ normal; } \\ \approx 0, \text{ chordwise}$$

$$\gamma = \frac{\rho a c R}{m}$$

$$\phi = \frac{\omega c}{2U}$$

$C(\phi)$  = Theodorsen's lift deficiency function

Note that this dynamic amplification factor must be applied to the bending moment due to the  $n$ th harmonic airload.

The bending frequencies of the nonrotating blade are a function of the blade geometry, stiffness, and mass distribution. For the 15-ft Cycloturbine these values are:

$$EI = 1.3 \times 10^6 \text{ lb-in}^2 = 0.903 \times 10^4 \text{ lb-ft}^2$$

$$m = \frac{W}{g \ell} = \frac{21}{32.2(8)} = .0815 \text{ slugs/ft}$$

$$\bar{\ell} = 4.67 \text{ ft}$$

Calculated bending frequencies are given in Table 4-7.

Table 4-7. Bending Frequencies of Nonrotating Blade.

Mode k	$\omega_{k_0}$		
	Rad/Sec	Hz	cpm
1	151	24	1,440
2	603	96	5,760
3	1,356	216	12,960

In the rotating system, the first blade frequency is given by  $k = 2$ . It is seen that the blade flatwise (normal) bending frequencies are so high that no dynamic amplification of the loading as given by Equation (4-70) occurs for harmonic airloads at least to 6/rev.

The aeroelastic phenomena called flutter is of concern in any machine subjected to aerodynamic loading. Flutter is classically a function of the torsional frequency of the structure (Reference 19). If the structure is made torsionally stiff, flutter is generally precluded. For a closed structural section, such as the blade, the torsional frequency is given by

$$\omega_{T_k} = k\pi \sqrt{\frac{GJ}{I_f \ell^2}} \quad (4-71)$$

For the Cycloturbine blade,

$$GJ = 2.6 \times 10^5 \text{ lb-in}^2 = 0.18 \times 10^4 \text{ lb-ft}^2$$

$$I_f = \frac{m c^2}{30} = \frac{.0815(1)^2}{30} = .00272 \text{ slug-ft}^2/\text{ft}$$

Calculated torsional frequencies are given in Table 4-8.

Table 4-8. Blade Torsional Frequencies.

Mode k	$\omega_T$		
	Rad/Sec	Hz	cpm
1	547	87	5,226
2	1,094	174	10,452
3	1,356	261	15,678

Therefore, torsional frequency of the blade structure is so high that classical flutter is unlikely to occur.

Vibration in the main shaft was found to be a problem in early models of the Cycloturbine. The shaft diameter was increased to preclude vibrational frequencies within the operational range of the machines. Based on experience, it is dynamically smoother to run significantly below critical shaft speeds while running supercritical to the first tower bending frequency.

#### 4.6.2 DYNAMIC RESPONSE OF CYCLOTURBINE/TOWER SYSTEM

A wind machine mounted on its tower represents a coupled dynamic system which can experience adverse interactions or excessive response to unsteady wind inputs. Such interactions have been observed in actual installation of wind machines. Therefore, a simplified dynamic response analysis was performed for the machine/tower system.

The dynamic response of a system subjected to an external forcing function can be determined in a number of ways. One of the common solutions employed in engineering practice is the normal mode solution in which the displacement characteristics of the structure are defined in terms of the normal mode characteristics.

The normal mode solution uncouples the equations of motion so that in matrix form,

$$\{\ddot{\eta}\} + 2[\zeta\omega]\{\dot{\eta}\} + [\omega^2]\{\eta\} = \frac{[\phi]^T}{[M]}\{Q\} \quad (4-72)$$

where

$$[M] = [\phi]^T [m] [\phi]$$

$$2[\zeta\omega] = [c]/[M]$$

$$[\omega^2] = [K]/[M]$$

$$[K] = [\phi]^T [k] [\phi]$$

$$[c] = [\phi]^T [c] [\phi]$$

and

$\phi_i$  = mode shape of the ith mode

$\eta_i$  = displacement in the ith mode

$m_j$  = discrete masses used to represent system components

$\zeta_i$  = damping ratio for the ith mode

$$c_j = 2\gamma_j m_j \omega_j$$

$\gamma_j$  = viscous damping ratio for jth mass

$\omega_j$  = frequency of jth mode

$k_j$  = stiffness of jth element of structural model

Then, in terms of series, the generalized mass,  $M_i$ , for each mode is

$$M_i = \sum_j \phi_i^{(j)} m_j \quad (4-73)$$

where  $i$  refers to mode and  $j$  refers to mass.

The forcing function,  $Q$ , is the aerodynamic force applied to the Cyclo-turbine. If it is sinusoidal, then the dynamic response can be obtained in closed form by classical methods. Thus, it is convenient to simplify the analytical approach used in Subsection 4.1 in order to determine the aerodynamic harmonics.

The instantaneous force in the downwind direction due to one turbine blade is given by Equation (4-9). Assume that, for nominal operational conditions, lift increases linearly and that the drag is small so that the drag coefficient is constant, or

$$C_{L\alpha} = a = \text{constant}$$

$$C_{D_0} = \text{constant}$$

If, in addition, the angle of attack,  $\alpha = \theta + \phi$ , remains small and that for mechanical reasons, the blade pitch is limited to small angles, then Equation (4-9) becomes by applying Equations (4-1) and (4-2),

$$\begin{aligned} \Delta H = \frac{1}{2} \rho c l U^2 [a(\theta \cos \phi + \sin \phi) (\cos \psi \cos \phi - \sin \psi \sin \phi) \\ + C_{D_0} (\sin \psi \cos \phi + \sin \phi \cos \psi)] \end{aligned} \quad (4-74)$$

The combined loading in the drag direction due to three blades located at angular increments of  $\Delta\psi = \frac{2\pi}{b}$  where  $b$  is the number of blades is

$$H = \Delta H_1(\psi) + \Delta H_2 \left( \psi + \frac{2\pi}{3} \right) + \Delta H_3 \left( \psi + \frac{4\pi}{3} \right) \quad (4-75)$$

Substituting Equation (4-74) in (4-75) at the appropriate phase angles, applying Equations (4-5), (4-6) and (4-18), and by recognizing that  $U \approx \Omega R(1 + \lambda_1 \sin \psi)$ , the total drag load on the turbine expressed in harmonics is

$$\begin{aligned}
 H = \frac{3}{2} \rho c l (\Omega R)^2 & \left\{ \frac{1}{2} [a \theta_{1c} + (a + 3 C_{D_o}) \lambda_o] \right. \\
 & + \frac{1}{4} [(a - C_{D_o}) \lambda_{1c}] \cos 3\psi + \frac{1}{4} [C_{D_o} \lambda_{1c}^2 \\
 & \left. + a(\theta_{1c} \lambda_o + \theta_o \lambda_{1c})] \sin 3\psi \right\} \quad (4-76)
 \end{aligned}$$

$$= 3 a_o \{a_1 + a_2 \cos \omega t + a_3 \sin \omega t\} \quad (4-77)$$

where

$$\omega t = 3 \Omega t = 3 \psi$$

$$\omega = \text{forcing frequency}$$

Thus, the aerodynamic load on the turbine in the drag direction is conveniently in harmonic form with a forcing frequency of 3/rev as expected for a 3-bladed machine.

If the mode shapes,  $\phi_i$ , are known then the modal displacements,  $\eta_i$ , can be determined from Equation (4-72) and the displacement,  $x$ , at any mass station can be determined from

$$x = \sum_{i=1}^{\infty} \phi_i \eta_i \quad (4-78)$$

Typical results for a turbine weight of 450 lbs on a 34-ft tower are shown in Figure 4-35. Since the dynamic characteristics of the tower were not known,

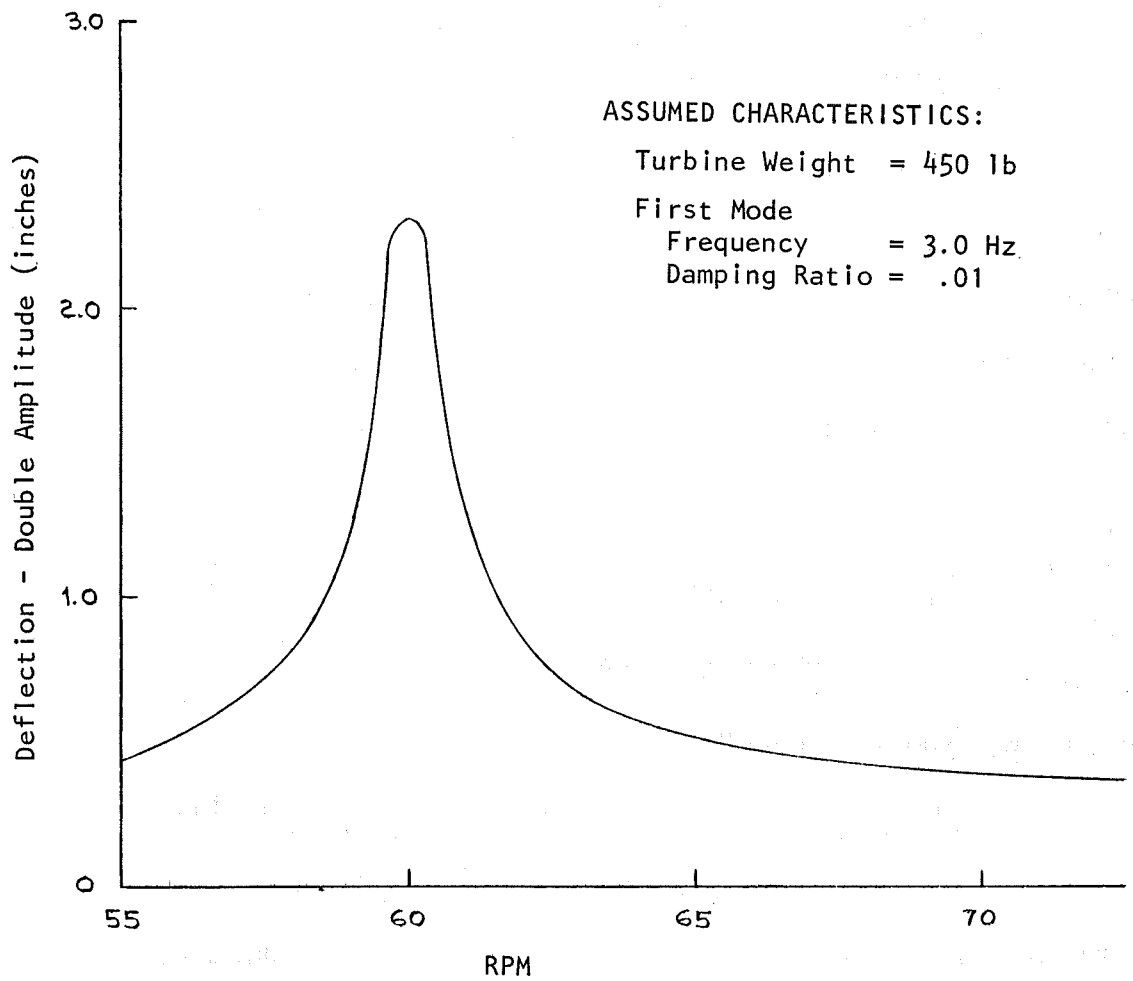


Figure 4-35. Cycloturbine/Tower Dynamic Response at Cycloturbine.

assumed mode shapes, natural frequencies and damping were used. The first mode frequency was assumed to be 3.0 Hz which is similar to observed data. The calculated deflection at the turbine exhibits a peak of 60 RPM which is the excitation frequency of a 3/rev forcing function at the tower frequency. Experimental determination of tower natural frequencies is discussed in Section 8.

#### 4.7 TOTAL SYSTEM PERFORMANCE

The electrical system of the Cycloturbine converts the mechanical power from the main shaft into a regulated source of direct current to charge a battery over the operational range. In order that the turbine perform at its highest efficiency, it operates at variable speeds, producing usable power from 28 to 160 RPM at the main shaft. To accomplish this, a three-phase alternator has been designed (see Subsection 3.2.2.1) whose input power characteristics closely match that available from the turbine. For best dynamic stability of the rotor, there should always be a "full" load on the turbine at rated wind speed and above. This requires matching the alternator characteristics to the turbine performance (see Subsection 4.3) for a given gear ratio and wind speed profile (see Subsection 2.7).

These elements were combined in a computer program (see Section 5, Volume III) in order to optimize system output such as the annual energy production or the maximum attainable power. The program employed an iterative process and started by assuming the turbine was running at optimum  $\Omega R/V$  and then computed the load imposed on the turbine by the generator through the selected gear ratio. Loads were calculated and then the turbine speed was modified until all loads matched to some specified error limit. This produced the expected power output,  $\Omega R/V$  and shaft speeds for a given range of wind speeds. These data were then used with the wind speed profile to determine the energy production for an average wind speed regime.

Results for the 1-kW Cycloturbine SWECS are given in Figure 4-36. The power attainable for the operational range was also determined for the average wind speed of 10 mph as shown in Figure 4-37.

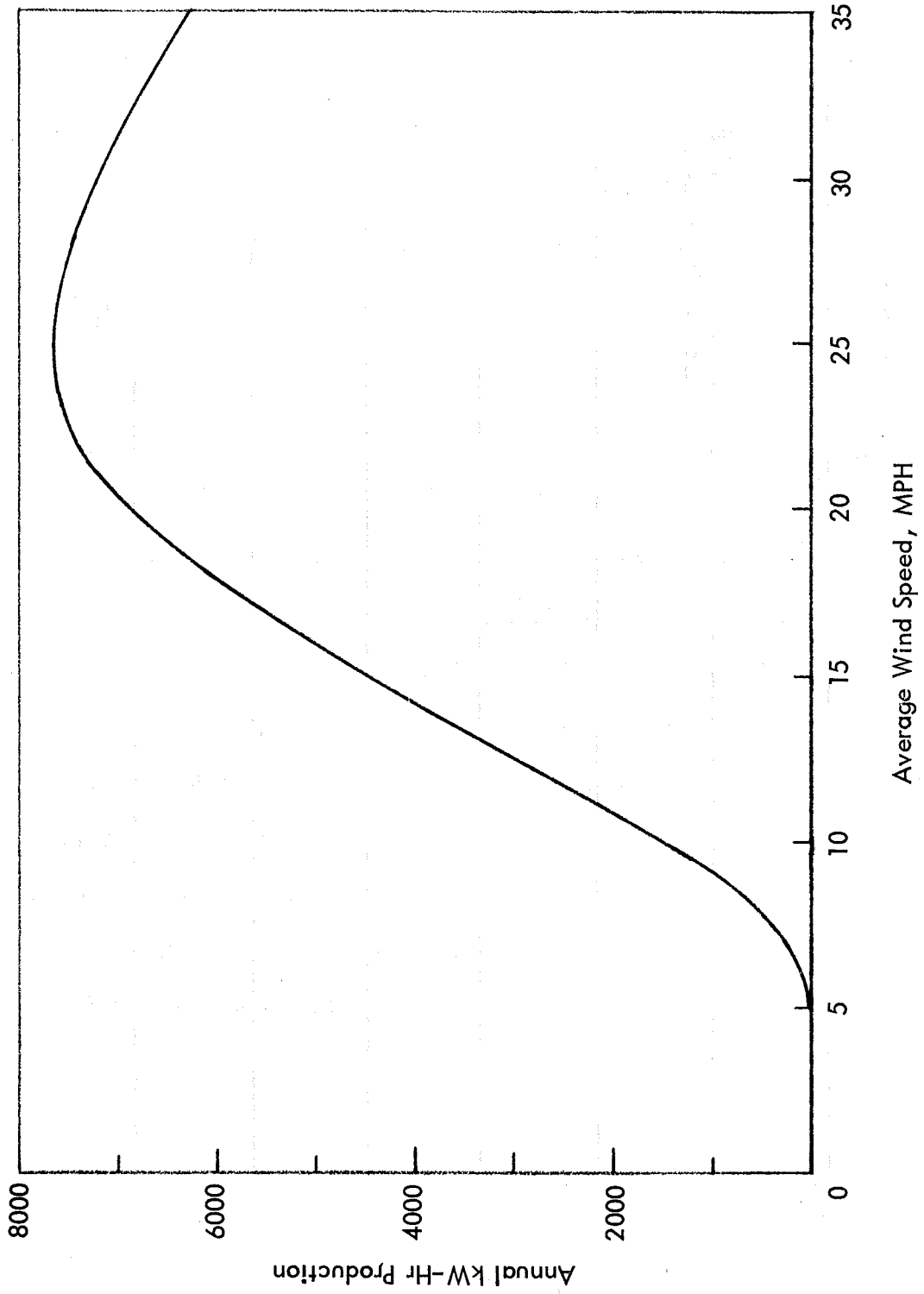


Figure 4-36. High-Reliability Cycloturbine Annual Energy Production.

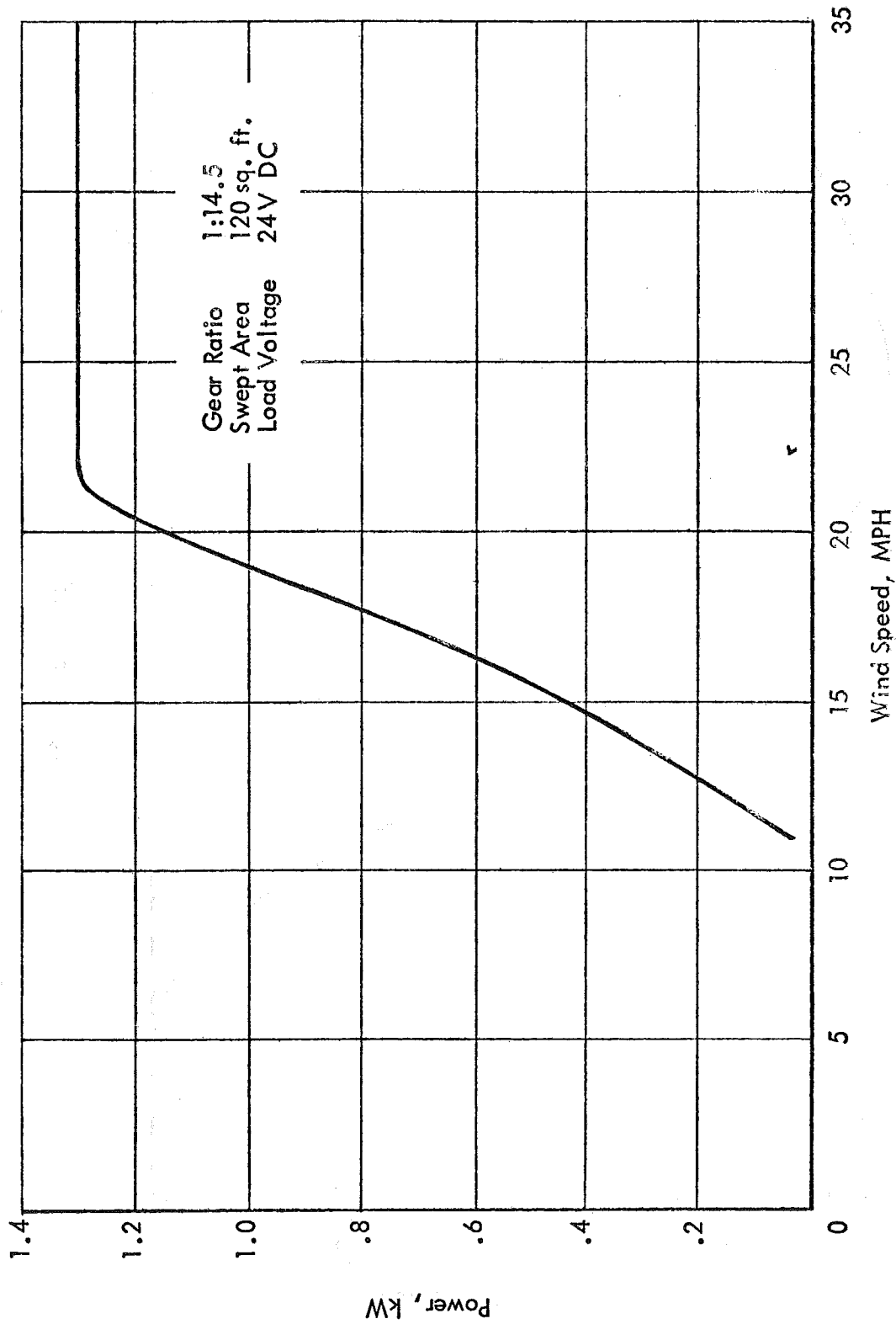


Figure 4-37. High-Reliability Cycloturbine Power Output.

## SECTION 5

### DEVELOPMENTAL TESTING

Tests were performed during the design phase in order to provide experimental data to verify analytical techniques and the design itself. A major test program was established to verify the performance and structural stress characteristics of the Cycloturbine. Other testing was done on critical components and subassemblies to verify their design loads, to ensure proper performance, and to increase confidence in their reliability.

#### 5.1 CYCLOTURBINE

##### 5.1.1 MEASUREMENT OF PERFORMANCE AND STRESS LEVELS

Due to the unique configuration of the Cycloturbine, traditional aerodynamic analytical methods cannot be used with a high degree of confidence to predict the aerodynamic forces that the turbine must withstand. For this reason, the analytical aerodynamic analysis (Subsection 4.1) has been augmented with experimental test data generated by a test program using an instrumented Cycloturbine of the type commercially available from Pinson Energy Corporation (Model C2E). From the comparison of analytical and experimental results, a more accurate prediction of aerodynamic operating conditions was formulated. This "real world" information was valuable in laying an experimental data base for the 1-kW high-reliability Cycloturbine development.

#### 5.1.1.1 TEST EQUIPMENT AND PROCEDURES

##### Instrumented Cycloturbine Model C2E

The Pinson Cycloturbine Model C2E has a rated output of 2-kW in a 24 mph wind. It has a 12-ft radius and an 8-ft blade span with 96 square feet of projected area. Photographs of the turbine are shown in Figure 1-1.

The Cycloturbine C2E is similar in configuration to the machine described for the high-reliability program (see Subsection 3.1). It consists of a central vertical main shaft held by two ball bearings mounted in either end of the bearing support tube. The bearing support tube is an integrally welded part of the transmission and generator mounts. This module is bolted atop a Natural Power, Inc. 35-ft Octahedron tower. Attached to the upper part of the main shaft are three pairs of horizontal struts. Each pair of struts holds a blade with a bearing allowing it to pitch as the turbine rotates. Each blade's pitch is controlled cyclically by a push rod connected to an eccentric cam located on top of the main shaft. The eccentric cam is oriented into the wind by the tailvane so that as the turbine turns through a complete revolution a blade pitches from  $10^{\circ}$  trailing edge inboard at its upwind position to  $10^{\circ}$  trailing edge outboard at its downwind position (see Figure 3-4).

The rotor delivers mechanical power to the 4-kW Winco generator through the transmission which is illustrated in Figure 5-1. It is a two stage timing belt system using Uniroyal HTD belts and pulleys. Power is transmitted through the first stage (speed ratio: 3.29:1) to the jackshaft. From here the speed is stepped up another 2.37:1 in the second stage to turn the Winco alternator. The total transmission ratio is 7.8:1.

The wind driven tests were conducted at the Pinson Energy Test Facility at New Seabury, Massachusetts. The test site is located on a thirty-foot bluff overlooking

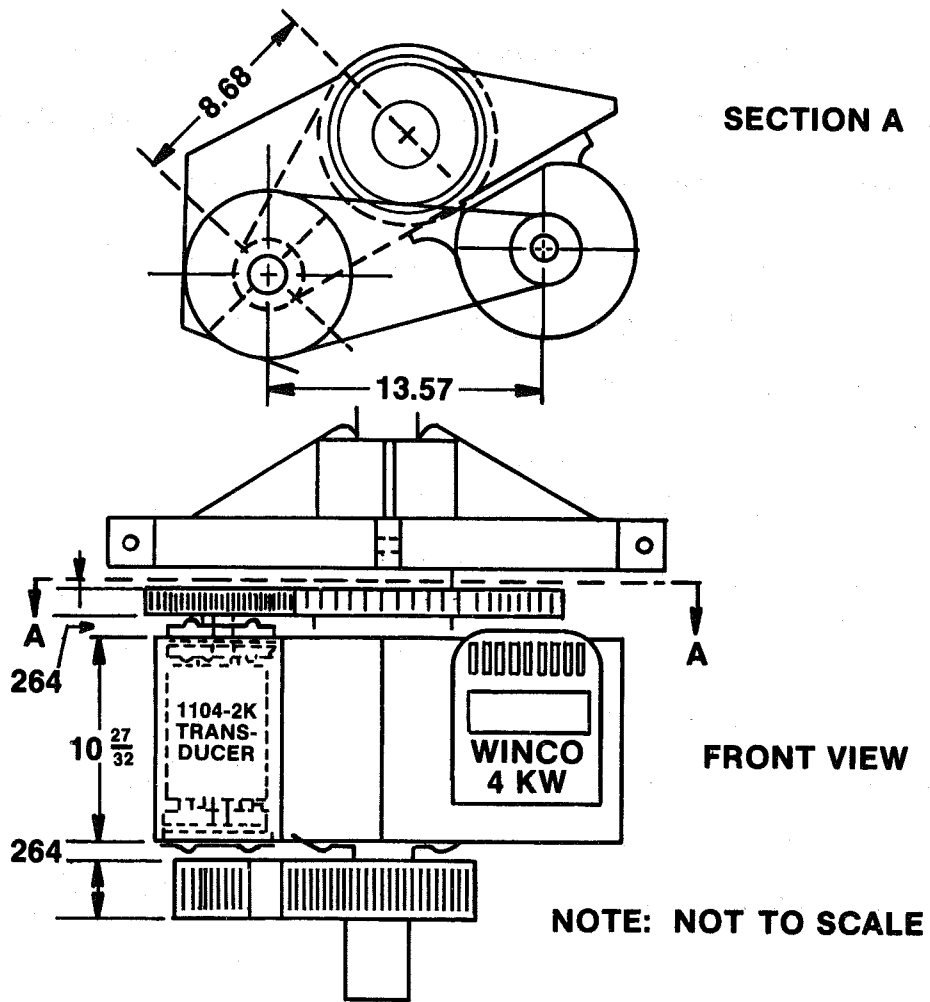


Figure 5-1. C2E Transmission and Weldment.

Nantucket Sound and enjoys 160 degrees of unobstructed wind off of the water from a compass heading of southeast to west-northwest. The area around the base of the tower is clear (except for a few low scrub pine) for one-quarter mile around the remaining points of the compass. The predominant spring and summer wind direction is from the southwest and the test site is ideally suited for the wind direction. The center of the rotor is located at thirty-six feet above ground level of approximately sixty-six feet above sea level. This results in a turbulence level which is very low when the wind is from the water as compared to wooded or hilly locations.

#### Test Measurements and Instrumentation

The test program consisted of two types of tests: performance tests and force tests. The performance tests measured the horsepower output of the Cycloturbine and correlated it to wind speed, RPM and electrical power output of the generator. The force tests measured strut root force and blade center spar force, and correlated them to wind speed, RPM, power output of the turbine and the rotor azimuth angle. Figure 5-2 shows the location of the instrumentation.

Mechanical power in the jackshaft was sensed by a Lebow 1104H-2K Torque Sensor (Figure 5-1). Output from the torque sensor was measured using an internal, high sensitivity, 4-active-arm strain gauge bridge, and RPM was measured from an internal magnetic pickup. Torque and RPM inputs supplied continuous horsepower data on the jackshaft of the transmission.

Forces were sensed by four-active-arm strain gauge bridges. One bridge was located on the strut root and measured in-plane bending forces on the strut. The other bridge was mounted on the blade spar and measured the flatwise bending of the blade. In order to get the data signal from the rotating strain gauge bridges to the

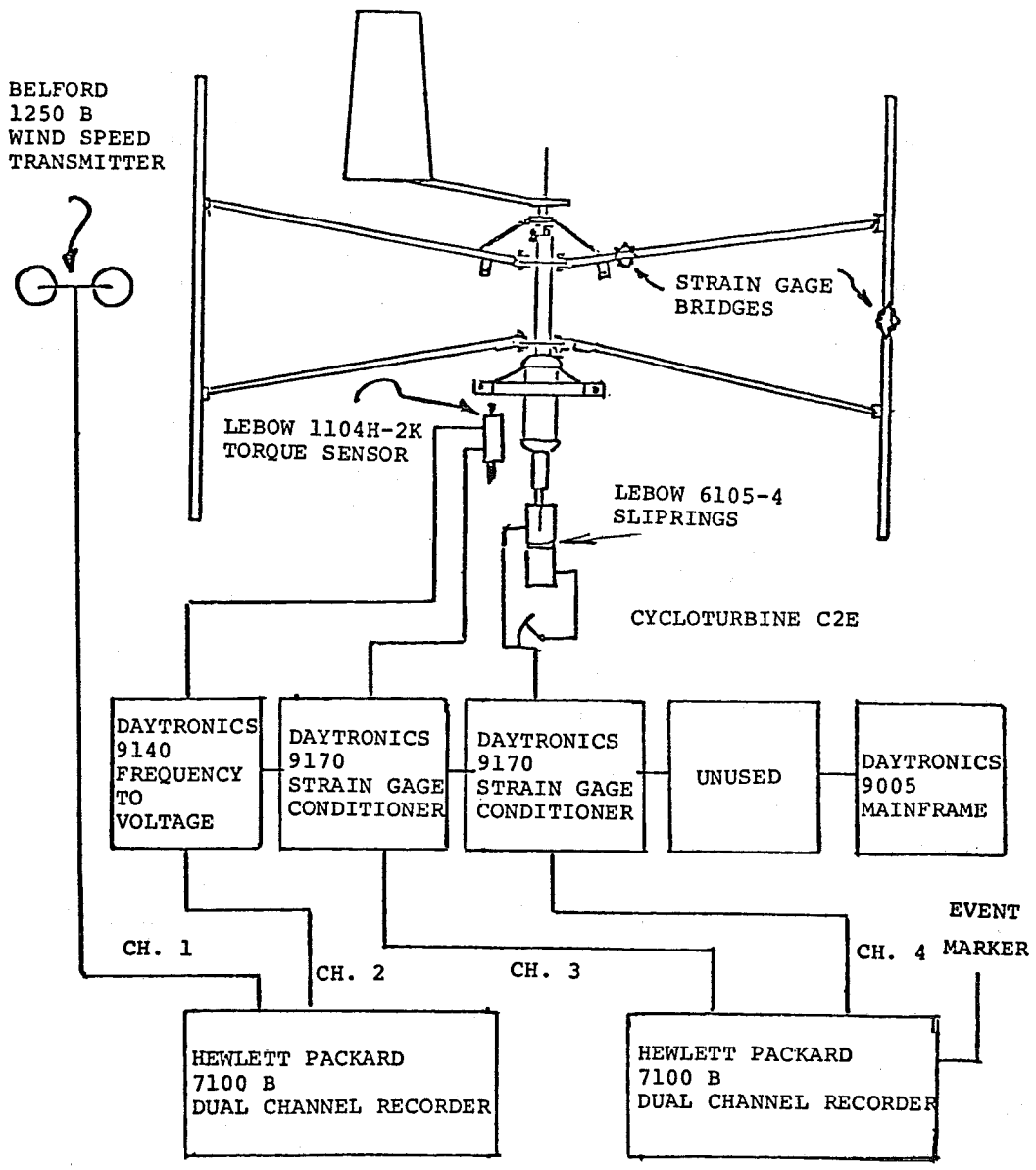


Figure 5-2. Instrumentation Block Diagram.

ground, a pair of Lebow 6105-4 Slip Rings was used. They were mounted at the bottom of the turbine main shaft.

The wind speed sensor for these tests was a Belfort 1250B Wind Speed Transmitter. The sensor was mounted 2-1/2 Cycloturbine diameters upstream into the prevailing wind which is from the south-southeast off Nantucket Sound.

Alternator output was single phase, 3-wire AC power which was fed to a 5000-watt variable capacity load bank located in the instrument building beneath the tower.

The rotor azimuth angle sensor was a miniature reed switch positioned upwind of the rotor shaft which was activated by a small permanent magnet attached to the instrumented strut. Each time the instrumented strut passed directly upwind, the circuit was closed and an impulse was recorded on the strip chart recorders.

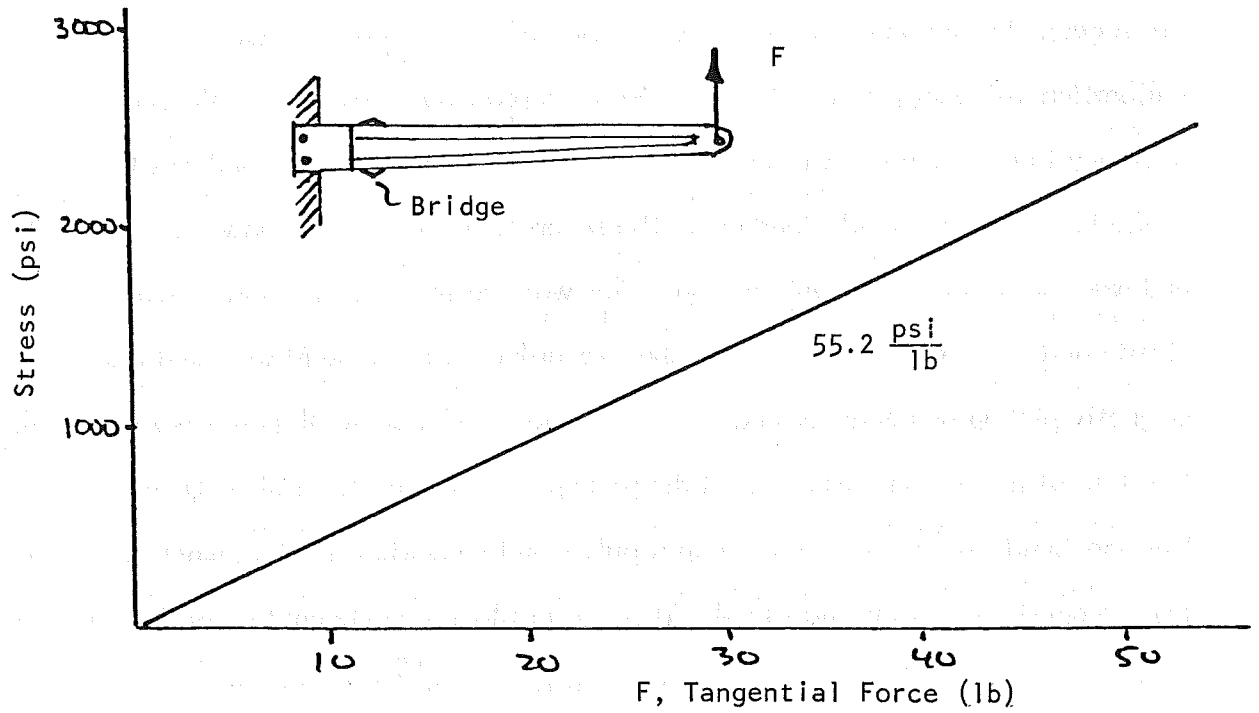
#### Data Recording and Calibration

The sensors located in the rotor were connected with Belden instrumentation cable to the conditioners, amplifiers and recorders located in the instrumentation building. Figure 5-2 illustrates the connection of the sensors to their respective amplifiers and to the recorders.

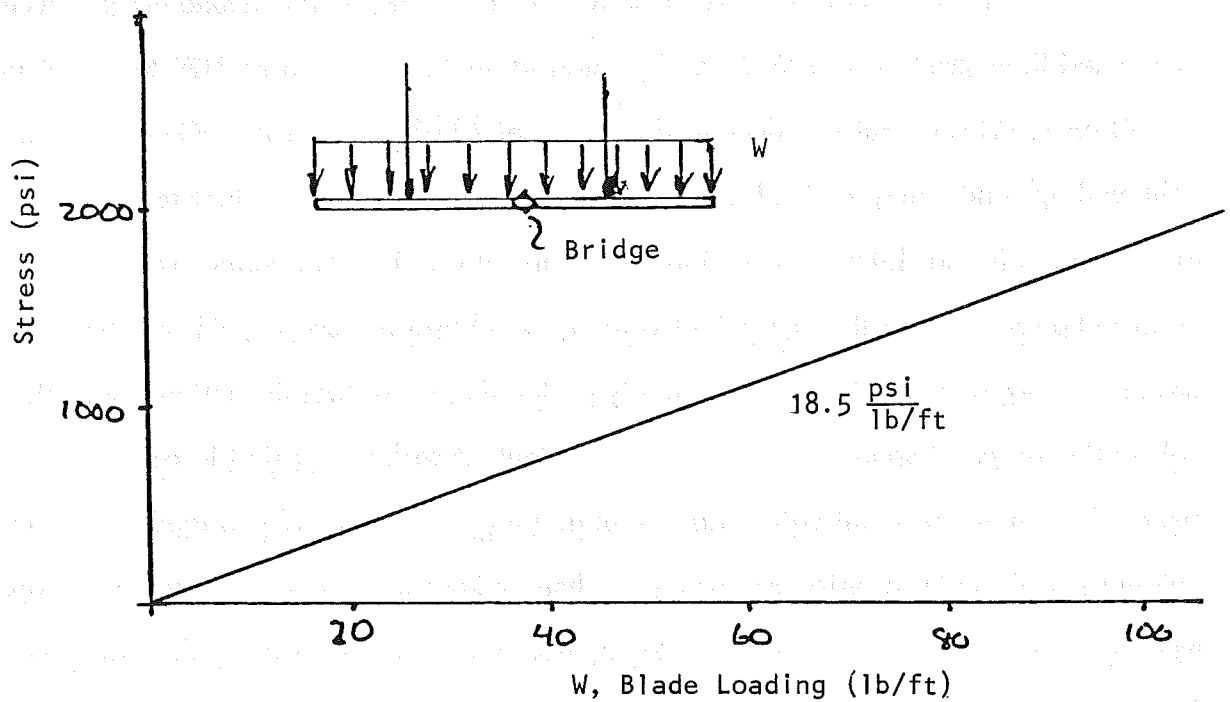
The torque output from the Lebow torque sensor was connected to a Daytronics 9170 Strain Gauge Conditioner and the output of the conditioner was plugged into channel #3 of the Hewlett Packard 7100B Strip Chart Recorder. To calibrate the torque system before running a test, all components were allowed to warm up and stabilize for ten minutes. All applied torque was removed from the torque sensor shaft and the strain gauge bridge was balanced to zero output using the balance control in the Daytronics 9170 Conditioner. Next, the output span was set to the Lebow factory calibration by applying the Lebow calibration shunt across one arm of the

strain gauge bridge and setting the output span of the conditioning amplifier to the calibration value supplied by Lebow. With the procedure completed, the published accuracy from Lebow was within  $\pm 0.05$  percent of the torque level and was traceable to the National Bureau of Standards. The recorder accuracy was, however,  $\pm 5$  in-lbs and was constant over the output span. This was due to a combination of scale readability and repeatability of the strip chart recorder. Turbine RPM was read from a magnetic pickup which generated a pulse as a tooth of a 60-tooth gear revolving with the shaft of the torque sensor passed the pickup. A Daytronics 9140 Frequency-to-Voltage Conditioner counted the output pulses and converted this frequency to a voltage level proportional to the shaft RPM. This was displayed on channel #2 of the recorder. Calibration was set using an internal crystal reference in the Daytronics 9140. The recorder accuracy was  $\pm 1/2$  RPM and was constant over the output span.

The strut root force was sensed by a strain gauge Wheatstone bridge circuit connected through the Lebow 6105-4 Slip Rings to another Daytronics 9170 Strain Gauge Conditioner. This output was displayed on channel #4 of the recorder. Calibration was achieved by conducting a "dead weight" calibration and transferring that to an equivalent input value for later shunt calibration. This allowed a dead weight calibration point to be replaced by the equivalent value of a calibration resistor. Then, the calibration resistor was used instead of actually performing a deadweight calibration. The calibration process began by zeroing the bridge output with no applied force on the strut. An equivalent input value was calculated for the bridge and was used to set the output span of the Daytronics conditioner. Then, a known sequence of ascending loads was applied to the strut tip and the bridge output was recorded. This calibration curve (Figure 5-3a) was used to reduce the test data. The calibration accuracy was  $\pm 1$  lb and was limited by the accuracy of the force scale used in calibration. It was also constant over the output span of the system.



a) Strut Root



b) Blade Spar Center Spar

Figure 5-3. Experimental Calibration Curves.

The blade spar force was calibrated by placing sand-filled bags on the blade to simulate a distributed load and was recorded to  $\pm 1$  lb accuracy on the recorders. Figure 5-3b shows the resulting calibration curves. The blade spar force tests were done separately because only two strain gauge conditioning channels were available. The results, however, were correlated to wind speed, RPM, and either torque sensor output or strut force.

#### General Test Procedure

A specific test began by setting up all equipment, calibrating each measurement system and then watching each system for at least one-half hour and re-calibrating, if necessary. Next, the series of tests runs was outlined in the test log and the tests performed. Every test run was carefully documented in the log and on the recorder chart paper. Periodic zero and calibration checks were made throughout the tests and, at the end of the tests, a careful calibration check was performed on all systems to spot any zero drift or change in calibration.

#### 5.1.1.2 TEST RESULTS

##### Performance Measurements

Cycloturbine performance data points were collected for a range of wind speeds by taking measurements on days when the wind was from the ocean at the New Seabury Test Facility. From this direction, wind speed is the steadiest and, therefore, near steady-state measurements could be taken. Data were collected on the two chart recorders, one recording wind speed and rotor RPM and the other reading the signal from the torque transducer. During a particular run, a range of loads (including no-load) was connected to the alternator.

The data were reduced by keying the recordings from the charts, choosing and numbering representative data points, and transcribing the points to a data reduction sheet. A sample data run is seen in Figure 5-4 and a sample data reduction sheet is given in Figure 5-5. The tip speed ratio for each data point was calculated from the measured wind speed and RPM. Similarly, power output was calculated using RPM and torque data and the results then used to calculate the power coefficient.

These points were then plotted to determine the shape of the power coefficient ( $C_p$ ) versus tip speed ratio ( $\lambda$ ) curve. Figure 5-6 shows the data of Figure 5-5 taken when the turbine was loaded (upper left) and when it was unloaded electrically (lower right). Note that an absolute no-load condition is not possible with the test equipment used because of bearing and belt drag and powering of the field circuitry in the Winco alternator. The loaded-condition grouping shows a mean power coefficient and tip speed ratio of about 0.45 and 3, respectively. A trend is noted also whereby higher tip speed ratios yield higher power coefficients.

A study was made of the sensitivity of the data to error in wind speed reading since this is the most difficult parameter to obtain accurately. A one-mph error, either high or low, in wind speed reading was assumed for representative values of  $C_p$  and  $\lambda$  based on experimental observations. A calculation on the effect on  $C_p$  and  $\lambda$  was then made while RPM and torque were held constant. Results for the point,  $C_p = 0.4$  and  $\lambda = 3.0$ , are given in Figure 5-7a and typical results are shown in Figure 5-7b along with similar data for the base points:  $C_p = 0.3$  and  $\lambda = 2.5$ ; and  $C_p = 0.175$  and  $\lambda = 3.5$  for various assumed wind velocities.

It is seen that at low wind speeds, the data are more sensitive to error resulting from a misreading of wind speed, than at the higher velocities. Also, data points at higher tip speed ratios are more susceptible to an error in the tip speed ratio

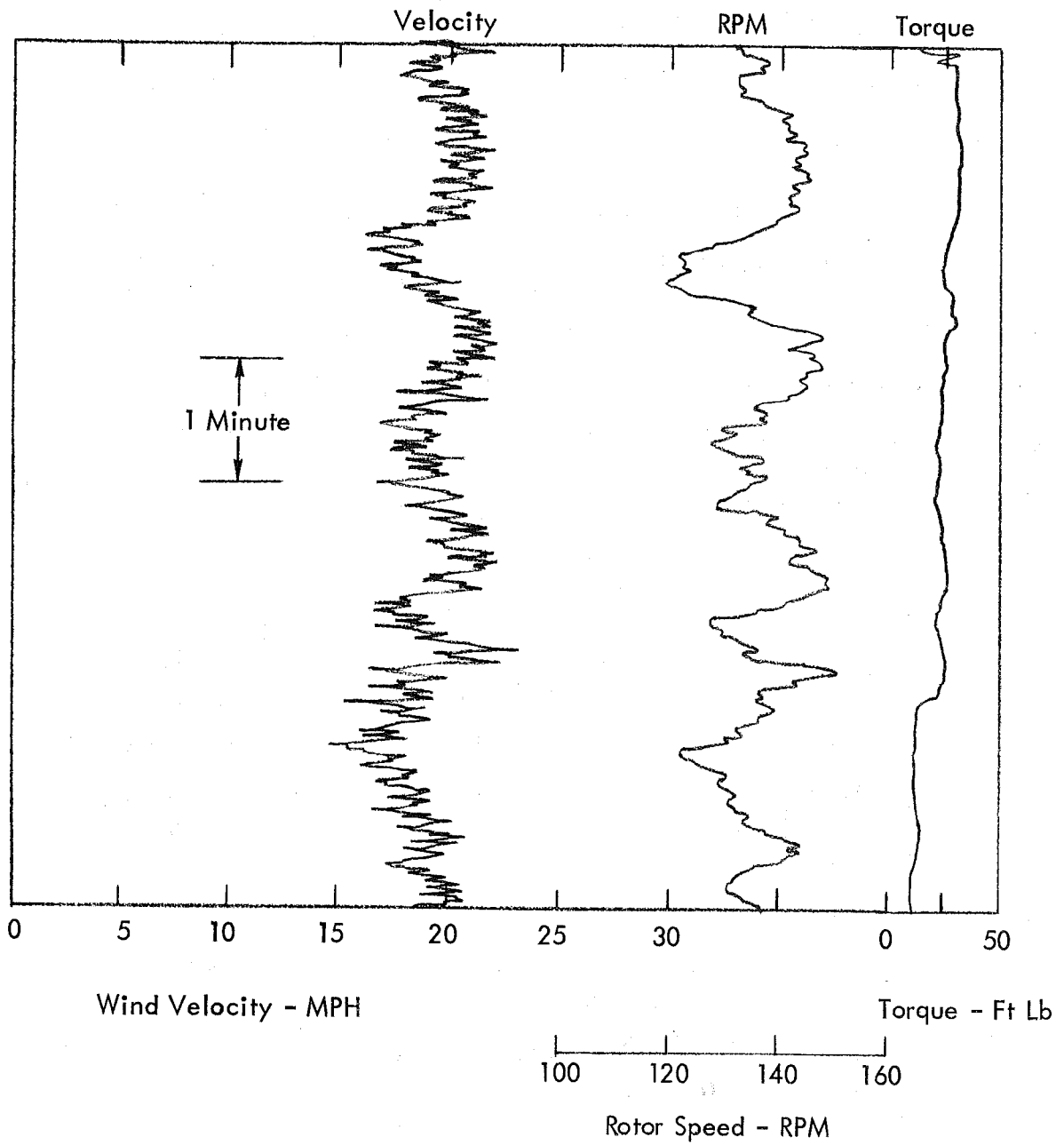


Figure 5-4. Sample Performance Data Run (Scale: 1 inch = 1 minute).

Point No.	V (MPH)	RPM	$\lambda$	Torque (Ft/Lb)	P (Watts)	$C_p$	Load/Field
1	10.5	90.0	3.67	9	115	0.203	V
2	11.0	91.0	3.54	9	116	0.178	
3	11.5	72.0	2.68	30	307	0.413	IV
4	11.5	71.0	2.64	29	292	0.393	
5	11.0	69.5	2.71	28	276	0.424	
6	11.0	71.5	2.78	22	223	0.343	III
7	10.5	70.0	2.86	22	219	0.387	
8	11.0	73.0	2.84	24	249	0.382	
9	11.0	72.0	2.80	23	235	0.361	
10	10.5	69.5	2.84	22	217	0.383	
11	9.5	64.0	2.89	28	164	0.391	
12	9.5	66.0	2.98	19	178	0.425	
13	10.0	68.5	2.93	21	204	0.417	
14	10.0	65.5	2.81	19	177	0.362	
15	9.0	63.0	3.00	18	161	0.452	
16	9.5	66.0	2.98	18	169	0.403	IIb
17	9.5	67.0	3.02	19	181	0.432	
18	10.0	68.0	2.91	22	212	0.434	
19	11.0	69.0	2.69	23	225	0.346	
20	8.75	66.0	3.23	18	169	0.516	
21	10.5	69.0	2.81	23	225	0.398	
22	10.0	67.0	2.87	20	190	0.389	
23	8.5	62.0	3.12	15	132	0.440	
24	9.0	66.0	3.14	18	169	0.475	
25	9.5	67.0	3.02	27	162	0.387	
26	9.0	67.0	3.19	18	171	0.480	
27	9.5	66.0	2.98	17	159	0.379	
28	8.0	76.0	4.07	4	43	0.172	V
29	9.5	82.0	3.70	4	47	0.112	
30	9.0	81.0	3.86	4	46	0.138	
31	9.25	78.0	3.61	5	55	0.142	
32	8.5	75.0	3.78	5	53	0.177	

Figure 5-5. Sample Data Reduction Sheet.

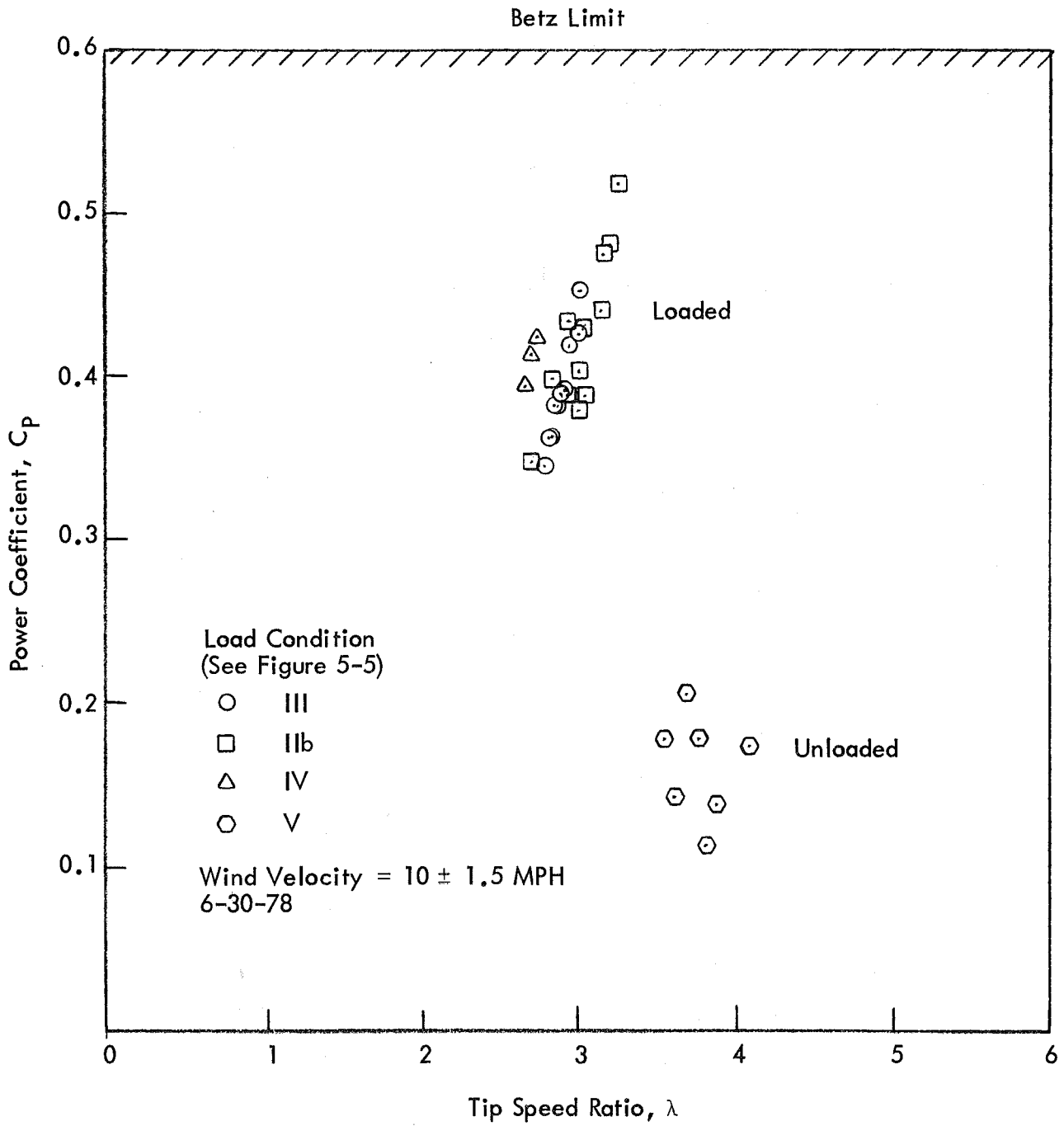
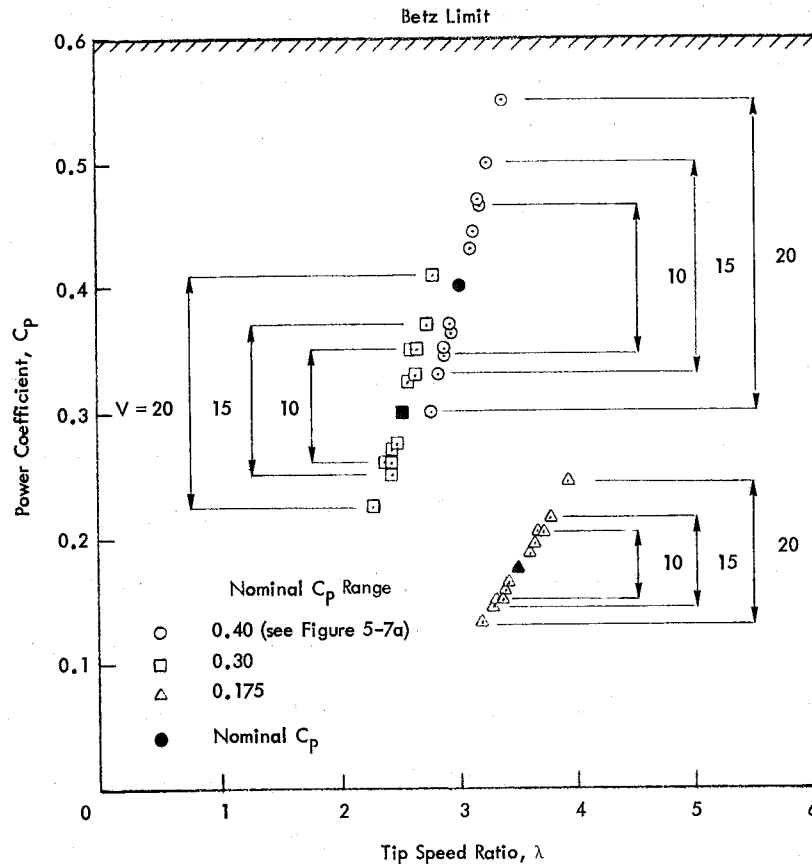


Figure 5-6. Sample Performance Data.

V (MPH)	RPM	$\lambda$	Torque (Ft/Lb)	P (Watts)	$C_p$	Error Band
9.0	70	3.33	19.66	195.4	0.548	$V = 10 \pm 1.0$ $\lambda = 3.0 \pm 0.30$ $C_p = 0.4 + 0.148; -0.100$
9.5	70	3.16	19.66	195.4	0.467	
10.0*	70	3.00*	19.66	195.4	0.400*	
10.5	70	2.85	19.66	195.4	0.346	
11.0	70	2.73	19.66	195.4	0.300	
14.0	105	3.21	44.23	659.2	0.492	$V = 15 \pm 1.0$ $\lambda = 3.0 \pm 0.20$ $C_p = 0.4 + 0.092; -0.071$
14.5	105	3.10	44.23	659.2	0.443	
15.0*	105	3.00*	44.23	659.2	0.400*	
15.5	105	2.90	44.23	659.2	0.362	
16.0	105	2.81	44.23	659.2	0.329	
19.0	140	3.16	78.64	1563.2	0.466	$V = 20 \pm 1.0$ $\lambda = 3.0 \pm 0.15$ $C_p = 0.4 + 0.066; -0.055$
19.5	140	3.07	78.64	1563.2	0.432	
20.0*	140	3.00*	78.64	1563.2	0.400*	
20.5	140	2.92	78.64	1563.2	0.371	
21.0	140	2.85	78.64	1563.2	0.345	

\*Nominal Value

a) Sample Error Band Calculations



b) Calculated Error Band

Figure 5-7. Effect of Wind Speed Reading Error.

value itself than those for lower tip speed ratios. Similarly, the higher the power coefficient, the larger the error band for those power coefficients. Finally, a non-linear (cubic) trend is seen which makes the power coefficient more sensitive to a low wind speed reading than to a high reading. In summary, the trends shown in Figure 5-7 indicate that the wind speed readings are most important when attempting to take a measurement on a loaded turbine in a low enough wind speed where transients due to turbulence are less.

The performance measurements of the Cycloturbine C2E were continued for three months and the data were collected only at near steady-state conditions. The data fall within the data band shown in Figure 5-8 and are seen to agree well with the curve calculated from the computer analysis having an assumed value on "additional drag coefficient" of 0.005 (see Subsection 4.3.2). The maximum power coefficient of about 0.40 occurs around a tip speed ratio of 3.

#### Force Measurements

The procedure for measuring the cyclic stresses on the strut root and blade center spar was complicated by recurrent problems with wiring continuity. Because of this, three chart recorders were employed. Two chart recorders, one displaying wind speed and RPM and the other displaying torque and blade or strut stress signals, were synchronized to each other at a relatively low chart speed of 6 inches per minute. The torque trace appeared as a wide band. The third recorder which had a chart speed capability of 2 inches per second was used to record a clear trace of the stress fluctuation. It was turned on when a near steady wind speed was observed and the RPM was relatively constant. Then two or three seconds of stress measurements were recorded. Azimuth position of the strut or blade relative to the wind direction was indicated by a

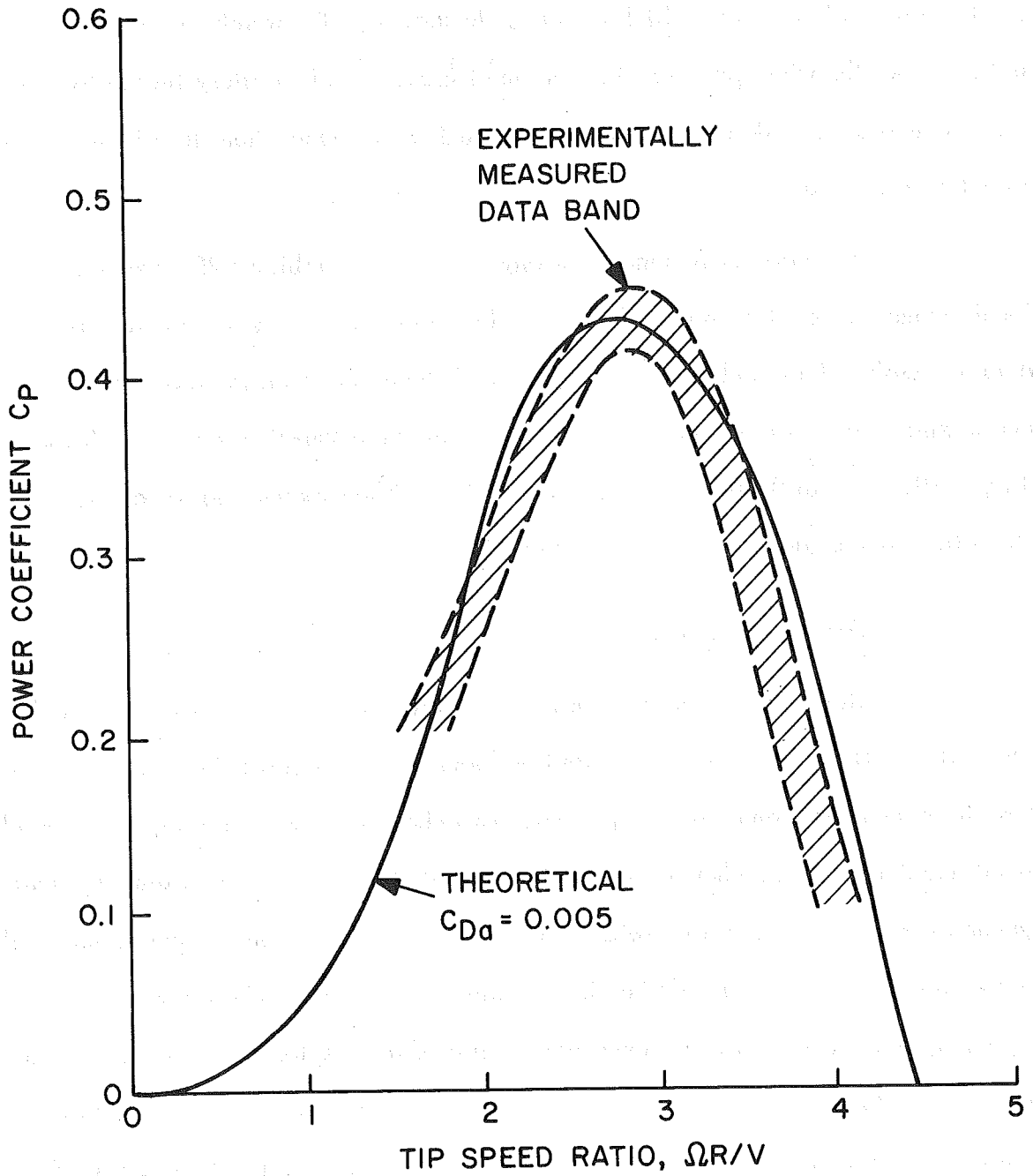


Figure 5-8. Comparison of Experimental and Analytical Performance.

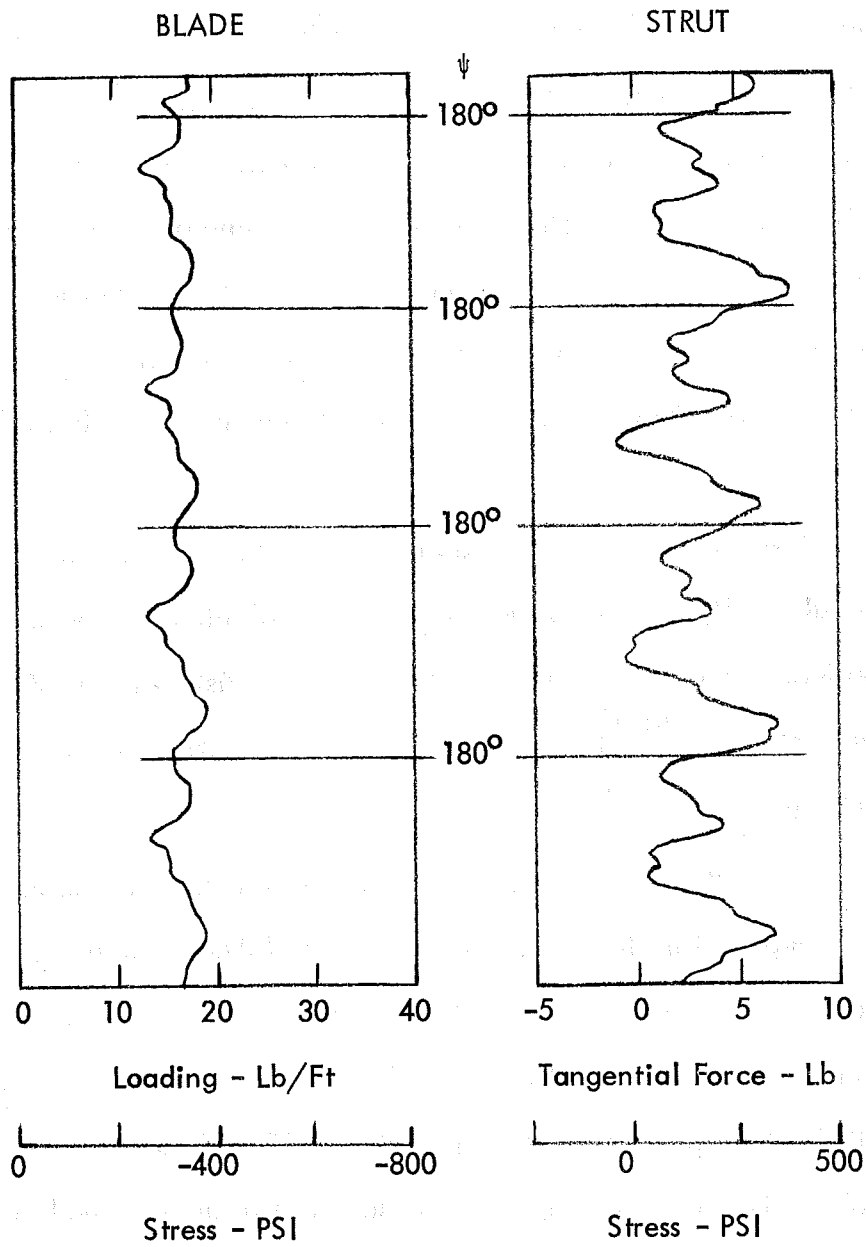
reed switch and recorded. Although  $\psi = 0$  was taken to be downwind of the center of rotation, the switch was placed on the upwind side in the test runs so that each contact indicated  $\psi = 180^\circ$ . Thus, the recorder response was removed as a variable.

Data from test runs at very similar conditions were selected for comparison and to combine blade and strut stress readings which could only be taken separately. Figure 5-9 shows matched runs of blade and strut stress traces for different loading conditions, that is, different  $C_p$  and tip speed ratios ( $\lambda$  in the figure) at the same wind speed of 20 mph. A difference in waveform shape is seen especially in the strut stress trace.

The results of the matched blade/stress data traces were compared to curves generated analytically (see Subsection 4.5). The calibration curves of Figure 5-3 were used to transform the measured data to blade chordwise distributed loads  $\left(\frac{dC}{d\ell}\right)$  and blade normal distributed load  $\left(\frac{dN}{d\ell}\right)$ . The comparisons of experimental and analytical results are shown in Figure 5-10.

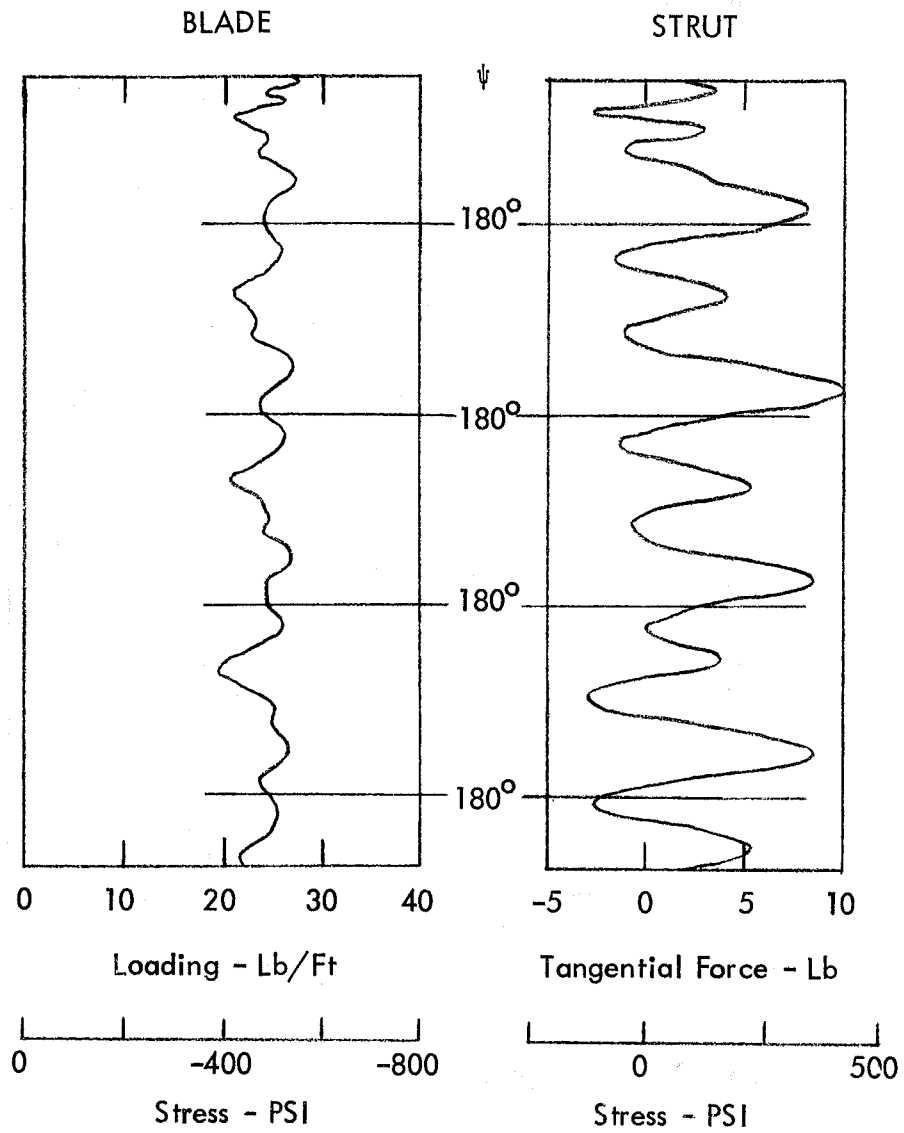
It is seen that the blade chordwise load results (taken from the strut root readings) compare well in shape but that the measured data seem to lag the calculated results. Additionally, the negative peaks (related to the blades driving the turbine around) are more pronounced. Although further measurements are needed, possible causes for the difference between the calculated and the measured data could be dynamic stall of the blades causing increases in aerodynamic drag and/or a lag in the lift buildup due to the unsteady nature of the loading. The lag may also be caused by a phase difference between the aerodynamic harmonic inputs and a natural frequency of the Cycloturbine.

The results from the blade normal force measurements do not correlate well. Although the curves show similar behavior from  $\psi = 270^\circ$  to  $\psi = 90^\circ$ , the measured normal load does not follow the calculated load at  $\psi = 180^\circ$ . The difference can be



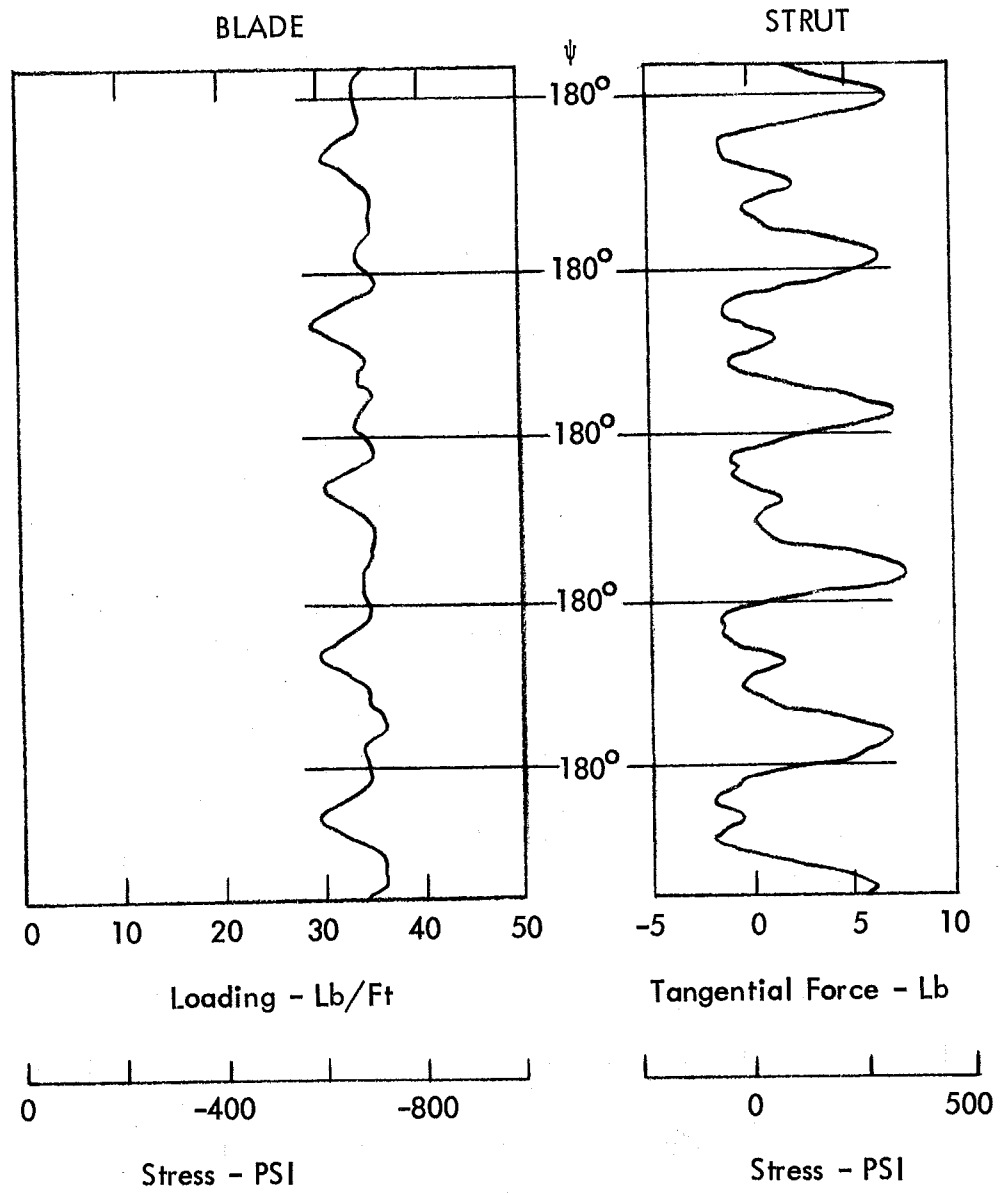
a)  $\lambda = 2.36$

Figure 5-9. Blade and Strut Loading Waveform.



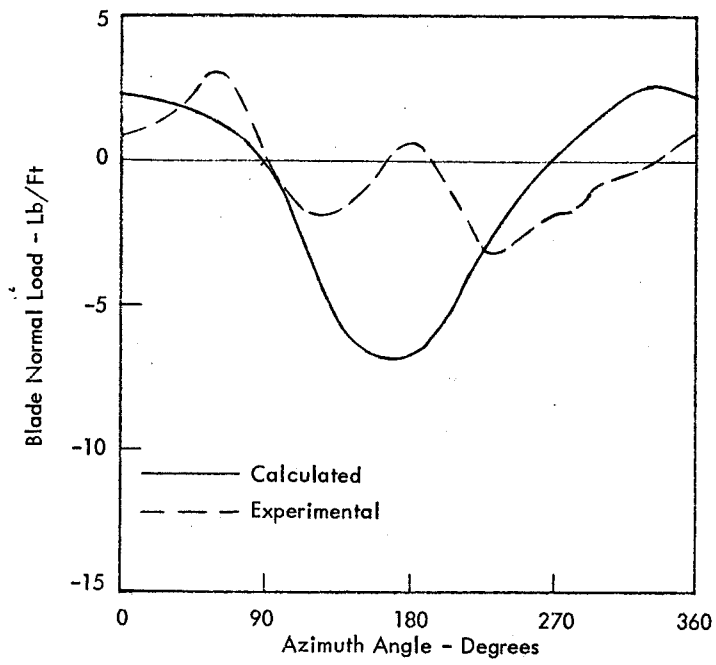
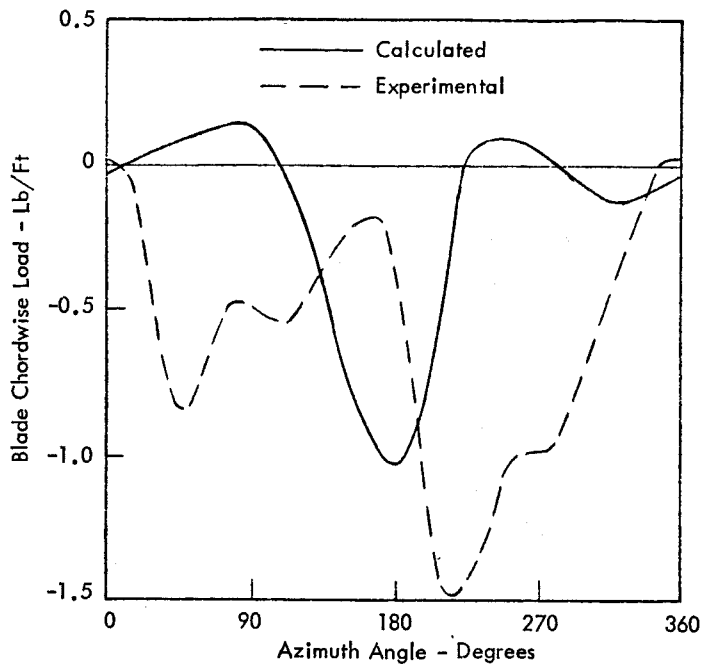
b)  $\lambda = 2.87$

Figure 5-9. Blade and Strut Loading Waveform (Continued).



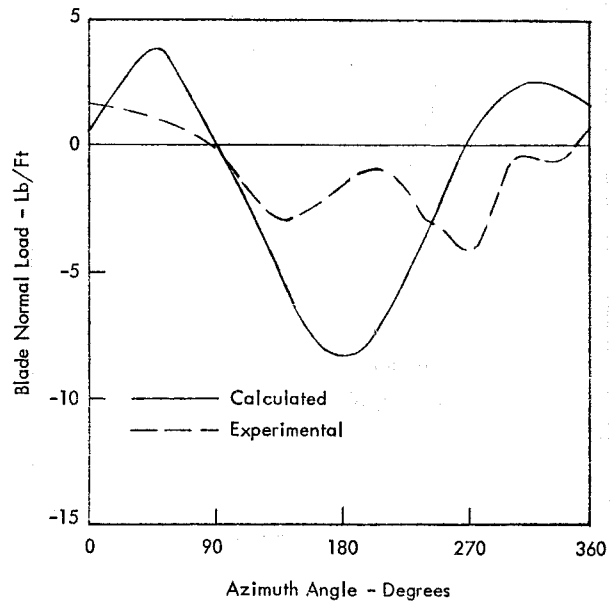
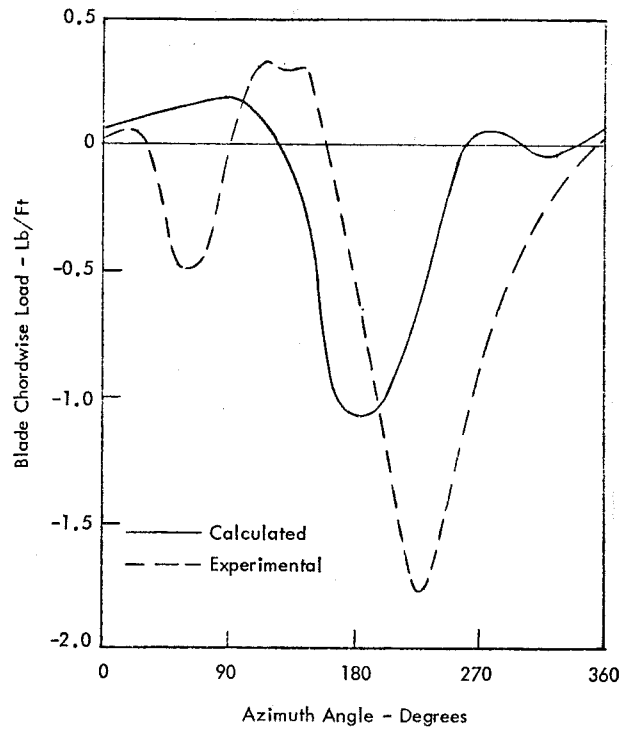
c)  $\lambda = 3.43$

Figure 5-9. Blade and Strut Loading Waveform (Concluded).



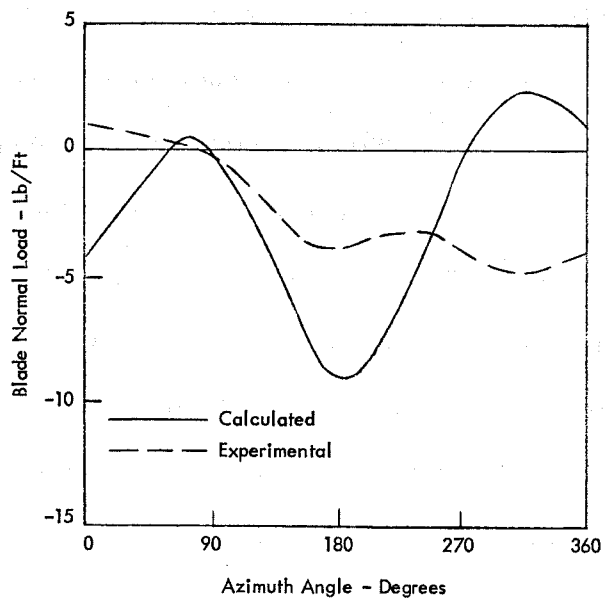
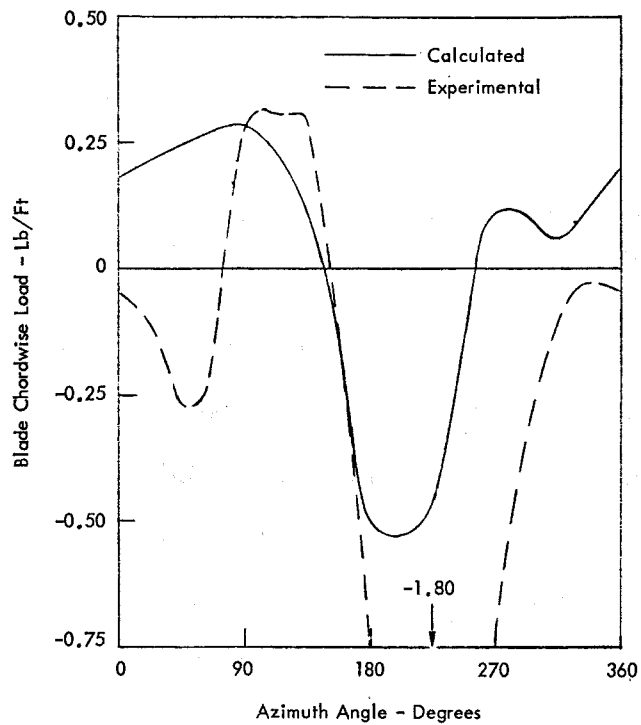
a)  $\lambda = 2.36$

Figure 5-10. Comparison of Experimental and Analytical Blade Loads.



b)  $\lambda = 2.87$

Figure 5-10. Comparison of Experimental and Analytical Blade Loads (Continued).



c)  $\lambda = 3.43$

Figure 5-10. Comparison of Experimental and Analytical Blade Loads (Concluded).

accounted for as stall but it is thought more likely that it is due to load taken up by the skin of the blade (only the spar inside the blade was instrumented).

Attempts were made to measure the effect of dynamic stall on the Cycloturbine C2E. Two effects were noted both of which negated the measured results. The first effect is that the  $C_p$  curve in the neighborhood of the dynamic stall point (see Figure 4-9) is extremely sensitive to small changes in wind speed. Unless a constant wind speed is achieved, the exact  $C_p$  cannot be identified. The second effect is that as dynamic stall occurs, suction is lost on the leading edge of the blade and chordwise force decreases rapidly. The result is that the rotor slows down and will stop unless the tip speed ratio increases. Thus, dynamic stall causes a transient situation in which precise measurements are difficult to achieve in the field.

### Conclusions

The data collected in the test program on the Cycloturbine C2E were adequate to verify the analyses developed for the aerodynamic loads, performance, and structural stresses. Performance was predicted within ten percent. Although the predicted loads and stresses did not correlate well over the operational cycle, their amplitude was of the same order of magnitude. The analysis could, therefore, be applied with increased confidence.

A more controlled environment is needed to be able to obtain data with better resolutions. The variable nature of the wind in the real environment is a problem in that steady wind conditions are required in order to obtain the desired measurements. A wind tunnel study should be considered as future work.

#### 5.1.2 STRUT OUTBOARD TANG STRUCTURAL TEST

A critical portion of the Cycloturbine strut is the outboard tang which provides the means of attaching the blade to the strut. The tang also acts as a hinge to allow the blade to change its angle-of-attack. The tang is subjected to the aerodynamic loads produced on the blades and transmitted to the struts, and to high tensile forces due to inertial effects of the blade weight and to centrifugal acceleration.

Theoretically, failure modes of the tang, as depicted in Figure 5-11 include: 1) double shear of hinge bolt; 2) double shear in tang; 3) tension; and 4) distortion due to bearing load. Yield loads for the first three modes were calculated and were found to be 16,570 lbs, 8,600 lbs, and 6,015 lbs, respectively. Thus, failure in tension was the expected failure mode.

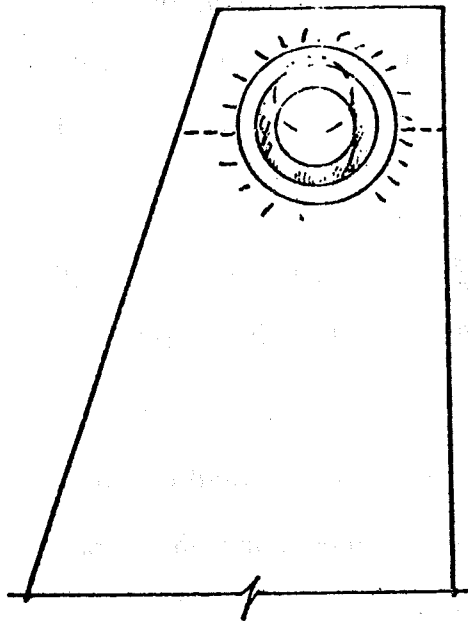
Tests were conducted in a tension/compression testing machine. A steel jig was constructed to support the tang in exactly the same manner as it acts in operation. The jig fit into the top set of jaws of the testing machine.

The tang was loaded in tension to failure. Failure occurred at 6,600 lbs which exceeded the predicted 6,015 lbs. This test provided assurance that the theoretical design load was conservative. It should be noted that the material failed and not the welds attaching the tang to its support structure.

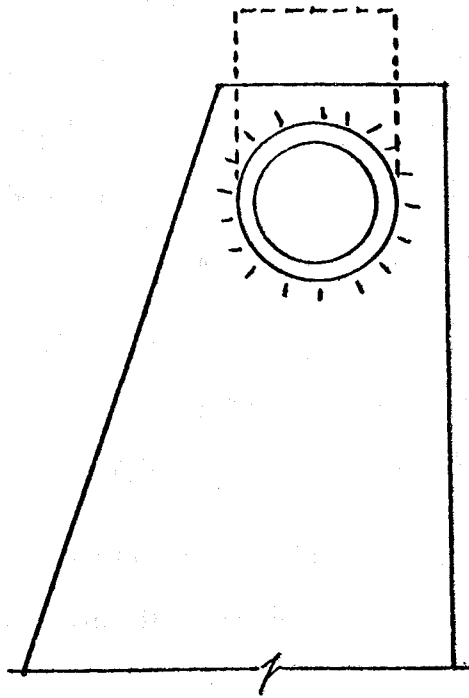
### 5.1.3 TILT-CAM CONTROL SYSTEM OPERATIONAL TESTS

A prototype tilt-cam control system was constructed to replace the pitch actuation control system originally incorporated in the instrumented Cycloturbine C2E used for testing at New Seabury. The tilt-cam design as conceived provides improved performance. It is also expected that the tilt-cam will be a higher reliability system because of the type of loads experienced and the bearings that can be used.

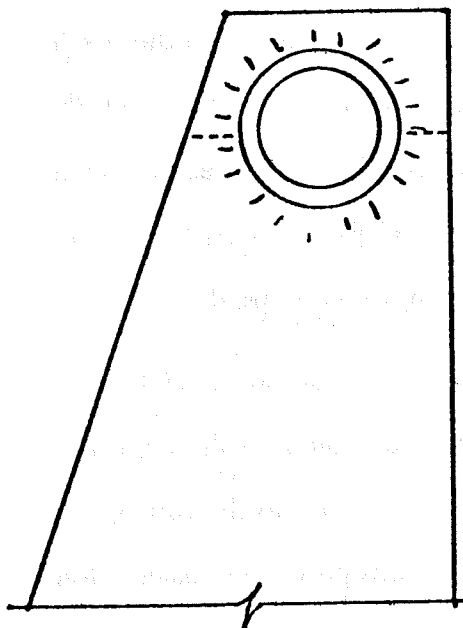
Installation of the tilt-cam control system on the Cycloturbine C2E revealed the need for several modifications. Design changes were made in the control linkage and in the location of the attachment of the control pull rods to the blades. The original attachment point was aft of the blade hinge but this produced compression loads (when averaged over a cycle) on the rods when actuated by the tilt-cam system. This was rectified by placing the attachment point ahead of the hinge (see Figure 6-3) which was accomplished by a design retrofit. Initial tests indicated that the system



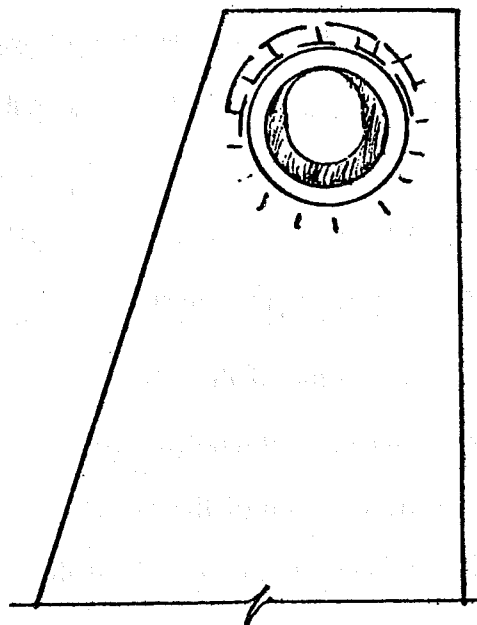
a) Double Shear of Bolt.



b) Double Shear in Tang.



c) Tensile Failure.



d) Bearing - Distortion Failure.

Figure 5-11. Strut Outboard Tang Failure Modes.

operates as expected, that is, the average cyclic load is in tension, and that the load levels are similar to those predicted.

## 5.2 ELECTRICAL SYSTEM

Testing was done to check the temperature stability of the voltage regulator A2A4 and the dump load control A2A2. Also a test was run on the power rectifier A2A3 to determine the temperature rise of the rectifier case at full power. Testing was done on the transient suppression network A1A2 and A2A1 to determine if it clamped voltages at a safe level. Also, as noted in Subsection 3.2.2.1, testing was done on the proposed alternator.

### 5.2.1 ELECTRICAL CIRCUIT TEMPERATURE TESTS

Low temperature tests were conducted on the voltage control relay (dump load) and voltage limiter control (regulator) circuits. An insulated box was fabricated with appropriate connectors and test points. Low temperatures down to  $-40^{\circ}\text{C}$  were achieved using liquid  $\text{CO}_2$  with a boiling point of  $-78^{\circ}\text{C}$ . The temperature was determined by measuring the resistance of a nickel wire resistance temperature device and comparing it to a known calibration table. The voltages that characterized the circuits performance (preset switching points and power supply voltage) were monitored externally.

It was possible to obtain temperatures between  $-40^{\circ}\text{C}$  and  $20^{\circ}\text{C}$  using the box. The circuits were then transferred to a refrigerator equipped with a heater and thermostat in which the temperature could be ranged from  $10^{\circ}\text{C}$  to  $60^{\circ}\text{C}$ . The same measurements were taken as above. Results of the temperature tests are shown in Figures 5-12 and 5-13.

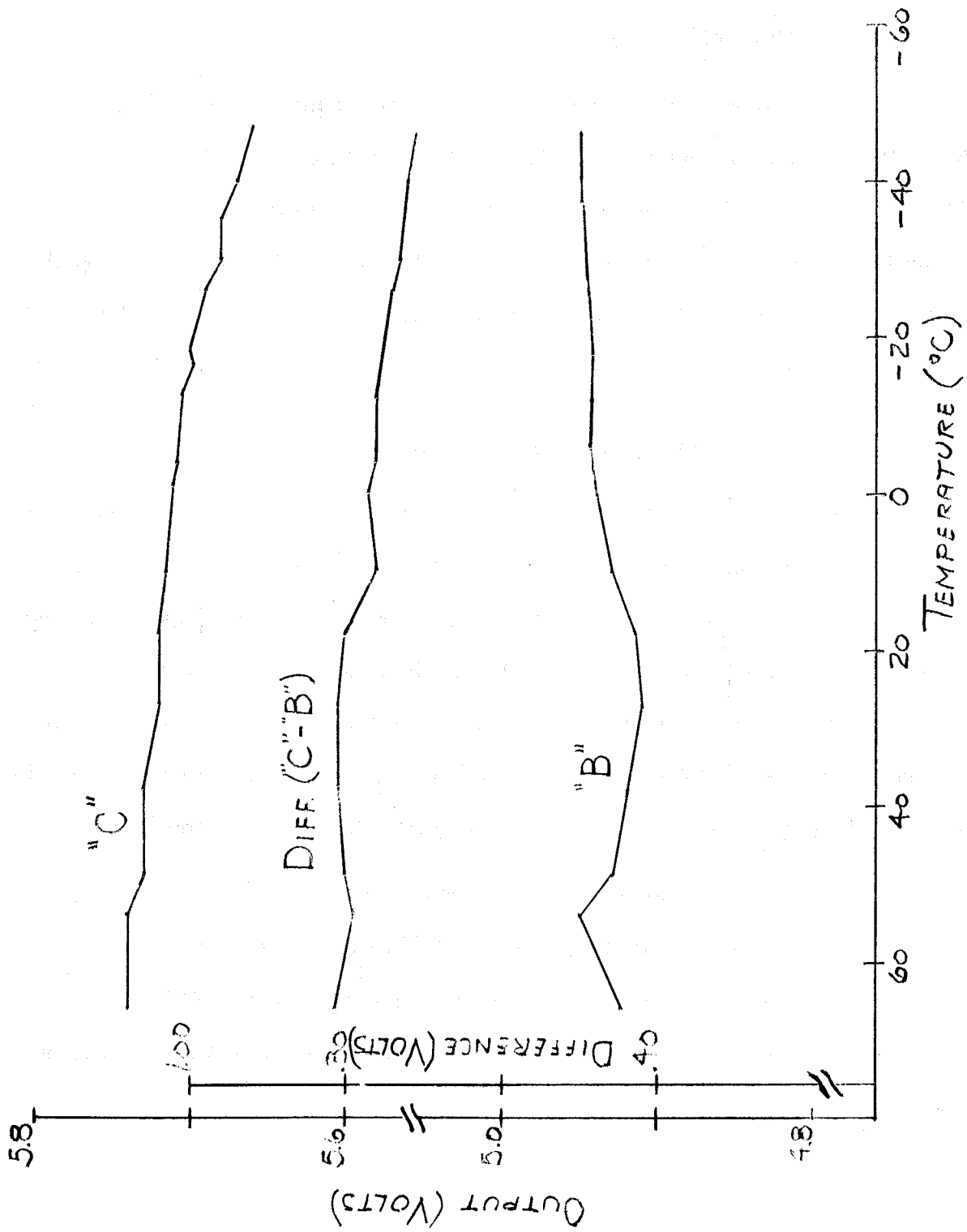


Figure 5-12. Voltage Control Relay Temperature Test Data.

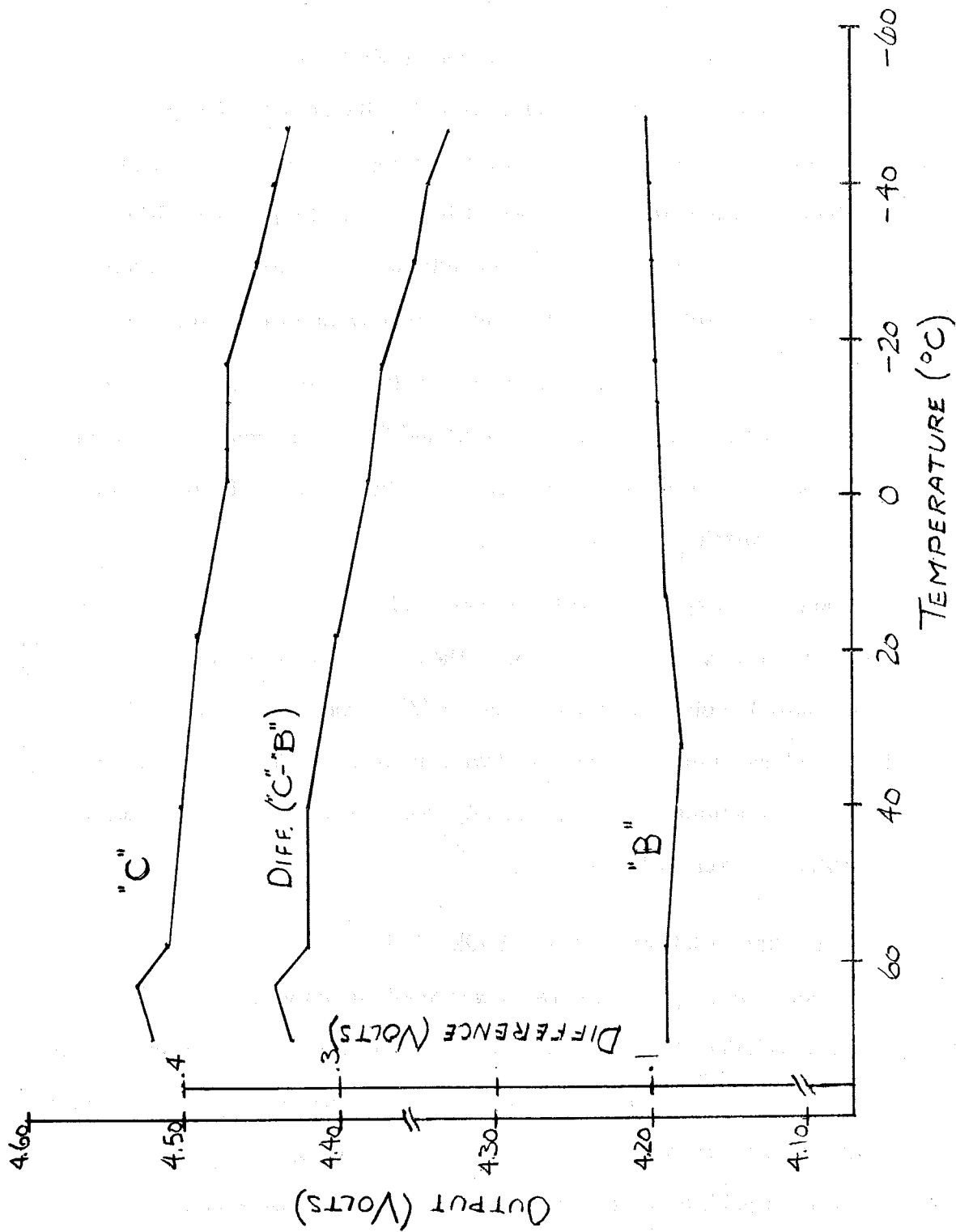


Figure 5-13. Voltage Limiter Control Temperature Test Data.

Curve B in Figures 5-12 and 5-13 is the voltage present at the inverting (i.e., the negative) terminal of the operational amplifiers (op amp). The op amps are shown in Figure 3-25 as CA3130 in the dump load (A2A2) and regulator (A2A4) circuits. Curve C in the figures is the voltage present at the noninverting (i.e., the positive) terminal of the op amp. In operation, the voltage at the inverting input is proportional to battery voltage and the voltage at the noninverting terminal is a reference voltage, which depends on the output state of the circuit. The current was adjusted to have zero error at room temperature, a convenient calibration point.

The effect of temperature on the stability of the circuits is shown by the difference between Curves B and C in Figures 5-12 and 5-13. The voltage regulator circuit was very stable but the dump load circuit had to be modified slightly to maintain voltage variations within acceptable levels.

A heat sink temperature test was performed on the main rectifier circuit to determine the temperature rise in the circuit. The temperature rise was achieved by drawing a DC current equivalent to the expected AC current through the rectifier assembly. The case temperature was monitored with the above resistance thermometer. The test was allowed to continue until the assembly remained stable in temperature for 15 minutes. Results are given in Figure 5-14.

#### 5.2.2 TRANSIENT SUPPRESSION NETWORK TESTS

The transient suppression network was required due to the possibility of high voltage transients induced by lightning strikes or near "hits". The network design was tested to voltage and amperage levels which could be generated both economically and safely in the available facilities. A 40  $\mu$ f laser discharge capacitor was charged to 2,000 volts and discharged into the circuit. Voltage and current waveforms were recorded on a storage oscilloscope. Initial tests indicated that the varistor in the

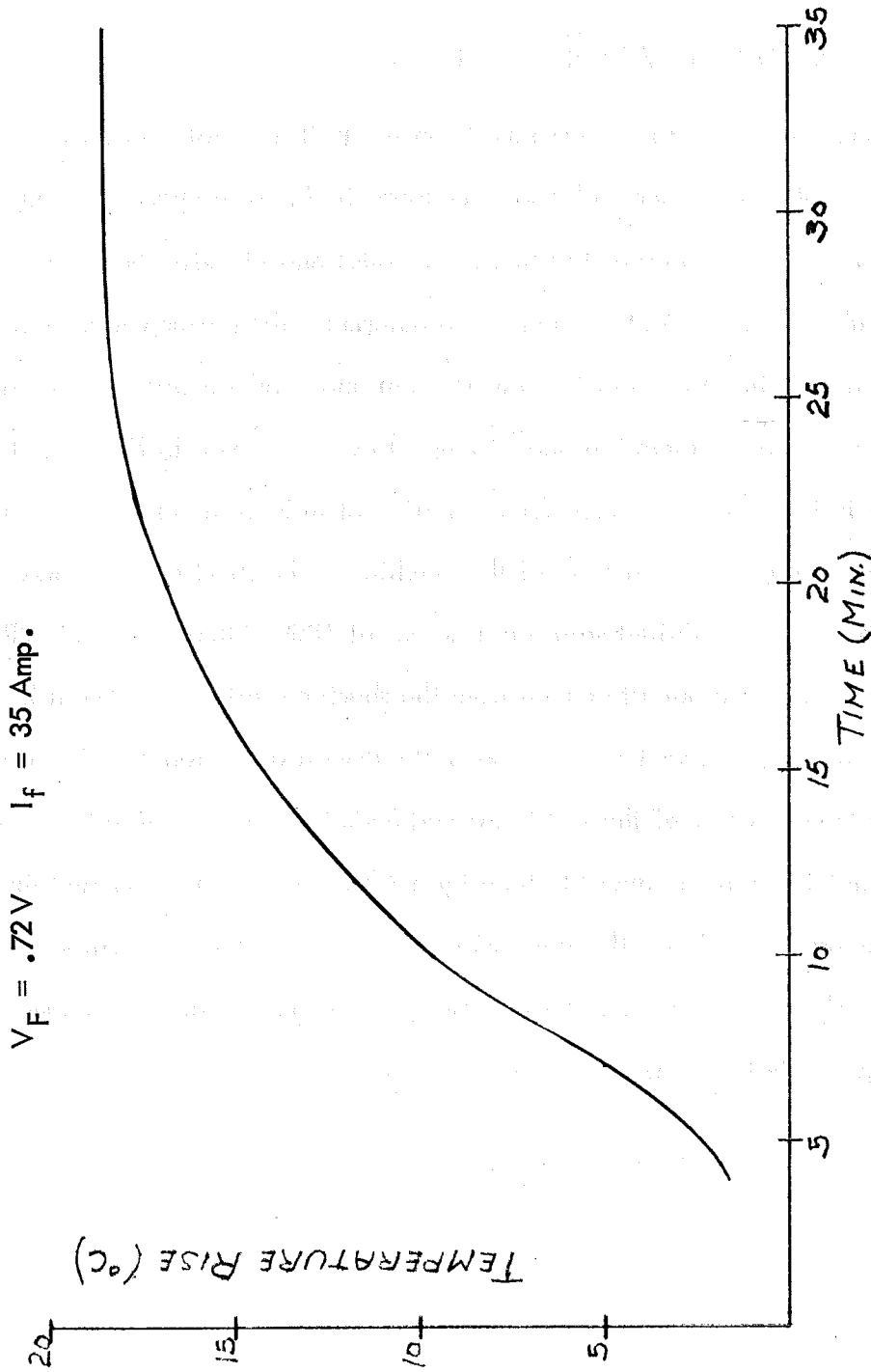


Figure 5-14. Main Rectifier Heat Sink Temperature Test.

circuit did not appear to clamp voltages at proper levels. Subsequent tests on a re-designed circuit with twice the series inductance showed that voltages were properly clamped and that the spark gaps worked as expected.

### 5.2.3 ALTERNATOR CHARACTERISTICS TESTS

A series of standard tests were made on the NPI alternator to characterize the performance of the alternator and also to measure its internal operating temperatures. These results were required in order to attempt to model analytically the alternator performance (see Subsection 3.2.2.1). In order to determine the power conversion efficiency of the NPI alternator, the effects of bearing friction and windage were measured on a dynamometer. The measured friction and windage losses are given in Figure 5-15. An open circuit test such as conducted for conventional induction machines was run to determine the air gap characteristics of the machine. The short circuit characteristics were also measured. The resultant saturation curves at 1800, 2000, and 3600 RPM are shown in Figure 5-16. The output current from the short-circuit test is shown in Figure 5-16a. The temperature tests were carried out with a resistance temperature device wound into the center of the field coil and a similar device glued to an output coil. The alternator was then caused to heat by applying external power and the temperature responses recorded. The time history of the measured temperature is shown in Figure 5-17. The temperature rise was measured from ambient at a maximum current condition (500  $\mu$ A), that is, a worst case condition.

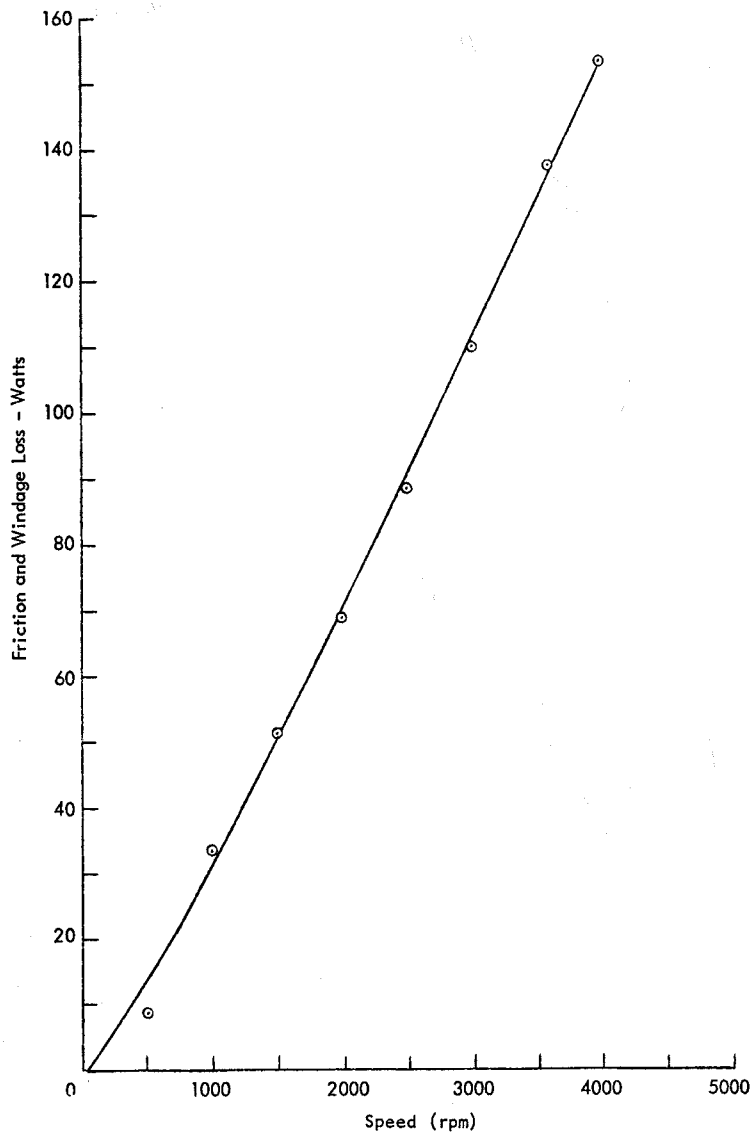
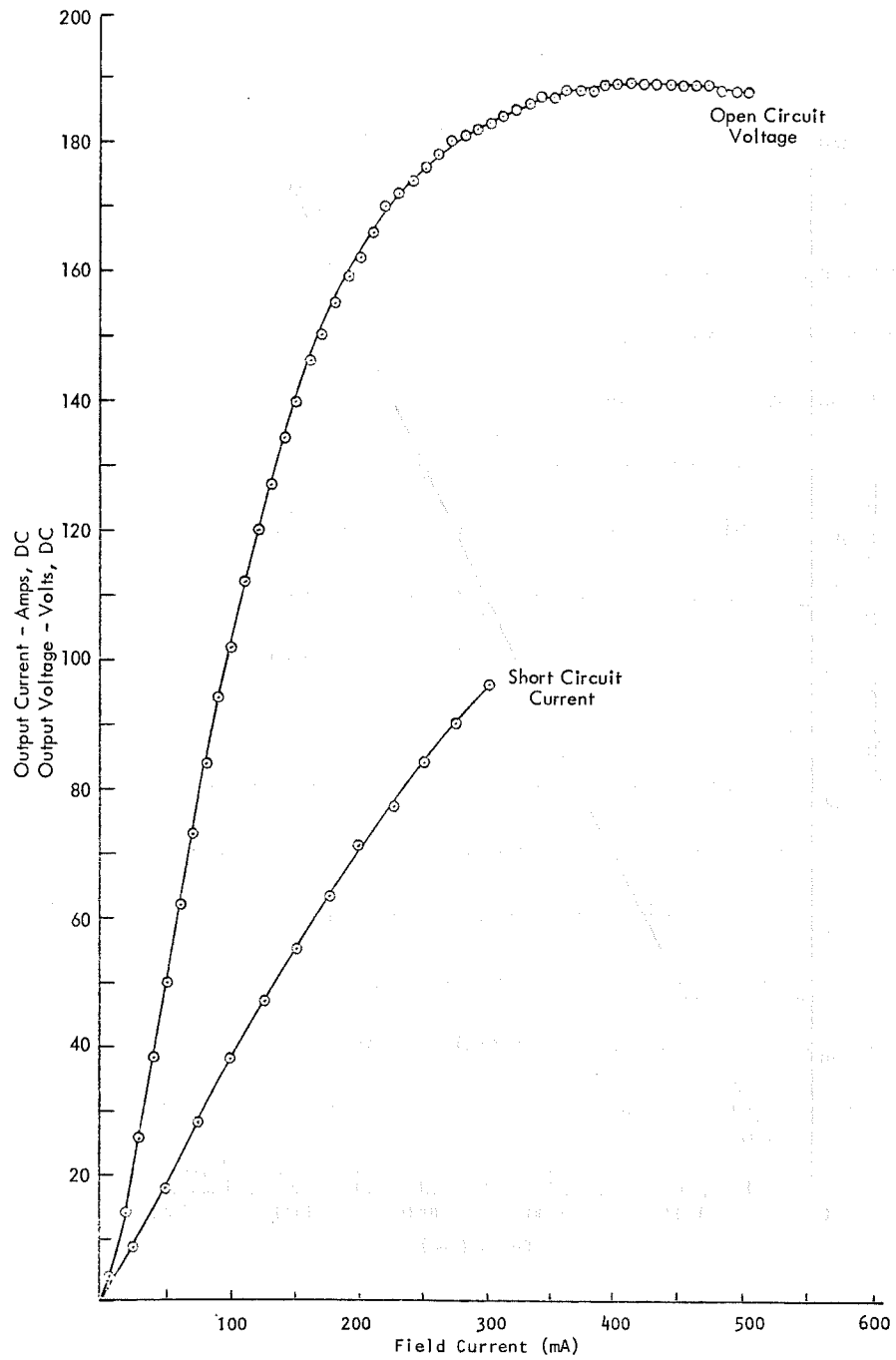
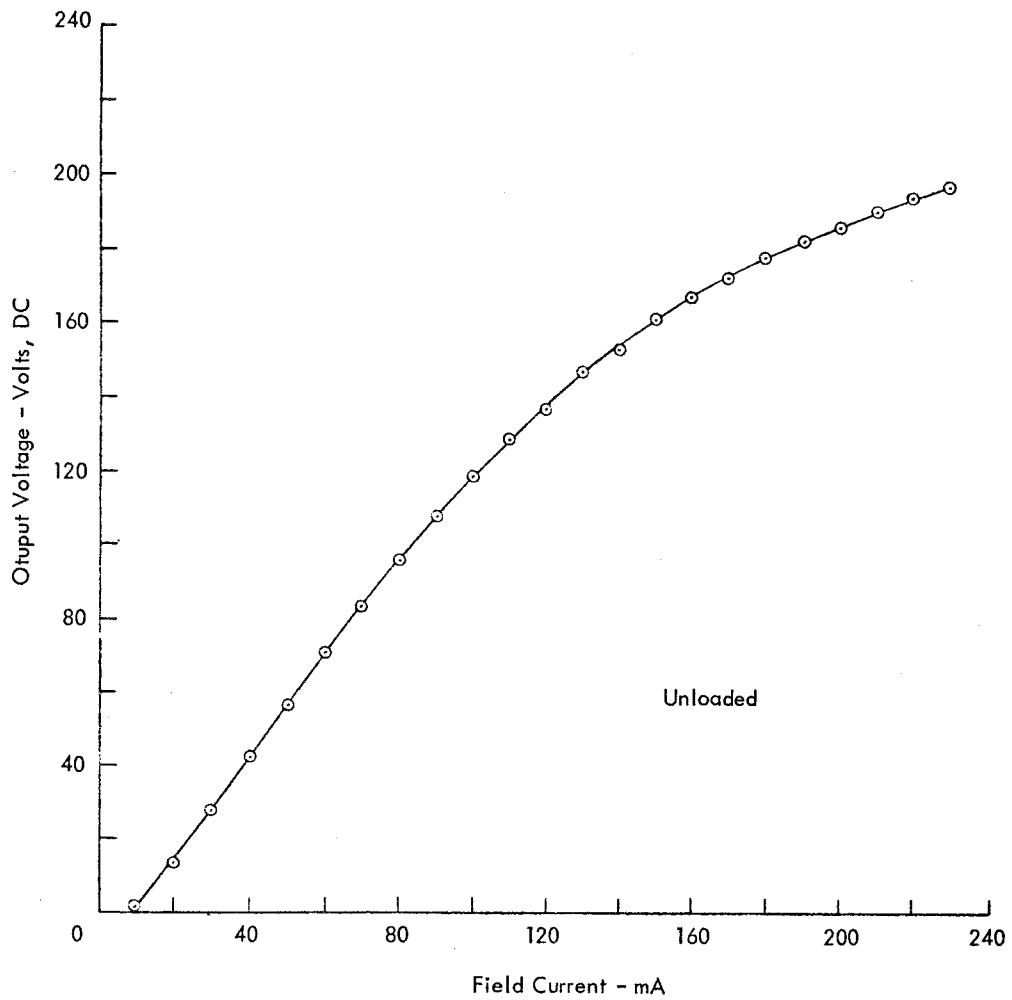


Figure 5-15. NPI Alternator Friction and Windage Loss.



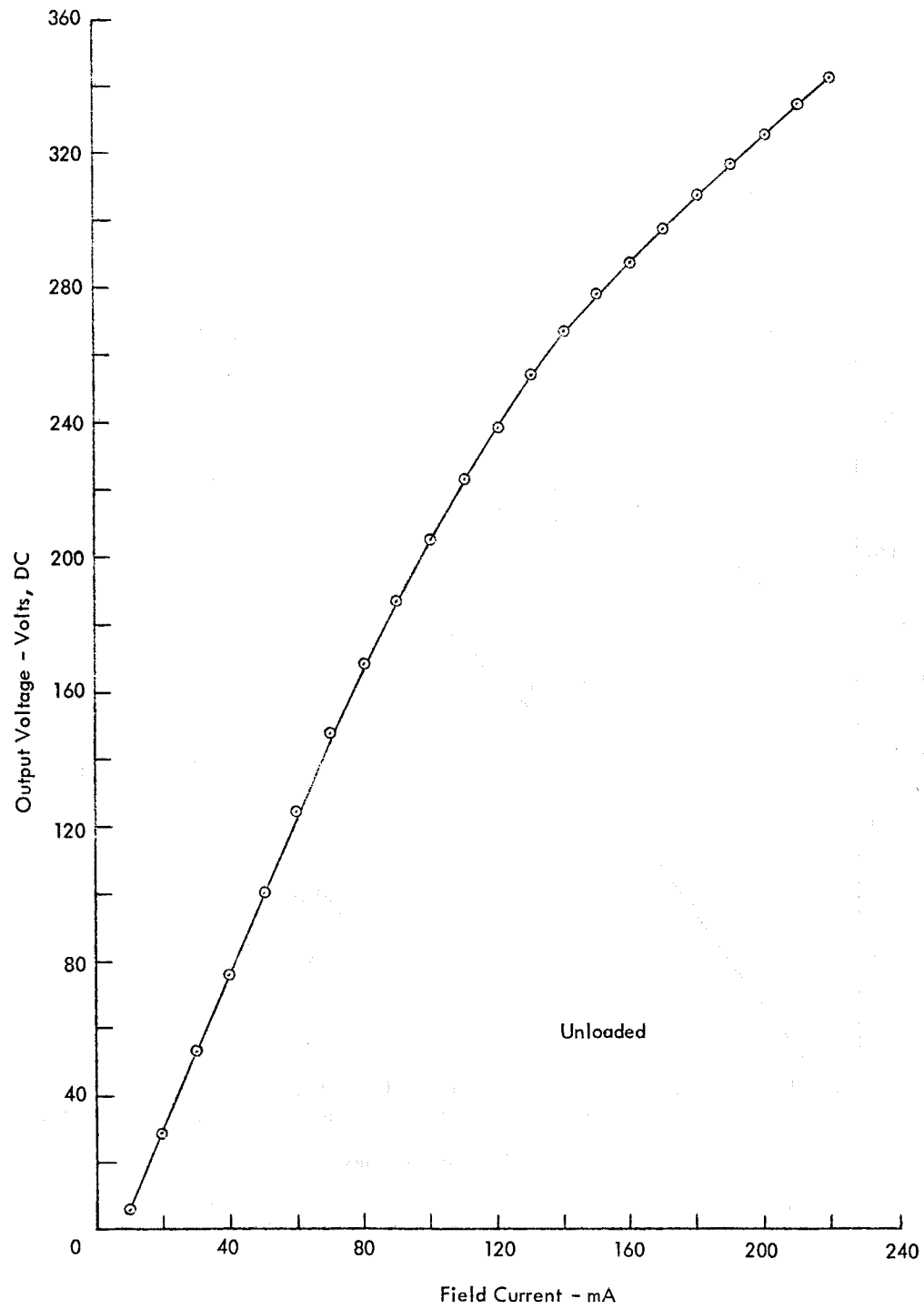
a) 1800 RPM

Figure 5-16. NPI Alternator Saturation Curve.



b) 2000 RPM

Figure 5-16. NPI Alternator Saturation Curve (Continued).



c) 3600 RPM

Figure 5-16. NPI Alternator Saturation Curve (Concluded).

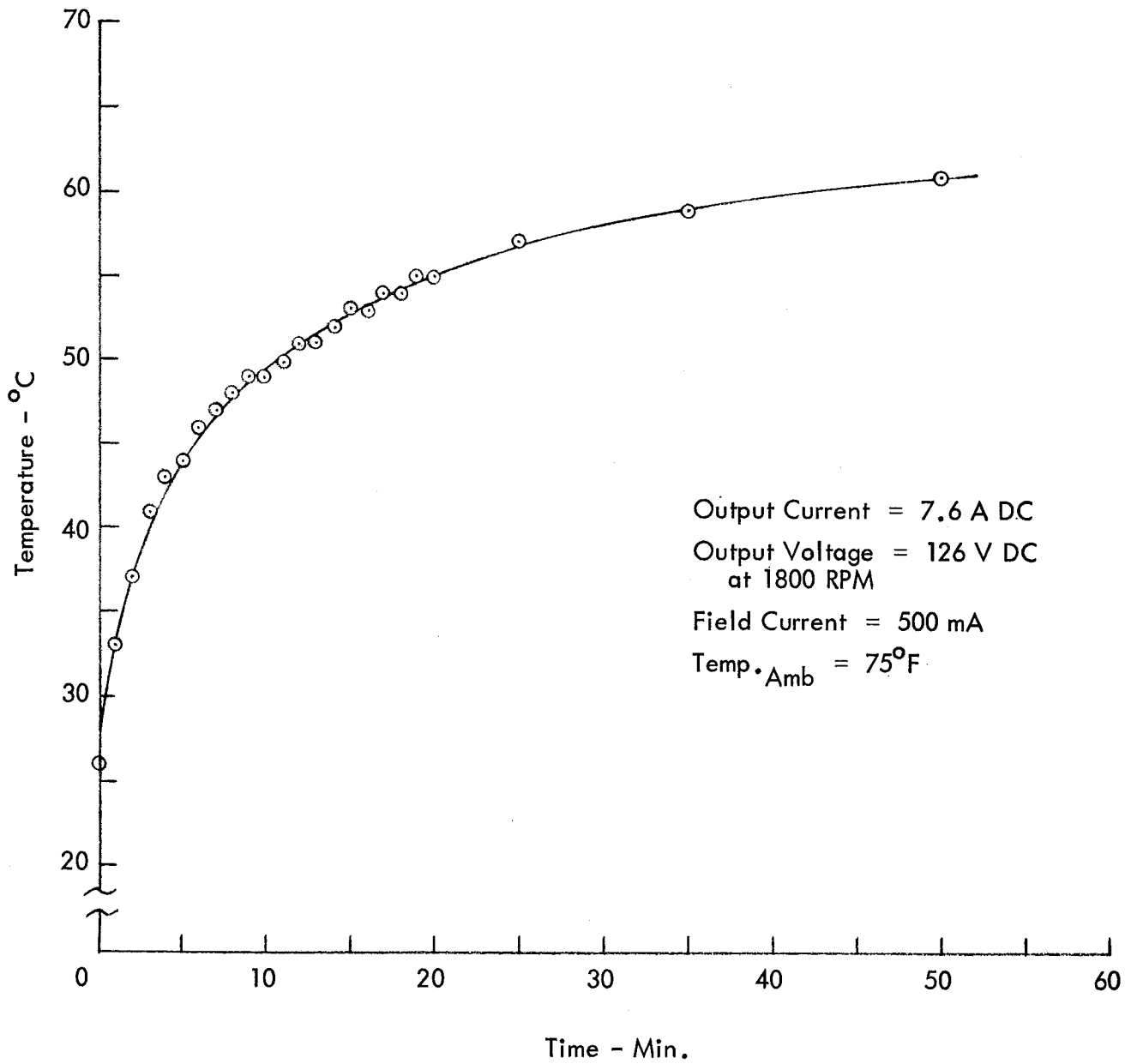


Figure 5-17. Temperature Rise in NPI Alternator.

## SECTION 6

### RELIABILITY

A principal requirement of the 1-kW machine design is that it be a high-reliability machine. High reliability is defined as having the capability to meet the following goals:

Reliability	The goal is to design for the utmost reliability. The mean time between failure (MTBF) shall be no less than ten (10) years.
Maintainability	The design goal shall be a maximum of one (1) scheduled maintenance day per year.
Durability	The machine shall be designed to operate continuously in extreme weather conditions.
System Life	The design goal is twenty-five (25) years minimum.

To meet these goals, a reliability program was established. The program consisted of the following elements:

- A failure mode effects analysis (FMEA) to identify critical components.
- Determination of areas requiring specific analysis or test.
- Estimation of failure rates for individual components.
- Justification of failure rates which had to be approximated.
- Quantitative prediction of overall system reliability.
- Establishment of a maintenance schedule.
- Establishment of test procedures to establish failure rates and to predict component life.

These seven elements are discussed in the following subsections.

## 6.1 FAILURE MODE EFFECTS ANALYSIS (FMEA)

A thorough understanding of the machine components and their interrelationships is required in order to perform a failure mode effects analysis. The principal components and subsystems of the Cycloturbine and its electrical system are shown in Figure 6-1. The figure shows the Cycloturbine rotor, transmission, alternator, and transient suppressor mounted on an Octahedron tower. The remainder of the electrical system is located in a protective control building on the ground and is connected to the tower by a transmission line.

The functional relationships among the Cycloturbine and electrical system components are shown in Figure 6-2. The numbers in each block correspond to the numbers shown in Figure 6-1. The functional blocks for the Cycloturbine components, that is, Blocks 1 through 9, are laid out in their relative physical positions. The dashed lines connecting Blocks 4 and 6, and Blocks 4 and 8 indicate that the components are physically connected but do not represent a continuous load path. Thus, the tilt-cam control system is mounted on the mainshaft via a bearing which allows the tilt-cam and mainshaft to rotate independently. Similarly, the mainshaft is mounted in a bearing cartridge which connects the Cycloturbine to the tower. The mainshaft rotates in the cartridge and transmits torque directly to the transmission as shown in Figure 6-1a.

Components designated by Blocks 1, 2, 3, 4, and 8 in Figure 6-2 constitute the Cycloturbine rotor whereas Blocks 5, 6, and 7 are the tilt-cam actuation control system. The function of each of these blocks as well as Blocks 9 through 14 are described in the following paragraphs:

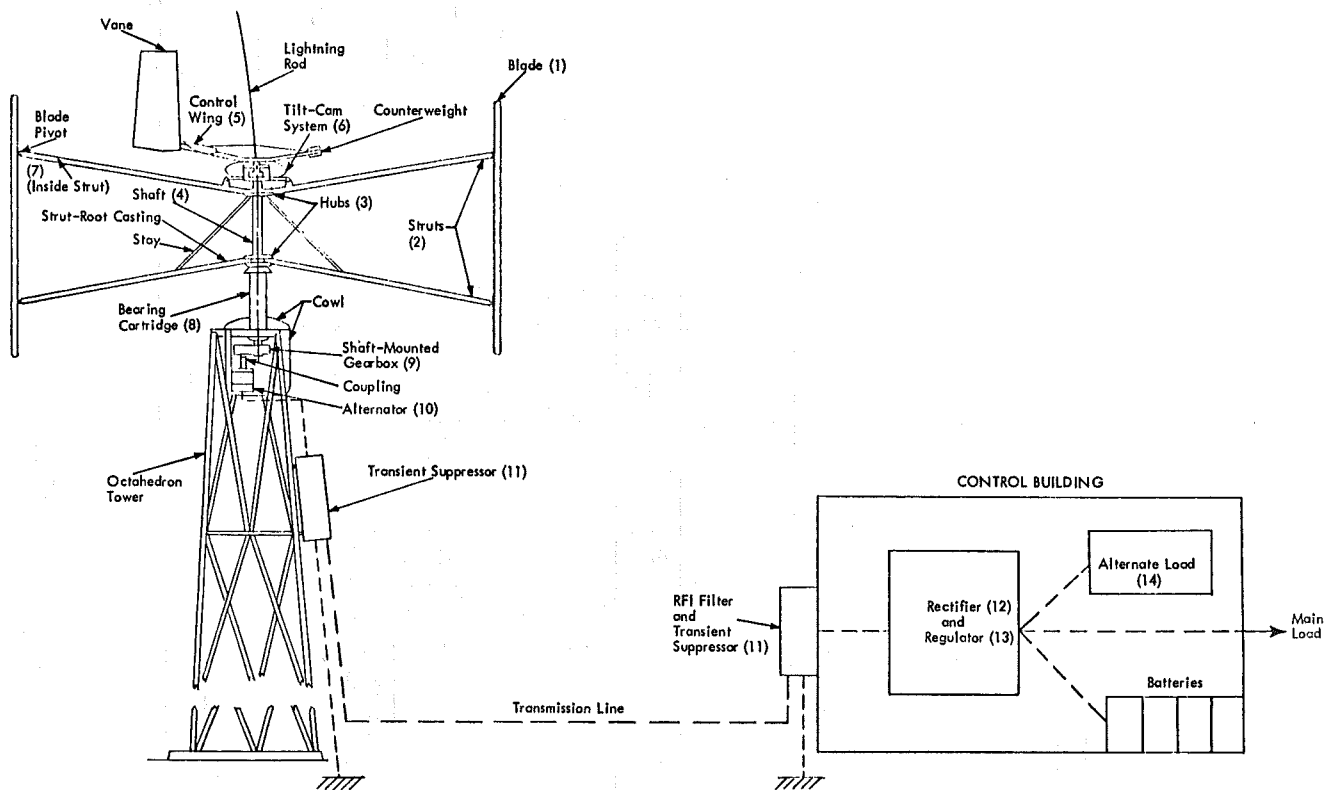


Figure 6-1. 1-kW High-Reliability SWECS Components.

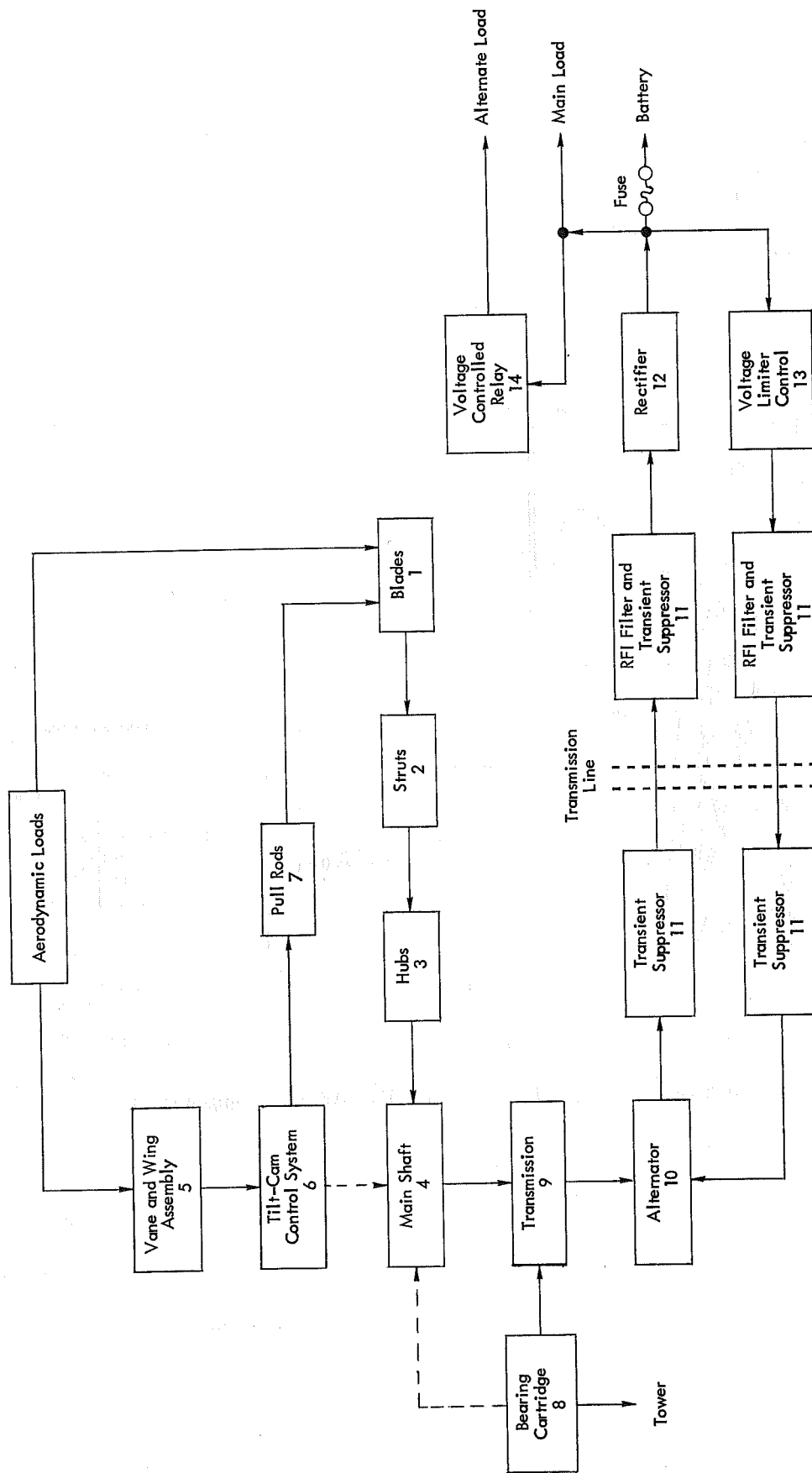


Figure 6-2. 1-kW High-Reliability SWECS Functional Flow Chart.

- Blades (Block 1)

The rotor has three blades set 120 degrees apart on a 7.5-ft radius. The blades are constructed of aluminum in the shape of an NACA 0015 airfoil. The blades extract energy from the wind in the form of aerodynamic loads which cause a torque on the rotor shaft. Each blade pivots about hinge pins that secure bell crank yokes on the blades to a set of struts (Block 2). The aerodynamic load is controlled by controlling the pitch angle of each blade. The pull-rods (Block 7) from the tilt-cam control system (Block 6) connect to the blades forward of the blade hinges. A swivel-type bearing is used in this joint.

- Struts (Block 2)

Each blade is mounted on two struts which are bolted to hubs (Block 3) on the main shaft (Block 4). The blade bell cranks fit between tangs at the outboard end of the struts. The blade hinge pin passes through a bearing in each tang. The struts are made from an aluminum extrusion with an NACA 0015 airfoil shape. The in-board end of each strut is welded to an aluminum casting which is bolted to the hub plates. A stay (shown in Figure 6-1a) passes from the upper hub to the lower strut to provide additional support to resist ice loads.

- Hubs (Block 3)

The hubs consist of two sets of flame-cut steel disks through which the main shaft (Block 4) passes. The lower disk of the upper set is welded to the main shaft as is the upper disk of the lower set. The strut root castings are fit between the hub plates and are bolted in place.

- Main Shaft (Block 4)

The main shaft is a 3-inch steel tube which is the central support for the struts and blades. The shaft turns in two flange-mounted ball bearings set in either end of the bearing cartridge (Block 8). The lower end of the shaft is affixed to the gear-box transmission (Block 9). The upper end of the shaft houses two cam steady bearings which support the tilt-cam control system (Block 6). The tilt-cam rotates independently of the main shaft.

- Bearing Cartridge (Block 8)

The steel bearing cartridge houses the two main bearings which support the main shaft. This cartridge is part of a welded triangular steel structure which bolts to the top of the tower.

- Vane and Wing Assembly (Block 5)

The vane and wing assembly provide orientation and shutdown control for the tilt-cam actuation control system. The purpose of the control

system is to provide a prescribed angle-of-attack schedule, that is, the angle between the blade chord and the relative wind, for each of the blades as they rotate through each cycle. The vane is attached to a boom (see Figure 6-1a) which, in turn, is rigidly attached to the tilt-cam. As the wind changes direction, the aerodynamic loads on the vane cause it to rotate, thereby, reorienting the tilt-cam. This action ensures that the blade angle schedule is oriented relative to the wind.

The wing is an aerodynamic surface mounted horizontally to the vane boom. It is designed to produce a download with increasing wind velocity. At a prescribed aerodynamic load, calibrated to a selected wind speed, the download on the wing offsets the balance weight located at the end of the boom (see Figure 6-1a). This causes the tilt-cam angle to increase which results in a reduction in the blade pitch angles. The effect is to decrease the aerodynamic forces on the blades which reduces the torque and causes the Cycloturbine to shut-down. The same effect will occur if the wing is heavily loaded with ice.

- Tilt-Cam Control System (Block 6)

The actuation control system consists of a tilt-cam and a series of mechanical linkages which activate pull rods (Block 7) which in turn rotate the blades about their hinge point. The control system, pull rods and blades are shown in Figure 6-3. Bearing locations are also identified. The tilt-cam which is shown in Figure 3-19 is mounted on the main shaft but rotates independently of the shaft through two cam steady bearings. The position of the cam is dependent on the orientation of the vane assembly (Block 5).

Since the linkages and pull rods for each blade are identical, as the tilt angle of the cam increases the moment arms attained by the linkages become different for each blade. The structure to which the links are attached to the tilt-cam is free to rotate with the main shaft relative to the tilt-cam. As the main shaft rotates, the tilt of the cam causes the blade position to change. Thus, the tilt-cam introduces an eccentricity into the system, hence, becoming a cam in terms of motion. The angular position of the blades is a function of the tilt-angle of the cam. In addition, if the attachment point of the linkage to the free rotating structure of the tilt-cam is different for each blade, then the pitch schedule can be modified from sinusoidal.

The tilt-angle is preselected by balancing the vane system and by proper selection of the tilt-cam hinge point. The angle is controlled by aerodynamic loads on the wing (Block 5).

- Pull Rods (Block 7)

The pull rods transmit control forces from the tilt-cam system (Block 6) to the blades (Block 1). The rods are located internally in the upper struts (Block 2) and pass through sliders which prevent the rods from striking the strut itself. The rods connect to the control links at one

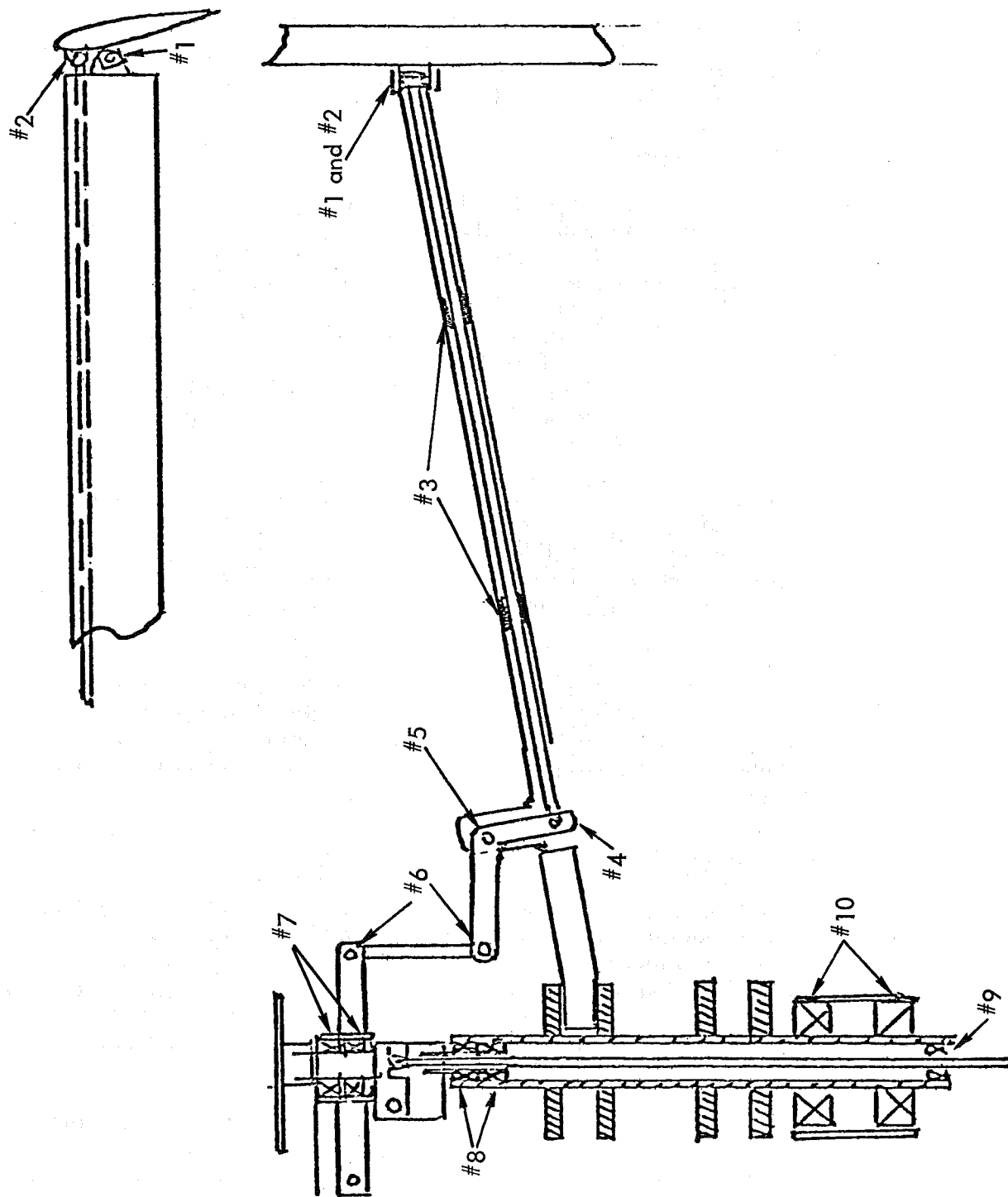


Figure 6-3. Cycloturbine Tilt-Cam Control System and Bearing Location.

end and to the blades forward of the blade hinge point (see Figure 6-3).

- Transmission (Block 9)

The transmission is a Morse gearbox with a 15:1 step-up ratio. The gearbox is mounted on the tower top structure and is driven directly by the main shaft. A coupling is attached to the gearbox output and connects it to the alternator (Block 10).

- Alternator (Block 10)

The mechanical torque produced by the Cycloturbine is converted to electrical power through an alternator. The alternator is mounted on the tower top and is driven by the transmission through a coupling. The alternator provides conversion efficiencies as high as 75 percent and weighs only 35 pounds. It has only one moving part, a low inertia flux-switching rotor which provides for generation of electrical energy without the use of slip rings, brushes or commutators. Both field and output windings are stationary. All coils are impregnated and the magnetic structure is conformal coated to enhance environmental resistance.

The magnetic design is optimized for lightweight, low inertia and high output at low speed, providing a cut-in point at about 900 rpm and full power at 1,800 RPM. The input power characteristic has been designed to allow the turbine shaft to increase in RPM with increasing wind speed to provide good matching of the respective torque characteristics.

The rotor, which incorporates the internal cooling fan, is supported at the input shaft end by a heavy-duty sealed roller bearing, and at the opposite end by a sealed ball bearing incorporating a grease reservoir. A synthetic grease will provide lubrication over the specified ambient temperature range.

- Transient Suppressor and RFI Filter (Block 11)

These assemblies are designed to protect the devices at the transmission line terminations from transient voltages and high frequency electromagnetic radiation. High frequency radiation is dissipated during normal operation by an inductor capacitor (LC). This L-type (shape) LC filter is designed to attenuate the radiation 3 db at 100 kHz, that is, an input signal at 100 kHz has its amplitude reduced by approximately 71 percent and its power cut in half.

The assembly protects the device on its inboard side by clamping the voltage to ground with a voltage variable resistor. If the transient is of the high current type, a series inductor limits the surge current into the protected device by means of an inductor. A gas filled spark gap is connected to the outboard side of the inductor. If the transient

disturbance contains sufficient energy, the  $L \frac{di}{dt}$  voltage across the inductor will cause the spark gap to fire. The energy will then be diverted to ground.

The failure rate of this assembly is dominated by the spark gap. The spark gap is capable of diverting 50 current pulses to 30,000 amperes. For a SWECS on a 40-ft tower, this translates to two strikes per year (global average) or an effective lifetime of 25 years. The spark gaps are removable in case periodic replacement is required due to more frequent lightning strikes.

- Rectifier (Block 12)

This assembly converts the three-phase AC power from the alternator to direct current. It also provides the power to excite the alternator field through a separate rectifier.

The main rectifier contains six silicon rectifier diodes arranged as a full wave bridge rectifier. This assembly is located in the control building to group it with the other semiconductors that need to be protected from low temperature extremes. This placement also affords better protection from transients. Three diodes are used in a half-wave bridge rectifier configuration to isolate the field from the battery. The return path for the field current is through the main rectifier.

- Voltage Limiter Control (Block 13)

This assembly is designed to regulate the output voltage of the alternator in the event that the main load or dump load associated with the voltage controlled relay (Block 14) cannot dissipate all the energy available. The limiter control circuit and the voltage controlled relay are redundant systems. The operation of either is sufficient to maintain the battery voltage within 24 to 28 volts.

The voltage limiter control operates as a switching regulator to control the average current to the alternator field coil. This circuit produces a constant pulse of field current with a variable repetition rate. This minimizes the power dissipated in the pass transistor and the power stress level thereby increasing the lifetime of the assembly.

- Voltage Controlled Relay (Block 14) (Optional)

The voltage controlled relay circuit is used to increase the load on the battery when the battery becomes fully charged. In order that the SWECS supply 100 percent of the energy required by the load, the SWECS must produce an excess of energy for most of its operation. The bulk of the excess energy will occur in the winter months when the efficiency of the battery can be enhanced by heating. The relay circuit also enhances the lifetime of the wind turbine by ensuring that the turbine will have a load when operating in high wind speeds.

This assembly incorporates a voltage sensitive switch with hysteresis to control a solenoid-type relay. It also incorporates a one-minute delay on turn-off. Due to the internal impedance of the battery, the terminal voltage is higher when it is being charged than when being discharged. Thus, hysteresis is required to prevent oscillation. The time delay is included to enhance the lifetime of the relay by reducing the number of cycles to which it is subjected.

This unit is set to operate just before the voltage limiter (Block 13). The failure rate of the assembly is dominated by the relay.

A Failure Mode and Effects Analysis (FMEA) was performed for the Cyclo-turbine and its electrical system based on the above described component functions and their interrelationships. The FMEA was used to determine critical failure modes and the resulting effects. All possible failures, both those actually experienced with previous equipment as well as those that could reasonably be expected to occur, were considered, and their cause and effect noted. The FMEA results are presented in Table 6-1.

## 6.2 CRITICAL COMPONENTS

The FMEA results presented in Table 6-1 were used to identify critical components. In the development of the FMEA, it is assumed that the structure of the Cyclo-turbine is adequately designed so that all beams, tubes, bolts, rivets, etc., are of sufficient size and strength to withstand design loads. In addition, it is assumed that structural welds done by a certified welder, will also withstand design loads. As a result, the rotor structure will meet the 25-year design lifetime and the probability of occurrence of failure of the structure is extremely small even when taking into account the given environmental factors. The unlimited fatigue life demonstrated by use of the Soderberg diagram (Figure 4-25) and the margins of safety given in Table 4-4 provide confidence in these assumptions.

The following critical components or subsystems have been identified as having higher failure rates than the remaining parts of the turbine and electrical system:

TABLE 6-1. 1-KW HIGH-RELIABILITY SWECS FAILURE MODES AND EFFECTS ANALYSIS.

Item No.	Component Description	Failure			Preventive Action	Corrective Action
		Mode	Cause	Effect		
1	<p><u>Blade System</u></p> <p>Three straight, constant cross-section blades provide the torque that powers the machine. The blades use NACA 0015 coordinates, on 11-1/2" chord and 8 ft length, giving an aspect ratio of 8.35.</p> <p>The blades are cyclically pitched by the pitch controlling system, which consists of an orientation vane, a stainless steel camshaft, and several pullrod and bellcrank assemblies.</p> <p>Centrifugal forces from the weight of the blades in motion, working in conjunction with the cam-controlled tracking system, aerodynamically feather the machine at high wind velocities.</p>	<ol style="list-style-type: none"> <li>1) Blade not pitching.</li> <li>2) Blade flapping uncontrolled.</li> <li>3) Blade pitch altered.</li> <li>4) Blade thrown.</li> <li>5) Blades and pivots loos.</li> </ol>	<p>Bent pullrod.</p> <p>Broken pullrod.</p> <p>Bent pullrod.</p> <p>Broken strut or strut tang.</p> <p>Severe rotor rime ice build-up.</p>	<p>Some power loss.</p> <p>Power loss and detrimental dynamic effects.</p> <p>Some power loss.</p> <p>Total power loss.</p> <p>Turbine shut down.</p>	<p>Use adequate pullrod material and correct bearing placement.</p> <p>Unlikely failure, due to newly specified hardware.</p> <p>Proper bearing placement.</p> <p>Unlikely failure, due to high factor of safety in design.</p> <p>Extremely severe icing will require manual de-icing, heating elements, or chemical blade coatings.</p>	<p>Restraighten/replace pullrod.</p> <p>Replace pullrod.</p> <p>Restraighten/replace pullrod.</p> <p>Repair damage and replace parts where necessary.</p> <p>De-ice machine where necessary.</p>
1A	<p><u>Hinge Bearing Assembly</u></p> <p>The NMB stainless steel 3/8" spherical bearing, which is TFE lined, is pressed into a hole in the outboard tang casting. The casting is welded into the rear cavity of the 6" NACA 0015 strut extrusion.</p>	<ol style="list-style-type: none"> <li>1) Hinge bearing seized or sticking.</li> </ol>	<p>Contamination by dirt, salt, etc.</p>	<p>Some power loss due to friction.</p>	<p>Use of a protective silicone rubber convoluted boot to protect bearing assembly.</p>	<p>Replace bearing and/or boot where necessary.</p>

FAILURE MODES AND EFFECTS ANALYSIS (Continued)

Item No.	Component Description	Failure			Preventive Action	Corrective Action
		Mode	Cause	Effect		
1B	<p><u>Bellcrank Assembly</u></p> <p>The bellcranks consist of rectangular sections of aluminum welded to the leading edge extrusion of the blade. A 5/16" NMB all-stainless TFE-lined rod and is used on the top bellcrank to pitch the blade.</p>	<p>1) No pitching.</p>	<p>Broken rod end.</p>	<p>Machine power loss.</p>	<p>A highly unlikely failure. The NMB rod ends now in use on the outboard locations are among the strongest and most reliable pieces available.</p>	<p>Replace rod end if necessary.</p>
1C	<p><u>Blade Construction</u></p> <p>The machine blades consist of a 3-1/2" leading edge extrusion of 6061-T6 alloy which is designed with a leading edge fillet ballast to achieve an airfoil center of gravity at 25% chord; a brake-formed trailing edge and internal "C" spar make up the rear portion of the airfoil. These two pieces are riveted to a 1" x 0.055" step on the rear of the extrusion with stainless steel pop rivets.</p>	<p>2) Ineffective pitching.</p>	<p>Worn rod end.</p>	<p>Machine power loss.</p>	<p>Unlikely failure. Number of rivets used give high safety factor.</p>	<p>Replace trailing edge.</p>
2	<p><u>Struts</u></p> <p>The strut assemblies consist of a 6" 0015 aluminum extrusion in a 6061-T6 alloy. The inboard strut casting is welded to the strut and bolts to the mainshaft hub plates. The outboard casting is welded into the rear cavity of the extrusion and acts as a support for the NMB blade pivot bearing. The six struts are bolted to the inner mainshaft hub plates with 1/2" UNF bolts using elastic locking nuts.</p>	<p>1) Trailing edge breaking away from the extrusion.</p> <p>2) Blade aerodynamics altered.</p>	<p>Rivet failure.</p> <p>Severe icing.</p>	<p>Machine power loss.</p> <p>Performance loss.</p>	<p>Normal blade flexing will help eliminate icing.</p>	<p>Possible low-friction coating on blades would reduce ice build-up.</p>
		<p>1) Loss of strut.</p> <p>2) Aerodynamic lead-lag.</p>	<p>Broken strut or casting.</p> <p>Misaligned holes inboard casting or hub plates.</p>	<p>Total power loss.</p> <p>Performance loss.</p>	<p>Assure casting quality control.</p> <p>Assure quality control in drilling mounting holes.</p>	<p>Replace broken pieces.</p> <p>Use acceptable castings.</p>

FAILURE MODES AND EFFECTS ANALYSIS (Continued)

Item No.	Component Description	Failure			Preventive Action	Corrective Action
		Mode	Cause	Effect		
3	<p><u>Hub Plates</u> The hub plates are 1" flame-cut sections, machined internally to fit the mainshaft tube, and finish-machined externally for appearance.</p>	1) Aerodynamic lag.	Incorrect hole alignment.	Performance loss.	Quality control in boring holes in hub plates.	Correct alignment.
4	<p><u>Mainshaft Tube</u> The tube used is 3" OD, 1/4" wall DOM tubing; it is centerless ground to 2-15/16" where it passes thru the "Seal Master" heavy duty bearings, and the tubing is turned to 2-7/8" between bearings.</p>	1) Seized bearings.	Inadequate lubrication.	Performance loss.	Regular greasing and maintenance.	Bearing replacement.
5	<p><u>Vane and Wing Assembly</u> The vane and wing are constructed of mild aluminum sheet formed to a slightly cambered airfoil, which are attached to a rectangular aluminum tubular boom. The boom attaches to the tilt-cam by means of a metal plate and tubing assembly.</p>	<p>1) Vane turning with machine rotation.</p> <p>2) Vane vibration.</p> <p>3) Vane turning on camshaft.</p>	<p>Poor bearing lubrication.</p> <p>Loose stabilizing cable.</p> <p>Loss of vane plate set screw.</p>	<p>Machine performance loss.</p> <p>Machine performance loss; bad vibrational affects.</p> <p>Machine performance loss.</p>	<p>Proper bearing lubrication and maintenance.</p> <p>Install cable with locking clamps to prevent accidental loosening.</p> <p>Use of correct size locking screws with proper locking compound.</p>	<p>Replace/regrease bearings where necessary.</p> <p>Re-tighten cable and install clamps where necessary.</p>

FAILURE MODES AND EFFECTS ANALYSIS (Continued)

Item No.	Component Description	Failure			Preventive Action	Corrective Action
		Mode	Cause	Effect		
6	<p><u>Tilt-Cam Actuation Control System</u></p> <p><u>Camshaft</u></p> <p>The camshaft consists of two lengths of 1" stainless shafting pressed into a mild steel cam block. The top length is standard 316 stainless, while the bottom length is 440 C stainless, case hardened to 50-54 Rc, and polished to 20-24 RMS.</p>	<p>1) Roller bearing failure.</p> <p>2) Machine speed regulation inoperable.</p>	<p>Poor bearing lubrication.</p> <p>Ice build-up under cam block.</p>	<p>Machine performance loss.</p> <p>Possible overspeed damage.</p>	<p>Proper bearing lubrication and maintenance.</p> <p>Use silicone rubber con-voluted boot to protect bottom shaft on cam to prevent ice build-up.</p>	<p>Replace/regrease bearing where necessary.</p> <p>Supply cam boot on turbine.</p>
6A		<p><u>Camshaft Plate</u></p> <p>The plate consists of a triangular plate with 3 rod end tabs welded onto the plate 120° apart. The plate rotates about the cam section by means of a small roller bearing.</p>	<p>1) Bearing failure.</p>	<p>Lack of proper lubrication.</p>	<p>Machine power loss.</p>	<p>A protective boot to seal the entire cam and bearing assemblies would help in protecting the system.</p>
6C	<p><u>Link Rod Tubes</u></p> <p>The tubes are of 304 stainless steel tubing with a .4375" O.D., .27" I.D., 5/16" Alinabal nylon race rod ends are used on each end of the link, which attaches to the pull rod swivel point, and the cam plate clevis attachment point. The link rod serves as a device to transfer cam motion to the pull rod.</p>	<p>1) Buckling.</p>	<p>a) High compressive loading.</p> <p>b) Radical cam movement.</p>	<p>Performance loss.</p> <p>Performance loss.</p>	<p>The prototype tilt-cam assembly is being designed to employ the link rods in tension, to avoid compressive buckling.</p> <p>The tilt-cam geometry is also being designed to act smooth in operation, but not to be extremely sensitive.</p>	<p>Replace link rods.</p>

FAILURE MODES AND EFFECTS ANALYSIS (Continued)

Item No.	Component Description	Failure			Preventive Action	Corrective Action
		Mode	Cause	Effect		
6D	<p><u>Link Rod/Pull Rod Swivel Point</u> The swivel consists of two sections of aluminum channel which are welded to the 0015 strut in such a position so as to act as a swivel point for the link and pull rods. A small welded swing arm transfers vertical motion into horizontal. Stainless hardware is employed.</p>	1) Stricking swivel.	<p>a) Frozen bearings. b) Icing build-up.</p>	Performance loss.	Assure quality control in bearing assembly.	Correct tight bearing condition. Possible boot application for ice build-up prevention.
7	<p><u>Pull Rod Tube</u> These tubes are of the same construction as the link rods, and use rod ends in each receiving end, the inner rod end being an Alinabal 5/16" piece, and the outer rod end an all stainless NMB 5/16" TFE lined rod end. The tubes are supported by three TFE Duralon bearings, and fit inside the front chamber of the 0015 strut extrusion. A clevis acts as a link on the outboard pull rod end.</p>	<p>1) Pull rod buckling.  2) Clevis failure. 3) Worn bearing.</p>	<p>Insufficient number of bearing supports.  Extreme loading. Rough pull rod surface.</p>	<p>Performance loss.  Performance loss; machine shutdown. Noisy operation.</p>	<p>The bearing supports are being designed so as to prevent buckling. The TFE Duralon bearings are of extremely low friction wear resistant construction. The pull rods are constantly in tension due to centrifugal forces, so compressive loading is non-existent.  Polish pull rods.</p>	<p>Restraighten/replace pull rod.</p>

FAILURE MODES AND EFFECTS ANALYSIS (Continued).

Item No.	Component Description	Failure			Preventive Action	Corrective Action
		Mode	Cause	Effect		
8	<p><u>Transmission/Cartridge</u></p> <p>The cartridge tubing is 6-3/4" O.D., 1/4" wall DOM stock with triangular gusset plates welded to a triangular frame, which has tabs positioned to accept the tower legs.</p> <p>The transmission is a speed-increaser with an NPI alternator mounted directly below the vertical main-shaft. A machined bushing which fits inside the main-shaft, joins the Morse double-reduction 15 to 1 speed-increaser, which uses a special synthetic low-temperature lubricant. The NPI generator is mated to the speed-increaser output shaft by means of a Gerbing G-500 industrial coupling, which uses a urethane plastic spider insert.</p>	<ol style="list-style-type: none"> <li>1) Gearbox failure.</li> <li>2) Bushing failure.</li> <li>3) Coupling failure.</li> </ol>	<p>Loss of oil due to faulty oil seals.</p> <p>Sheared set screws or Woodruff key.</p> <p>Sheared set screws or Woodruff key.</p>	<p>Performance loss.</p> <p>Performance loss.</p> <p>Performance loss.</p>	<p>Special low temperature heavy duty seals.</p> <p>Specify correct number and size of set screws and/or Woodruff key.</p> <p>Specify correct number and size of set screws and/or Woodruff key.</p>	<p>Replace seals.</p> <p>Repair set screws and keys.</p> <p>Repair set screws and keys.</p>
9	<p><u>Transmission</u></p> <p>The high-reliability transmission consists of an adapter bushing, a Morse 15 to 1 double reduction speed increaser, a Gerbing industrial coupling, and an NPI alternator. The main shaft attaches to the speed increaser by means of a machined bushing. The speed increaser is lined to the alternator by means of a Gerbing G-500 coupling, which uses an internal resilient urethane spider.</p>	<ol style="list-style-type: none"> <li>1) Transfer bushing not turning.</li> <li>2) Gearbox failure.</li> <li>3) Coupling failure.</li> </ol>	<p>Sheared set screws.</p> <p>Loss of lubricant</p> <p>Internal spider failure.</p>	<p>Loss of power transmission.</p> <p>Loss of power transmission.</p> <p>Slight power loss.</p>	<p>Specification of stronger set screws and/or Woodruff keys.</p> <p>Specification of heavy duty low-temperature oil seals.</p> <p>Unlikely failure due to high factor of safety.</p>	<p>Repair/replace shaft and/or set screws.</p> <p>Replacement of seals and/or gear box.</p> <p>Replace spider.</p>

FAILURE MODES AND EFFECTS ANALYSIS (Continued)

Item No.	Component Description	Failure			Preventive Action	Corrective Action
		Mode	Cause	Effect		
10	<p><u>Alternator</u>                      Alternator (A1A1); 1.3 kW switched flux self-excited, with stationary field and armature windings and rotating flux-switching magnetic structure. Field coil is single solenoid, layer wound on nylon bobbin. Rotor is press-fit assembly of steel insert pressed into aluminum casting which is cast on magnetic structure. Shaft is pressed into steel insert.                      Alternator shaft is driven by cog Woodruff-keyed to shaft, and secured with pinned castellated nut. Armature windings are layer-wound on nylon bobbins which are locked to the magnetic structure by FRP keeper strips.</p>	<ol style="list-style-type: none"> <li>1) Shaft won't turn.</li> <li>2) Shaft wobble.</li> <li>3) Bearing drag.</li> <li>4) Reduced output.</li> <li>5) No output.</li> </ol>	<p>Frozen bearing.                      Broken bearing, ball or roller, bent shaft.                      Broken bearing, ball or roller.</p> <p>a) Open or shorted armature winding.                      b) Partially shorted field winding.                      a) Open or fully shorted field winding.</p>	<p>Total loss of output.                      Progressive deterioration of bearing to ultimate failure, allowing rotor to strike or jam against stator.                      Reduction in system efficiency and output capability. See shaft wobble.                      Reduced output power capability. Reduced system utility.                      Total loss of system utility.</p>	<p>Scheduled periodic lubrication. Inspection at scheduled maintenance.                      See above.                      See above.                      See above.                      High potential insulation; measure inductance during scheduled maintenance.                      See above.</p>	<p>Increase size of bearings or change bearing type.                      See above.                      See above.                      Investigating other insulating materials for insulated wire. Improving winding techniques.                      See above.</p>

FAILURE MODES AND EFFECTS ANALYSIS (Continued)

Item No.	Component Description	Failure			Preventive Action	Corrective Action
		Mode	Cause	Effect		
11	<p><u>Lightning Protection</u></p> <p>Transient suppressors/RFI filters, A1A2 and A2A1, provided direct data to ground for dissipation of energy of lightning strokes and also prevent radiation of EMI generated within control cabinet.</p>	<p>1) Failure to adequately divert lightning strike energy.</p> <p>2) Loss of continuity or shorted ground.</p> <p>3) Loss of RFI filtering.</p>	<p>Deteriorated spark gap.</p> <p>Open induction or shorted varistor or capacitor. Possibly due to lightning strike.</p> <p>Open bypass capacitor or shorted inductor might be caused by lightning strike.</p>	<p>Damage to alternator and/or control circuits on lightning stroke making system inoperative or deteriorating performance.</p> <p>Reduction of system capability.</p> <p>Possible interference with communication.</p>	<p>Measure spark gap breakdown with hi-pot, at scheduled maintenance intervals; replacing if deteriorated.</p> <p>Periodic inspections.</p> <p>Inspection and test at scheduled maintenance intervals.</p>	<p>Change to heavier spark gaps and/or add more gaps.</p> <p>Increase safety factor.</p> <p>Analyze fault and increase safety factor.</p>

FAILURE MODES AND EFFECTS ANALYSIS (Concluded)

Item No.	Component Description	Failure			Preventive Action	Corrective Action
		Mode	Cause	Effect		
12	<p><u>Rectifier</u> Rectifier Assembly, A2A3, rectifies alternator AC output to produce DC output power, and also DC excitation for alternator field.</p>	<ol style="list-style-type: none"> <li>1) Low output (loss of one phase).</li> <li>2) No output (loss of two phases).</li> </ol>	<p>Shorted or open rectifier.</p> <p>Multiple rectifier failure.</p>	<p>Reduced output capability, possible battery deterioration.</p> <p>Total loss of output.</p>	<p>Inspection and test at scheduled maintenance intervals.</p> <p>Same as above.</p>	<p>Analyze fault and increase safety factor.</p> <p>Same as above.</p>
13	<p><u>Voltage Limiter Control</u> Voltage limiter control, A2A4, serves to reduce alternator output current at pre-set voltage to prevent battery over-charge or excessive no-load alternator output voltage.</p>	<ol style="list-style-type: none"> <li>1) No output.</li> <li>2) Change in voltage setting.</li> <li>3) Output fully ON.</li> </ol>	<p>Failure of A2A4 in open output mode.</p> <p>Component deterioration.</p> <p>Component deterioration or failure.</p>	<p>Total loss of output.</p> <p>Reduction or loss of output.</p> <p>Possible over-charge of battery.</p>	<p>Test operation during scheduled maintenance.</p> <p>Exercise and test during scheduled maintenance.</p> <p>Test during scheduled maintenance.</p>	<p>Analyze fault and increase safety factor.</p> <p>Same as above.</p> <p>Same as above.</p>
14	<p><u>Voltage Controlled Relay</u> Voltage controlled relay, A2A2, diverts alternator output to alternate load to prevent battery over-charge if battery voltage rises to charge limit.</p>	<ol style="list-style-type: none"> <li>1) Inoperative, fully OFF.</li> <li>2) Change in setting or fully ON.</li> </ol>	<p>Component failure.</p> <p>Component change or failure.</p>	<p>Loss of potential energy. Possible battery over-charge.</p> <p>Reduced battery charge.</p>	<p>Exercise and test during scheduled maintenance.</p> <p>Same as above.</p>	<p>Analyze fault and increase safety factor.</p> <p>Same as above.</p>

- Cycloturbine Bearings.
- Cycloturbine Bearing Surfaces.
- Spark Gaps in Lightning Protection System.
- Relay in Dynamic Loading Switch.
- Dump Load Circuit.
- Alternator Bearings.

These components are the principal contributors to the system failure rates.

### 6.3 COMPONENT FAILURE RATES AND RELIABILITY

Failure rate data are required in order to calculate the mean time between failure (MTBF) for the 1-kW wind machine. These data are readily available for electronic components and were also available for the alternator. However, valid statistical samples of failure data on system, subsystem, or component level do not exist for the Cycloturbine. Therefore, preliminary failure rate and MTBF estimates were derived for the bearings using manufacturer's bearing life data. These estimates are discussed in the next subsection.

#### 6.3.1 CYCLOTURBINE FAILURE RATE ESTIMATES

The Cycloturbine bearings are identified in Figure 6-3 and are key numbered from 1 to 10. Of these bearings, nine are identified as critical components in the FMEA; only Bearing 9 is noncritical.

It was assumed that the failure of a critical bearing is a random event so that the probability of failure at a given time, that is, the probability density function,  $f(t)$ , can be expressed as being exponential in time. Classically, this condition is achieved when the hazard rate,  $h(t)$ , is constant, that is,

$$h(t) = \lambda \quad (6-1)$$

where the constant,  $\lambda$ , is called the failure rate.

The reliability,  $R(t)$ , which is the probability of nonfailure in a specified time period,  $t$ , is written

$$R(t) = e^{-\lambda t} \quad (6-2)$$

Thus, the reliability of the component is a function of the component failure rate,  $\lambda$ , and the time period,  $t$ , under consideration, in this case 364 days or 8,736 hours (annual operating period less one maintenance day). For the exponential failure distribution, the MTBF (mean time before failure) becomes,

$$MTBF = 1/\lambda \quad (6-3)$$

Thus, the failure rate and the reliability of a component can be determined from Equations (6-2) and (6-3) using life data for the component. The MTBF for each bearing is obtained from the manufacturer. Most of the bearings used in the Cycloturbine are designed and tested to a minimum wear specification. For example, the rod-end and spherical bearings all meet a military requirement of .006 inches of wear after 25,000 cycles at maximum load. Test data for catastrophic failure of bearings were generally unavailable. Thus, the reliability analysis of the Cycloturbine was based on data which reflect a minimum wear condition of the bearings. The MTBF for each component is then adjusted to account for actual-to-rated load and speed. In order to develop these ratios, it is necessary to determine the load capacities of the bearings and the loads to which they are subjected. Table 6-2 lists the bearings keyed to Figure 6-3, their load

Table 6-2. Critical Bearings List.

Key No.	Item	Nominal Load* (lbs)	Maximum Load** (lbs)	Type of Load	Bearing Choice	Manufacturers Recommended Maximum Load (MRML)	Number/Turbine
1	Blade Hinge Bearing	130	500	Radial; Oscillating to 20° Max.; Moderate Shock	0.375" Bore; NMB Spherical Ball; TFE Lined	6,400 lbs	6 (2 per Blade)
2	Bellcrank Bearing	75	200	Radial; Oscillating to 20° Max.; Moderate Shock	0.3125" Bore; NMB Rodend; TFE Lined	2,770 lbs	3 (1 per Blade)
3	Pull Rod Slider or Guide Bearing	20	50	Linear Motion; 5/16" Amplitude	0.4375" Bore; Duralon Journal Bearing; TFE Lined	11,780 lbs	3 (1 per Blade)
4	Pull Rod/Swivel Connector Bearing	60	233	Radial; Oscillating to 20° Max.; Moderate Shock	0.3125" Bore; NMB Rodend; TFE Lined	2,770 lbs	3 (1 per Blade)
5	Link Rod/Swivel Connector Bearing	60	233	Radial; Oscillating to 20° Max.; Moderate Shock	0.3125" Bore; NMB Journal Bearing; TFE Lined	11,780 lbs	3 (1 per Blade)
6	Swivel Bearing	60	233	Radial; Oscillating to 20° Max.; Moderate Shock	0.3125" Bore; NMB Rodend; TFE Lined	2,770 lbs	6 (2 per Blade)
7	Cam Bearings	100	200	Radial and Axial (Equal); Full Rotation; Moderate Shock	1" Bore Timken; Double Taper	1,710 lbs Radial 590 lbs Thrust	2
8	Cam Steady Bearings	100	200	Radial and Axial (Equal); Full Rotation; Moderate Shock	1" Bore Timken; Double Taper	1,710 lbs Radial 590 lbs Thrust	2
9	Actuator Rod Guide Bearing	5	30	Radial and Rotary; No Shock	Delrin Bushing	Not Important	1
10	Main Bearings	250 500	750 500	Radial; Full Rotation Axial; Full Rotation	Sealmaster SFC; Standard Duty; 2-15/16" Bore	6,100 lbs	2

\*Nominal Loading - It is assumed in arriving at these figures that the wind turbine operates in an environment which has an average wind speed of 15 mph and a rotor speed of 100 rpm. Assume that this is the continuous loading.

\*\*Maximum Loading - Here it is assumed that the maximum rotor speed is 200 rpm, wind speed 30 mph and the control system will not allow higher rotor loading.

Note: Both nominal and maximum loading are assumed to be dynamic in nature.

Since during annual maintenance some of the bearings can be replaced, it is useful to know the number of cycles the bearing is expected to undergo within a year.

Nominal @ 100 rpm constant: 52,560,000 cycles/year

Maximum @ 200 rpm constant: 105,120,000 cycles/year

magnitude and type, and manufacturer's specifications. Bearings 7, 8, and 10 are subjected to combined radial-axial loading. A resultant load was determined as follows (see Reference 20):

Bearings 7 and 8 (Timken)

$$P = .66 P_r + k P_a \quad (6-4)$$

where

$$P_r = \text{radial load}$$

$$P_a = \text{axial load}$$

$$k = 1.45 \text{ for bearings used}$$

Therefore, using values from Table 6-2 in Equation (6-4), yields

$$P_{\text{Rated}} = 1984 \text{ lbs}$$

$$P_{\text{Max}} = 422 \text{ lbs}$$

$$P_{\text{Nom}} = 211 \text{ lbs}$$

Bearing 10 (SKF)

$$P = P_r + y P_a \quad (6-5)$$

where

$$y = 1.5$$

Then, using values from Table 6-2 in Equation (6-5), yields

$$P_{\text{Rated}} = 6100 \text{ lbs}$$

$$P_{\text{Max}} = 1500 \text{ lbs}$$

$$P_{\text{Nom}} = 1000 \text{ lbs}$$

The actual MTBF or life of each bearing was determined as follows using the data provided in Table 6-2:

$$(\text{Life})_{\text{Actual}} = (\text{Life})_{\text{Rated}} (\text{Service Factor}) \quad (6-6)$$

where  $(\text{Life})_{\text{Rated}}$  is the manufacturer's estimated MTBF for wear failure under recommended load and speed conditions given as maximum continuous loading at a specified speed and shock condition.

Analysis of the reliability was conducted using three stages of increasing complexity and realism. Initially, a highly conservative approach was used with the life varying linearly with the inverse of the load. It was assumed that the machine was subjected to maximum loads at a maximum running speed of 200 RPM continuously for one year. In this case, the service factor was defined as:

$$\begin{aligned} \text{Service Factor} &= (\text{Speed Factor}) (\text{Load Factor}) \\ &= F_S F_L \end{aligned} \quad (6-7)$$

where

$$F_L = \frac{1}{2} F_L^I F_L^{II}$$

$$F_L^I = \frac{\text{Manufacturer's Recommended Maximum Load}}{\text{Actual Maximum Load}}$$

$$F_L^{II} = \frac{\text{Actual Level of Shock}}{\text{Design Level of Shock}}$$

and  $F_S$  is a function of actual RPM and load rating RPM. Whereas  $F_L^I$  is based on Table 6-2,  $F_S$  is given by the following schedule:

<u>F<sub>s</sub></u>	<u>Actual RPM</u>	<u>Load</u>
3.22	15	Average Oscillatory
2.75	25	
2.16	50	
1.71	100	Nominal
1.44	150	
1.36	200	Maximum
1.18	250	

This approach provided a worst-case reliability based on extreme running conditions. Therefore, more reasonable running conditions using nominal loads at a continuous operational speed of 100 RPM were used to reevaluate the bearing reliability. In addition, the service factor was modified to be consistent with a widely applied bearing equation. The resultant life equation was (see, e.g., Reference 20)

$$(\text{Life})_{\text{Actual}} = \left( \frac{\text{Load}_{\text{Rated}}}{\text{Load}_{\text{Actual}}} \right)^{\frac{10}{3}} \left( \frac{\omega_{\text{Rated}}}{\omega_{\text{Actual}}} \right) (\text{Life})_{\text{Rated}} \quad (6-8)$$

where  $\omega$  is the rotational speed of the bearing.

Results obtained with Equation (6-8) were overly optimistic. This was not unexpected since this is a general equation applied to ball or roller bearings to achieve an average result (e.g., References 21 to 23). Depending on the type of bearing, the exponent on the load factor has a value between 3 and 4.

It is important to note, however, that Bearings 1 through 6 of the Cyclo-turbine (see Table 6-2) are not of the ball bearing type, but are nonlubricated Teflon

lined spherical balls, rod ends or sleeves. Thus, it was necessary to determine the life equations applicable to each type of bearing. The following equations based on manufacturer life data were used:

Bearings 1,2,4, and 6

$$(\text{Life})_{\text{Actual}} = \left( \frac{\text{Load}_{\text{Rated}}}{\text{Load}_{\text{Actual}}} \right)^2 \left( \frac{\gamma_{\text{Rated}}}{\gamma_{\text{Actual}}} \right) (\text{Life})_{\text{Rated}} \quad (6-9)$$

where  $\gamma$  is the total angle of oscillation.

Bearings 3 and 5

$$(\text{Life})_{\text{Actual}} = \left( \frac{\text{Load}_{\text{Rated}}}{\text{Load}_{\text{Actual}}} \right)^{1.8} \left[ \frac{(\gamma\omega)_{\text{Rated}}}{(\gamma\omega)_{\text{Actual}}} \right] (\text{Life})_{\text{Rated}} \quad (6-10)$$

where  $\gamma$  is the total angle of oscillation and  $\omega$  is rotational speed.

Bearings 7, 8 and 10

$$(\text{Life})_{\text{Actual}} = \left( \frac{\text{Load}_{\text{Rated}}}{\text{Load}_{\text{Actual}}} \right)^3 \left( \frac{\omega_{\text{Rated}}}{\omega_{\text{Actual}}} \right) (\text{Life})_{\text{Rated}} \quad (6-11)$$

where  $\omega$  = rotational speed.

The actual life was calculated based on the rated life and the resultant MTBF was used in Equation (6-3) to calculate the failure rate,  $\lambda$ . The reliability between scheduled maintenance, that is,  $R(t) = R(8736)$  was determined from Equation (6-2). The MTBF in years,  $\lambda$  in terms of failures per million hours, and  $R(8736)$  are given in Table 6-3 for the Cycloturbine bearings for the three approaches described previously. The Conservative results were obtained using Equations (6-6)

Table 6-3. Bearing MTBF and Reliability.

Key No.	Item	Comment	Conservative		General		Detailed			
			MTBF (Yrs.)	$\lambda \times 10^6$	MTBF (Yrs.)	$\lambda \times 10^6$	MTBF (Yrs.)	$\lambda \times 10^6$	R (8736)	R (8736)
1	Blade Hinge Bearing	Spherical Bearing (Stainless)	9.62	11.90	205	.559	28.80	3.97	.96591	.96591
2	Bellcrank Bearing	One/Blade Teflon Rod End Bearing	10.30	11.11	79	1.45	27.01	4.24	.96366	.96366
3	Pull Rod Slider or Guide Bearing	Moved to Half Radius	17.63	6.49	$4.6 \times 10^6$	$.25 \times 10^{-4}$	2860.	.004	.99997	.99997
4	Pull Rod/Swivel Connector Bearing	Rod End; Nylon Lined	7.10	16.13	166	.689	42.21	2.71	.97659	.97659
5	Link Rod/Swivel Connector Bearing	Rod End; Nylon Lined	12.82	8.93	2481	.046	49.00	2.34	.97977	.97977
6	Swivel Bearing	Rod End; Nylon Lined	6.64	17.24	166	.689	42.21	2.71	.97659	.97659
7	Cam Bearing	Two Cam Bearings	8.01	14.29	2492	.046	1190.	.096	.99916	.99916
8	Cam Steady Bearings	Ball Bearings	6.64	17.24	2492	.046	1190.	.096	.99916	.99916
9	Actuator Rod Guide Bearing	Not Required	-	-	-	-	-	-	-	-
10	Main Bearings	Not Required	7.78	14.71	590	.194	325.	.352	.99861	.99861

and (6-7), based on the extreme running conditions. The General results were obtained using Equation (6-8) and the Detailed results were calculated with Equations (6-9), (6-10), and (6-11). The General and Detailed results were based on nominal loads (see Table 6-2) at a continuous operational speed of 100 RPM. The Detailed results were used in evaluating the total Cycloturbine reliability since they were based on the best available equations for each type of bearing applied at a reasonable operational condition.

### 6.3.2 ELECTRICAL SYSTEM FAILURE RATES

The sections of the electrical system described in the FMEA (Table 6-1) are circuits or subassemblies of the electrical system composed of many electronic parts. A detailed part stress analysis was performed for each of these parts using the techniques described in Reference 8. For this analysis, the alternator was assumed to be in a ground mobile environment as it was subject to vibration. All other components were assumed to be in the ground fixed environment. Parts with the highest established reliability rating (i.e., JAN TX) were used wherever available. Details of the parts stress analysis are not included herein. However, the parts stress analysis techniques in Reference 8 include those for:

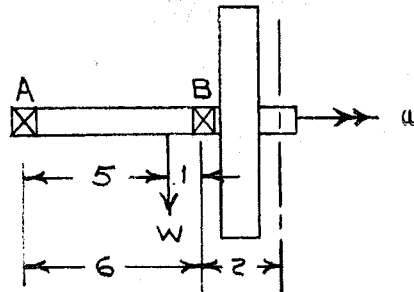
- Microelectronics.
- Discrete Semiconductors.
- Resistors.
- Capacitors.
- Inductive Devices.
- Rotary Devices.
- Relays.

- Switches.
- Connectors.
- Wire and Printed Wire Boards.

### 6.3.2.1 ALTERNATOR FAILURE RATE ANALYSIS

The failure rate analysis for the alternator is analagous to that for the Cyclo-turbine in that life data were available for the two shaft bearings. Test results were for the alternator in the belt-driven configuration shown in the sketch below. The data were:

- 1) Output ball bearing (A) averages life at 4000 rpm is 22,000 hours.
- 2) Input roller bearing (B) average life at 4000 rpm is 20,000 hours.
- 3) Horsepower to drive alternator at 75 percent efficiency is 2.7 HP.
- 4) Diameter of input pulley is 3 inches.
- 5) Pulley was belt driven.



Test Configuration

The tension,  $T$ , applied to the pulley through the drive belt is:

$$\begin{aligned}
 T &= \frac{63,000 (P) (f)}{\omega r} \\
 &= \frac{63,000 (2.7) (1.5)}{4,000 (1.5)} \\
 &= 42.5 \text{ lb}
 \end{aligned}$$

where

$P$  = power, HP

$f$  = drive belt factor

$\omega$  = shaft speed, RPM

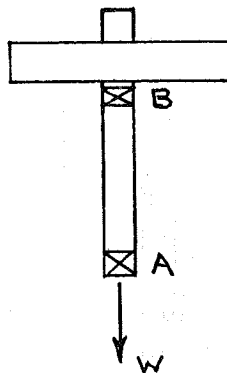
$r$  = pulley radius, in

The measured output load,  $W$ , was 15 lbs. Then, using the dimensions in the sketch, the maximum radial loads on the bearings are computed to be:

Bearing A : 16.7 lbs

Bearing B : 69.1 lbs

In the wind machine application, the alternator coupled to the turbine shaft is loaded as shown in the following sketch:



Turbine Configuration

In this configuration, only torsional load is transmitted from the turbine shaft to the alternator. The equivalent radial load at Bearing A due to the alternator rotor weight,  $W$ , is 15 lbs whereas the radial load at Bearing B is negligible.

The life of Bearing A can be related to the test data by Equation (6-8). For an alternator shaft speed of 2000 RPM, the life of Bearing A is 62,932 hours. Therefore, the life of Bearing A would be 7.2 years.

Bearing A is obviously critical and will be replaced with a tapered roller bearing with a thrust capacity three times that of the original ball bearing. From Equation (6-8), the life then becomes 2,450,610 hours or 281 years. Since the radial load on Bearing B is negligible, it has a life considerably longer than that of Bearing A. The alternator bearing failure rate is, therefore,  $.408 \text{ failures}/10^6 \text{ hours}$ .

The alternator contains one field coil, and twelve output coils configured in three sets of four to provide 3-phase voltage. In order to compute the part stress level for these coils, the alternator was assumed to be a lower quality audio transformer operating in a ground mobile environment. The coils have a class B insulation. Since the part stress for the coils is subject to the hot spot temperature, it was necessary to measure these temperatures.

The hot spot temperature at the center of the field coil was obtained by winding on RTD-type temperature probe into it and measuring the probe resistance while the alternator was operating. This resulted in a reading of  $50^{\circ}\text{C}$  above ambient at 1800 RPM which is a hot spot temperature of  $110^{\circ}\text{C}$ . The calculated failure rate (see Reference 8) for the field coil is  $.065/10^6 \text{ hours}$ .

A probe was also cemented with thermally conductive epoxy in the slot between two output coils. The alternator was run at full power at 1800 RPM and allowed to stabilize in temperature. The alternator was then stopped and a maximum reading of  $20^{\circ}\text{C}$  above ambient, that is,  $80^{\circ}\text{C}$  was obtained. The failure rate for an output coil was calculated to be  $.029/10^6 \text{ hours}$  or  $.351/10^6 \text{ hours}$  for the twelve coils.

The failure rate for the alternator based on the bearings, the field coil, and the twelve output coils being in series is  $.824/10^6$  hours.

#### 6.3.2.2 SUBSYSTEM FAILURE RATE ESTIMATES

The failure rates determined from the parts stress analysis for the electronic subsystems and for the alternator are given in Table 6-4. Also shown in the table are the MTBF for each and the reliability for the one year period between annual one-day shutdown for maintenance.

Table 6-4. Electrical System Reliability.

Key (Figure 6-1)	Assembly	Failures $10^6$ Hrs.	MTBF - Years	One Year Reliability
10	A1A1	.8240	138.9	.99283
11	A1A2	.2395	477.9	.99791
11'	A2A1	.2395	477.9	.99791
14	A2A2	.5410	211.6	.99528
12	A2A3	3.700	30.9	.96819
13	A2A4	.4006	285.7	.99651

#### 6.4 SYSTEM RELIABILITY

The reliability values developed in Section 6.3 for the components and subsystems are used to determine the overall reliability of the machine. The Cycloturbine and the electrical system reliabilities are discussed separately in the following subsections.

#### 6.4.1 CYCLOTURBINE RELIABILITY

The reliability of the turbine system would normally be determined by multiplying the component values together implying a set of series dependencies. This is based on the premise that a total failure (or catastrophic failure) in one part directly affects the reliability of other parts. However, data for catastrophic failures were not available for the bearings which are the prime contributors to reducing Cycloturbine reliability.

The approach used in the reliability analysis by ASI was to determine the probability of nonfailure of the system where failure is defined as excessive wear. Thus, the MTBF defined for the Cycloturbine is one in which the machine would continue to function but with parts exceeding wear tolerances, the result of which would eventually lead to degraded performance or failure of a more serious nature.

The physical relationship of the Cycloturbine critical components, that is, the bearings, is shown in Figure 6-3. A system block diagram of the Cycloturbine bearings is shown in Figure 6-4. This diagram shows the functional relationships among the bearings which reflect the assumptions used in the reliability analysis for wear failure. Although the effects of wear on one part do affect other parts of the machine eventually, the effects are indirect and very difficult to predict. Therefore, it was assumed that only adjacent parts are directly affected (that is, are in series) and that load sharing occurs between bearings furnished in pairs.

In this latter case, failure in one bearing can increase the probability of failure of the other, that is, since the blades work in parallel to carry the imposed loads, failure of one bearing means that the remaining bearing can be assumed to carry the full load alone. If  $h_1(t)$  is the failure rate of one of two operating bearings and

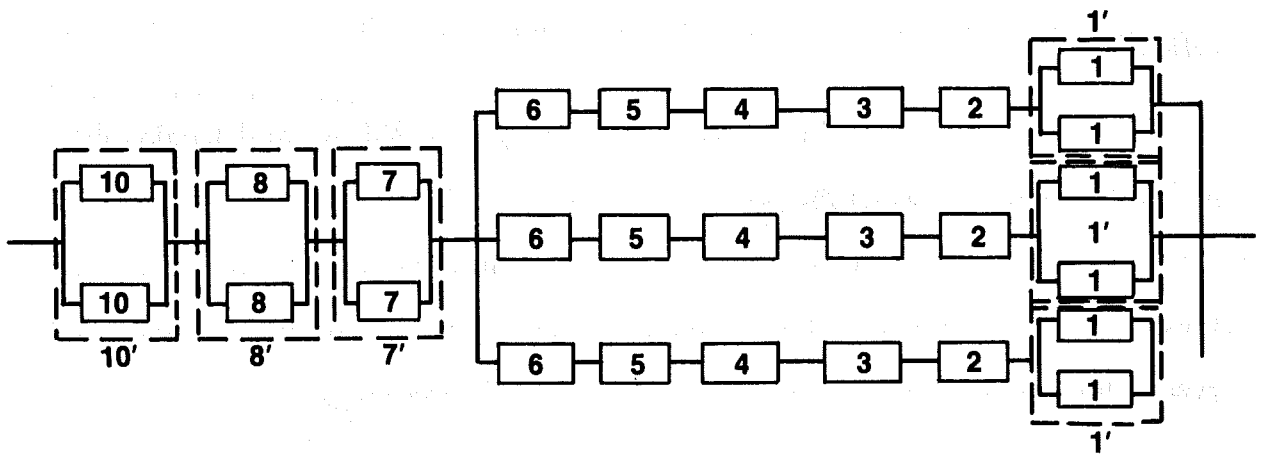


Figure 6-4. System Block Diagram of Cycloturbine.

$h_2(t)$  is the failure rate of a remaining bearing given the other bearing of the pair has failed, then the following model can be used:

$$p_0(t) = \exp \left[ -2 \int_0^t h_1(t) dt \right] = e^{-2\lambda t}$$

and

$$p_1(t) = h_2(t) \exp \left[ - \int_0^t h_2(t) dt \right] = 2\lambda t e^{-2\lambda t}$$

where

$p_0(t)$  = probability of both bearings operating satisfactorily at time,  $t$

$p_1(t)$  = probability of the remaining bearing operating after failure of one of the pair of bearings

with

$$h_1(t) = \lambda = \text{constant}$$

and

$$h_2(t) = 2\lambda = \text{constant}$$

if the stress is assumed to be linear.

The resulting reliability of the pair of bearings serving a particular function is:

$$R'(t) = \sum_{i=0}^{n-1} e^{-n\lambda t} \frac{(n\lambda t)^i}{i!} \quad (6-12)$$

$$= e^{-2\lambda t} [1 + 2\lambda t] \text{ for } n = 2$$

The blade hinge bearings (Key 1) constitute complementary bearings which share the load. However, because of the distances between them, it is not obvious how much load would be transferred from one to another of the bearings. If bearing failure is defined simply as excessive wear of the lining, then the previous assumption can be said to hold. To be more realistic though, it is assumed that the blade hinge bearings are subject not to linear but to parabolic stress, that is, the remaining intact bearing carries a higher than proportional stress. This is approximated by letting  $n = 4$  in Equation (6-12). The reliability of the bearing pair is given in Table 6-5.

Table 6-5. Bearing Pair Reliability.

Bearing Pair Key	Detailed		
	$\lambda \times 10^6$	R(8736)	R'(8736)
1	3.97	.96591	.99122
7	.096	.99916	.99999
8	.096	.99916	.99999
10	.352	.99693	.99998

The main bearings, cam steady bearings, and cam bearings serve all three blade assemblies. As each of these three bearings consists of a set of two identical bearings, Equation (6-12) is applicable. The resulting reliability of the bearing pairs is given in Table 6-5.

This kind of distribution (Erlang) is a reasonable assumption where parallel components share the load and where the failure rate of each is a direct function of the load carried by the component. The assumption is made plausible by the large degree of overdesign of the bearings.

The three blade systems required a different approach. Wear in one blade bearing or other part of one blade system does not immediately impact on the other blade systems. On the other hand, the blade systems are not totally independent, that is, they are not redundant. Therefore, the three blade systems were assumed to be partially in parallel which is a standard technique used in reliability analyses for systems which are obviously not in series but are also not redundant. This phenomena can be assumed if at least two blade assemblies stay in reasonable controllable operation.

The reliability of this partially parallel blade system is expressed as

$$R_{BS}(t) = 3 R_B(t)^2 - 2 R_B(t)^3 \quad (6-13)$$

where the resulting system reliability,  $R_B(t)$ , for each blade assembly can be expressed as

$$R_B(t) = R_6(t) R_5(t) R_4(t) R_3(t) R_2(t) R_1'(t) \quad (6-14)$$

Similarly, the common system reliability

$$R_C(t) = R_{10}'(t) R_8'(t) R_7'(t) \quad (6-15)$$

Then, the total Cycloturbine reliability based on the wear out (but not breakage) of one blade assembly bearings which permits the turbine to at least temporarily continue operating is

$$R_T(t) = R_C(t) R_{BS}(t) \quad (6-16)$$

The Cycloturbine one-year reliability based on the Detailed failure rates (Subsection 6.3.1) is:

Failure/10 <sup>6</sup> Hrs.	3.75
MTBF (Yrs.)	30.6
R (8736 Hrs.)	.96780

#### 6.4.2 ELECTRICAL RELIABILITY

The electrical system reliability was determined both with and without the optional dump load (Assembly A2A2). The electrical system reliability without the dump load is the product of the subsystem reliabilities given in Table 6-4 or

$$\begin{aligned}
 R_E(t) &= R_{10}(5) R_{11}(t) R_{11'}(t) R_{12}(t) R_{13}(t) \\
 &= .95389
 \end{aligned}
 \tag{6-17}$$

and MTBF = 21.18 years for  $\lambda = 5.404$  failures/10<sup>6</sup> hours.

When the dump load option is included, Assemblies A2A2 and A2A4 (Key 13 and 14 in Table 6-4) are redundant. This enhances the system reliability since the reliabilities  $R_{13}$  and  $R_{14}$  are combined to yield

$$\begin{aligned}
 R_r(t) &= R_{13}(t) + R_{14}(t) - R_{13}(t) R_{14}(t) \\
 &= .99998
 \end{aligned}
 \tag{6-18}$$

The reliability of the electrical system with the dump load is

$$\begin{aligned}
 R_E(t) &= R_{10}(t) R_{11}(t) R_{11'}(t) R_{12}(t) R_r(t) \\
 &= .95722
 \end{aligned}
 \tag{6-19}$$

and MTBF = 22.87 years for  $\lambda = 5.005$  failures/10<sup>6</sup> hours.

#### 6.4.3 TOTAL SYSTEM RELIABILITY

The overall reliability of the total system comprising the Cycloturbine and the electrical system is determined as the product of the reliability of each system, that is

$$R_S(t) = R_T(t) R_E(t) \quad (6-20)$$

The total machine reliability was determined using the Detailed results for the Cycloturbine and the electrical system with dump load. The resultant system reliability is:

<u>System</u>	<u>Failures/ 10<sup>6</sup> Hrs.</u>	<u>MTBF (Yrs.)</u>	<u>One-Year Reliability</u>
Cycloturbine	3.750	30.60	.96780
Electrical System	5.005	22.87	.95722
Total Machine	8.755	13.07	.92640

The detailed bearing reliability analysis was repeated to incorporate structural reliability. Rather than include the structural reliability as a single value, failure rates were included for the following components (see Figure 6-3 for bearing locations):

- Tower Foundation
- Tower
- Bearing Cartridge
- Transmission
- Coupling
- Main Shaft
- Hubs
- Struts
- Blades
- Vane/Wing Assembly
- Tilt-Cam
- Tilt-Cam Frame Link (between Bearings 6 and 7)

- Link Between Bearings 6 and 6
- Link Between Bearings 6 and 5
- Pull Rod (Between Bearings 4 and 2)

Basically, the reliability logic of Subsection 6.4.1 was applied. The structure and bearings associated with the struts, blades, control links, and bearings in each blade assembly were assumed to be in series. The blade systems were assumed to be partially parallel. All other systems (except parallel bearings) were assumed to be in series.

Since data for the failure rates of the structural components are not available, it was necessary to select values based on reasonable estimates. The loads analysis presented at the FDR had verified that by using standard engineering practices to assess the fatigue capabilities of the Cycloturbine design, it was shown that fatigue was not a problem. On this basis, it could be expected that the reliability of the structure should be very high, that is, at least .99999. Therefore, selected values of failure rates should yield reliabilities in that neighborhood. With this background as a basis, the following values were selected:

- Foundation  $\lambda = .001 \text{ failures}/10^6 \text{ Hours}$  or  $R = .99999$
- Transmission - The two bearings basically carry the weight of the transmission with very low radial loads. To account for reliability of seals and gears, let  

$$\lambda = .1 \text{ failures}/10^6 \text{ hours}$$
 or  $R = .99913$
- All Other Components  $\lambda = .01 \text{ failures}/10^6 \text{ hours}$  or  $R = .99991$

Applying these failure rates in conjunction with the bearing failure rates, the following results for the total 1-kW system were obtained:

<u>System</u>	<u>Failures/ 10<sup>6</sup> Hrs.</u>	<u>MTBF (Yrs.)</u>	<u>One-Year Reliability</u>
Cycloturbine	5.720	20.00	.95123
Electrical System	5.005	22.87	.95722
Total Machine	10.725	10.80	.91054
Machine and Tower and Foundation	10.736	10.66	.91047

Reevaluation of the 1-kW high-reliability Cycloturbine SWECS including structural components, and even the tower and foundation which is not required by the contract, shows that the requirement of MTBF of 10 years is satisfied. This result was achieved by a more specific representation of the bearing life equations and by using more realistic load and operational conditions.

#### 6.5 MAINTENANCE

The 1-kW high-reliability wind machine will be shut down for a 24-hour period each year for maintenance (see Table 2-1). A maintenance schedule has been established based on the FMEA, the reliability analysis, and experience with similar equipment. The schedule is as follows:

Period	Required Maintenance		
Yearly	<u>Grease:</u> Cam Bearing Main Bearing Alternator Bearings	<u>Inspect:</u> Paint Hardware (for Tightness) Structure (for Integrity) Seals Tolerances Spark Gaps Alternator Performance (Test) Voltage Controlled Relay (Test)	<u>Replace:</u> Gearbox Oil Bushings (if Necessary) Pins (if Necessary) Guides (if Necessary) Bearings (if Necessary) End Caps (if Necessary)
Every Five Years	--	--	Alternator Bearings (Replace Alternator)
Every Ten Years	--	--	Spark Gaps

## 6.6 CRITICAL COMPONENT TESTS

Critical components or subassemblies have been identified in the FMEA presented in Section 6.1 or in previous versions of the FMEA. A number of tests have been completed on components to ensure proper performance and to provide some indication of reliability (see Section 5). Other tests are planned or have been proposed (see Section 10).

Several areas have been identified which relate directly to the operational reliability of the 1-kW high-reliability wind machine. These areas and a synopsis of approach for each are discussed in the following subsections.

### 6.6.1 BEARINGS

The bearings selected for use in the Cycloturbine and the alternator are of a high-reliability type. It is recognized that the life values obtained for the bearings may be overly conservative. This is due to the fact that the manufacturer-supplied failure data are wear failure rates. It is expected that these are the highest or most likely failure rates. It may be possible, by comparison with failure results published for other bearings, to identify failure rates for catastrophic modes. Thus, the failure rate for certain bearings may be significantly reduced which may improve the overall machine reliability.

### 6.6.2 CASTINGS

Castings are to be used at the strut roots for connection to the main shaft hubs. Castings, like the weld areas, represent an area in which the structural lifetime is less certain than for other structural areas. The design of castings is a specialized area in which particular expertise is necessary in order to achieve a design that is reliable in terms of structural integrity, cost effectiveness, timely in terms of fabrication

schedule, distributes loads without undue stress concentration, and which is readily assembled without undue finishing and machining. These criteria are best met by the utilization of personnel experienced in the design, production, and finishing of castings. Thus, the need exists to use the services of a consultant well-versed in the casting area.

### 6.6.3 TILT-CAM VANE/WING ASSEMBLY TESTS

The tilt-cam control system includes a vane/wing assembly (see Section 6.1) which provides orientation and shutdown control of the Cycloturbine through aerodynamic forces. In order to work properly, it is essential that the vane/wing assembly be accurately calibrated so that the exact location, positioning, and balance on the assembly boom can be determined.

Vane design and positioning has been determined by several years of trial and error procedures to enhance performance. This experience, however, is for a 12-ft diameter rotor only. The wing control represents a new concept for which test results on an operational machine are not available. Limited results have been obtained by mounting the wing on a truck and driving at test speeds. However, the truck is a blunt body which induces an erratic, turbulent airflow over the wing, thereby making a precise calibration impossible.

In order to assure that the vane/wing assembly operates properly, it is necessary to obtain operational data on the assembly. This can be done in a wind tunnel where the wind velocity is controlled and force measurements on the assembly can be made. Force data are quickly available, and changes in the vane and wing orientation and position are readily made for a new series of tests. If this mode of tests is not practical, then operational field tests should be conducted to verify proper operation of the shutdown control for the machine.

#### 6.6.4 TRANSIENT-SUPPRESSION CIRCUIT TESTS

A limited test of high voltage transients has been made on the transient suppression network as discussed in Subsection 5.2.2. However, since the potentially most damaging transients are those caused by lightning strikes, the need exists to expose the circuit to high voltage and high amperage transients. The recommended test would expose the system to the output of a high current generator, one producing upwards of 200,000 amperes at between 60,000 and 200,000 volts. It is expected that circuit design would have to be adjusted following the test and the test repeated. This procedure would most likely be completed within three to four iterations.

#### 6.7 SUMMARY OF CONCLUSIONS

The reliability analysis performed for the 1-kW High-Reliability Cycloturbine SWECS indicates that the machine is capable of meeting the reliability goals. Several improvements can be made to the analysis which will make it more realistic and possibly more general. These include: 1) a spectrum analysis of the machine loads; 2) failure rates for failures other than wear; and 3) analysis of reliability for catastrophic failure. The spectrum analysis will consist of using a typical wind velocity distribution to determine RPM and load as a variable based on wind speed and running time at that speed. As an example of the latter condition, the Boston wind profile results in a running time for the alternator of 3,850 hours/year if it is assumed that the turbine begins turning in a one mph wind and that the alternator runs at 2000 RPM. Failure rate data for seized, cracked, or broken bearings will be sought for the bearings used. If unavailable, estimates of these will be made based on failure rates of similar bearings. It is expected that these failure rates will be less than those for wear. Closely related to the revised failure rates will be the method of reliability analysis. A series analysis will be used to reflect the catastrophic nature of the bearing failures.

## SECTION 7

### MANUFACTURING COSTS

Manufacturing cost estimates were determined for both prototype units and a mass-produced 1000th unit. Cost estimates for a prototype Cycloturbine were readily obtained based on the experience of PEC in the manufacture of commercial units. Learning curves and company growth estimates were combined with this experience to arrive at estimates for the 1000th production unit. A similar situation exists for production of the alternator by NPI. However, for the electronic portion of the electrical system, estimates for the 1000th unit were based on established production figures which are available for mass-produced electronic components. The Cycloturbine and electrical system manufacturing costs are discussed separately in this section. All costs are in 1977 dollars.

#### 7.1 CYCLOTURBINE

##### 7.1.1 COST IMPROVEMENT CURVE CONSIDERATIONS

A synthesis of practical assumptions of company behavior with cumulative average productivity as a function of number of units produced from the Wright Theory Cost Improvement Curve (see Figure 7-1) was used in estimating manufacturing costs for the 1000th production Cycloturbine. The 80 percent loglinear slope is recommended for use for a new product coming out of development.

Since the labor time (or cost) of the nth unit depends on the labor time to produce the first machine, an estimate of the first unit labor time is required. This is obtained by listing and estimating labor time for each operation in the manufacturing process. The estimates are summarized in Table 7-1 and delineated per component in Table 7-2. Labor is divided between "semi and unskilled" and "skilled" which were assigned pay

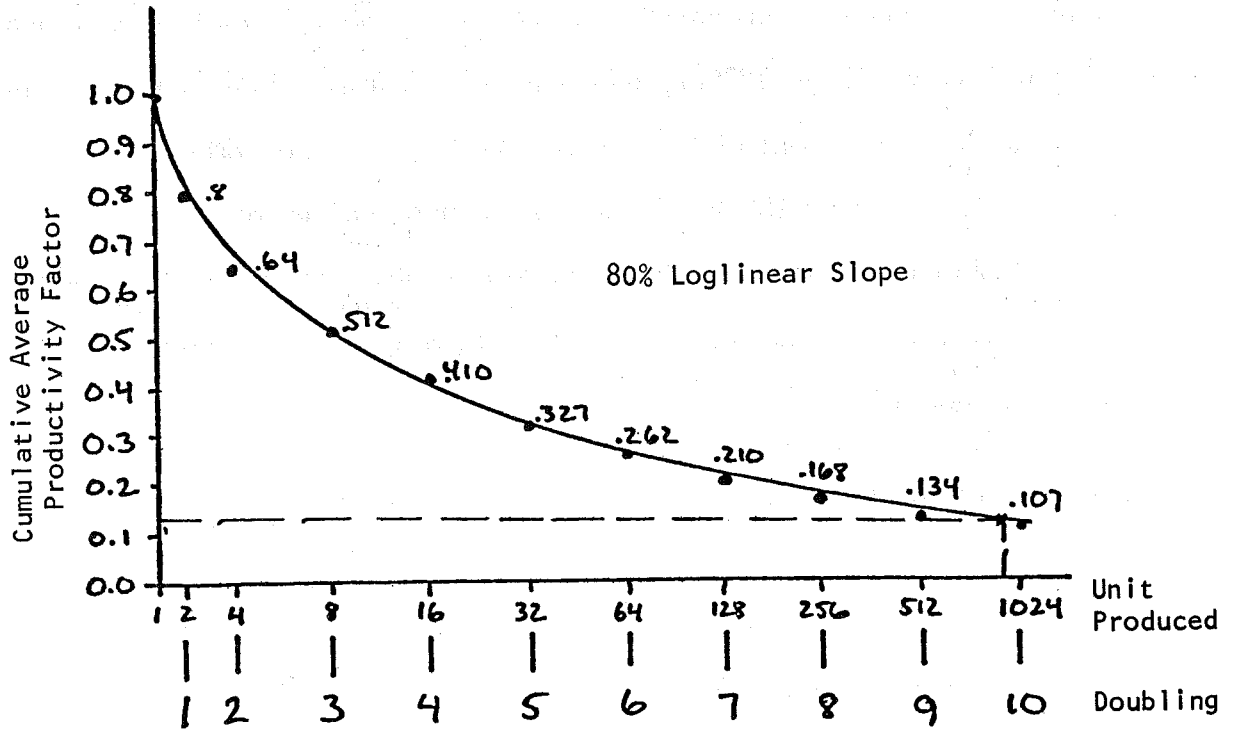


Figure 7-1. Cycloturbine Cumulative Average Productivity Factor versus Unit Number Produced.

**Table 7-1. Summary of Cycloturbine First Unit Manufacturing Labor Hours.**

Item	Hours	
	Semi and Unskilled	Skilled
Blades	15.75	1.25
Struts	20.50	2.0
Shaft	15.25	4.0
Bearing Cartridge	2.85	10.4
Vane	7.45	0.25
Tilt Cam	8.0	2.5
Final Check and Packaging	3.60	-
<b>Totals</b>	<b>73.40</b>	<b>20.4</b>
<b>Total Production Hours</b>	<b>93.8</b>	

Table 7-2. Cycloturbine First Unit Manufacturing Labor Hours.

a) Blades (3/Unit)

Item	Hours	
	Semi and Unskilled	Skilled
Pivot Tabs - Shear and Drill	1.0	.5
Slot Extrusion	1.0	-
Weld Pivot Tabs to Extrusions	-	.75
Drill Outer Skin	.75	-
Form Outer Skin	.5	-
Form C - Spar	.5	-
Clamp Assembly	.75	-
Drill Rivet Holes	1.25	-
Deburr Rivet Holes	1.0	-
Clamp and Rivet	2.5	-
Install End Caps	1.5	-
Seal	2.0	-
Etch, Prime, Paint	3.0	-
Totals	15.75	1.25
Total Production Hours	17.0	

Table 7-2. Cycloturbine First Unit Manufacturing Labor Hours (Continued).

b) Struts (6/Unit)

Item	Hours	
	Semi and Unskilled	Skilled
Clean and Prep Blade and Hub Castings	3.0	-
Clean and Prep Pull Rod Slider Castings	2.0	-
Cut Extrusions	1.75	-
Fabricate Strut Stay Tangs	.75	-
Weld Extrusion Castings	-	2.0
Etch, Prime and Paint Strut Assemblies	4.5	-
Fabricate Pull Rods	1.5	-
Clean, Paint and Install L-Links	3.5	-
Fabricate and Install Stainless Stays	1.5	-
Install Blade Boot	2.0	-
<b>Totals</b>	<b>20.50</b>	<b>2.0</b>
<b>Total Production Hours</b>	<b>22.50</b>	

Table 7-2. Cycloturbine First Unit Manufacturing Labor Hours (Continued).

c) Main Shaft

Item	Hours	
	Semi and Unskilled	Skilled
Fabricate Bottom Bushing	2.0	-
Weld	-	0.5
Turn Shaft ID	-	1.0
Mill Key Way	-	0.5
Machine Hub Plates	3.0	-
Drill Mounting Holes in Shaft	1.5	-
Weld Hub Plates	-	0.5
Clean, Prime and Paint Shaft	1.75	-
Fabricate Gearbox Flange Assembly	4.0	1.0
Machine and Mount Brake Disc	1.5	0.5
Machine Control Bushing	1.5	-
<b>Totals</b>	<b>15.25</b>	<b>4.0</b>
<b>Total Production Hours</b>	<b>19.25</b>	

Table 7-2. Cycloturbine First Unit Manufacturing Labor Hours (Continued).

d) Bearing Cartridge

Item	Hours	
	Semi and Unskilled	Skilled
Cut Straps	0.35	-
Bend Straps	-	0.4
Cut Plate	-	0.75
Cut Gussets	-	0.75
Machine End Flanges	1.5	-
Weld Cartridge	-	3.5
Fabricate Drive and Generator Frame	-	2.0
Clean and Prep Cartridge	1.0	-
Galvanize	-	3.0
<b>Totals</b>	<b>2.85</b>	<b>10.4</b>
<b>Total Production Hours</b>	<b>13.25</b>	

Table 7-2. Cycloturbine First Unit Manufacturing Labor Hours (Concluded).

e) Vane

Item	Hours	
	Semi and Unskilled	Skilled
Drill Vane Skins	1.0	-
Deburr Vane Skins	0.5	-
Bend Vane Skins	0.5	-
Bend Vane Spar	0.25	-
Cut Gussets	0.25	-
Assemble Gussets and Spar	0.35	-
Machine and Assemble Vane Plate	1.25	0.25
Assemble Vane Skin to Spar	0.50	-
Assemble Spar to Plate	0.35	-
Etch, Prime and Paint	2.0	-
String	0.5	-
<b>Totals</b>	<b>7.45</b>	<b>0.25</b>
<b>Total Production Hours</b>	<b>7.7</b>	

rates of \$3.90/hr. and \$18/hr., respectively. An average labor rate of \$6.97/hr. was found which is used to find the labor cost of the 1000th machine (see Subsection 7.1.3).

## 7.1.2 GROWTH ESTIMATES

Assumptions must be established relative to company growth in order to determine future company production capability. These assumptions concerning sales, production level and work force are delineated in the following subsections.

### 7.1.2.1 SALES

1979 - 1980: Wind turbine sales will be primarily to a market comprised of institutions, remote uses and telecommunication applications. Some help in sales to individuals will result from federal and state tax incentives. Widespread market acceptance is slowed by consumer information lags and the time required to develop marketing networks and achieve manufacturing cost reductions. Energy prices will continue to rise.

1980 - on: Sales increase dramatically due to increased creditability of wind energy alternatives and achievement of cost effectiveness for SWECS brought on by increasing fossil fuel prices and manufacturer's refinements.

### 7.1.2.2 PRODUCTION LEVELS

The assumed production rate for PEC is given in Figure 7-2.

Quarters 1 - 6: (Beginning in 1979) are marked by incremental improvements in machine shop style production.

Quarters 7 - 9: Implement automation of repetitious operations.

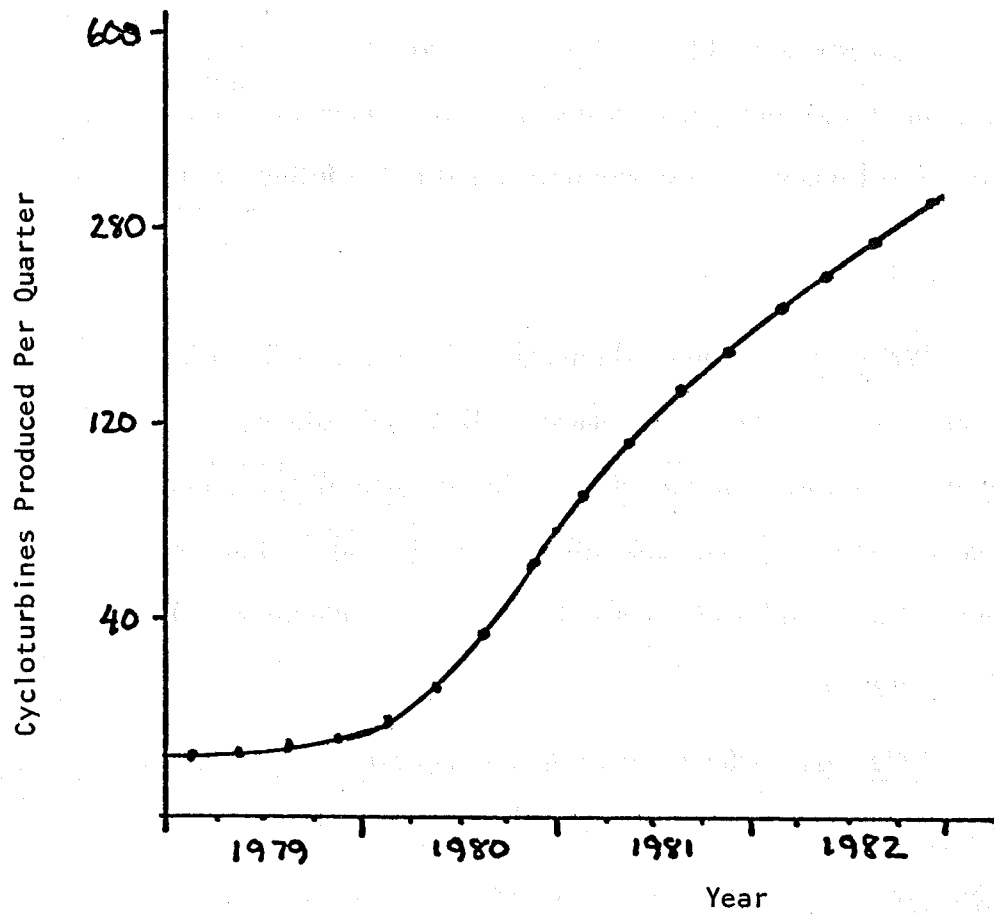


Figure 7-2. Assumed Cycloturbine Production Rate.

Quarters 10, 11: Reflect the implementation of full automation and some redesign of the turbine for high mass production.

Quarters 11 - 14: Demonstrate the completion of full automation and achievement of large scale production.

### 7.1.2.3 HIRING AND EMPLOYMENT

Quarters 1 - 9: Improved management acumen and production techniques allow three workers to meet production levels.

PEC is operating in the high slope region of the learning curve (Figure 7-1) where continued production at lower levels results in high learning efficiencies.

Quarters 10 - 14: In the 10th quarter, production of 120 Cycloturbines will necessitate hiring of one additional man. In the 12th quarter, production of 200 turbines necessitates hiring 2 more. Some concern exists that hiring mandated by a high level of production would result in lowering the overall efficiency of the workforce. However, at such a high volume of production, new workers progress rapidly down the steepest section of the learning curve.

### 7.1.3 LABOR COST

In the 14th production quarter (second quarter of 1982), the 1000th machine is made (see Figure 7-3). Production for the quarter is 250 machines. Five workers and a foreman are engaged directly in production. The cumulative average productivity factor is 0.107 as seen in Figure 7-1.

It is estimated that the first machine made will require 93.8 manhours to complete (see Table 7-1). Utilizing the cumulative average productivity factor, the 1000th unit will require 10.04 manhours to produce. Note that the total manhours available for labor in the 14th quarter (6 workers) is 3120 manhours. At the production rate of 250 units per quarter, 12.48 manhours are available per Cycloturbine made which

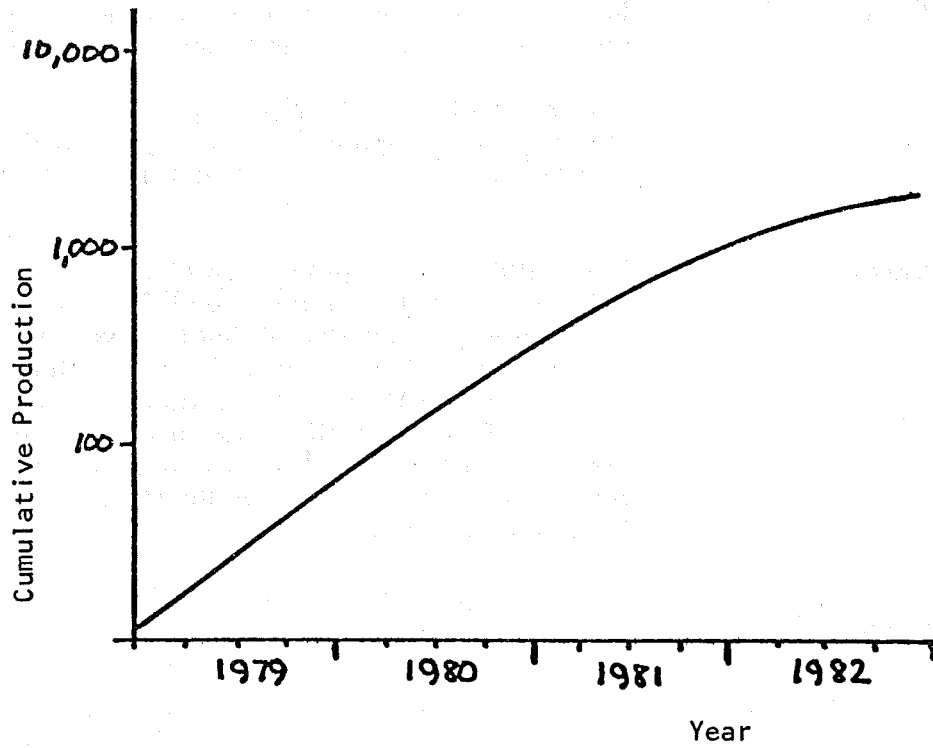


Figure 7-3. Assumed Cycloturbine Cumulative Production.

agrees well with that found. Taking 10.04 manhours and multiplying by the average rate of \$6.97 per hour, the manufacturing labor cost will be \$70.00 for the 1000th unit.

#### 7.1.4 MATERIALS AND PARTS COSTS

In determining the cost of materials and parts of the 1000th Cycloturbine produced, a quote survey was made by mail to all suppliers of Cycloturbine components. Requested information included price per unit when ordered in quantities of 500, 1000 and 1500; OEM price if different from that listed, approximate delivery time, and name and position of individual providing the quotation. A summary of the materials cost for the Cycloturbine is given in Table 7-3, and Table 7-4 provides a materials cost breakdown for each major component. The total materials cost for the 1000th Cycloturbine is \$720.

#### 7.1.5 TOTAL COST

The labor cost and the materials cost with appropriate profit and burden rates for a manufacturing plant are summarized in Table 7-5. A total cost of \$1,099 is obtained for the 1,000 production unit. The weight of the turbine is 508 pounds (see Table 7-6) making the turbine price per pound \$2.16.

**Table 7-3. Summary of Cycloturbine Materials and Parts Costs.**

Part	Number per Machine	Price per Machine in Quantities of 1000
Blades	3	\$ 69.65
Struts	6	198.06
Shaft	1	93.43
Bearing Cartridge	1	99.73
Transmission	1	223.87
Control System	1	34.78
<b>Total</b>		<b>\$719.52</b>

Table 7-4. Cycloturbine Materials and Parts Costs.

a) Blades

Part	Weight or No. per Machine	Price per Machine in Quantities of 1000
Leading Edge Extrusion	42.75 lbs	\$42.75
C - Spar 6061 T-6 .025 in.	6.36 lbs	6.36
Blade Skin 6061 T-6 .025 in.	12.71 lbs	12.71
Rivets 5/32 x 1/8 Marson Klik Fast (Stainless)	300 Rivets	5.00
Pivot Tabs	.60	.51
End Caps	6	.12
Pivot Pins	6	2.20
<b>Total</b>		<b>\$69.65</b>

Table 7-4. Cycloturbine Materials and Parts Cost (Continued).

b) Struts

Part	Weight or No. per Machine	Price per Machine in Quantities of 1000
NACA 0015 Extrusion	74.80 lbs	\$ 74.80
Strut Castings	24	45.00
Spherical Bearings	6	12.46
Boot	6	12.00
TFE Bushings	9	2.40
Pull Rod, Stay Rod (Stainless)	24 ft	16.00
Rod End Bearings	6	21.00
L - Link	3	9.00
Swivel Pins	3	1.50
Swivel Brackets	24	3.00
Stay Tang	6	.90
<b>Total</b>		<b>\$198.06</b>

Table 7-4. Cycloturbine Materials and Parts Cost (Continued).

c) Shaft

Part	Number per Machine	Price per Machine in Quantities of 1000
Centerless Ground Steel Shaft Tube	-	\$72.00
Gearbox Adaptor Bushing	1	4.00
Brake Disc and Mount	1	4.03
Brake Calipers 375 m2	1	5.65
Hub Plates	4	7.75
<b>Total</b>		<b>\$93.43</b>

Table 7-4. Cycloturbine Materials and Parts Cost (Continued).

d) Bearing Cartridge

Part	Weight or No. per Machine	Price per Machine in Quantities of 1000
Cartridge Tube	34.72 lbs	\$14.00
End Flanges	11 lbs	8.25
Triangle Straps	32.51 lbs	7.43
Gussets	4.46 lbs	.74
Triangle Plate	14.46 lbs	3.09
Frame	22.44 lbs	4.51
Bearings SFC - 47	2	58.36
Bearing Mounting Bolts	8	3.35
<b>Total</b>		<b>\$99.73</b>

Table 7-4. Cycloturbine Materials and Parts Cost (Continued).

e) Transmission

Part	Number per Machine	Price per Machine in Quantities of 1000
Gearbox 115D 15	1	\$185.16
Flexible Coupling Gerbing G - 5000	1	11.21
Cowling-Plastic Injection Mold	1	7.50
Mounting Flanges	1	20.00
Total		\$223.87

Table 7-4. Cycloturbine Materials and Parts Cost (Concluded).

f) Control System

Part	Weight or No. per Machine	Price per Machine in Quantities of 1000
Vane Skin	1.5 lbs	\$ 1.50
Vane Boom	3183 ft	4.71
Gussets	1.4 lbs	1.84
Vane Plates	1	1.93
Eye Bolt	1	0.75
Hardware	-	0.43
End Cap (Plastic)	2	0.03
Rivets (Stainless)	50	1.55
Tie Cable	4 ft	0.04
Tilt Cam Assembly	1	22.00
<b>Total</b>		<b>\$34.78</b>

Table 7-5. Summary of Cycloturbine Cost Elements.

1000th Production Unit

1977 Dollars

Cost Elements	Cost
Direct Material	\$ 720.
Material Overhead (10%)	72.
Direct Engineering Labor	8.
Engineering Overhead (150%)	13.
Direct Manufacturing Labor	70.
Manufacturing Overhead (100%)	70.
Other Costs	18.
Subtotal	<u>\$ 971.</u>
General and Administrative Expenses (5%)	48.
Subtotal	<u>\$1,019.</u>
Profit (8%)	80.
Total Price per Unit	<u>\$1,099.</u>

**Table 7-6. 1-kW High-Reliability Cycloturbine Weight Estimation.**

Components	Weight (Lbs.)	Total (Lbs.)
Blades	3 @ 21 (ea.)	63
Struts and Joiner Plates	6 @ 15	90
Strut Root Castings	6 @ 8	48
Main Shaft with Hubs	1 @ 90	90
Main Shaft Cartridge	1 @ 70	70
Control System	1 @ 25	25
Gearbox, Coupling, Alternator	1 @ 120	120
<b>Total</b>		<b>508</b>

## 7.2 ELECTRICAL SYSTEM

### 7.2.1 MANUFACTURING COST CONSIDERATIONS

Manufacturing cost estimates for unit quantities were based on NPI's manufacturing experience that the cost of a new design would be spread equally between parts, labor and testing. Manufacturing cost estimates for the electrical system in quantities of 1000 units per year were developed based on established times for performing all tasks related to the manufacture of the electrical system. The cost of conducting required acceptance tests during manufacturing (see Table 7-7) is included in these estimates. Tests specifically for quality control are not included.

Table 7-7. Electrical System Manufacturing Testing.

#### Alternator

- Output and Field Coil Resistance
- Insulation Resistance
- Output Coil Orientation
- Performance (Output Power and RPM)

#### Transient Protection Network

- Spark Gap Firing Voltage
- Varistor Clamping Voltage
- Insulation Resistance
- Surge Protector Clamping Voltage

#### Main Rectifier Assembly

- Low Current Voltage Drop; Each Diode
- 48 Hour Power Burn-In

#### Voltage Regulator Card

- Functional Test Before and After Burn-In
- 48 Hour Power Burn-In

#### Dump Load Card

- Functional Test Before, During and After Burn-In

### 7.2.2 GROWTH ESTIMATES

In order to produce 1000 units per year, approximately 20 units must be built each week. Power burn-in and alternator varnishing are the pacing activities for the system production. Personnel required to build 20 units per week include 8.4 people to build the main control, 1.3 people to build the alternators, and 7.8 people to handle the remaining tasks. If another 2.5 people are added to account for division of labor inefficiencies, the total personnel requirement is 20.

Labor saving techniques and equipment viable for production of 1000 units per year were developed and included in the cost estimates. Projections of new equipment and space for manufacturing, research and offices were developed consistent with the production level (see Table 7-8). Learning curves were not required.

New equipment was specified not only to improve cost of production but also to improve reliability through quality control. Since there are many screws used in the construction of the electrical system, care was taken in the design to use similar screws wherever possible. This will allow the use of a pneumatic screwdriver to speed production. In the interest of reliability, a wave soldering machine was included in the required capital equipment. While the quantity does not justify the expense, the wave soldering technique makes it easier to locate soldering problems. This is because the machine eliminates random errors, that is, if it is working correctly, all boards in a particular run will be acceptable; otherwise, if an error occurs on one board it will most likely be on all boards. Once the problem is detected, all boards in that run could be reworked. If the same set were hand soldered, any individual joint

Table 7-8. Electrical System Manufacturing Capital Improvements.

<u>Equipment to Produce 1000 Units per Year:</u>	
Pneumatic Screwdriving System	
Wave Soldering System	
Lead Forming Tools	
P.C. Board Assembly Stations	
Electric Solder Pot	
Automatic Wire Cutter	
Automatic Wire Stripper	
Degreasing Tank	
Oscilloscopes	
<u>Area Required to Manufacture:</u>	
20 People Bench Space @ 30 ft <sup>2</sup>	600
Burn-In Area	96
Wave Solder and Cleaner	200
Drill Press	20
Saw	20
Miscellaneous	100
Shipping	520
Electrical Lab	400
Offices	400
Miscellaneous (Aisles, Common Areas)	400
Stock Room (90 Day Inventory - 240 Units)	<u>1200</u>
	3956 ft <sup>2</sup>

could be left unsoldered or have a cold joint - problems much more difficult to detect. Simple forming aids would be used to preform resistor and capacitor leads and to reduce strain on the component. An automatic wire stripper and cutter would be used to speed production of wiring harnesses. A solder pot would be employed to tie ends of the wire braid used to connect several high power sections of the circuit. The required printed circuit boards would be built stacked three high and three wide to reduce handling. These boards would then be broken apart much like a model airplane kit when complete. The larger size also facilitates support and provides for ease of handling. A special milling cutter would be used to deburr and remove the anodizing on heat sink holes. The capital required for the equipment was amortized over seven years of operation with a 10 percent salvage value and manufacturing space was assumed to cost \$8/square foot/year.

### 7.2.3 LABOR COST

The labor cost for each major subassembly for the production of the 1000th unit is delineated in Table 7-9. The labor cost at an average rate of \$5 per hour for the 1000th unit will be \$68.

### 7.2.4 MATERIALS AND PARTS COST

Materials and parts costs were determined from available catalogs and established costs for manufactured subassemblies. The materials and parts costs for each major subassembly for the 1000th unit are given in Table 7-9. The material and parts cost for the 1000th unit will be \$570.

Table 7-9. Summary of Electrical System Materials and Manufacturing Labor Costs.

1000th Production Unit

1977 Dollars

Description	Materials and Parts	Manufacturing Labor
A1A1	\$118.	\$ 9.80
A1A2	38.	14.00
A2A1	74.	14.00
A2A3	77.	6.52
A2A4	71.	5.67
Control Box	90.	18.00
Transmission Line	102.	-
Total	\$570.	\$67.99

### 7.2.5 TOTAL COST

The electrical system labor cost and the materials cost with appropriate profit and burden rates for a manufacturing plant are summarized in Table 7-10. A total cost of \$895 is obtained for the 1000th production unit.

Table 7-10. Summary of Electrical System Cost Elements.

1000th Production Unit

1977 Dollars

Cost Elements	Electrical System
Direct Material	\$570.
Material Overhead (10%)	57.
Direct Engineering Labor	4.
Engineering Overhead (150%)	7.
Direct Manufacturing Labor	68.
Manufacturing Overhead (100%)	68.
Other Costs	16.
Subtotal	<u>\$790.</u>
General and Administrative Expenses (5%)	39.
Subtotal	<u>\$829.</u>
Profit (8%)	66.
Total Price per Unit	<u>\$895.</u>

### 7.3 CYCLOTURBINE AND ELECTRICAL SYSTEM TOTAL COST

Combining the costs for the Cycloturbine and the electrical system from the previous subsections gives the total system costs for the 1000th production unit presented in Table 7-11.

Table 7-11. Summary of Total System Cost Elements.

1000th Production Unit

1977 Dollars

Cost Elements	Cycloturbine	Electrical	Total
Direct Material	\$ 720	\$570	\$1,290
Material Overhead (10%)	72	57	129
Direct Engineering Labor	8	4	12
Engineering Overhead (150%)	13	7	20
Direct Manufacturing Labor	70	68	138
Manufacturing Overhead (100%)	70	68	138
Other Costs	18	16	34
Subtotal	\$ 971	\$790	\$1,761
General and Administrative Expenses (5%)	48	39	87
Subtotal	\$1,019	\$829	\$1,848
Profit (8%)	80	66	146
Total Price per Unit	\$1,099	\$895	\$1,994

## SECTION 8

### TOWER SPECIFICATION

The total SWECS for high reliability applications requires both the wind turbine system and a support structure, that is, a tower. Although a tower was not to be designed nor supplied with the 1-kW high-reliability SWECS, it was necessary to specify the characteristics of the tower, preferably by recommending a specific tower. This specification is discussed in this section.

#### 8.1 FOUNDATION SPECIFICATION

Commercial versions of the Cycloturbine have been installed in the field. A tower often provided as part of the installed system by PEC is the NPI Octahedron tower manufactured by Thompson Engineering. The Octahedron tower, shown in Figure 1-1, is a fully triangulated, nonredundant structure offering high strength at low weight. Its ease of transport, and simplicity of construction which permits erection without a crane make it attractive for SWECS applications, particularly at remote locations.

Because of the successful application by PEC for the Cycloturbines, a 34-ft version of the Octahedron tower was recommended early in the design phase. Full scale drawings of the base area were provided to Rockwell International to enable design of a concrete pad to be initiated.

Additional effort was expended for nonconcrete footings. Where soil conditions permit, the guyed tower footings shown in Figure 8-1 can be used. Rock anchors for the guy wires are used, if necessary. In compressible soils, the steel pads would be buried to provide additional support at the footings.

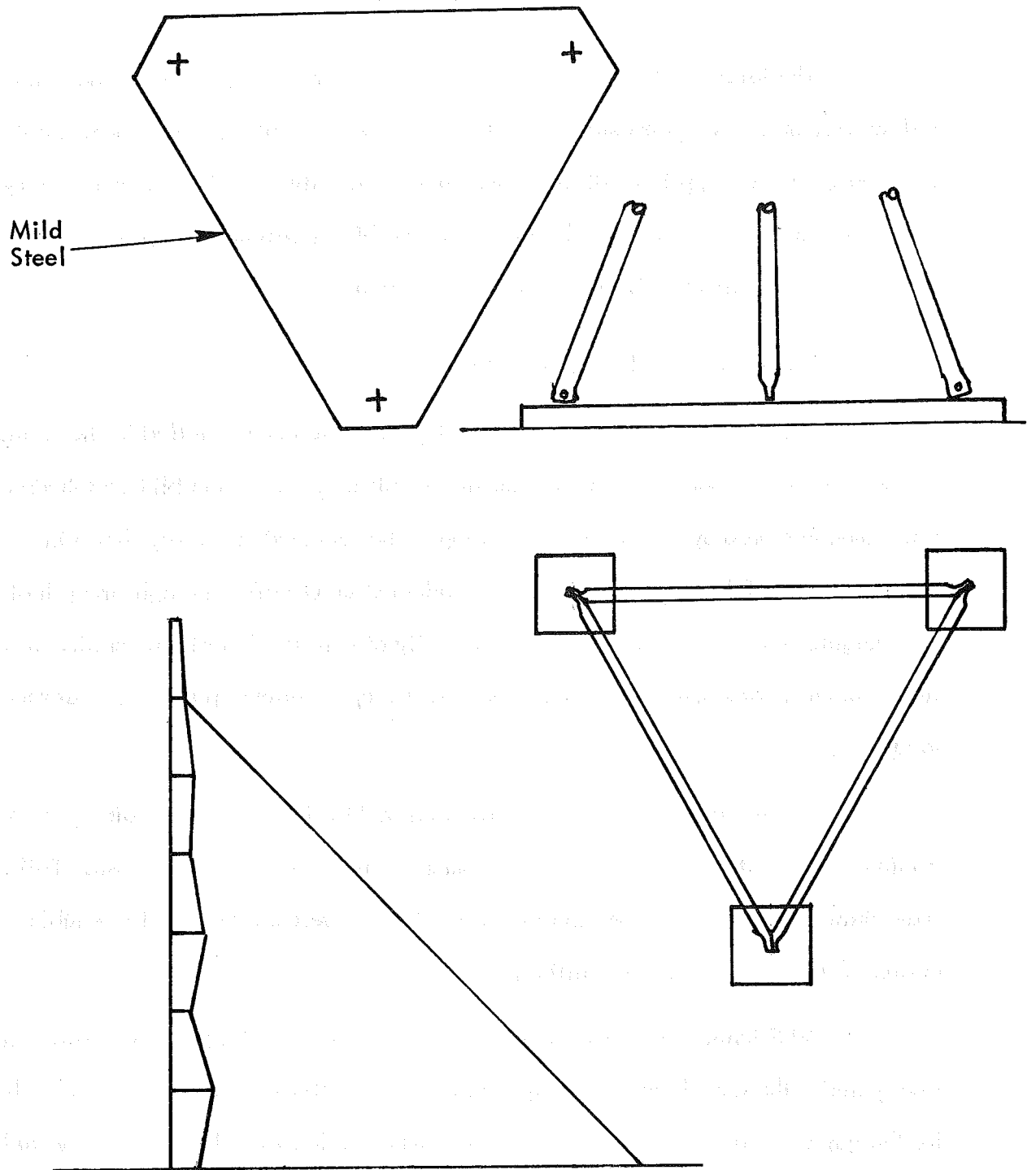


Figure 8-1. Nonconcrete, Guyed Footings.

## 8.2 TOWER SPECIFICATION

A wind machine mounted on its tower represents a coupled dynamic system which can experience adverse interactions or excessive response to unsteady wind inputs. A SWECS cannot be considered reliable and totally safe under all environmental conditions without studying the coupled tower/rotor system. Resonant conditions have been observed of Cycloturbines mounted on Octahedron towers. Therefore, before specification of a tower was made, analysis and test verification were necessary for the coupled Cycloturbine/tower system.

### 8.2.1 CYCLOTURBINE/TOWER SYSTEM ANALYSIS

A simplified dynamic response analysis for the coupled machine/tower system was outlined in Subsection 4.6.2. As was shown in Figure 4-35, if the third aerodynamic harmonic and the tower first natural frequency are coincident, a significant dynamic response can occur unless sufficient damping exists in the system. This fact is further emphasized by the parametric study results shown in Figure 8-2. An increase in Cycloturbine weight tends to reduce the dynamic response (note that for this study, the tower frequencies were held constant); however, the deflection at the Cycloturbine is affected more by the damping.

Although it seemed reasonable based on the results shown in Figure 8-2 to specify that maximum deflections at resonance have a double amplitude of less than 2 inches and that the fundamental mode damping ratio be greater than 0.01, these criteria required further investigation for several reasons. First, the damping ratio used in the analysis is the modal damping ratio based on viscous damping rather than structural damping normally used for structural analysis. Second, a double amplitude of 2 inches may be excessive. Finally, the tower characteristics used in the analysis were assumed since actual tower dynamic characteristics were not available either from analysis or test.

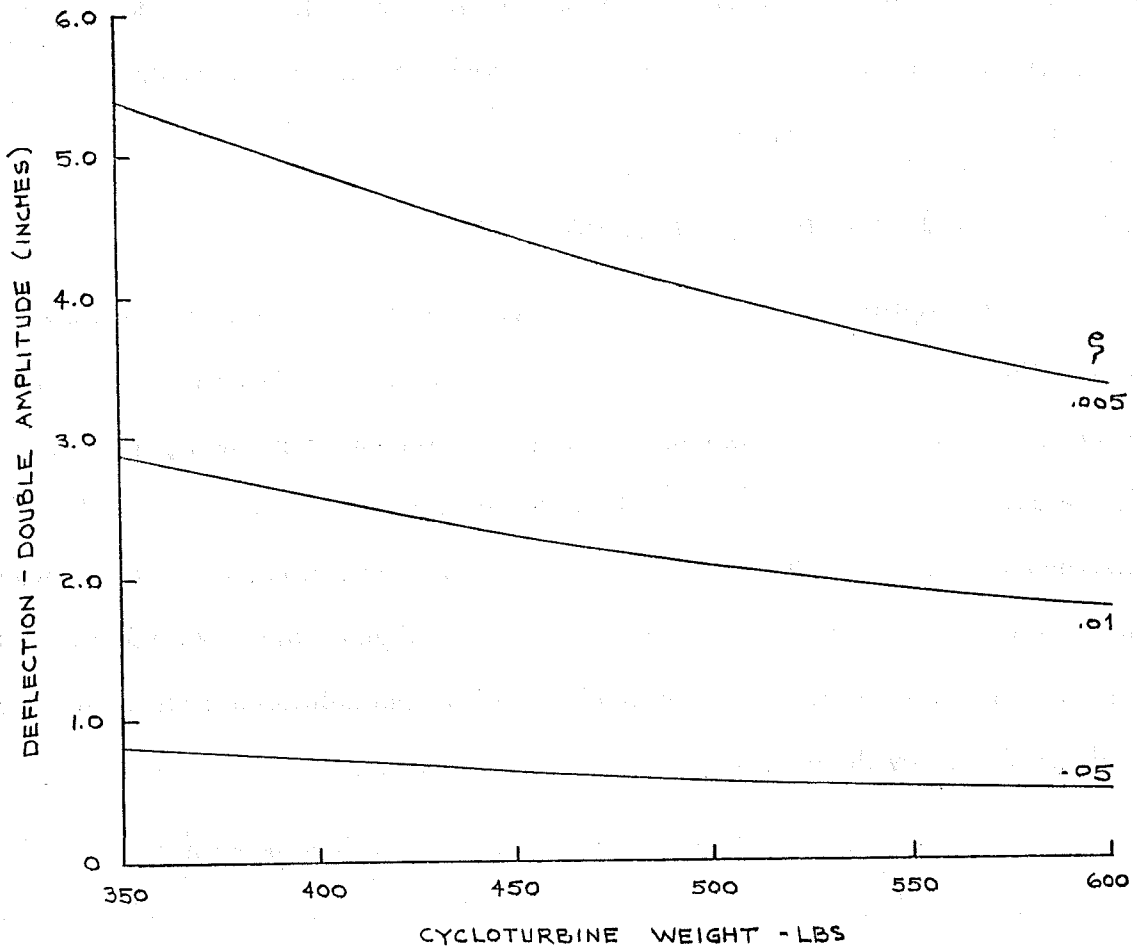


Figure 8-2. Effect of Weight and Damping Ratio On Cycloturbine/Tower Dynamic Response.

## 8.2.2 PRELIMINARY TOWER CHARACTERISTICS

The lack of tower dynamic characteristics was the most significant shortcoming of the dynamic response analysis because it precluded the use of the analysis for an actual tower. In order to specify the tower, therefore, it became necessary to obtain dynamic characteristics for towers of interest. Because of the observed coupled response of the Cycloturbine/Octahedron system, PEC had investigated other available towers. Several installations were made with the Rohn SSV tower. The two towers of interest are shown in Figure 8-3.

Since a number of the Cycloturbine installations were readily available, PEC after arrangement with the machine owners, performed a preliminary vibration test of several Cycloturbine/Octahedron towers. The test consisted of having someone climb to the tower top and excite the first natural mode by rocking back and forth. At the resonant condition (which is easily recognized), the number of cycles were counted over a short time period usually 10 seconds. This would be done several times to verify the results. These data for different tower heights and approximately the same Cycloturbine weight are compared in Figure 8-4. As expected, the frequency of the first or fundamental mode decreases with tower height. Also shown and compared to the tower frequency scale is the rotor RPM which, for a 3/rev excitation, would result in resonance.

Only one Rohn tower was available for test, a 40-ft SSV, owned by PEC. The tower was tested with and without weight mounted on it. Results of these tests, shown in Figure 8-5, indicate the decrease in natural frequency with increase in weight on top of the tower.

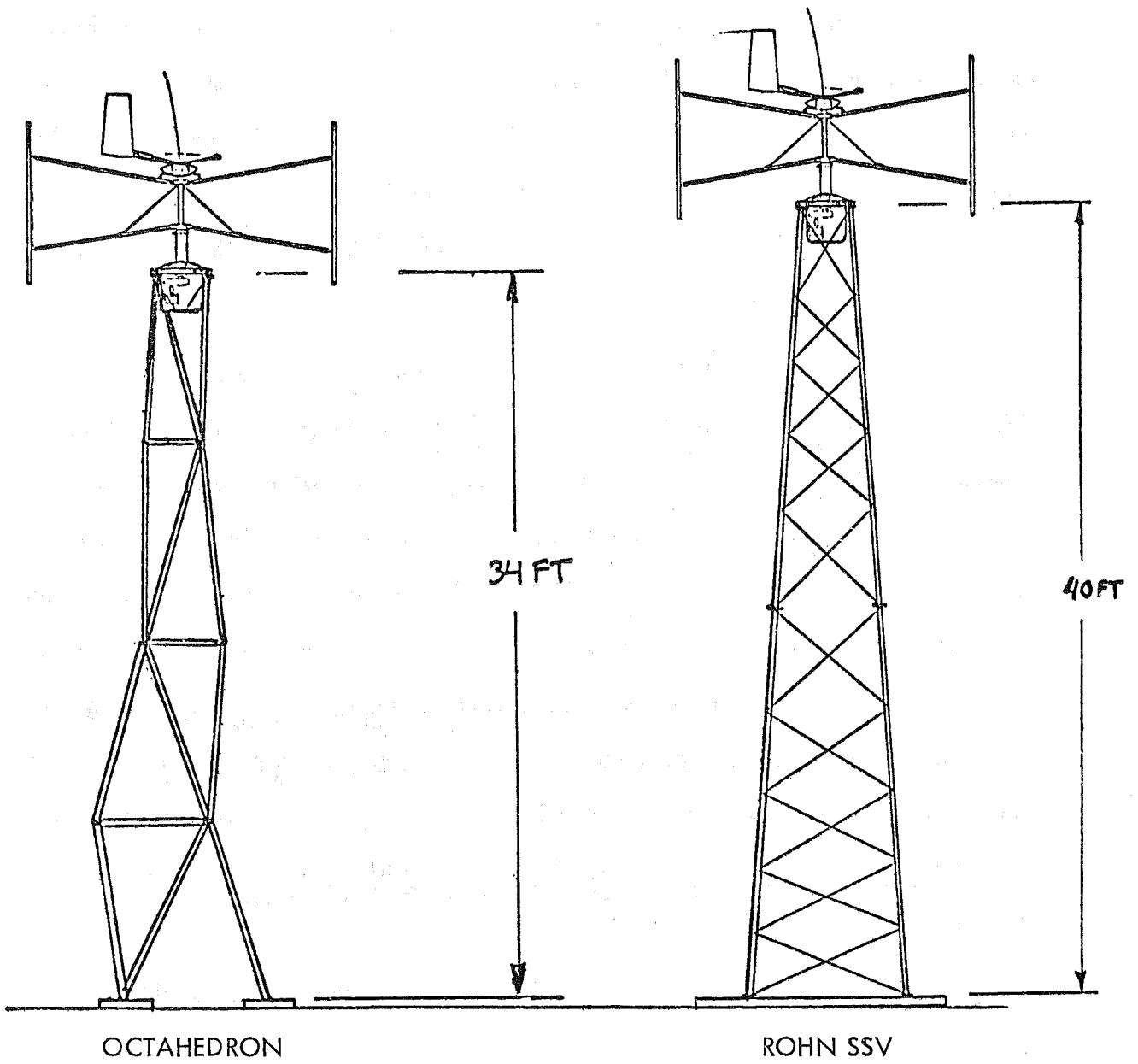


Figure 8-3. Towers Under Consideration.

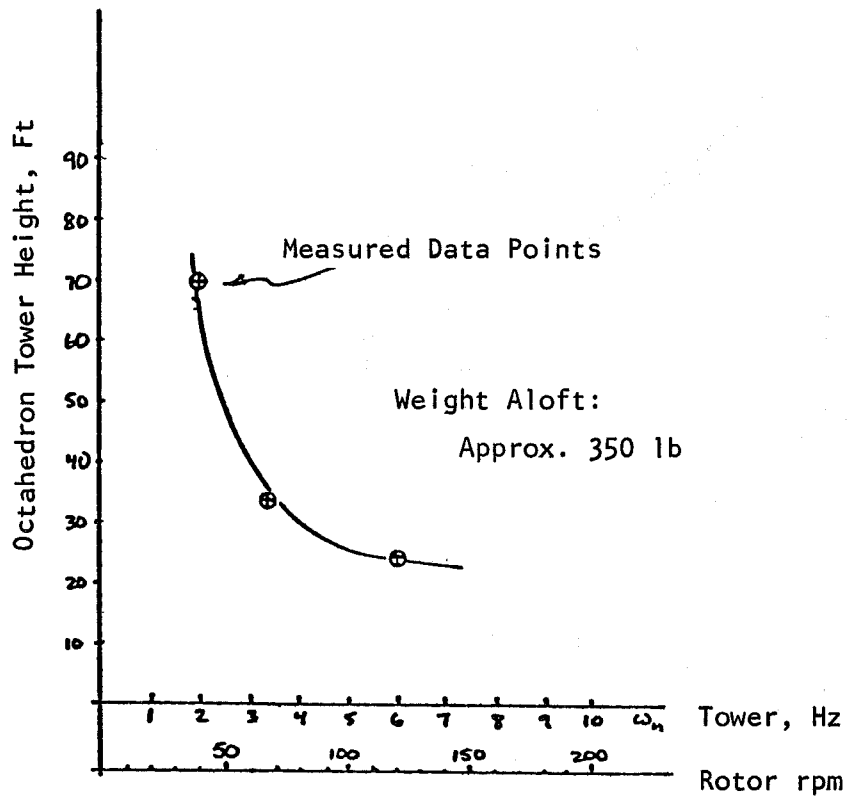


Figure 8-4. Octahedron Tower First Mode Natural Frequency versus Tower Height.

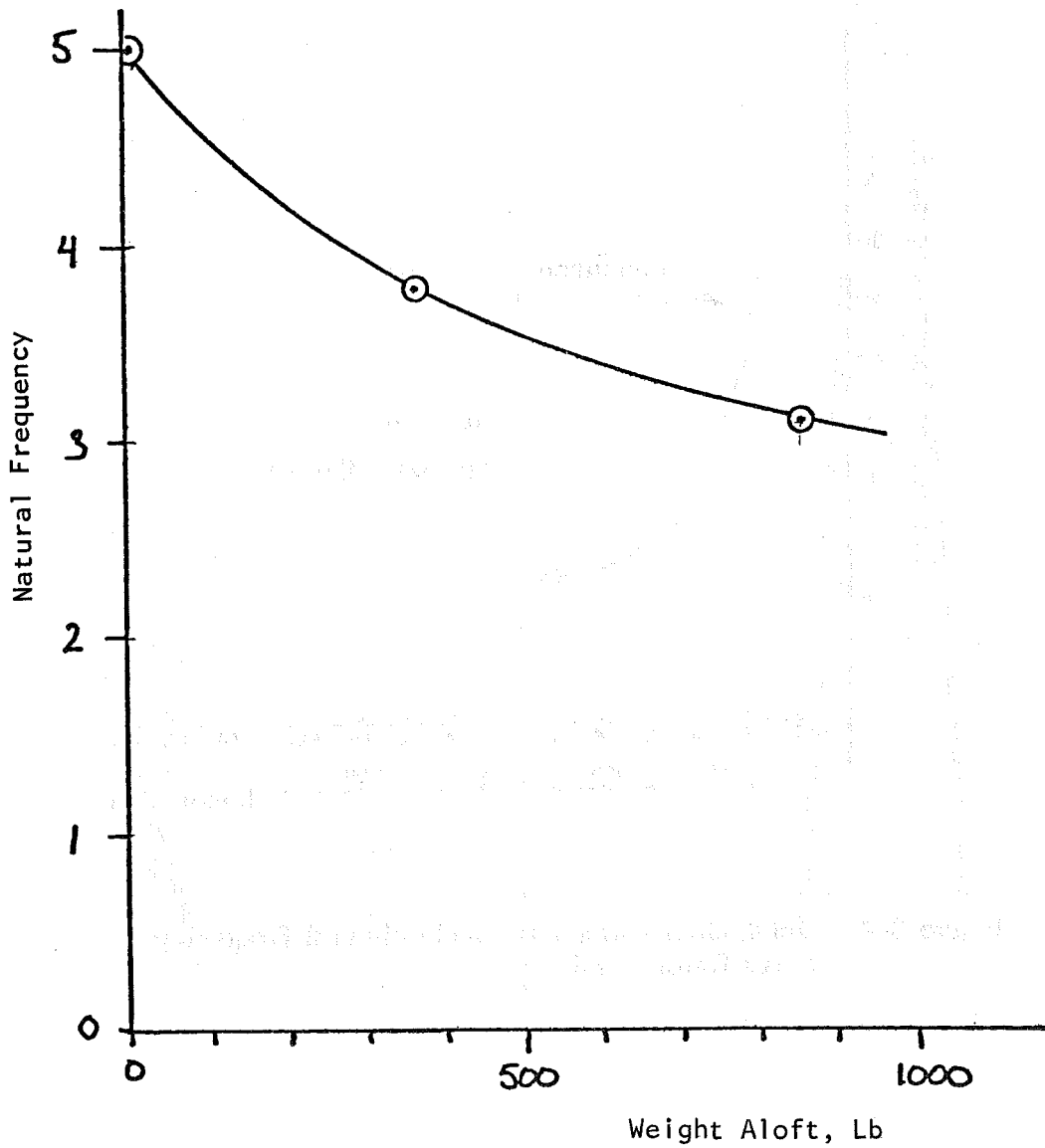


Figure 8-5. Preliminary Measurement of Natural Frequency versus Weight Aloft for 40-ft Rohn SSV Tower.

### 8.2.3 TOWER TEST PROGRAM

The preliminary test results shown in Figure 8-4 and 8-5 revealed that Octahedron and Rohn towers had fundamental frequencies in the range of 3 to 4 Hz. In order to relate these and other tower data to the Cycloturbine, the tower frequencies are shown relative to Cycloturbine RPM and aerodynamic harmonics in Figure 8-6. Two aerodynamic harmonics are shown, the 1/rev (1p) and the 3/rev (3p). The 1/rev is not a primary input for the Cycloturbine unless an unbalance occurs in the generation of the aerodynamic forces. In that case, if the 1/rev occurs, it can cause loads in excess of the usual 3/rev. Therefore, in selecting a tower, one criteria is that the fundamental tower frequency should be greater than the Cycloturbine 1/rev excitation band. Since the Cycloturbine running speed range is about 60 RPM to 160 RPM, it is seen from Figure 8-6 that to satisfy this criteria the fundamental tower frequency should be about 3 Hz or greater.

The 3/rev, as discussed before, is the dominant aerodynamic harmonic and can be troublesome at resonant conditions. Therefore, operating at an RPM which can cause resonance should be avoided. As seen in Figure 8-6, tower frequencies above 3 HZ tend to lie within the Cycloturbine operating range. Therefore, to preclude resonance, the tower should be "soft" (that is, have a low fundamental frequency) so that the Cycloturbine operates above the tower frequency or should be stiff enough so that the Cycloturbine always operates below the tower frequency. The soft tower can present static aeroelastic problems and the stiff tower introduces problems of cost, weight, transportability, etc.

A compromise solution was sought wherein the Cycloturbine, if exciting the tower frequency would do so at reduced load levels, that is, at the lower end of the operating range. As seen in Figure 8-6, both the 34-ft heavy-duty Octahedron and the

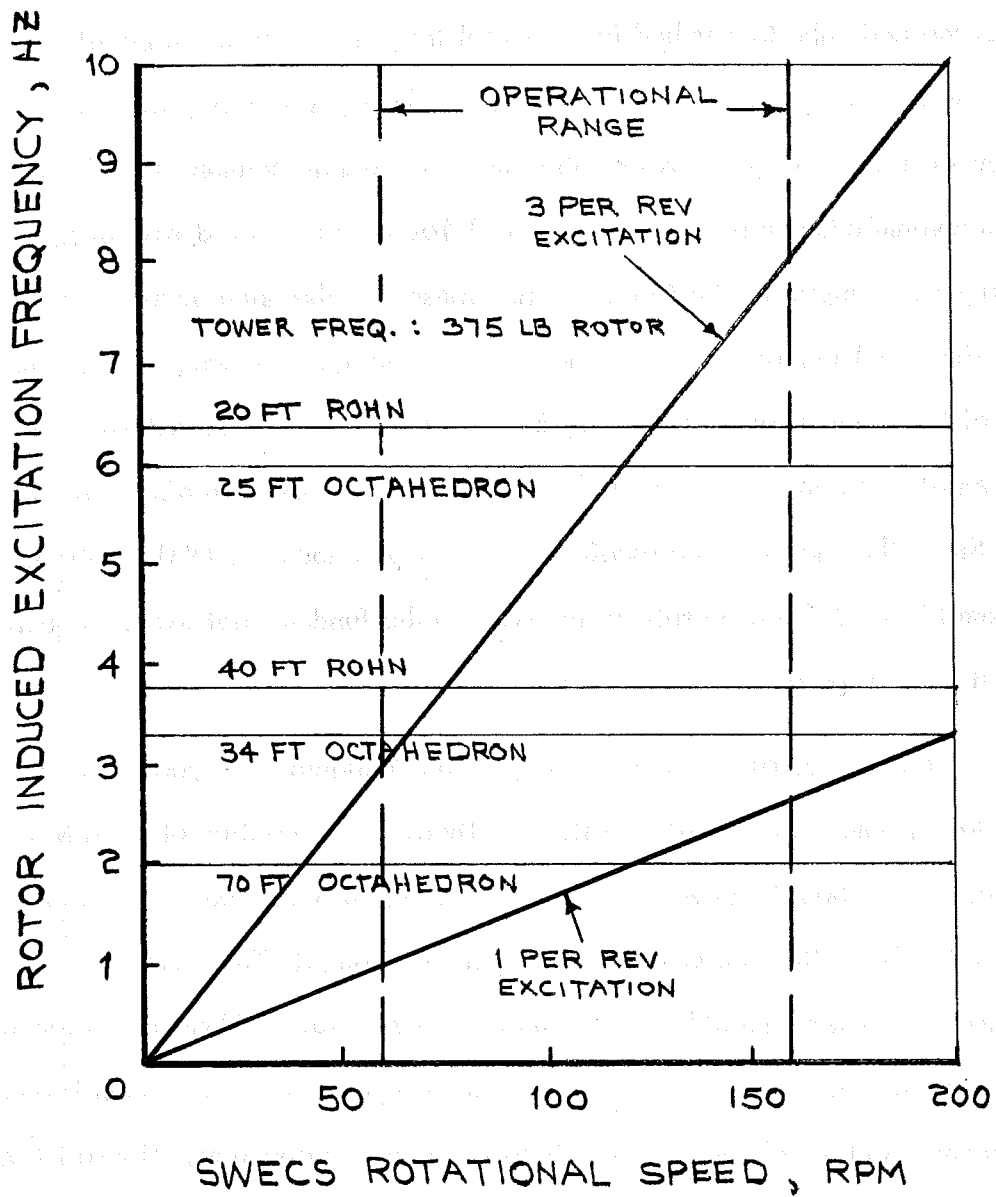


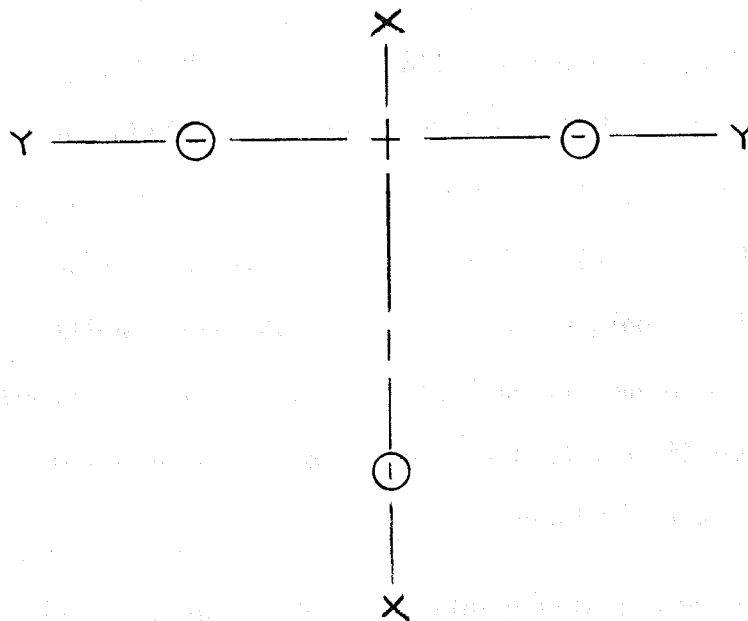
Figure 8-6. Excitation Frequency versus SWECS RPM.

40-ft Rohn towers became viable candidates. In order to select a tower, it became essential to determine the fundamental frequency accurately and, if possible, to determine the damping characteristics.

A test program was performed in order to establish the dynamic characteristics of a 34.5-ft, heavy-duty Octahedron tower with a 500 lb Cycloturbine, and a 40-ft Rohn SSV tower with a 570 lb deadweight. Electronic equipment used for obtaining data consisted of two 2262-C-25 Endevco piezoresistive accelerometers, a 9170 Daytronics conditioning unit, and two 7132-A Hewlett-Packard dual pen chart recorders. The accelerometers were mounted on brackets at the Cycloturbine or tower top to measure in directions  $90^\circ$  apart. The conditioning equipment and recorders were located on the ground near the tower.

The tower was excited by attaching a rope to the top of the test tower and to the back of a pick-up truck. A shackle-and-pin assembly was used to release the rope. An initial tension was applied to the tower by the truck. The pin was then pulled from the shackle, allowing the tower to vibrate in its fundamental mode. The accelerometer signals were recorded until the vibrations dampened.

After the field testing was completed, the fundamental frequency was determined from the acceleration traces, and the damping factors,  $\zeta$ , were calculated by using logarithmic decrement curves for the damped data. A structural dynamics equation for cantilever beam applications was then used to calculate moment of inertia values for the towers. Results for the Octahedron tower and the 40-ft Rohn are summarized in Figure 8-7 and details are given in Appendix B. The figure defines the two excitation axes,  $90^\circ$  apart, along which the accelerometers were placed. As is seen from the frequency and damping data, the towers have very similar characteristics.



OCTAHEDRON

500 lb Cycloturbine

34-Ft Height

Frequency:

X-X: 4.25 Hz

Y-Y: 4.4 Hz

Damping:

X-X: .0059

Y-Y: .0083

ROHN

570 lb Dead Weight

40-Ft Height

Frequency:

X-X: 3.92 Hz

Y-Y: 3.55 Hz

Damping:

X-X: .0082

Y-Y: .0017

Figure 8-7. Tower Test Data.

It was concluded that both towers are acceptable for use in the 1-kW high-reliability Cycloturbine test program. However, a 42.5-ft heavy-duty Octahedron tower was recommended since this tower meets the height criteria and, because the construction is the same as the 34-ft tower, the natural frequency is lower. The frequency is expected to be between 3.8 and 4.0 Hz. The Octahedron tower is preferred to the Rohn tower because it can be erected more easily by hand at remote locations and because PEC has more experience with the Cycloturbine on Octahedron towers.

However, in order to provide the greatest latitude and flexibility in selecting the tower, three options were offered, namely:

Option 1:

- Purchase 42.5-ft Octahedron and 40-ft Rohn.
- Locate Octahedron at New Seabury for prototype tests.
- Locate Rohn at Rocky Flats for test program.
- Deliver Octahedron to Rocky Flats with third prototype.

Option 2:

- Purchase two (2) 42.5-ft Octahedrons.
- Locate at New Seabury and Rocky Flats as in Plan 1.

Option 3:

- Purchase 42.5-ft Octahedron tower for Rocky Flats tests.

## SECTION 9

### PRODUCT LIABILITY AND SAFETY

The development of commercially-viable SWECS has reached the point where wide spread distribution of these machines to the public is imminent. Public acceptance of SWECS is based not only on their technical performance and reliability but also on other factors such as noise, esthetic value, and safety. The latter factor can have significant impact on the SWECS industry because of the need to satisfy local, state and federal codes that exist for the erection and operation of equipment in a manner designed to protect the public interest. Since these codes were established in a general sense, they can impose in some cases strict limitations on SWECS which can limit performance of the equipment or require costly modification.

Closely tied to safety considerations is the need for product liability insurance. Changes in product liability laws and court decisions in recent years have resulted in a financial dilemma for manufacturers (see, e.g., Reference 24). For the SWECS industry, product liability considerations could require unnecessary design changes which can result in more costly machines. These costs in addition to the high cost of product liability insurance will directly impose a further barrier to commercialization.

Thus, product liability insurance coverage and safety requirements imposed on SWECS could hamper rapid commercialization of these systems. The material in this section is a result of a limited investigation into the cost and availability of products liability insurance for manufacturers and users of small wind energy conversion systems. Also considered was the extent of safety requirements presently in existence which could impact on the commercialization of SWECS.

## 9.1 PRODUCT LIABILITY

One of the many institutional barriers to the rapid commercialization of SWECS is the lack of Products Liability insurance coverage at a reasonable rate. The rates, as illustrated by the following information, gathered for Phase I, are restrictively high in view of the fact that the majority of the companies involved in the development and manufacture of SWECS are relatively young industries, supplying a limited market.

The following paragraphs, excerpted from a response from an insurance company to an inquiry regarding product liability coverage, illustrate the current state of the problem:

"I am pleased to be in a position to offer any quote on this coverage which on an industry-wide basis is in a crisis situation. Users of products are suing manufacturers more frequently and for larger amounts, and the defense costs alone reach outrageous proportions. A product like yours is viewed by the insurance companies as an above average hazard because of the blades spinning. Even though you feel it is extremely safe, the insurance companies are difficult to convince. The helicopter blades that caused injury and damage in a New York City accident recently is an example of the concern the companies have for suits".

"The quote is for \$300,000.00 Combined Single Limit of coverage for Bodily Injury and Property Damage with a \$500.00 deductible per loss. The Minimum and Deposit annual premium is \$10,400.00 (including premium tax), with an adjustable rate at audit of \$10.00 per \$100.00 of sales. Although this figure seems staggering compared to your other insurance costs, it is really quite reasonable for products liability coverage".

Up to the present time, no standards have been set as to the requirements of SWECS and very little statistical information is available to the insurance companies. Because Products Liability costs are based solely upon statistics, insurance companies presently impose the highest rates. Until the insurance companies are provided with

statistical information and until such time that standards are developed for the manufacture of SWECS, the premium rates for Products Liability will remain prohibitive.

Conceivably, these costs could remain only a short term barrier to the commercialization of the wind industry. The development of an adequate statistical data base for SWECS through the continued testing by Federal agencies utilizing facilities such as those at Rocky Flats, and the development of manufacturing standards by Federal agencies will make available to the insurance companies the information needed to set rates in accordance with the reliability and safety of products.

## 9.2 SAFETY REQUIREMENTS

Presently, there are very few requirements regarding safety during manufacture, installation or use of small wind energy conversion systems. This also inhibits the insurance companies and adds to their reluctance to lower rates.

OSHA has no specific safety requirements for SWECS. The safety requirements for employees of manufacturers of SWECS, for the present, fall under the same nonspecific regulations applicable to all manufacturing firms. The general regulations and requirements are enumerated under the "General Standards 29 Code Federal Regulations 1910" (Reference 25). The applicable categories are:

- Accident Record Keeping Requirements.
- Drive Belts.
- Electrical Installations.
- Gears.
- General Duty Clause.
- Ladders, Fixed.
- Machine Guarding.

- Machinery, Fixed.
- Power Transmission, Mechanical.
- Pulleys.
- Stationary Electrical Devices.

Until such time that specific regulations and safety requirements are set, either by the insurance companies or Federal Agencies, it is advisable that the following safety measures be taken:

During Manufacturing:

Apply "General Standards 29 Code Federal Regulations 1910", (Reference 25).

During Installation:

- Hardhats.
- Safety climbing belts.
- Warning signs.
- Use of personnel qualified to work with cranes, on towers, etc., that is, experienced erection crews.
- Keep tower work to a minimum (use of cranes, etc.).
- When it is not possible to use a crane and bucket truck, either a crane alone or a platform which adheres to OSHA standards should be used.

On Site Safety Measures:

- Fences.
- Warnings Signs.
- Measures should be taken to inhibit tower climbing, e.g., remove bottom 20' of ladder.

## SECTION 10

### PHASE II TEST PLAN

The test program to be carried out during Phase II will consist of three parts, namely: 1) weld tests; 2) test stand tests; and 3) prototype tests. The test stand is a specially constructed Cycloturbine designed to accept advanced-design components such as the tilt-cam actuation control system and an extruded strut. Prototype tests will be conducted on the three models to be delivered to Rocky Flats. The tests are described in the following sections.

#### 10.1 WELD TESTS

##### Objective

To determine the fatigue life of welded specimens to be used in verifying the life capabilities of the welded structure.

##### Test Description

A degree of confidence in the capability of welds to accept design loads was achieved by the results of the strut tang test (Subsection 5.1.2). However, the strut welds are to be subjected largely to oscillatory loads which is a more critical condition than the steady state loads. Therefore, a fatigue test of a welded structure is planned. The test specimen will be placed in a fixture and oscillatory loads applied by a motor with an eccentric. The specimen will be tested to failure at a prescribed stress level. Other specimens will be tested to failure at different stress levels. The results will be used to produce S-N curves for the welded structure.

Additional fatigue data will also be obtained for rod ends to be used on the Cycloturbine. It is planned to link the drive motor to the test specimen with a rod end so that the rod end will also be exposed to the fatigue load.

## 10.2 TEST STAND TESTS

The test stand consists of the following major components:

- C2E blades modified to have pull rod connection ahead of hinge point and balanced to have the center of gravity at the quarter chord.
- Struts constructed of extruded aluminum NACA 0015 Section each 7-ft in length.
- C2E main shaft.
- C2E hubs.
- C2E bearing cartridge.
- Tilt-cam actuation control system.

The following instrumentation are available for all tests:

- Torque transducer.
- Strain gage at strut root.
- RPM sensor.

In addition, wind speed is detected by two anemometers and electrical output can be recorded in the instrumentation shed.

### 10.2.1 CYCLOTURBINE

#### 10.2.1.1 COMPONENT DYNAMIC TESTS

##### Objective

To determine the natural frequency of selected components both as individual members and when connected in a subassembly. These data will be used to help interpret operational test results and the subsequent correlation with analytical results.

The data will also be used in interpreting dynamic response of the Cycloturbine/tower system.

### Test Description

Dynamic tests will be conducted on Cycloturbine components both on the bench and when installed as the test stand. Bench tests will be conducted on a blade, strut, pull rod and main shaft as individual components. The components will be supported in a manner similar to that in which they will be supported in the test stand. The component will be excited by striking to excite the fundamental mode. Data will be recorded using the accelerometers provided by Rockwell.

Dynamic tests will be performed on the same components when assembled in the test stand and mounted on the Octahedron tower at New Seabury. Accelerometers will be mounted on the components to record the natural frequency of the component. In the case of the pull rod, it may be necessary to strain gage the rod in order to record the frequency.

Excitation of the total system will be made by a rope attached to the tower (see Subsection 8.2.3). Pulls will be made in several directions to determine any assymetry due to tower motions. If the results are dominated by the tower frequency, a variable speed motor with an eccentric will be attached to the tower to allow a frequency sweep in order to excite the various components of interest.

Tower data will be recorded with the machine both stopped and running. The frequency data obtained from the series of tests will be used to help interpret operational test results and their correlation with analytical results.

## 10.2.1.2 OPERATIONAL TESTS

### Objective

To determine the performance and load characteristics of the Cycloturbine tilt-cam control system over a wide range of operational conditions. Continuous running of the machine in the operational environment will yield valuable insight into the reliability of the tilt-cam system.

### Test Description

The test stand machine will be installed at the New Seabury test site and will be run throughout the windy winter season. The machine will be subjected to high winds, salt fog, and icing. The operational and load characteristics of the tilt-cam system will be observed. In addition, the continued running of the machine in the operational environment will yield valuable information on the reliability of the tilt-cam system.

Parameters to be recorded are:

- Torque.
- Wind speed.
- RPM.
- Strain at strut root.
- Electrical output.

Data will be recorded at wind speeds throughout the operational range of the Cycloturbine as well as at high velocities normally encountered during the winter season. The machine will be inspected periodically especially after periods of high wind velocity.

### 10.2.1.3 EFFECT OF CYCLIC PITCH SCHEDULE - $\theta_{1c}$

#### Objective

To determine the effect of various maximum cyclic pitch angles,  $\theta_{1c}$ , on the performance of the Cycloturbine and to select the cyclic pitch angle consistent with performance and reliability goals.

#### Test Description

The original pitch actuation control system was operated with a maximum cyclic pitch angle,  $\theta_{1c}$ , of -10 degrees. The tilt-cam actuation control system is designed to operate at lower values of  $\theta_{1c}$ . The test stand machine will be operated at different schedules of  $\theta_{1c}$  from zero degrees to -10 degrees. These tests will be conducted in conjunction with the operational tests (see Subsection 10.2.1.2).

### 10.2.1.4 STOPPED ROTOR LOADS

#### Objective

To determine the loads on the stopped rotor and to establish the shut-down and restart capabilities of the machine.

#### Test Description

The Cycloturbine is designed to shutdown at wind speeds in excess of 40 mph. The loads in the strut will be measured under these conditions. Wind speed and RPM will also be measured.

These tests are dependent on the wind conditions. In addition to the measured loads, the shut down and restart capabilities of the tilt-cam system will be established.

#### 10.2.1.5 ICING EFFECTS

##### Objective

To determine the effect of ice build-up on the performance and loads of the Cycloturbine.

##### Test Description

During the winter testing season, icing conditions will be encountered. The test stand machine will be observed during icing periods to determine its operation and the effect of icing. If possible, the extent of icing and the amount of build-up on the machine will be determined. Performance and loads will be measured during operation under icing conditions. These tests will be conducted in conjunction with operational tests (see Subsection 10.2.1.2).

#### 10.2.1.6 DYNAMIC STALL

##### Objective

To determine the effect of dynamic stall on the Cycloturbine performance.

##### Test Description

Dynamic stall, when it occurs, is a transient condition on the Cycloturbine. During the operational tests, at wind speeds less than 20 mph, attempts will be made to induce a dynamic stall condition and to obtain data during the transitional operational condition.

## 10.2.2 ELECTRICAL SYSTEM

### 10.2.2.1 BURN-IN

#### Objective

To detect components with low mortality rates and to ensure proper operation of all circuit components.

#### Test Description

Transient suppression networks, main rectifier circuit, voltage limiter control, and voltage controlled relay have all been bread-boarded for Phase I. These subassemblies will be connected and an alternator (standard unit) will be provided to constitute the full electrical system. This assembled system will undergo a 48-hour power burn-in. The burn-in will aid in detecting components with premature mortality. Functional tests will be conducted before, during and after burn-in to ensure proper operation of all circuit components.

### 10.2.2.2 OPERATIONAL TESTS

#### Objective

To verify the proper functioning of the electrical system in the operational environment and to provide a realistic load to the Cycloturbine.

#### Test Description

The fully-assembled bread-board version of the electrical system will be delivered to PEC and installed on the test stand machine. It will be used during operational tests conducted during the winter season (see Subsection 10.2.1.2). Electrical output from the test stand will be recorded.

### 10.3 PROTOTYPE TESTS

Three prototype units of the 1-kW high-reliability Cycloturbine SWECS will be delivered to Rocky Flats. Extensive testing will be performed with the first prototype. This machine will undergo limited testing at New Seabury prior to delivery to Rocky Flats.

#### 10.3.1 CYCLOTURBINE

The following instrumentation will be available on the first prototype:

- Torque transducer.
- Strain gauges at selected points including blade center spar and strut root.
- RPM sensor.
- Blade pitch angle sensor.
- Thermocouples at selected points including alternator field coil.

This instrumentation will be supplied by Rockwell. Brackets for attaching similar instrumentation will be provided on the second and third prototypes.

##### 10.3.1.1 COMPONENT DYNAMIC TESTS

###### Objective

To determine the natural frequency of selected components both as individual members and as parts of a subassembly. These data will be used to aid in the interpretation of operational test results and in the subsequent correlation with analytical results. The data will also be used in interpreting dynamic response of the Cycloturbine/tower system.

###### Test Description

The component dynamic tests described in Subsection 10.2.1.1 for the test stand machine will be repeated for the first prototype. These dynamic data will be used in the

interpretation of tests results and for correlation to analytical results. The experience gained in the test stand tests will facilitate the implementation of these data for the prototype.

### 10.3.1.2 OPERATIONAL TESTS

#### Objective

To verify the proper operation of the fully-assembled prototype, to provide performance and load data of the prototype, and to implement design modifications, if necessary.

#### Test Description

Limited operational tests will be conducted on the first prototype at New Seabury. Tests to be conducted and data to be recorded will parallel that of the test stand operational tests (Subsection 10.2.1.2). These tests will be on a limited scale compared to the test stand tests. Sufficient data at available wind speeds will be recorded at steady-state conditions to allow comparison to analytical results.

If operational problems are encountered, design modifications will be implemented and the redesign tested. The prototype will be approved for delivery to Rocky Flats when the machine is deemed to be free of operational problems.

### 10.3.2 ELECTRICAL SYSTEM

#### 10.3.2.1 SUBASSEMBLY TESTS

#### Objective

To detect out-of-spec performance of components, to verify proper operation of subassemblies, and to determine components with premature mortality.

## Test Description

The following tests will be performed:

- Alternator (A1A1)

Five tests for output and field coil resistance to detect intercoil shortcircuits and to determine wire tension during coil fabrication.

Five tests for insulation resistance to detect short circuits between coils and the frame of the alternator.

One test for output coil orientation to find coils that are 180° electrically out of phase, while it is still easy to reverse them.

One performance test as a final check of all components and to detect machining errors as well as electrical faults.

- Transient Protection Network (A1A2)

One test of spark gap firing voltage which is a nondestructive test to verify operation of the gap.

One test of varistor clamping voltage which is a nondestructive test to determine if device is within nominal specifications.

One test of insulation resistance as a final check for short circuits to ground and the insulation impedance.

- Transient Protection Network (A2A1)

One test of surge protector clamping voltage to determine if the suppressor is within nominal specifications.

- Main Rectifier Assembly (A2A3)

Two tests for low current voltage drop for each diode to detect damage to the rectifier junction, which it is not possible to observe.

48-hour power burn-in with A2A2 and A2A4 to cull out infant mortalities in the assemblies.

- Dump Load Card A2A2

48-hour power burn-in with A2A3 and A2A4 to cull out infant mortalities in the assemblies.

Functional test before and after burn-in to ensure proper operation of all circuit components.

Three functional tests during burn-in to speed throughput of this operation as it may gate the entire assembly procedure.

- Voltage Limiter Control (A2A4)

48-hour power burn-in with A2A2 and A2A3 to cull out infant mortalities in the assemblies.

### 10.3.2.2 OPERATIONAL TESTS

#### Objective

To verify the proper functioning of the prototype electrical system in the operational environment and to provide the proper load resistance to the Cycloturbine.

#### Test Description

The first prototype electrical system will be mounted on the Cycloturbine, tower, and instrumentation building as designed. Temperature of the alternator field coil will be observed and electrical output at the battery will be measured.

## REFERENCES

1. Drees, H. M., "An Analytical and Experimental Investigation of a Darrieus Wind Turbine Employing Cyclic Blade Pitch Variation". M.S. Thesis, Massachusetts Institute of Technology, Cambridge, Massachusetts, 1976.
2. Noll, R. B.; Drees, H. M.; and Nichols, L., "Development of the 1-2 kW Cycloturbine". Presented at the American Wind Energy Conference (Amarillo, Texas), March 1 - 5, 1978.
3. Brinkman, W. A. R., "Climatological Study of Strong Downslope Winds in the Boulder Area". NCAR Cooperative Thesis No. 27, University of Colorado, Department of Geography, 1973.
4. Marin, J., "Engineering Materials". Prentice-Hall, Inc. (New York), 1952.
5. Frost, W. and Long, B. H., "Engineering Handbook on the Atmospheric Environmental Guidelines for Use in Wind Turbine Generator Development". The University of Tennessee Space Institute, November 1977.
6. Wentink, T., Jr., "Wind Power Potential of Alaska: Part I - Surface Wind Data from Specific Coastal Sites". University of Alaska, Geophysical Institute, UAG R-225, August 1974.
7. Justus, C. G.; Hargraves, W. R.; and Mikhail, A., "Reference Wind Speed Distributions and Height Profiles for Wind Turbine Design and Performance Evaluation Applications". ORO/5108-7614 UC 60, August 1976.
8. Anon., "Reliability Prediction of Electronic Equipment". Department of Defense, Military Standardization Handbook, MIL-HDBK-217B, September 20, 1974.
9. Templin, R. J., "Aerodynamic Performance Theory for the NRC Vertical-Axis Wind Turbines". National Research Council of Canada, LTR-LA-160, June 1974.
10. Ashley, H., "Some Contributions to Aerodynamic Theory for Vertical-Axis Wind Turbines". J. of Energy, Vol. 2, No. 2, March - April 1978, pp. 113-119.
11. Blackwell, B. F.; Sheldahl, R. E.; and Feltz, L. V., "Wind Tunnel Performance Data for the Darrieus Wind Turbine with NACA 0012 Blades". Sandia Laboratories, SAND 76-0130, May 1976.
12. Sheldahl, R. F. and Blackwell, B. F., "Aerodynamic Characteristics of Four Symmetrical Airfoil Sections through 180 Degrees Angle of Attack at Low Reynolds Numbers". Vertical-Axis Wind Turbine Technology Workshop, May 17-20, 1976.
13. Fanucci, J. B. and Walters, R. E., "The Theoretical Performance of a Vertical-Axis Wind Turbine". Proceedings of the Vertical-Axis Wind Turbine Technology Workshop, Sandia Labs, May 1972.

14. Ham, N. D. and Garelick, M. S., "Dynamic Stall Considerations in Helicopter Rotors". Journal of the American Helicopter Society, April 1968, pp. 49-55.
15. Johnson, W. and Ham, N. D., "On the Mechanism of Dynamic Stall". Journal of the American Helicopter Society, October 1972, pp. 36-45.
16. Johnson, W., "The Effect of Dynamic Stall on the Response and Airloadings of Helicopter Rotor Blades". Journal of the American Helicopter Society, April 1969, pp. 68-79.
17. Etkin, B., "Dynamics of Flight: Stability and Control". John Wiley and Sons, Inc., 1959, p. 314.
18. Ham, N. D.: "Aeroelastic Analysis of the Troposkien-Type Wind Turbine". Sandia Labs, SAND77-0026, April 1977.
19. Ham, N. D.: "Helicopter Blade Flutter". AGARD-R-607, January 1973.
20. Marks, L. S. (Ed.), "Mechanical Engineer Handbook (see "Bearings with Rolling Contact" by G. A. Ungar)". McGraw-Hill Book Co., Inc. (New York), 1941.
21. Palmgren, A.: "Ball and Roller Bearing Engineering". S. H. Burbank and Co., Inc., 1959.
22. Wilcock, D. F. and Booser, E. R., "Bearing Design and Application". McGraw-Hill Book Co., (New York), 1957.
23. Harris, T. A., "Roller-Bearing Analysis". John Wiley & Sons, Inc. (New York), 1966.
24. "The Devils in the Product Liability Laws". Business Week, February 12, 1979.
25. U.S. Department of Labor Occupational Safety and Health Administration, OSHA 2201, revised June 1975.

APPENDIX A

NOMENCLATURE

APPENDIX A  
NOMENCLATURE

A	total blade aerodynamic load acting on main shaft
$A_S$	material cross-sectional area of main shaft
$A_{k_n}$	blade dynamic amplification factor for bending in the $k^{\text{th}}$ mode in response to the $n^{\text{th}}$ harmonic airload
AC	alternating current
ASI	Aerospace Systems, Inc.
a	blade lift curve slope (Section 4.2) = $V_B^2/Rg$ ; centrifugal acceleration in g's (Section 4.5) main shaft dimension; see Figure 4-18 Wentink wind distribution parameter; see Equation (2-2)
$a_c$	location of blade aerodynamic center in percent of chord
$a_{p_i}$	axial acceleration of pull rod
ac	aerodynamic center
$B_1$	radial load on upper main bearing
$B_2$	radial load on lower main bearing
b	number of blades blade dimension; see Figure 4-20 main shaft dimension; see Figure 4-18
C	blade chordwise aerodynamic force
$C(\phi)$	Theodorsen's lift deficiency function
$C_D$	blade drag coefficient
$C_{D_a}$	additional drag coefficient; see Equation (4-27)

## NOMENCLATURE (Continued)

$C_{D_{\text{strut}}}$	$= C_{D_a}$
$C_{D_o}$	constant drag coefficient
$C_H$	turbine drag coefficient
$C_L$	blade lift coefficient
$C_{L_\alpha}$	lift curve slope
$C_P$	turbine power coefficient
$C_l$	$= C_L$ ; blade lift coefficient; see Figure 4-7
$C_m$	blade pitching moment coefficient; see Figure 4-7
$c$	Weibull wind distribution parameter; see Equation (2-3) main shaft dimension; see Figure 4-18
$c_i$	$= 2 \gamma_i m_i \omega_i$
cg	center of gravity
D	blade drag axial load in strut due to distributed weight; see Equation (4-40)
DC	direct current
d	main shaft dimension; see Figure 4-18
$dC/dl$	blade chordwise force distribution
$dN/dl$	blade normal force distribution
E	cam eccentricity; see Equation (4-50) Young's modulus of elasticity (Section 4.6)
e	relative change in length of pull rod linkage caused by cam eccentricity; see Equation (4-50)

## NOMENCLATURE (Continued)

F	axial load on strut due to blade load; see Equation (4-39) allowable structural stress (Section 4.5.3)
$F_G$	gust factor
$F_L$	total load factor for bearing
$F'_L$	bearing load ratio
$F''_L$	bearing shock load ratio
$F_S$	bearing speed factor
$F_a$	force exerted by blade on pull rod
$F_{ap}$	axial force on pull rod due to blade
$F_{as}$	side force on pull rod due to blade
$F_p$	total axial force on pull rod
$F_{pc}$	centrifugal force on pull rod
$F_{pi}$	oscillating inertial force on pull rod
FDR	Final Design Review
FMEA	Failure Mode and Effects Analysis
f	actual or calculated structural stress (Section 4.5.3) drive belt factor (Section 6.3.3.1)
$f(x)$	probability density function
G	torsional modulus of elasticity
g	acceleration of gravity

## NOMENCLATURE (Continued)

H	mean drag force in wind direction; see Equations (4-10) and (4-76) constant blade tension force component parallel to axis of rotation; see Equation (4-66)
$H_z$	time in hours that wind speed is equal to or exceeds the value, V
h	distance between blade cg and pivot; see Figure 4-20
$h(t), h_1(t), h_2(t)$	hazard rate
I	blade bending moment of inertia
$I_B$	blade moment of inertia about the blade pivot
$I_{cc}$	moment of inertia of blade spar
$I_f$	alternator field current $= \frac{mc^2}{30}$ (Section 4.6.1)
$I_{ss}$	main shaft polar moment of inertia
$I_{xx}$	moment of inertia of the strut
i	summation index; see Equation (6-19)
J	blade polar moment of inertia
j	blade dimension; see Figure 4-20
K	inflow ratio parameter; see Equation (4-16) Weibull wind distribution parameter; see Equation (2-3)
k	Wentink wind distribution parameter; see Equation (2-2) mode number; see Equation (4-67) bearing load weighting factor; see Equation (6-9)
$k_i$	stiffness of the $i^{\text{th}}$ element of the structural model

## NOMENCLATURE (Continued)

kW	kilowatt
L	blade lift total blade length (Section 4.5)
$L_s$	length of blade spar
Life	bearing life
Load	bearing load
$l$	blade length
$\bar{l}$	distance between two blade supports; see Figure 4-34
$l_c$	length of blade tip cap
$l_s$	length between end of blade spar and blade/strut connection
$l_t$	$= l_c + l_s$
M	bending moment on turbine blade; see Equation (4-66)
$M_H$	total blade moment about the blade pivot
$M_{H_a}$	aerodynamic pitching moment of blade about its pivot
$M_{H_c}$	centrifugal moment of blade about its pivot
$M_{H_I}$	inertial moment of blade about its pivot
$M_{a_1}$	aerodynamic bending moment at blade spar center
$M_{a_2}$	aerodynamic bending moment at blade/strut connection
$M_{cc}$	centrifugal bending moment on blade tip caps
$M_i$	generalized mass of $i^{\text{th}}$ mode

## NOMENCLATURE (Continued)

$M_i$	bending moment
$M_s$	bending moment on strut due to tangential aerodynamic force
$M_1$	total bending moment at blade spar center
$M_{1c}$	centrifugal bending moment at blade spar center
$M_2$	total bending moment at blade/strut connection
$M_{2c}$	centrifugal bending moment at blade/strut connection
$M_4$	bending moment on main shaft
MOV	metal oxide varistor
mph	miles per hour
MRML	manufacturer's recommended maximum load
MS	margin of safety
MTBF	Mean Time Before Failure
m	blade mass
$m(\xi)$	blade mass element; see Equation (4-66)
$m_g$	damping coefficient of any mode; $= \frac{\gamma}{2} C(\phi)$ , normal; $\approx 0$ , chordwise
$m_i$	blade mass element; see Equation (4-56)
$m_i$	discrete mass used to represent system components (Section 4.6.2)
$m_p$	pull rod mass
N	blade normal force

## NOMENCLATURE (Continued)

NLL	no-lift line
NPI	Natural Power, Inc.
n	airload harmonic number; see Equation (4-70) number of bearings sharing a function; see Equation (6-19)
OSHA	Occupational Safety and Health Administration
P	turbine mean power resultant load on bearing; see Equations (6-9) and (6-10)
$P_a$	axial load on bearing
$P_r$	radial load on bearing
P.C.	printed circuit
PEC	Pinson Energy Corporation
p	blade dimension; see Figure 4-20
$\underline{p}$	number of events per revolution; also ___/rev
$p_o(t)$	probability of both bearings in a pair operating satisfactorily at time, t
$p_1(t)$	probability of remaining bearing operating after failure of one of a pair of bearings
Q	aerodynamic force on the turbine
q	blade dimension; see Figure 4-20
R	turbine radius
R(t)	reliability; probability of nonfailure
$R'(t)$	reliability of a pair of bearings serving a particular function
$R_B$	reliability of one blade assembly
$R_{BS}$	reliability of a partially parallel blade system

## NOMENCLATURE (Continued)

$R_E$	total reliability of electrical system
$R_S$	total system reliability; see Equation (6-27)
$R_T$	total reliability of turbine
$R_C$	reliability of common system; see Equation (6-22)
$R_e$	Reynold's number
$R_r$	reliability of a redundant system
RPM	revolutions per minute
$r$	radial station of strut from shaft center; see Figure 4-15 pulley radius (Section 6.3.3.1)
$r_i$	distance of a blade mass element from pivot
$r_o$	distance between cam center and inner end of pull rod
$S_{a1}$	stress at blade spar center due to aerodynamic moment
$S_{a2}$	stress at blade/strut connection due to aerodynamic moment
$S_{a3}$	stress at strut root due to aerodynamic load
$S_{c1}$	stress at blade spar center due to centrifugal moment
$S_{c2}$	stress at blade/strut connection due to centrifugal moment
$S_{c3}$	stress at strut root due to centrifugal load
$S_i$	stress due to bending moment
$S_1$	total bending stress at blade spar center

## NOMENCLATURE (Continued)

$S_2$	total stress at blade/strut connection
$S_3$	total strut axial stress
$S_4$	bending stress in main shaft
$S_5$	axial stress in pull rod
S-N	fatigue curves of stress (S) versus number of cycles (N) at a given stress level
SWECS	Small Wind Energy Conversion System
T	tangential force on strut
t	time
U	relative wind speed
V	wind velocity volts (electrical system)
$\bar{V}$	mean wind speed
$V_B$	= $\Omega R$
$V_G$	gust velocity; see Equation (2-1)
$\bar{V}_z$	mean wind speed at elevation z; see Equation (2-4)
$V_f$	alternator field voltage
v	inflow velocity
$v_G$	velocity amplitude of a discrete gust (Section 4.4)
$v_o$	mean inflow velocity
W	thrust on alternator bearing (Section 6.3.3.1) blade weight (Section 4.6)

## NOMENCLATURE (Continued)

$w_a$	= $dN/dl$ ; distributed aerodynamic normal load
$w_b$	blade weight; see Equation (4-56)
$w_p$	pull rod weight
$w_s$	distributed weight of strut
$w_1$	distributed weight of blade spar, ribs and skin
$w_2$	distributed weight of blade skin of tip caps
$x$	= $V/\bar{V}$ ; see Equation (2-2) = $V/c$ ; see Equation (2-3) displacement at any mass station; see Equation (4-78) distance along undeflected blade; see Figure 4-34
$\bar{x}_{cc}$	distance from hub center to outer fibers of strut
$y$	blade deflection; see Figure 4-34 bearing load weighting factor; see Equation (6-10)
$\bar{y}$	distance from chord line to outer fiber of blade; see Equation (4-36) maximum blade deflection; see Equation (4-67)
$y_k$	blade deflection in $k^{\text{th}}$ mode
$z$	elevation above ground level; see Equation (2-4)
$\bar{z}$	main shaft radius
$\alpha$	blade angle-of-attack
$\alpha_{DS}$	dynamic stall angle-of-attack
$\gamma$	total angle of oscillation of bearing; see Equations (6-14) and (6-15) = $\frac{\rho a c R}{m}$ ; (Section 4.6.1)
$\Delta H, \Delta H_1,$ $\Delta H_2, \Delta H_3$	instantaneous force in downwind direction due to one turbine blade

## NOMENCLATURE (Continued)

$\Delta \psi$	charge in azimuth angle due to change in wind direction (Section 4.3.3) azimuthal angular distance between blades (Section 4.6.2)
$\zeta$	angular position of blade cg; see Figure 4-20
$\zeta_i$	damping ratio for the $i^{\text{th}}$ mode
$\eta_i$	displacement in the $i^{\text{th}}$ mode
$\theta$	blade instantaneous pitch angle; see Figure 4-1
$\theta_o$	blade collective pitch angle
$\theta_{1c}$	blade cyclic pitch angle
$\lambda$	$= \frac{\Omega R}{V}$ ; tip speed ratio (Section 5) failure rate; see Equation (6-1)
$\lambda_i$	inflow ratio
$\lambda_o$	mean inflow ratio
$\lambda_{1c}$	magnitude of harmonic variation of inflow velocity
$\nu_k$	$= \frac{\omega_k}{\Omega}$ ; nondimensional natural frequency of the $k^{\text{th}}$ mode
$\xi$	blade station; see Figure 4-34 cant angle of strut; see Figure 4-15b
$\pi$	$= 3.141529624$
$\rho$	density of air
$\rho_i$	density of ice

## NOMENCLATURE (Concluded)

$\sigma$	$= \frac{bc}{2R}$ ; turbine solidity
$\phi$	blade inflow angle; see Figure 4-1 $= \frac{\omega c}{2U}$ ; (Section 4.6.1)
$\phi_i$	mode shape of the $i^{\text{th}}$ mode
$\psi$	blade azimuth position; see Figure 4-1
$\psi_y$	phase angle in tilt cam
$\Omega$	turbine rotational speed
$\omega$	gust frequency; see Equation (4-28) rotational speed of bearing; see Equation (6-13) forcing frequency; see Equation (4-77)
$\omega_{T_k}$	blade frequency of the $k^{\text{th}}$ torsional mode
$\omega_i$	frequency of the $i^{\text{th}}$ mode (Section 4.6.2)
$\omega_k$	blade frequency of $k^{\text{th}}$ bending mode; see Equation (4-69)
<u>Subscripts</u>	
Actual	actual or calculated value
MAX, max	maximum value
Nom	nominal load
Rated	manufacturer's rated load
<u>Other</u>	
.	single dot above a parameter indicates rate
..	double dot above a parameter indicates acceleration

APPENDIX B

TOWER VIBRATION TEST DATA FOR:

- 34-ft Octahedron (500 lb Cycloturbine)
- 40-ft Rohn (570 lb Deadweight)

TOWER VIBRATION TEST DATA

34-Ft Octahedron (500 Lb Cycloturbine)

Excitation Direction: X-X

Conditions:

$$\begin{aligned}
 f_N &= 4.25 \text{ cps} \\
 &= 255 \text{ RPM} \\
 &= 85 \text{ RPM 3/rev excitation}
 \end{aligned}$$

Results:

Test No. 1

$$\left. \begin{aligned}
 \frac{1}{6} \quad \ln \left( \frac{14.5}{10.75} \right) &= 0.049 \\
 \frac{1}{12.5} \quad \ln \left( \frac{14.5}{8.75} \right) &= 0.040 \\
 \frac{1}{19} \quad \ln \left( \frac{14.5}{6.75} \right) &= 0.040 \\
 \frac{1}{25.5} \quad \ln \left( \frac{14.5}{5.5} \right) &= 0.038 \\
 \frac{1}{32} \quad \ln \left( \frac{14.5}{4.5} \right) &= 0.036
 \end{aligned} \right\} \delta_{\text{AVE}} = 0.041$$

$$\text{Damping Factor} = \zeta = \frac{\delta}{[(2\pi)^2 + \delta^2]^{1/2}}$$

$$\zeta_{XX} = 0.0061$$

Test No. 2

$$\frac{1}{6.5} \ln \left( \frac{11.25}{8.75} \right) = 0.038$$

$$\frac{1}{13} \ln \left( \frac{11.25}{7} \right) = 0.036$$

$$\frac{1}{19.5} \ln \left( \frac{11.25}{5.5} \right) = 0.036$$

$$\frac{1}{32} \ln \left( \frac{11.25}{3.5} \right) = 0.036$$

$$\frac{1}{38.5} \ln \left( \frac{11.25}{2.75} \right) = 0.036$$

$$\delta_{AVE} = 0.036$$

$$\text{Damping Factor} = \zeta = \frac{\delta}{[(2\pi)^2 + \delta^2]^{1/2}}$$

$$\zeta_{XX} = 0.0057$$

Excitation Direction: Y-Y

Conditions:

$$f_N = 4.4 \text{ cps}$$

$$= 264 \text{ RPM}$$

$$= 88 \text{ RPM } 3/\text{rev excitation}$$

Results:

Test No. 1

$$\frac{1}{6.5} \ln \left( \frac{29.75}{20.25} \right) = 0.059$$

$$\frac{1}{20} \ln \left( \frac{29.75}{11} \right) = 0.049$$

$$\frac{1}{26.5} \ln \left( \frac{29.75}{8} \right) = 0.049$$

$$\frac{1}{40} \ln \left( \frac{29.75}{4.75} \right) = 0.046$$

$$\frac{1}{46.5} \ln \left( \frac{29.75}{3.75} \right) = 0.044$$

$$\delta_{AVE} = 0.049$$

$$\text{Damping Factor} = \zeta = \frac{\delta}{[(2\pi)^2 + \delta^2]^{1/2}}$$

$$\zeta_{YY} = 0.0078$$

Test No. 2

$$\frac{1}{7} \quad \ln \left( \frac{34}{21.75} \right) = 0.064$$

$$\frac{1}{13.5} \quad \ln \left( \frac{34}{15} \right) = 0.061$$

$$\frac{1}{20} \quad \ln \left( \frac{34}{11.5} \right) = 0.054$$

$$\frac{1}{26.5} \quad \ln \left( \frac{34}{8.5} \right) = 0.052$$

$$\frac{1}{40} \quad \ln \left( \frac{34}{5} \right) = 0.048$$

$$\delta_{AVE} = 0.056$$

$$\text{Damping Factor} = \zeta = \frac{\delta}{[(2\pi)^2 + \delta^2]^{1/2}}$$

$$\zeta_{YY} = 0.0089$$

TOWER INERTIA CALCULATIONS

Excitation Direction: X-X

Conditions:

$$g = 386 \text{ in/sec}^2$$

$$M_B = 700 \text{ lbs}$$

$$l = 33' = 396''$$

$$M = 455 \text{ lbs}$$

Dynamic:

$$\omega_N = \sqrt{\frac{3EI}{l^3 (M + 0.23 M_B)}}$$

Using 4.25 cps as the natural frequency,  $\omega_N = 4.25 (2\pi) = 26.7 \text{ rad/sec}$

$E = \text{Modulus of Elasticity (Steel} = 30 \times 10^6)$

$$26.7 \text{ rad/sec} = \left[ \frac{3 (30) (10)^6 I}{(396)^3 \left( \frac{455}{386} + 0.23 \frac{700}{386} \right)} \right]^{1/2}$$

$$I_{XX} = 650 \text{ in.}^4$$

Excitation Direction: Y-Y

Dynamic:

Using 4.4 cps as the natural frequency,  $\omega_N = 4.4 (2\pi) = 27.6 \text{ rad/sec}$

$$27.6 \text{ rad/sec} = \left[ \frac{3 (30) (10)^6 I}{(396)^3 \left( \frac{455}{386} + 0.23 \frac{700}{386} \right)} \right]^{1/2}$$

$$I_{YY} = 840 \text{ in.}^4$$

## EXPECTED TOWER DEFLECTIONS

Excitation Direction: X-X

$$\Delta_{MAX} = 1 \text{ in.} = \frac{P l^3}{3EI}$$

$$1 \text{ in.} = \frac{P (396)^3}{3 (30) (10)^6 650}$$

Excitation Direction: Y-Y

$$\Delta_{MAX} = 1 \text{ in.} = \frac{P (396)^3}{3 (30) (10)^6 840}$$

$$P = 1,215 \text{ lbs}$$

TOWER VIBRATION TEST DATA  
40-Ft Rohn SSV (570 Lb Deadweight)

Excitation Direction: X-X

Conditions:

$$\begin{aligned}
 f_N &= 47/12 = 3.92 \text{ cps} \\
 &= 235 \text{ RPM} \\
 &= 78 \text{ RPM } 3/\text{rev excitation}
 \end{aligned}$$

Results:

Test No. 1

$$\frac{1}{4} \ln \left( \frac{26.25}{21} \right) = 0.056$$

$$\frac{1}{15.5} \ln \left( \frac{26.25}{11.5} \right) = 0.053$$

$$\frac{1}{19.5} \ln \left( \frac{26.25}{9.5} \right) = 0.052$$

$$\frac{1}{23.5} \ln \left( \frac{26.25}{8} \right) = 0.051$$

$$\frac{1}{27.5} \ln \left( \frac{26.25}{7} \right) = 0.048$$

$$\delta_{\text{AVE}} = 0.052$$

$$\text{Damping Factor} = \zeta = \frac{\delta}{[(2\pi)^2 + \delta^2]^{1/2}}$$

$$\zeta_{\text{XX}} = 0.0083$$

Test No. 2

$$\frac{1}{3.5} \ln \left( \frac{26.25}{21.5} \right) = 0.057$$

$$\frac{1}{15} \ln \left( \frac{26.25}{12} \right) = 0.052$$

$$\frac{1}{19} \ln \left( \frac{26.25}{10.25} \right) = 0.049$$

$$\frac{1}{27} \ln \left( \frac{26.25}{6.75} \right) = 0.050$$

$$\frac{1}{38.5} \ln \left( \frac{26.25}{4} \right) = 0.049$$

$$\delta_{AVE} = 0.051$$

$$\text{Damping Factor} = \zeta = \frac{\delta}{[(2\pi)^2 + \delta^2]^{1/2}}$$

$$\zeta_{XX} = 0.0082$$

Excitation Direction: Y-Y

Conditions:

$$f_N = 3.55 \text{ cps}$$

$$= 213 \text{ RPM}$$

$$= 71 \text{ RPM } 3/\text{rev excitation}$$

Results:

Test No. 1

$\frac{1}{3.5}$	$\ln$	$\left(\frac{15}{10}\right)$	$= 0.116$	] $\delta_{AVE} = 0.108$
$\frac{1}{7}$	$\ln$	$\left(\frac{15}{6}\right)$	$= 0.131$	
$\frac{1}{10.5}$	$\ln$	$\left(\frac{15}{4.5}\right)$	$= 0.115$	
$\frac{1}{14}$	$\ln$	$\left(\frac{15}{3.5}\right)$	$= 0.104$	
$\frac{1}{25}$	$\ln$	$\left(\frac{15}{2.25}\right)$	$= 0.076$	

$$\text{Damping Factor} = \zeta = \frac{\delta}{[(2\pi)^2 + \delta^2]^{1/2}}$$

$$\zeta_{YY} = 0.017$$

Test No. 2

$$\frac{1}{7} \quad \ln \quad \left( \frac{14.25}{5.5} \right) = 0.136$$

$$\frac{1}{10.5} \quad \ln \quad \left( \frac{14.25}{4} \right) = 0.121$$

$$\frac{1}{14} \quad \ln \quad \left( \frac{14.25}{3} \right) = 0.111$$

$$\frac{1}{17.5} \quad \ln \quad \left( \frac{14.25}{2.5} \right) = 0.099$$

$$\frac{1}{28.5} \quad \ln \quad \left( \frac{14.25}{1.25} \right) = 0.085$$

$$\delta_{AVE} = 0.110$$

$$\text{Damping Factor} = \zeta = \frac{\delta}{[(2\pi)^2 + \delta^2]^{1/2}}$$

$$\zeta_{YY} = 0.0175$$

TOWER INERTIA CALCULATIONS

Excitation Direction: X-X

Conditions:

$$g = 386 \text{ in/sec}^2$$

$$M_B = 1,025 \text{ lbs}$$

$$l = 40' = 480''$$

$$M = 570 \text{ lbs}$$

Dynamic:

$$\omega_N = \sqrt{\frac{3EI}{l^3 (M + 0.23 M_B)}}$$

Using 3.9 cps as natural frequency,  $\omega_N = 2\pi (3.9) = 24.5 \text{ rad/sec}$

where

$\omega_N$  = natural frequency in rad/sec

$E$  = modulus of elasticity (steel =  $3 \times 10^7$  psi)

$M$  = mass of weight at beam end

$M_B$  = beam (tower) mass

$l$  = beam length

$$24.5 \text{ rad/sec} = \left[ \frac{3 (3) (10)^7 I}{(480)^3 \left( \frac{570}{386} + 0.23 \frac{1,025}{386} \right)} \right]^{1/2}$$

$$I_{XX} = 1,540 \text{ in.}^4$$

Excitation Direction: Y-Y

Dynamic:

Using 3.55 cps as the natural frequency,  $\omega_N = 2\pi (3.55) \text{ cps} = 22.305 \text{ rad/sec}$

$$22.305 \text{ rad/sec} = \left[ \frac{3 (30) (10)^6 I}{(480)^3 \left( \frac{570}{386} + 0.23 \frac{1,025}{386} \right)} \right]^{1/2}$$

$$I_{YY} = 1,275 \text{ in.}^4$$

## EXPECTED TOWER DEFLECTIONS

Excitation Direction: X-X

$$\Delta_{\text{MAX}} = 1 \text{ in.} = \frac{P \ell^3}{3EI}$$

$$1 \text{ in.} = \frac{P (480)^3}{3 (30) (10)^6 1,540}$$

$$P = 1,250 \text{ lbs}$$

where

P = horizontal force at tower top

E = steel elastic modulus =  $30 (10)^6$  psi

I = inertia (in.<sup>4</sup>)

ℓ = tower height

Excitation Direction: Y-Y

$$\Delta_{\text{MAX}} = 1 \text{ in.} = \frac{P (480)^3}{3 (30) (10)^6 1,275}$$

$$P = 1,035 \text{ lbs}$$